The effect of hydrogen bonding on foldamer self-assembly

by

Michael-Phillip Smith

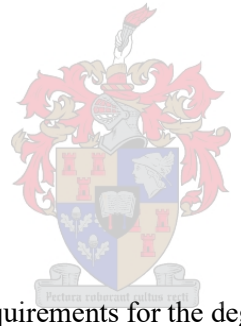

Thesis presented in fulfilment of the requirements for the degree of Master of Science in the Faculty of Science at Stellenbosch University

Supervisor: Prof B Klumperman

Co-supervisors: Dr R Pfukwa & Prof WAL van Otterlo

March 2023

1 Declaration

By submitting this thesis electronically, I declare that the entirety of the work contained therein is my own, original work, that I am the sole author thereof (save to the extent explicitly otherwise stated), that reproduction and publication thereof by Stellenbosch University will not infringe any third party rights and that I have not previously in its entirety or in part submitted it for obtaining any qualification.

March 2023

2 Abstract

Foldamers are chain molecules (oligomer or polymers) that fold into a conformationally ordered state when in solution. These polymers have been shown to have applications in host-guest chemistry, catalysis, and show great promise as responsive gel polymers. In previous literature, a large *para*-aryl triazole foldamer system with a diameter of 30 Å was developed and studied by Klumperman and co-workers. The foldamer's superhelical structures (helixes made of helixes) were shown to be unstable. Where the structures would collapse (forming spherical objects made of secondary structure helixes) at high percentage solvent compositions of the selective solvent (water) in the non-selective solvent (Dimethylformamide, (DMF)). This was hypothesized to have occurred because of the polymer being poorly solubilized in solution.

A library of polymers with varying amounts of hydrogen bond acceptors incorporated within the monomeric units was therefore synthesized and successfully characterized. The properties of the said library of polymers were then investigated *via* DLS (dynamic light scattering), LD (linear dichroism), CD (circular dichroism), and UV/Vis spectroscopy (ultraviolet-visible light spectroscopy). It was determined that the polymers with hydrogen bonding moieties incorporated within the monomeric units, would not fold with a change in solvent composition, instead, the polymers would form a conglomerated mass of polymer chains. This may be a result of two factors; firstly, although the hydrogen bonding was expected to increase the stabilization of the helical structure (simulated *via* molecular dynamic calculations), the amount of hydrogen bonding groups incorporated within the polymers could be too great and inhibited the polymers' ability to fold. Secondly, the polymers may have not folded as the molecular weights of the polymers may have not been sufficiently large enough to induce folding (polymer length would need to be 42 kDa). To confirm this hypothesis, ultrapure monomers would need to be synthesized (according to a new synthetic procedure) and a new polymerization methodology would need to be developed for the hydrogen bonding containing monomers to ensure higher molecular weights are easily achieved.

In the future, it would be ideal to investigate other streamlined methods to achieve the synthesis of the polymeric systems developed in this thesis, this would enable for the effective investigation of the properties of this system without having such synthetic hurdles as was encountered in this work. For example, the development of a triphenylphosphine-free methodology for a Sonagashira-Hagihara coupling reaction. It would also be ideal to develop another method of polymerization for the hydrogen bond-containing systems as the current polymerization technique may have not yielded polymer with high enough molecular weights to confirm that low molecular weights of the polymer systems were inhibiting the folding process. In addition, it would be ideal to develop another methodology to acquire

ultrapure monomer as this is a step growth polymerization and any impurities would drastically impact the molecular weight acquired.

3 Uittreksel

Voudamers is kettingmolekules (oligomeer of polimere) wat in 'n konformasie-geordende toestand vou wanneer dit in oplossing is. Daar is getoon dat hierdie polimere toepassings het in gasheer-gas chemie, katalise, en toon groot belofte as responsiewe gel polimere. In vorige literatuur is 'n groot para-ariel triasool voudamer sisteem met 'n deursnee van 30 Å ontwikkel en bestudeer deur Klumperman en medewerkers. Die voudamer se superheliese strukture (helikse gemaak van helikse) is as onstabiel getoon. Waar die strukture sou ineenstort (wat sferiese voorwerpe gemaak van sekondêre struktuurhelikse vorm) by hoë persentasie oplosmiddelsamestellings van die selektiewe oplosmiddel (water) in die nie-selektiewe oplosmiddel (Dimetielformamied, (DMF)). Dit is vermoedelik plaasgevind as gevolg van die polimeer wat swak opgelos is in oplossing.

'n Biblioteek van polimere met wisselende hoeveelhede waterstofbinding-aannemers wat binne die monomeriese eenhede geïnkorporeer is, is dus gesintetiseer en suksesvol gekarakteriseer. Die eienskappe van die genoemde biblioteek van polimere is daarna deur middel van DLS (dinamiese ligverstrooiing), LD (lineêre dichroïsme), CD (sirkulêre dichroïsme) en UV/Vis-spektroskopie (ultraviolet-sigbare ligspektroskopie) ondersoek. Daar is vasgestel dat die polimere met waterstofbindingsdele wat binne die monomeriese eenhede geïnkorporeer is, nie sou vou met 'n verandering in oplosmiddelsamestelling nie, eerder sou die polimere 'n geglomereerde massa polimeerkettings vorm. Dit kan die gevolg wees van twee faktore; eerstens, alhoewel die waterstofbinding na verwagting die stabilisering van die heliese struktuur sou verhoog (gesimuleer via molekulêre dinamiese berekeninge), kon die hoeveelheid waterstofbindingsgroepe wat binne die polimere geïnkorporeer is te groot wees en die polimere se vermoë om te vou belemmer. Tweedens het die polimere dalk nie gevou nie aangesien die molekulêre gewigte van die polimere dalk nie groot genoeg was om vou te veroorsaak nie (polimeerlengte sal 42 kDa moet wees). Om hierdie hipotese te bevestig, sal ultrasuiwer monomere gesintetiseer moet word (volgens 'n nuwe sintetiese prosedure) en 'n nuwe polimerisasiemetodologie sal ontwikkel moet word vir die waterstofbinding-bevattende monomere om te verseker dat hoër molekulêre gewigte maklik bereik word.

In die toekoms sal dit ideaal wees om ander vaartbelynde metodes te ondersoek om die sintese van die polimeriese sisteme wat in hierdie tesis ontwikkel is te bereik, dit sal die effektiewe ondersoek van die eienskappe van hierdie sisteem moontlik maak sonder om sulke sintetiese hindernisse te hê as wat in hierdie werk teëgekom is. . Byvoorbeeld, die ontwikkeling van 'n trifenylfosfienvrye metodologie vir 'n Sonagashira-Hagihara-koppelreaksie. Dit sal ook ideaal wees om 'n ander metode van polimerisasie vir die waterstofbinding-bevattende sisteme te ontwikkel aangesien die huidige polimerisasietegniek moontlik nie polimeer met hoog genoeg molekulêre gewigte opgelewer het om te bevestig dat lae molekulêre gewigte van die polimeerstelsels die vouproses inhibeer nie. Daarbenewens sal dit ideaal

wees om 'n ander metodologie te ontwikkel om ultrasuiwer monomeer te verkry, aangesien dit 'n stapgroeipolimerisasie is en enige onsuiwerhede die molekulêre gewig wat verkry word, drasties sal beïnvloed.

4 Dedication

This thesis is dedicated to my incredible wife, Nikki Smith.

5 Acknowledgments

Firstly, a big thank you to Professor Klumperman for all his guidance and mentorship throughout this project. I have developed a lot as a researcher under your guidance, and I feel that there is nothing I can do to ever repay you for all that you have done for me, but I can say that I will be forever grateful for your mentorship and what you have done. Secondly thank you to Doctor Pfukwa, for all your guidance in the lab and for showing me the ropes. You have taught me a lot in terms of lab skills, developing my ability to think critically and analyse papers, and teaching me to always make sure the work I do is thorough and reproducible. Thank you for also teaching me how to write in a more scientific manner, it is a greatly appreciated skill that I will always value. To Professor Van Otterlo, thank you for your infinite advice when it comes to synthetic techniques and skills. There were quite a few times where you really got me out of a synthetic hole that I had no idea how to get out of. So, thank you so much for that and for your assistance in developing me further as a research scientist and for instilling a sense of excitement for science and chemistry. I would then also like to give an enormous thank you to Professor Rodger, for all her amazing work and assistance on the LD side of things in this thesis. You have done amazing work that I could never repay you for, thank you so much. To Professor Lederer and her team in Dresden, for your help and expertise in determining the molecular weight of the polymers developed. Without your help, there would be a massive hole in the story. And finally, the CHPC for allowing me to utilize the licensing for the Schrodinger Suite, and specifically Doctor Krishna for his assistance with teaching me how to utilize the interface of the CHPC server and using the Schrodinger software. I would also like to thank the Wilhelm Frank Trust for funding me throughout my MSc studies. Without your support, none of this would have happened and I would have never been able to pursue my postgraduate studies.

I would like to give a huge thank you to Professor Arnott for being there for me. For always having your door open to me and being willing to chat about anything. I would like to thank Doctor De Villiers for opening her lab to me, for being so welcoming, and for allowing me to work there and use her UV machine so often, it proved to be the difference between finishing a master's and not, so thank you so much. A huge thank you to Doctor Brand and Elsa for all the assistance with the NMR instruments and the CD instrument. You were both so helpful and kept me calm when the spectra were, as we would say, far from ideal. I would also like to say thank you to Doctor H Pfukwa, for the assistance with all the training on the instruments in the building, without the correct guidance I would have probably broken something major by now. Also, a massive thank you to Erinda (who always had a big smile on her face that always made my day) for all her help with all the admin and short-notice deliveries I had done, it is greatly appreciated. Thank you to Debbi, Luluntu, Jim, Calvin, and Mienie for all your support, good mornings and good afternoons and for always checking in on me each morning.

Thank you to all the members of GOMOC for all the great memories in meetings and outdoor excursions and for accommodating me in your labs when our lab burnt down. I would like to give a huge thank you to Khaya Gould for all his synthetic advice on chemical procedures and the workings of a lab. Then I would also like to thank Jessica Thibaud for all her assistance regarding the computational work covered in this thesis and for teaching me how to process massive data sets. A huge thank you to Lauren Ball, Jaques Buys, Annerike, Cronje, and Leanne Kellerman for teaching me the ins and outs of polymer chemistry. What you have taught me is invaluable and will be passed on to others who join the lab. I would also like to thank all the members of the Free Radical Lab for being there for me, and for all the support, friendship, kindness, and helpful feedback you have given me over the years.

Thank you, mom, and dad, for being there for me, for supporting me, and for listening to me talk about my work, although it may not always make sense to you. Thank you for supporting me throughout my life and always encouraging me in whatever I do. Thank you, Hayley, for being the best little sister I could ask for. Your company is always appreciated. I would also like to give a massive thank you to my new in-law family, Werner Snr, Werner Jnr, Belinda, and Danielle. You have all been amazing to me and I appreciate all the support and love you all give me.

Lastly, saving the best for last, thank you to my amazing wife, Nikki, for all the support, friendship, and motivational talks you have given me. Without you, I feel this would have not been possible. This thesis is as much mine as it is yours.

6 Abbreviations

DMF	*N*,*N*-Dimethylformamide
UV/Vis	Ultraviolet/Visible spectroscopy
CD	Circular Dichroism
SEC	Size Exclusion Chromatography
NMR	Nuclear Magnetic Resonance spectroscopy
DLS	Dynamic Light Scattering
LD	Linear Dichroism
STEM	Standing Transmission Electron Microscopy
MS	Mass spectrometry
CAF	Central Analytical Facility
$Pd(PPh_3)_4$	Tetrakis(triphenylphosphine)palladium(0)
HFIP	Hexafluoroisopropanol
MALDI-Tof MS	Matrix assisted laser desorption ionization-time of flight mass spectrometry
DCC	*N*,*N*'-Dicyclohexylcarbodiimide
DMAP	4-Dimethylaminopyridine
HOBt	Hydroxybenzotriazole
DCM	Dichloromethane
EtOAc	Ethyl acetate
DIPEA	*N*,*N*-Diisopropylethylamine
n-BuOH	1-Butanol
THF	Tetrahydrofuran
^{1}H NMR	Proton Nuclear Magnetic Resonance spectroscopy
^{13}C NMR	Carbon Nuclear Magnetic Resonance spectroscopy
COSY	Correlation spectroscopy

HSQC	Heteronuclear single-quantum correlation spectroscopy
HMBC	Heteronuclear multiple-bond correlation spectroscopy
ROESY	Rotating frame Overhauser enhancement spectroscopy
ESI	Electrospray ionization
FTIR	Fourier transform infrared spectroscopy
TLC	Thin Layer Chromatography
TEA	Triethylamine

7 Table of Contents

8 List of Figures

9 List of Schemes

10 List of Tables

11 CHAPTER 1 – Introduction

11.1 Introduction

There has been a great injection of research towards the development of highly ordered helical polymers. As a product of this phenomenon, many static helical polymeric systems have been generated with sophisticated applications (poly(isocyanides)s and poly(acetylene)s in the medical field, and poly(amino acid)s in asymmetric catalysis).[1–3] Where a static helical polymeric system attains and retains its ordered structure because of the manner in which the monomer is polymerized and the steric interactions between adjacent monomeric units within the polymer (thus this polymer is inherently ordered as a result of its polymerization process). As a consequence of the polymer acquiring its helical shape as a product of steric repulsion, the helical structure is irreversibly formed (unless heated to high temperatures where the increased temperature promotes the breakdown of the ordered structure), and not as a result of any external stimulus exerted on the system. Thus, the ordered structure should not collapse unless chemical bonds are broken. As a result of this non-reversibility, the functionality of this class of polymer is limited. This explains the current effort toward reversibly forming higher-ordered polymers. One such example is that of foldamers, these are polymers that can reversibly form higher-ordered arrangements (primarily helical structures) under selective solvent conditions. In some cases, the ordered helices can pack together to form quaternary structures.[4,5]

This ordered quaternary structure is somewhat akin to that of fibrillar structures that can be found within the extracellular matrix (a hydrogel in itself).[6] It is expected that hydrogels composed of an ordered fibrillar network can exhibit a stress-strain behaviour that deviates from hydrogels with a more random network structure (e.g., strain hardening). This stress-strain behaviour could afford a stimulus-responsive (temperature or pH) hydrogel that would have interesting properties to investigate.[6–9]

Foldamers are organized structures primarily as a result of solvophobic effects (selective solvation of components in the monomeric units of the polymer), which are induced because of the structure of the monomers (namely the positioning, number, and type of functional groups present within the monomeric unit) that comprise the foldamer. In literature, it has been indicated that the functionalization of monomeric units with hydrogen bonding pendant chains has drastically changed the properties of ordered helical polymers.[10]

11.2 Aims and objectives

This effort will build upon the work previously conducted by Klumperman and co-workers,[11] where a foldamer backbone was developed and several non-hydrogen bonding achiral/chiral side chains were examined. The backbones of these foldamers were shown to form ordered helical structures upon the introduction of increasing amounts of water in dimethylformamide (DMF).[4,5] It was discovered that as the amount of DMF (percentage-wise) decreased (and thus the amount of water increased), so the

superhelical structures (large helixes made of smaller helixes) would collapse from ordered superhelix's into sphere-like structures made of helical secondary structures. The anomaly occurred at different percentages of DMF depending on the pedant chain length.[4] This is unsatisfactory, as in the future, the foldamer system would be subjected to various stimulus-responsive situations where the utilization of large amounts of a corrosive chemical (DMF) would be a limitation in terms of applications. To attain the ordered helical structure where there are low amounts of DMF, (< 5 %) the side chains on the backbone will be altered with the introduction of hydrogen bonding groups. The change in the side chains should result in the formation of hydrogen bonds within the foldamer's higher-ordered structure. This will be confirmed *via* a short computational study to determine if hydrogen bonding contributes to any degree toward helix stabilization. If there is stabilization, then it should in turn provide stability within the helical structure and should ultimately promote helix formation in higher quantities of water.

In this thesis, the aim was to synthesize a library of foldamers that contain varying degrees of hydrogen bond donors and acceptors within the polymer. The hydrogen bonding capabilities were incorporated within the pendant chains attached to the polymer backbone. Thereafter these foldamers were characterized and investigated *via* an array of analytical methods, namely ultraviolet/visible spectroscopy (UV/Vis), circular dichroism (CD), size exclusion chromatography (SEC), and nuclear magnetic resonance spectroscopy (NMR) to determine the impact the varying degrees of hydrogen bonding has on the foldamers system.

11.3 Organization of thesis

In this thesis, chapter two contains a literature review encompassing the topics covered. While chapter three includes a brief computational investigation into the foldamer library as well as all the synthetic procedures utilized for the synthesis of the library (related spectral data included), and the results from the spectral analysis of the library. Lastly, chapter four will include a summary of all the work, conclusions, and recommendations for future work.

12 CHAPTER 2 – Literature review

Biological macromolecules are highly interesting structures, which form the basis upon which life is built. These biological macromolecules are outstanding in that the complex structures are primarily constructed through the utilization of four categories of molecules (saccharides, amino acids, lipids, and nucleic acids).[12] These molecules are utilized in nature to produce a plethora of higher-order structures,[13] where function is acquired *via* the ordered self-assembly of the primary structure. If a variety of functional macrostructures could be produced from a limited pool of small molecule building blocks, it then begs to question of what can be achieved through the usage of synthetic chemicals that are at the disposal of a modern chemist. The array of synthetic polymers that could possibly be produced could be able to generate the same or similar functionality as the biological macromolecules, but still keeping in mind that the synthetic chemist in question needs to be able to synthesize these primary backbones with precise sequences that self-assemble into predictable structures with specific functions. With these ideas in mind, a field in its infancy is rapidly expanding, that of the development of highly ordered oligomers known as foldamers. A foldamer can be described as an oligomer that can fold into a well-defined conformation in solution.[14] These more ordered structures are often stabilized by a collection of noncovalent interactions between nonadjacent monomeric units. The transition between this unfolded and folded state is of great interest and often under study (Figure 12-1).

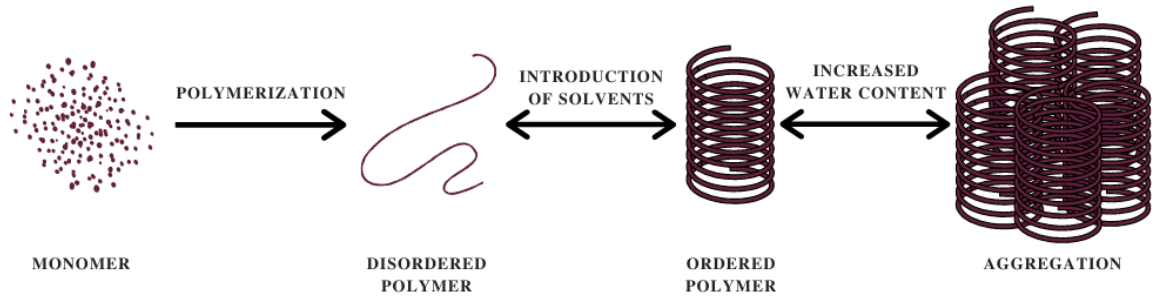

Figure 12-1: A general scheme for the route of foldamer formation and folding.

Therefore, through the introduction of solvents, the disordered primary structure can form a defined secondary structure, which can be designed to possess a specific function,[15] this concept will be further explain in more detail in the text to follow. As can be noted, this motif is similar to that of biological macromolecules (e.g., proteins), although showing much more promise in terms of a wider variety of functions as well as being more customizable in terms of the constituents that make up the primary structure and not being limited to a small pool of monomeric blocks, for example, the 20 amino acids from which proteins are derived. Although foldamers are primarily produced with non-native chemical backbones, there is a class of foldamers that have a primarily 'biotic' backbone i.e., amino acids,[16–24] or urea,[25–28] incorporated in the backbone structure. The alternative, which is the focus of this review, makes use of a more 'abiotic' backbone, these foldamers are known as synthetic foldamers.

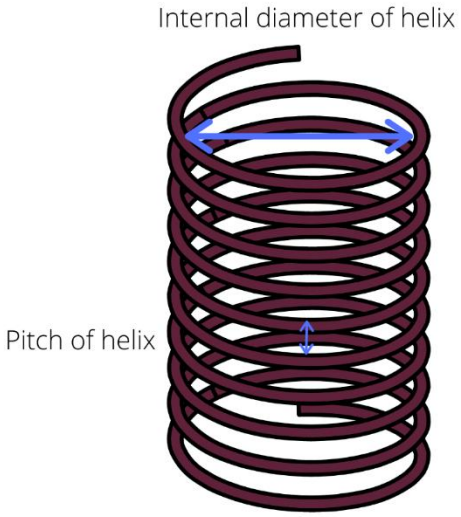

Figure 12-2: Pitch and internal diameter of a single-stranded helix.

Currently, the majority of foldamer structures are that of single-stranded helical structures,[29–33] although there have been instances where double-stranded helical foldamers have been synthesized and characterized.[34–36] In each instance the foldamer varies in terms of the pitch of the helix (the height acquired from a complete helical turn) as well as the internal diameter of the helix (Figure 12-2). Both properties, as well as the physical properties of the foldamer and the propensity of the polymer to form its ordered folded state, are determined by the monomer that is utilized. It is paramount therefore to further delve into the design of a monomeric unit of a foldamer and what interactions are of significance when designing a foldamer system. The careful design of the monomer assists in the formation of ordered structures as opposed to the formation of disordered globules (Figure 12-3).

12.1 Monomer design

Meticulous design or choice of the monomeric unit is of great importance, where the manner in which monomers are connected is crucial regarding the favouring of the folded state of the polymer as opposed to a linear disordered chain. This can be achieved *via* the introduction of attractive forces within the polymer itself. Firstly, between directly attached monomer units, where these interactions favour the bending of the polymer chain as opposed to a linear chain. This bending in turn favours the polymer to begin to fold on itself. Secondly, attractive forces between unattached monomeric units (interactions between different turns of the helix), these interactions stabilize the helix once it begins to form upon folding. The ordered state thus can be achieved through non-directional forces such as the solvophobic effect and local conformational preferences of the monomeric units,[37] as well as directional forces such as hydrogen bonding between the backbone structure of the monomeric unit or any pendant groups attached to the backbone structure.[1,38] These effects are often found to be acting in conjunction with one another to promote the folding process. The ideal foldamer system, as will be elucidated shortly, will

make use of as many of these interactions as possible, where solvophobic effects would act as the driving force to induce the folding of the disorganized polymer.

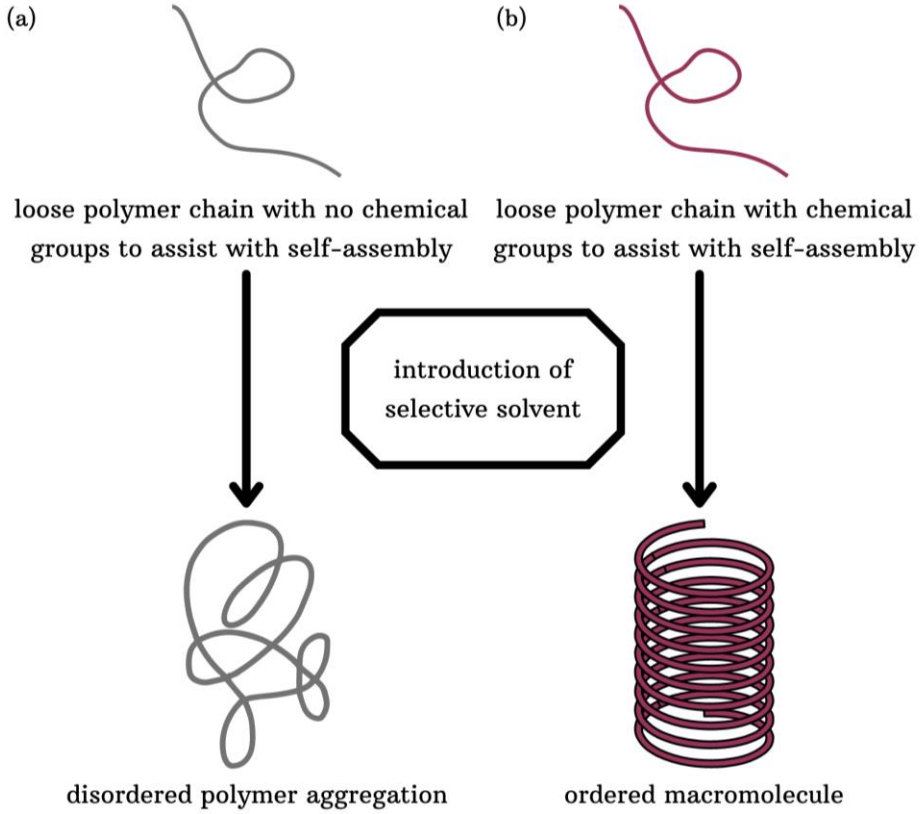

Figure 12-3: Comparison of outcomes of foldamers that were designed with or without inter and intra monomer interactions. a) the polymer was designed without intra and inter monomer interactions. The introduction of specific solvents results in the formation of a disordered polymer aggregation (a conglomeration) in comparison to b). In b) the polymer was designed such that there are intra and inter monomer interactions that result in the formation of a highly ordered macromolecular structure during the introduction of specific solvents.

12.1.1 Local conformational preferences

Monomers that utilize local conformational preferences make use of forces between directly connected monomeric units or within the monomeric unit itself. By utilizing interactions within the monomeric unit and between connected monomeric units, the degrees of rotational freedom within the macromolecule are limited. Reducing the degrees of rotational freedom, makes it simpler for the macromolecule to self-assemble into a higher-ordered structure. A commonly utilized technique is that of the introduction of hydrogen bonds between connected monomeric units, this motif is often applied in oligo-amide-based foldamers.[39] Another strategy employed to minimize the degrees of rotational freedom in and between monomeric units is *via* the introduction of multiple bonds such as triple bonds (this strategy is often accompanied with the use of specific linkage geometry which is utilized to induce bending i.e. aromatic rings),[1,30,40] or *via* the introduction of fixed planar structures such as aromatic rings.[36,39,41–43] In having multiple bonds between carbon atoms, these structures again limit the degrees of rotational freedom possible within the polymer.[30,44,45] This assists the polymer in self-assembling into a higher-ordered structure.

There are instances where helical structures form entirely based on local conformational preferences.[46] These helical structures operate on local conformational preferences and the sterically restricting manner in which the monomeric units are bound. This type of helical structure thus is not dependent on the polarity of the solvent, but the helicity is a product of the bonding between atoms in the structure. Therefore, these types of structures do not align with the definition of a foldamer,[14] in that the helicity of the macromolecular is a product of the polarity of the solvent. For the sake of this review polymers that do not exhibit dependency on solvent polarity will not be viewed as foldamers, but instead simply as helical structures. Thus, the ideal foldamer system would make use of local conformational preferences in conjunction with other forces to induce and stabilize folding respectively, while not utilizing local conformational preferences as the driving force for the folding process.

12.1.2 Intrastrand interactions

Intrastrand interactions are a category of interactions that occur between different topological levels of the supramolecular structure. These interactions occur once the higher-ordered structure forms and are utilized to stabilize the ordered structure. This added stabilization keeps the polymer in this ordered state as opposed to unravelling into its disordered loose-strand form. This category of interaction is often found in foldamer systems. A motif often used in foldamer design is that of aromatic monomeric backbone structures.[40,47–49] This structural property affords extra stability within the already formed foldamer helix due to π-π stacking.[42] In addition to this, it has been noticed in foldamer systems that hydrogen bonding has been utilized to stabilize the higher-ordered structures. These hydrogen bonds are formed between pendant groups that are attached to the foldamer backbone structure.[40,49] An example of this can be seen (Figure 12-4) where both hydrogen bonding and π-stacking interactions are present to stabilize the folded state.[49] These intrastrand interactions promote the folding process as well as retaining the folded form.

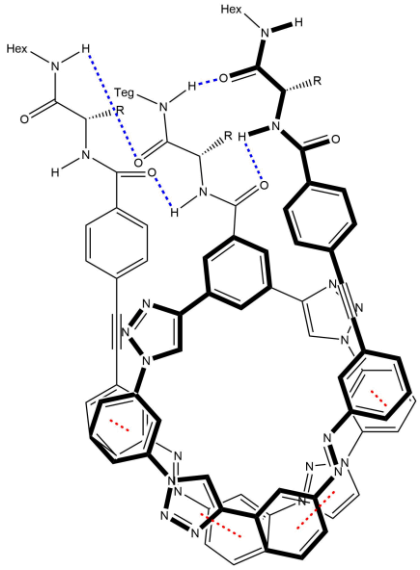

Figure 12-4:Example of foldamer that is stabilized by both hydrogen bonding (blue dotted lines) interactions as well as π-π stacking interactions (red dotted lines).[32] The image was adapted from literature.[32]Where hex implies hexyl and Teg implies tri(ethylene glycol) monomethyl ether units.

12.1.3 Solvophobic effects

It is of course important to acknowledge the very driving force of folding for foldamer systems, that of solvophobic effects. This is utilized to drive the formation of higher-ordered structures from originally disordered polymers as is highlighted in the definition of a foldamer system stated earlier and thus is the whole reason why foldamers as a class of polymers exist.

The solvophobic effect is a process where a polymer (i.e., a foldamer) is selectively solvated based on the different polarities present in the topology of the polymer (an amphiphilic polymer).[37] These different areas of the molecule will either, associate with the solvent, and in doing so those sections of the polymer will undergo a process whereby these components of the macromolecule will be further separated. This is because the components are said to bind or interact with the solvent i.e., the components are solvated. Or the topological surface of the polymer will be repelled by the solvent and all components that are of similar polarity will aggregate together. A schematic of this process is highlighted in Figure 12-5. It should be noted that this mode of aggregation is the same as that of the hydrophobic effect, where in literature water has been noted as an ideal solvent for non-directional interactions due to water being a small molecule and having low polarizability among other favourable properties.[50–53] It can thus be stated that the hydrophobic effect is a sub-class of the solvophobic effect where the selective solvent is that of water.[37] It can therefore be concluded that the ordered structures of proteins are a product of the protein being surrounded by a selective solvent i.e., water.

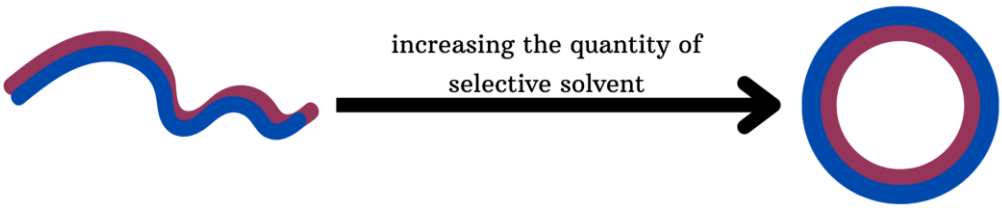

Figure 12-5: Mode of action of solvophobic effects. Red: Solvophobic component (component that is not solvated by solvent); Blue: Solvophilic component (component solvated by solvent).

A regular polymer (not a foldamer system) often does not have pre-organization within the monomeric unit, and few intrastrand interactions. Because of this, during the introduction of the selective solvent, the polymer does not collapse into an ordered macromolecular structure. Instead, it collapses into a globular structure with little to no order, a conglomerate. This process is akin to that of a hydrophobic collapse except it is not limited to aqueous settings. To prevent the foldamer from collapsing into a conglomerate of polymer, the foldamer is designed such that there is already a propensity for bending within the polymer backbone, the correct balance between polar and non-polar components in the polymers structure, as well as directional forces (i.e., hydrogen bonds) and non-directional forces (i.e., van der Waals forces, π-π stacking) to guide and stabilized the folding process as the collapsing processing occurs as a result of the solvophobic effect.

Both types of interactions (directional and non-directional) have their purposes in the formation of a foldamer system. The directional forces (i.e., hydrogen bonds, local steric conformations) can be used to induce directionality and stability during the folding process and assist in guiding the formation of the helix during the folding process as opposed to glomeration. While the non-directional forces (van der Waals forces, π-π stacking) incorporated within the polymer act to stabilize the helix once the folding process has taken place, noting that the folding is driven by solvophobic effects, begins.[54,55] To fully utilize these non-directional forces, it would be recommended that the backbone structure would have limited amounts of conformational freedom and have prior degrees of preorganization before the folding occurs. Therefore, the non-directional nature of the solvophobic effect can be utilised without concern of the foldamer collapsing into a disorganized globular state.

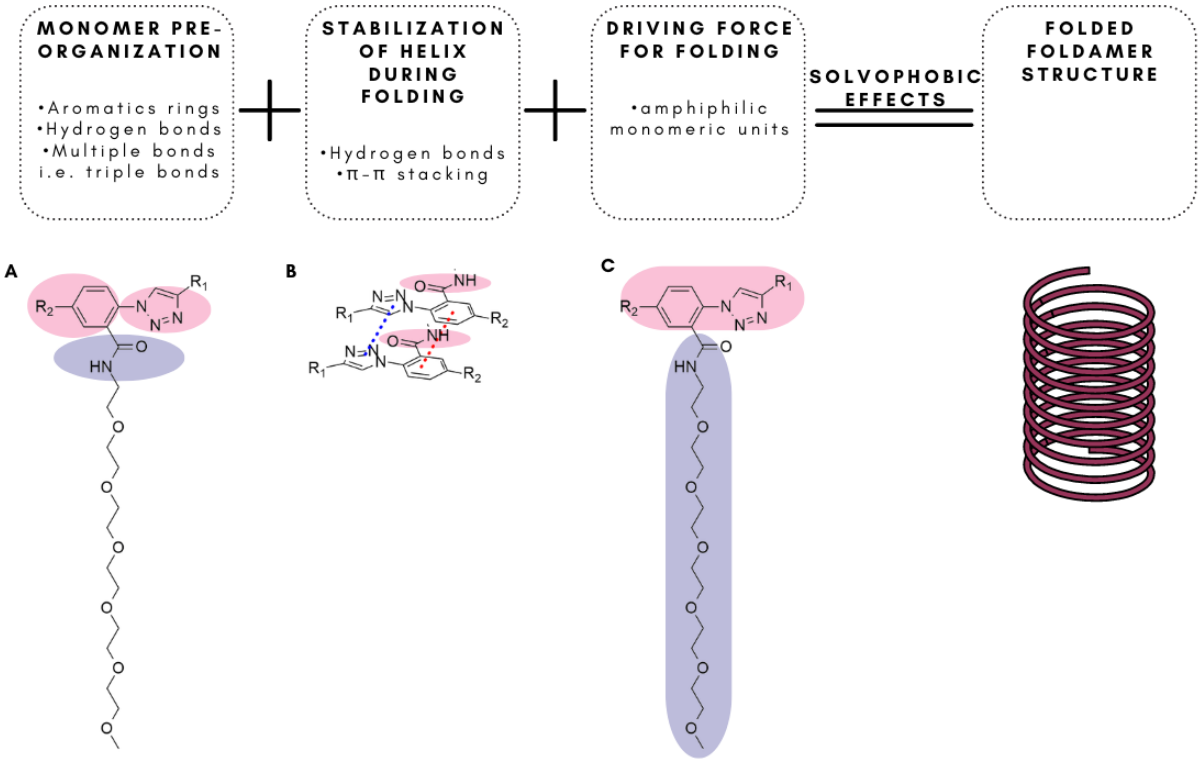

Figure 12-6:Summary of foldamer design based on foldamer system discussed in thesis. Note in Figure 6A there are examples of monomer pre-organization. Where there is an example of foldamer monomer with aromatic rings in pink, and in purple shading there are hydrogen bonding functional groups. In Figure 6B it is possible to note stabilizing forcing that are utilized to stabilize the helix once folding had taken place. Here there are hydrogen bonding groups to be utilized for stabilization during the collapsing process as well at ring stacking which is evident via the dotted lines (blue and red) between aromatic rings. In Figure 6C it is possible to note the carefully determined ratio in the amphiphilic nature of the monomer, with the hydrophobic component of the monomer highlighted in pink and the hydrophilic component in purple. This amphiphilic nature allows the monomer to act under solvophobic forces on the introduction of a selective solvent. In addition to stopping the polymer from precipitating out of solution on the introduction of a selective solvent.

As with peptides and proteins, ordered foldamer structures can be denatured. This can be achieved through the introduction of increasing proportions of a non-selective solvent,[56,57] or through high temperatures.[58] It has been shown that the denaturation process acts *via* a cooperative transition state.[37]

Which, as with proteins, can either occur in a two-state or one-state cooperative transition. Although it primarily occurs *via* a two-state cooperative system.[59]

On inspection, it can be noted that all the above-mentioned interactions are required to synthesize a successful foldamer system (Figure 12-6). Foldamers that incorporate two or more of these properties have been synthesized and have shown to have varying applications depending on the monomeric unit utilized. Some of these applications include areas such as anion binding or sensing,[32,48,60–65] molecular binding or sensing,[30,33,57,66,67] or as ion channels.[68,69]

Foldamer chemistry is still a rather young field of chemistry, with there being a huge explosion in terms of the discovery of new foldamer systems with different backbone structures. A few of these classes of foldamers include indolocarbazole,[62,70–74] m-phenylene ethynylene,[30,44,57,75–79] oligoamides,[39,80–86] oligocholic acid,[87–93] oligourea,[94–98] triazine,[99] and pyridine oxadiazole,[68,69] to name a few of the plethora of foldamer classes that exist currently (Figure 12-7). In this review, the focus will be on triazole-based foldamers, and their applications thus far. We have acknowledged that there are other foldamer classes, however, these have been extensively reviewed in the previous literature.[68,100–107] The next section will be dedicated to the discussion of triazole-based foldamers and their applications thus far in the literature.

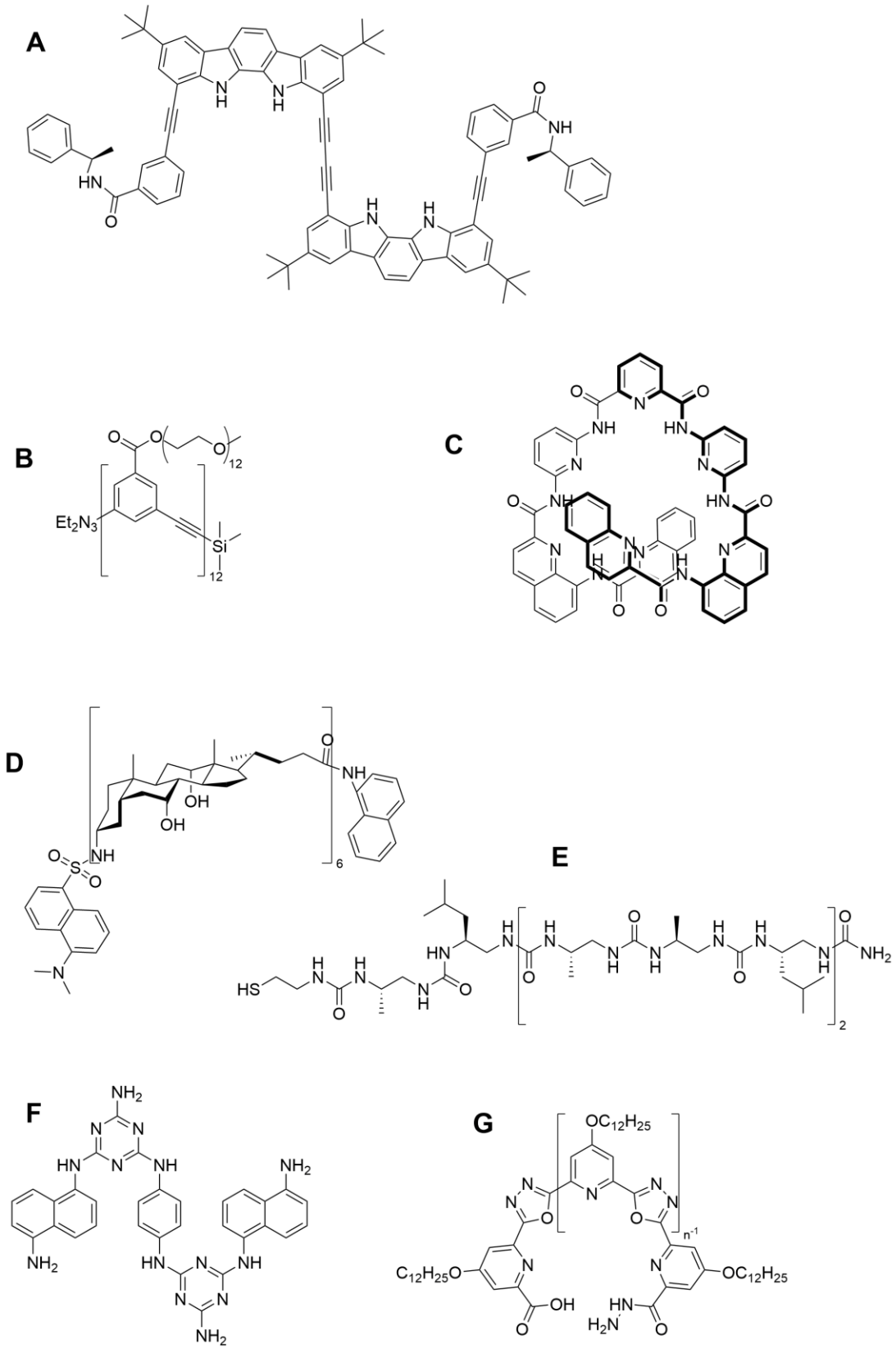

Figure 12-7: Examples of the different foldamer class: A) indolocarbazole,[70] B) m-phenylene ethynylene,[30] C) oligoamide,[151] D) oligocholic acid,[87] E) oligourea,[95] F) triazine,[99] and G) pyridine oxadiazole.[69]

12.2 Triazole-based foldamers

The 1,4-disubstituted-1,2,3-triazole motif is a remarkable chemical group. It has a large dipole moment (5 debye dipole) which is nearly colinear with the C-H bond of the 5-carbon atom of the triazole (Figure 12-8).[108] Due to the three nitrogen atoms all being on a single side of the ring, the collective electronegativity of the three nitrogen atoms causes the carbon side of the ring to become electron-deficient, this aiding the polarization of the C-H bond.[109] This polarization of the C-H bond on the triazole provides much of the functionality of the motif.

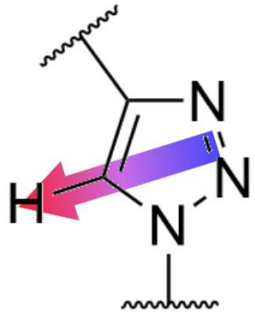

Figure 12-8: Dipole detected in triazole ring where the C-5 hydrogen atom has a partial positive charge. Red colour indicating a partial positive charge of dipole moment and blue colour that of the partial negative charge of the dipole moment in the triazole motif.

Common utilization of this motif is *via* the binding to halogens, this is often seen in the literature.[110] Foldamers have taken advantage of this trend and have been utilized to bind to halogens (halogen anions,[34,48,49,61,111–118] or in some cases halogen-containing organic compounds),[66] in solution. These halogens can be entrapped as guests in the cavity of the folded helix, and then be released upon the unfolding of the helical structure. Foldamers mostly fold as a result of the solvophobic effect, but in a few rare cases, helical folding can be trigger *via* host-guest binding.[65]

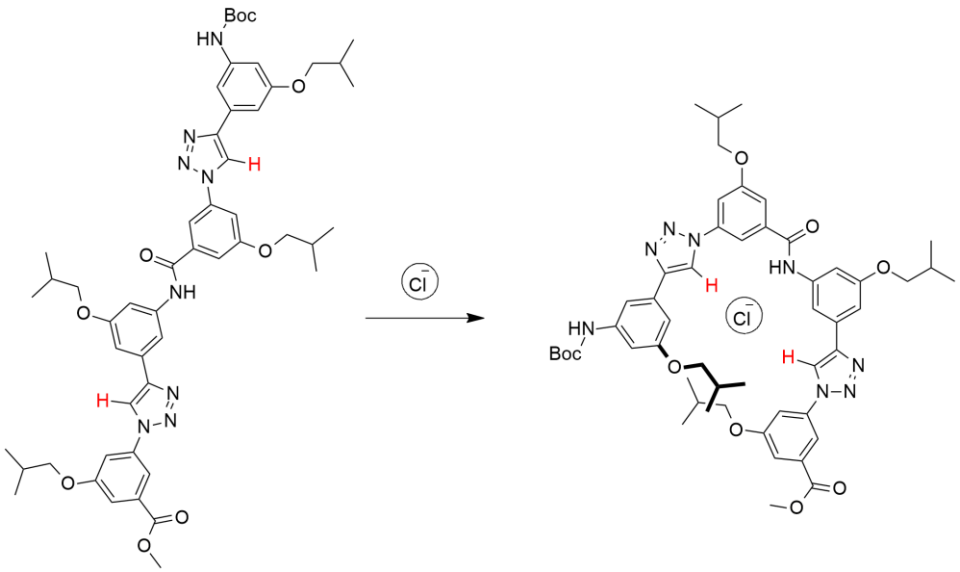

Figure 12-9: Directed polymer folding because of polymer coordination to chloride anion.[65]

These previously stated cases are of foldamer systems that utilized the C-H dipole moment on the triazole to bind to the halogen atoms (Figure 12-9), but foldamers can form host-guest associations with large organic molecules as was the case with a large foldamer system discovered by Klumperman and co-workers.[4] In this scenario, the foldamer system is wrapped around a poly(γ-benzyl-l-glutamate) guest.[4] The diameter of triazole foldamers can be varied by changing the substitution pattern of the aromatic rings that link the triazole units (Figure 12-10). The triazoles may be linked either *via* a *meta* or *para* relation to one another on the aromatic rings.

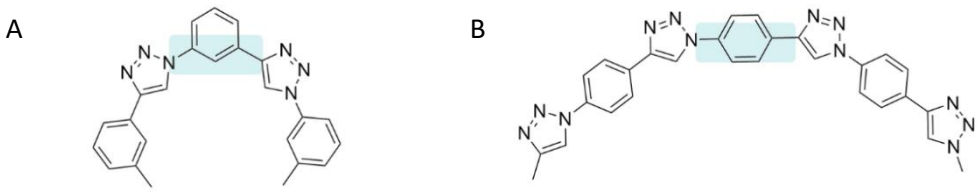

Figure 12-10:Impact on the curvature of the foldamer system based on A) meta and B) para substitution of the triazole motifs on the connecting benzene rings.

As is the case with macrocycles, the larger the diameter of the helix, the larger the guest that can be accommodated in host-guest interactions within the foldamer cavity. This is evident in the literature as meta-substituted triazole-based foldamer systems can only accommodate halogen atoms due to size limitations.[65,118] This contrasts with the foldamer system developed by Klumperman and co-workers, where the para-substituted triazole-based foldamer system can accommodate large polymer structures.[4] Triazole foldamers are a class of helical foldamer that are often found to be stabilized *via* π-π stacking, and hydrogen bonding.[34,48,65,118] This class of foldamer incorporates local conformational preferences in their monomeric units *via* the addition of triazole units to aromatic rings. This limits the degree of

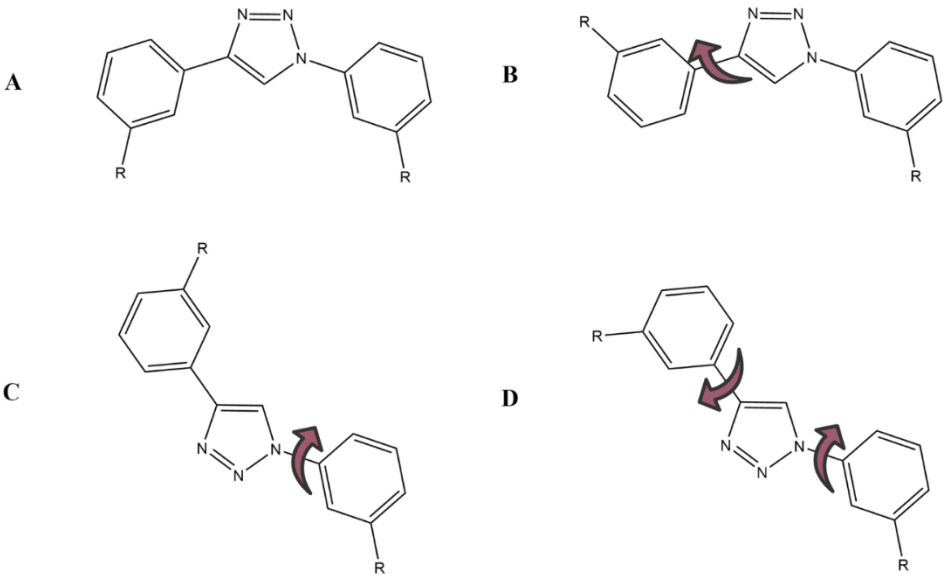

Figure 12-11: The forms of rotation that can occur within the foldamer monomeric units. There are various degrees of rotation from A to D as indicated by the red arrows. The limited degree of rotation assets the foldamer in forming a helical structure during the introduction of increasing amounts of a selective solvent.

rotation within the polymer structure to that of the rotation around the dihedral angle between the aromatic rings (Figure 12-11).[34,116,118]

Stabilization is primarily brought about by π-π stacking within the foldamer structure. This is a result of the polymer backbone consisting of alternating triazole and benzene ring repeat units that can stack atop one another. [65,111] On the other hand, hydrogen bonding is a form of stabilization that is sparsely explored within both larger (regarding diameter) and longer (regarding helix length) triazole foldamers. There has been one scenario where the effects of hydrogen bonding on a foldamer system (smaller and shorter system) have been studied .[49] It was shown that the hydrogen bonds between turns of the helical structure would provide greater influence on the stabilization of the helix than π-π stacking.[49] There have been other scenarios where *m*-phenylene ethynylenes foldamers have utilized hydrogen bonding.[40] In this scenario, Moore, and co-workers confirmed that the introduction of just a single hydrogen bond within a foldamer structure was sufficient to greatly stabilize it.[40] The work compares two foldamer systems, one with hydrogen bonding and another without (Figure 12-12). The system with hydrogen bonding present was found to form a more stable helix, which showed a greater tolerance towards the helix collapsing at high selective solvent compositions.

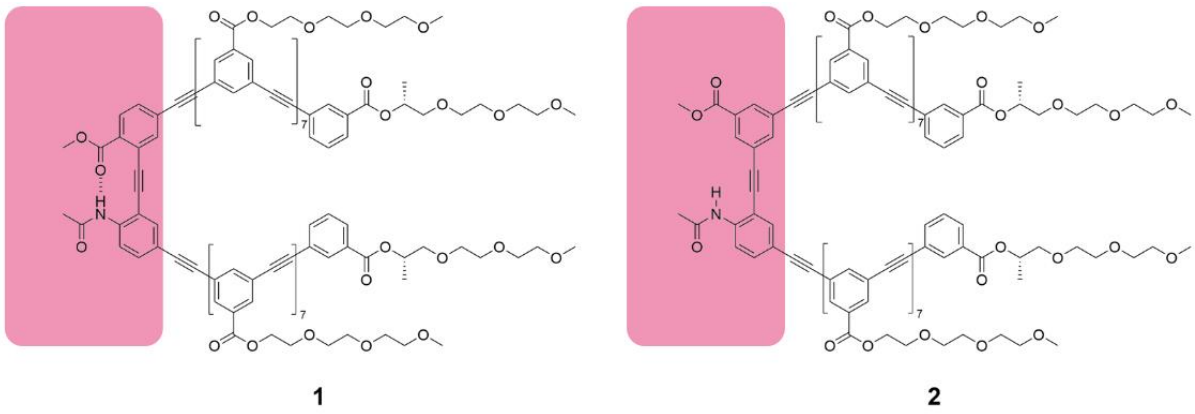

Figure 12-12: m-Phenylene ethynylene foldamers. 1) A foldamer containing a single hydrogen bond, 2) a foldamer system with no hydrogen bonds present.

A research project was thus birthed; asking the question if a foldamer system of larger proportions (as developed by Klumperman and co-workers),[4] could also be stabilized with hydrogen bonding, and if so, to what effect?

12.3 Foldamer system of interest

The research conducted builds upon the polymer backbone structure (*para*-aryl triazole motif, Figure 12-13) that was developed by Klumperman and co-workers.[4,11] Where the properties and folding characteristics of this foldamer system will be studied.

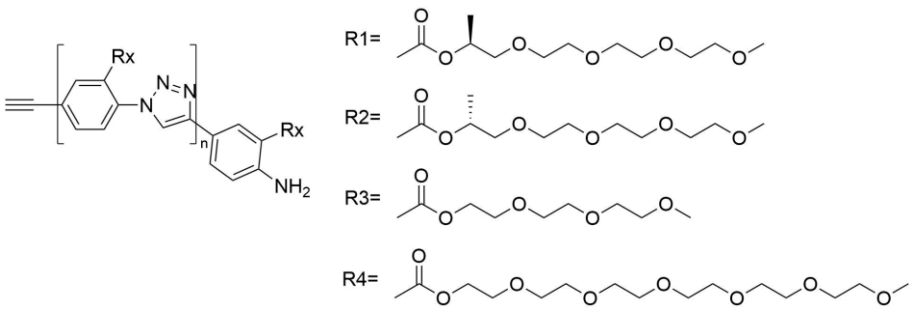

Figure 12-13:Foldamer system developed by Klumperman and coworkers.[4,11]

A foldamer system was developed which attained a highly ordered quaternary structure when in the presence of a specific ratio of water and *N*, *N*-dimethylformamide (DMF).[4] The specific ratio of water to DMF is dependent on the ratio of the hydrophilic component to the hydrophobic component of the monomeric unit of the foldamer, as well as the number and strength of the interactions between the helical strands that stabilize the higher-ordered structures.

To further enhance the applicability of this system, in stimulus-responsive applications as well as host-guest studies, a foldamer system will be developed that can form an ordered structure at higher percentage compositions of water. This is the case as DMF is both a toxic and corrosive chemical. To achieve stabilization of the higher ordered state of the foldamer system in higher contents of water, added stabilizing forces would need to be incorporated into the side chains attached to the *para*-(aryl) triazole backbone of the foldamer. The alteration would (as it falls within the hydrophilic pendant chains) stabilize the hydrophilic components of the foldamer monomeric units as it could possibly form a hydrogen bonding network within the foldamer system. This stabilization of the hydrophilic components could induce the formation of the higher-ordered state (a tight column-like helix, Figure 12-14) of the foldamer system at a higher water content.

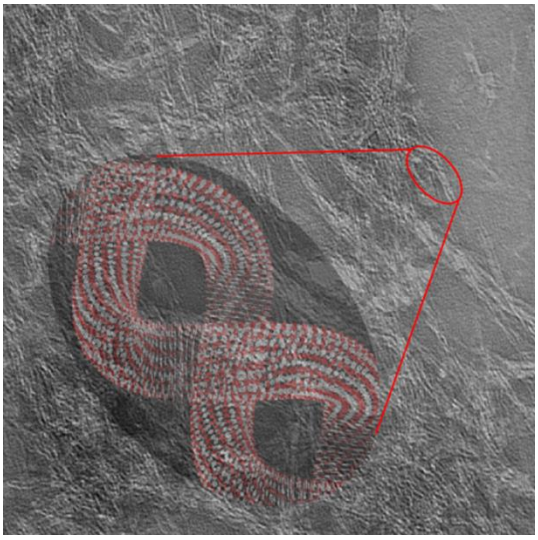

Figure 12-15: Higher ordered helical structure of the foldamer system developed by Klumperman and coworkers.[4,11] *This higher ordered structure is known as a super helix, or a helix composed of helixes. This image as taken from work by Carter et al.*[5]

Currently, the system developed by Klumperman, and co-workers lacks stabilization in the pendant chains, this results in the ordered superhelical structures collapsing and forming agglomerations (into spheres like structures thar are made of helixes) in higher water content.[5] In addition to this, it is hypothesized that the pendant chains were not large or polar enough to solubilize the polymer at high water compositions.[11] The ordering and collapsing is shown in Figure 12-15 where aggregates formed by loose strands (ordered) can be observed in Figure 12-15A where the solvent composition contains 15% water. These loose strands then form long superhelical structures in Figure 12-15B at 45% water. Finally, as stated earlier, the helixes agglomerate to form spherical structures (made of helixes) at 90% water (high water content), Figure 12-15C. This is a result of a lack of stabilization forces required for the foldamer system to maintain the ordered superhelical structure and thus it collapses. In addition, it may also be as a result of a lack of solubilization of the polymer provided by the pendant chains. The

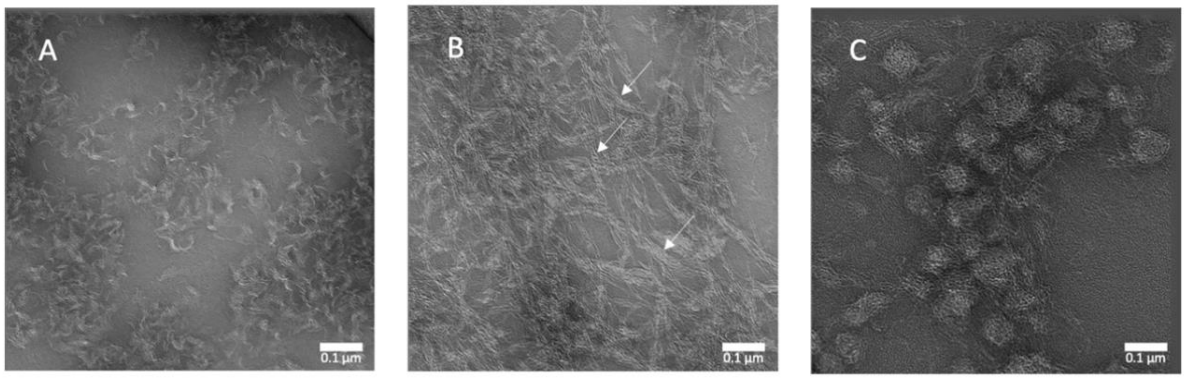

Figure 12-14: Negative stained TEM images of a foldamer system with a pendant chain of tetra(ethylene glycol) monomethyl ether. 15A is a TEM image of the foldamer system in 15% water. It should be noted that the strands are short and loose. In 15B the strands are tighter and long, this TEM image was taken at 45% water. 15C is a TEM image at 90% water, where the foldamer higher-ordered helical system has collapsed and agglomerated. This figure was taken from work by Carter et al. [5]

negative-stained TEM images belong to that of a foldamer system with pendant chains of tetra(ethylene glycol) monomethyl ether type chains.[5]

The tight helixes mentioned (Figure 12-14) are of importance as they are hypothesized to have properties similar to that of biological fibres and thus could exhibit great stress-strain properties.[3,10,119] These properties could ultimately be used to generate a stimulus-responsive hydrogel.

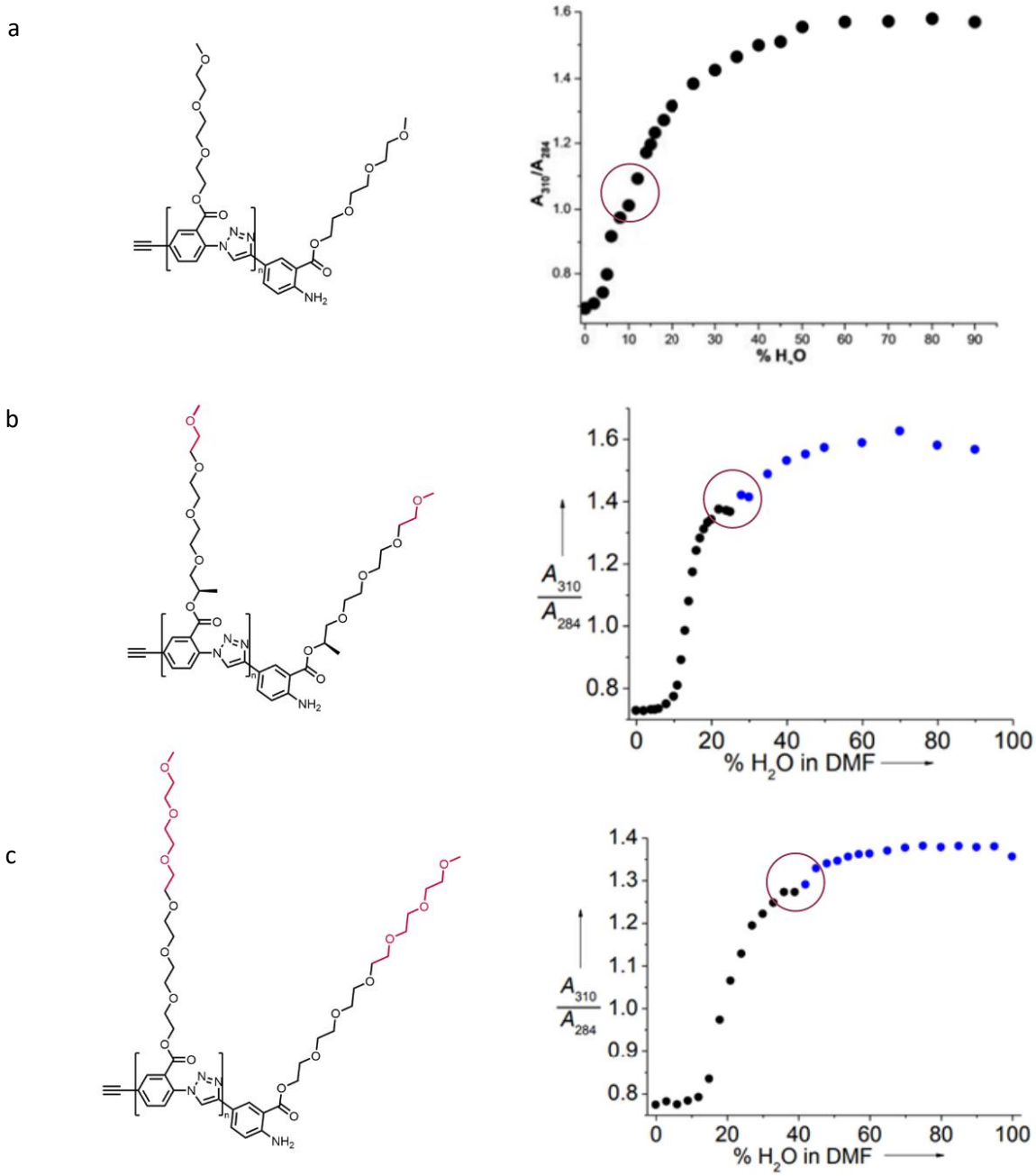

Figure 12-16: Diagrammatic representation of the impact that the size of the hydrophilic pendant group has on the folding kinetics. a) tri(ethylene glycol) monomethyl ether pendant group, b) a chiral tetra(ethylene glycol) monomethyl ether pendant group and c) hexa(ethylene glycol) monomethyl ether pendant group.

The folding kinetics could be altered in two ways, firstly *via* the alteration of the size of the hydrophilic pendant groups connected to the hydrophobic backbone structure. In doing this, one is able to fine-tune when the higher-ordering assembly occurs. A preliminary study of this has already been completed by Klumperman and co-workers and has been summarized in Figure 12-16.[4,11]

In Figure 12-16, it is important to note that as the size of the hydrophilic component in the foldamer monomeric unit increases, the occurrence of folding shifts to higher percentages of water contents mixed with DMF. Figure 12-17 describes the folding process that occurs at various compositions of water in Figure 12-16. Where above 40% water there is stacking of the helixes to form a column of helixes, a superhelix (Figure 12-14). In Figure 12-16 a-c, it is important to take note of the maroon circle which signifies the stacking of the shorter helixes into larger column-like helixes (Figure 12-17).

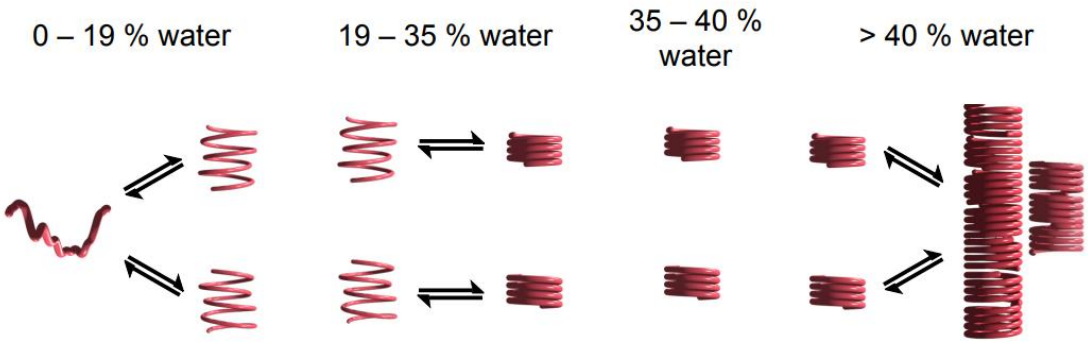

Figure 12-17: Folding kinetic of the foldamer system developed by Dr Pfukwa et al. The folding kinetic described in the figure are that of the foldamer system with a hexa(ethylene glycol) monomethyl ether pendant group. The figure was taken from work by Carter et al. [5]

It can thus be stated that as the hydrophilic pendant chain increases in length, the percentage of water required to induce folding, and the stacking of the helixes also increases. In this scenario, hexa(ethylene glycol) monomethyl ether-based monomeric units stacks at water percentages above 40% water as stated earlier. For the time being the exact folding process will be further discussed in more depth in Chapter 3. At the moment, it is sufficient to take note that the size of the hydrophilic pendant chain impacts the folding.

A second way stability can be imparted on the helix is *via* the introduction of stabilizing forces (hydrogen bonds) between the pendant chains. These stabilizing forces could stabilize the helix and thus assist the polymer in retaining its ordered form at higher contents of water as opposed to the structure collapsing at higher water content. A textbook example of said interaction is that of hydrogen bonding. If both hydrogen bond donors (HBD) and hydrogen bond acceptors (HBA) can be presented in the pendant chains, a network could be generated between the pendant groups attached within the foldamer as well as the surrounding water molecules in the environment.[10] These directional forces (hydrogen bonding) could then lock the helix in place once it forms as well as assist the helixes in stacking atop one another to ultimately form the column-like superhelix (Figure 12-14) at higher water

content.[40,120] The directional forces would also oppose the agglomeration that normally occurs at higher percentage water compositions *via* both stabilizing the superhelix as well as assisting in solubilizing the polymer/helix at higher water compositions.[5] It is hypothesized that hydrogen bonds in the pendant chains will provide stability to the foldamer system.[10]

As a result of this hypothesis, a library will be synthesized which will vary in terms of the number of hydrogen bond donors and acceptors (Figure 12-18). These hydrogen bond donors and acceptors will be introduced *via* the introduction of amide bonds as this motif is often utilized in nature.

It has been shown in the literature that the use of D-alanine-L-alanine in the pendant groups of another helical polymer (polyisocyanides) has improved the solubility of the system in water.[121] The enhancement in solubility could be accredited to the increased hydrogen bonding between one of the amino acids (that is accessible to the solvent) and the solvent in the D-alanine-L-alanine units in the pendant groups of the polymer.[10] It was also shown that this combination of alanine units had the highest amount of hydrogen bonding occurring compared to D-alanine-D-alanine or L-alanine-L-alanine or L-alanine-D-alanine.[121] The hydrogen bonding could then be utilized to stabilize the helix. Thus, taking inspiration, D-alanine-L-alanine will be added to the backbone developed by Klumperman and co-workers.[4]

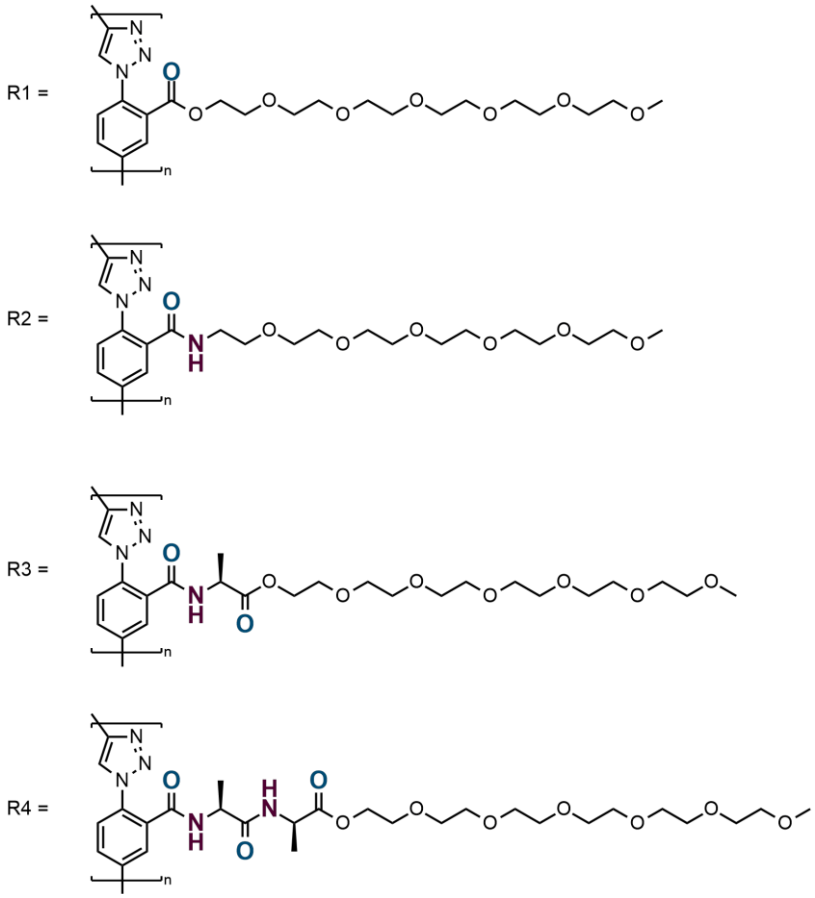

Figure 12-18: The library of foldamers to be synthesized. The foldamers range from pendant groups with no hydrogen bond acceptor and donor sites (R1), one hydrogen bond acceptor and one hydrogen bond donor (R2 and R3) and two hydrogen acceptor and donor sites(R4). Hydrogen bond donors are in red, and the hydrogen bond acceptors are in blue.

13 Chapter 3 – Computation, synthesis, and characterization of *para*-aryl triazole foldamer library

13.1 Computation

A library of foldamer systems with varying degrees of hydrogen bonding was synthesized (Figure 13-1).

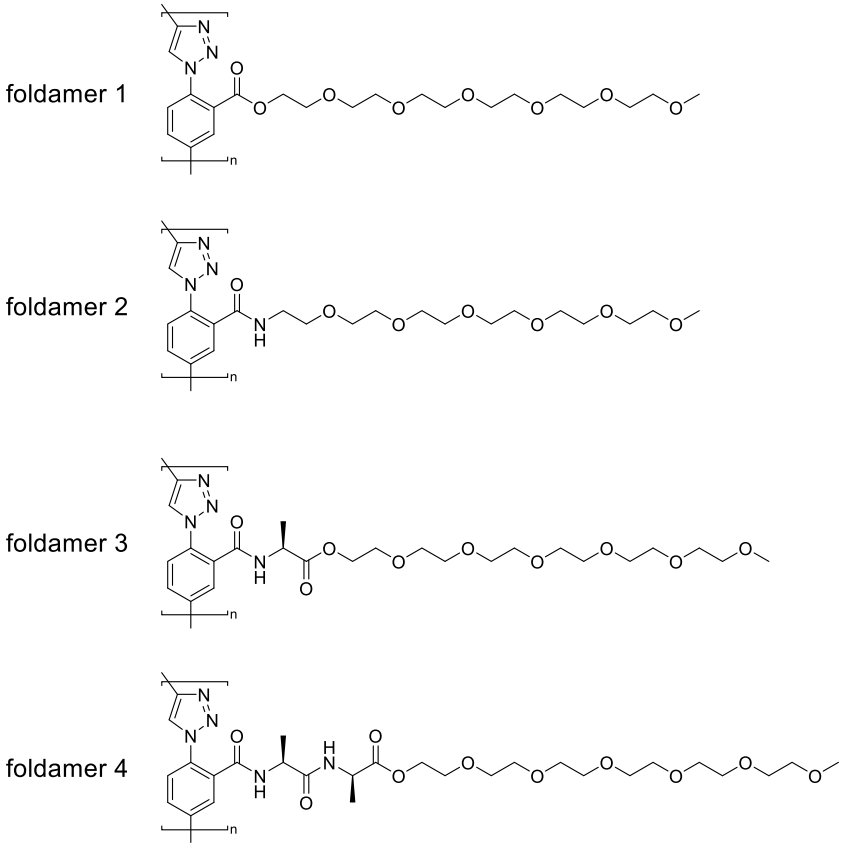

*Figure 13-1: Library of foldamer systems to be synthesized. Where foldamer **1** contains no hydrogen bond donors or acceptors. Foldamer **2** contains one hydrogen bond donor and one acceptor. Foldamer **3** contains two hydrogen bond acceptors and one hydrogen bond donor and foldamer **4** contains three hydrogen bond acceptors and two hydrogen bond donors.*

The library of foldamers is hypothesized to have increasing degrees of hydrogen bonding present (from foldamer **1** to foldamer **4**) within the resulting foldamer three-dimensional ordered structures, as well as with the surrounding solvent. These hydrogen bond interactions are hypothesized to stabilize the helical structure of the foldamer in water. This hypothesis was preliminarily investigated *in silico via* computational means in the Material Science program from the Schrodinger Suite. A workflow was developed whereby a foldamer structure was generated and thereafter subjected to molecular dynamic calculations (Figure 13-2).

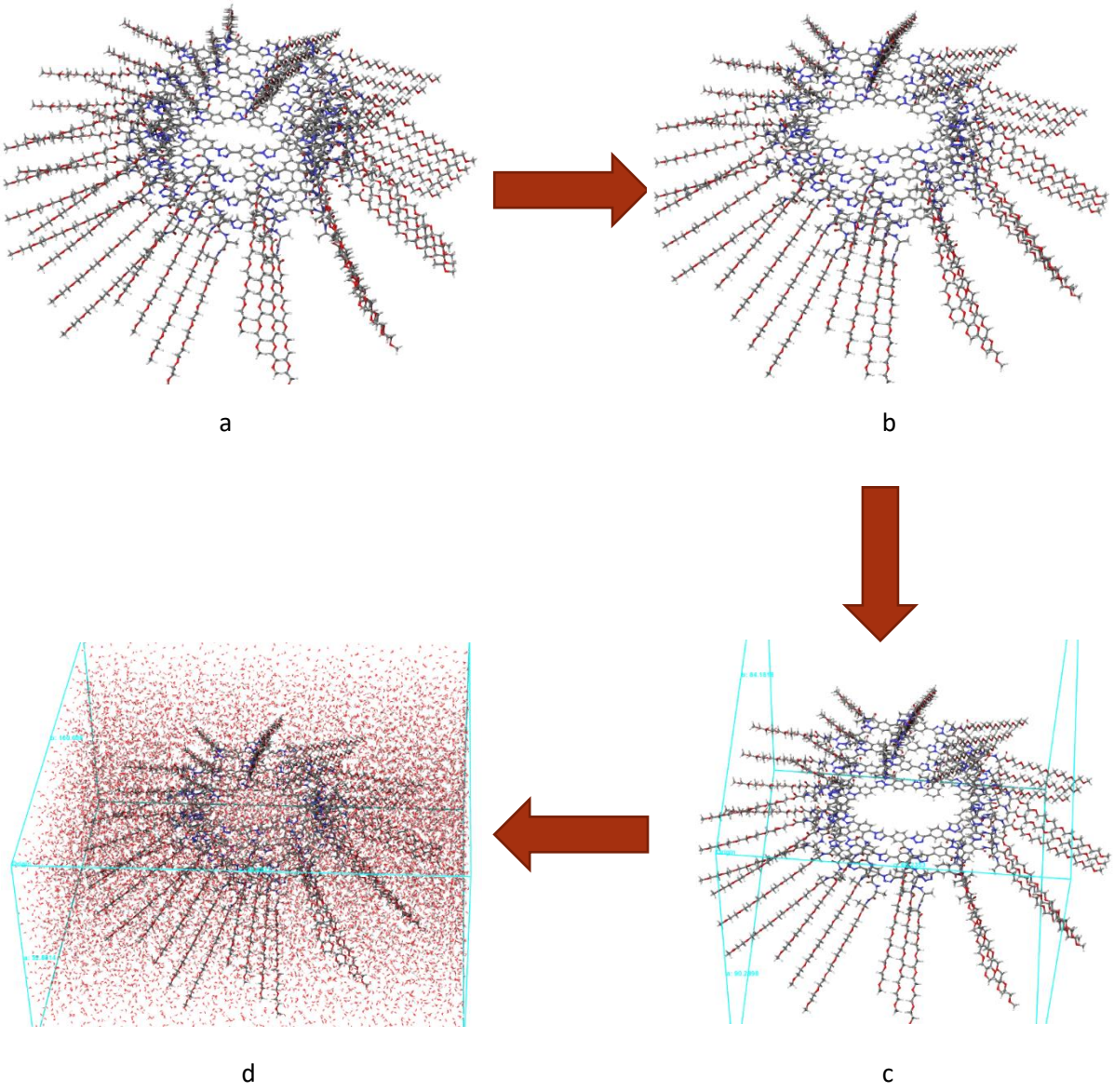

Figure 13-2:General workflow for the computation of the foldamer systems. a) The foldamer was generated in Material Science with 50 repeat units. b) The foldamer system was shortened to 40 repeat units. c) It was thereafter minimized according to the OPLS4 forcefield. d) The foldamer was finally surrounded with water (TIP4P solvent model) in a box according to the OPLS4 forcefield. The output of this program was then subjected to a molecular dynamic's workflow with Brownian minimization and molecular dynamics.

These simulations could act as tentative models of the system to offer some idea as to the possible impact of the inclusion of hydrogen bonding within the system as indicated. These representations should be and have been viewed with great diffidence as they are not completely accurate depictions of the system. In reality, the foldamer system often packs into large helical coils (a helix of helixes) which consist of hundreds to thousands of repeat units.[5] This could not be replicated perfectly *in silico* as this would computationally be too expensive. Instead, 40 repeat units were generated *in silico* and modelled to hint toward a theme/trend that may be observed later, experimentally. This model also does not consider the actual folding process, but instead only looks at the impact of hydrogen bonding on the foldamer system once it has successfully folded in pure water. The model was generated by making a 50-repeat unit foldamer and shortening it from its original 50 units to 40 repeat units as the end units

often started to fold on themselves and create odd discrepancies within the bulk helical structure. It was possible to remove these end units as the aim of the model was towards modelling the impact of hydrogen bonding on the internal structure of the helix and not to model the end-capping points of the helix. Thus, a uniform helical structure was generated in this manner.

In this method, OPLS4 was selected as the forcefield of choice regarding implicit solvation energy minimization calculations as it offers the latest improvements on the popular OPLS3e forcefield.[122] In addition, the TIP4P (water) solvent model was selected as the explicit solvation model as it offered a high level of computational accuracy without being the most computationally expensive model.[123] Further details on the exact computational procedure followed can be found in the supplementary information.

The output of said molecular dynamics simulation resulted in the below final output images.

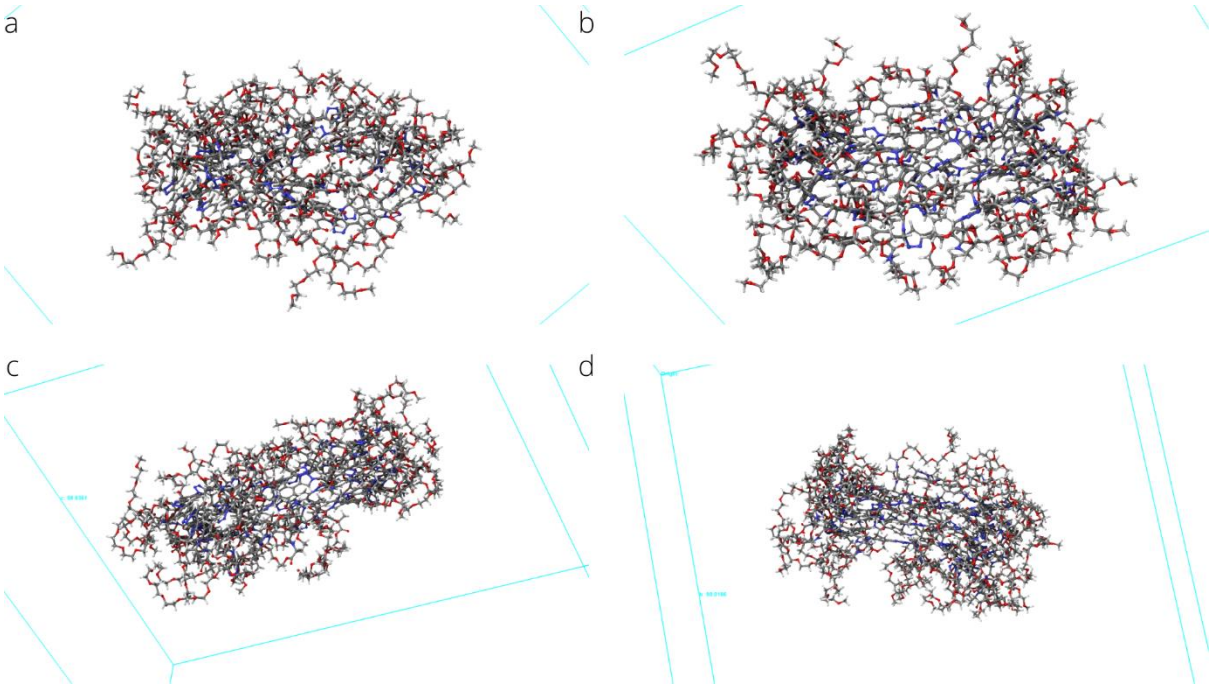

*Figure 13-3: Comparative images of the side profile of the foldamer systems. a) foldamer **1**; b) foldamer **2**; c) foldamer **3**; d) foldamer **4**.*

In Figure 13-3 it is important to note that as the number of hydrogen bond donors and acceptors increases from Figure 13-3a to Figure 13-3d, no added ordering of the ethylene glycol side chains takes place. Instead in each case, there are large amounts of disorder present in the pendant groups. In contrast to Figure 13-3, where no observable stabilization was provided *via* hydrogen bonding. In Figure 13-4 it can be noted that Figure 13-4b-Figure 13-4d has definite helical structures with an open cavity present in its structure. In contrast to this, Figure 13-4a seems to be in the process of collapsing in on itself. It was attempted to simulate for a longer simulation time, but this was not successfully achieved due to the calculation timed out on the CHPC server. The collapse, although not conclusively proved *via* longer simulation times, agrees with what has been observed with TEM and Cryo-TEM analysis in previous

work by Klumperman and co-workers.[4,5] It was proved that in nearly pure water compositions (80% – 100%), foldamer system 1 agglomerates. If it were possible to have longer simulation times, foldamer system 1 would likely collapse. In contrast to foldamer **1**, foldamers **2** - **4** show little to no signs of collapsing although longer simulation times would be needed to confirm this hypothesis.

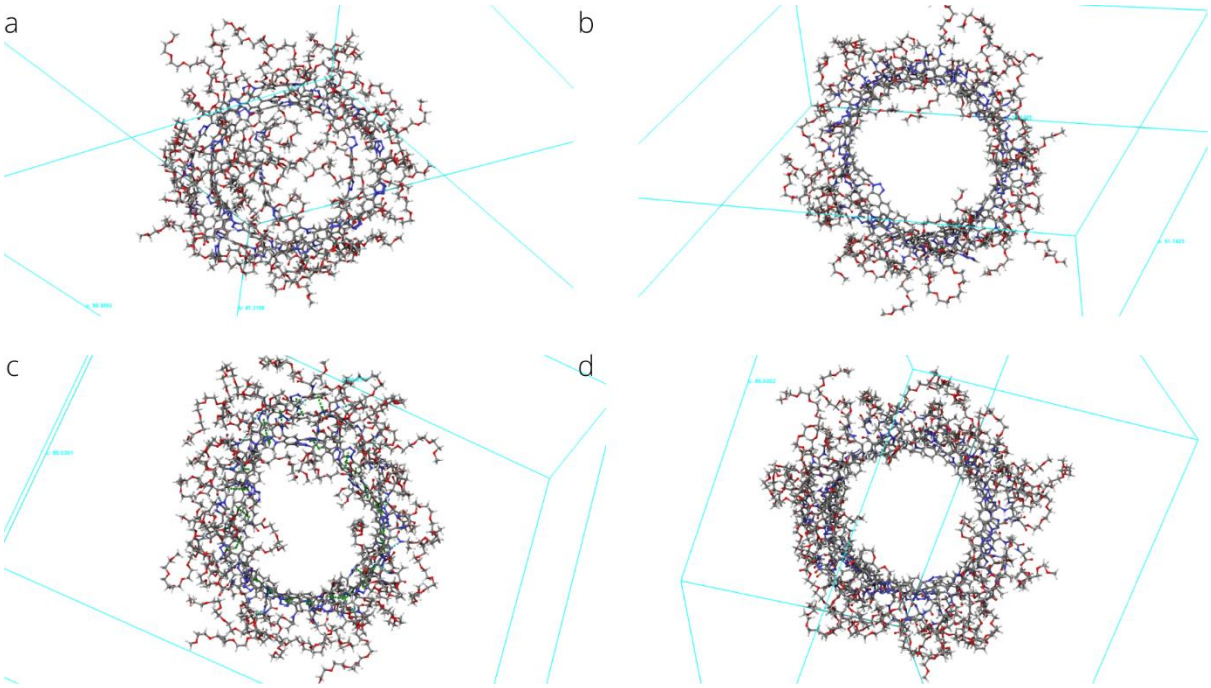

*Figure 13-4: Comparative image of the top-down profile of the foldamer systems. a) foldamer **1**; b) foldamer **2**; c) foldamer **3**; d) foldamer **4**.*

During this molecular dynamic simulation, it is possible to track several properties over time. One such property is the RMSD (root-mean-square deviation) of the atomic coordinates over time. This value is used to determine when the system has reached a state of equilibrium.[124] When inspecting large systems, a low RMSD value with little to no fluctuations is ideal. When the RMSD has equilibrated, it is possible to state that the system is in equilibrium and that the data from where the data has plateaued is more reliable than where there are large fluctuations in the RMSD. In Figure 13-5 the reference frame is taken as the final frame in the simulation and the RMSD reaches a plateau at roughly 20 ns. Because of this plateau, the data from 20 ns onwards can be considered more reliable than from 0 ns to 19 ns and the analysis of data to follow has been taken from the period of 20 ns – 100 ns. The zoomed/focused in area of Figure 13-5 depicts the data for the RMSD from 20 ns to 100 ns. These RMSD values are lower and vary minimally from the final frame in terms of variation. The data to follow is the summary of the output of data from this time range.

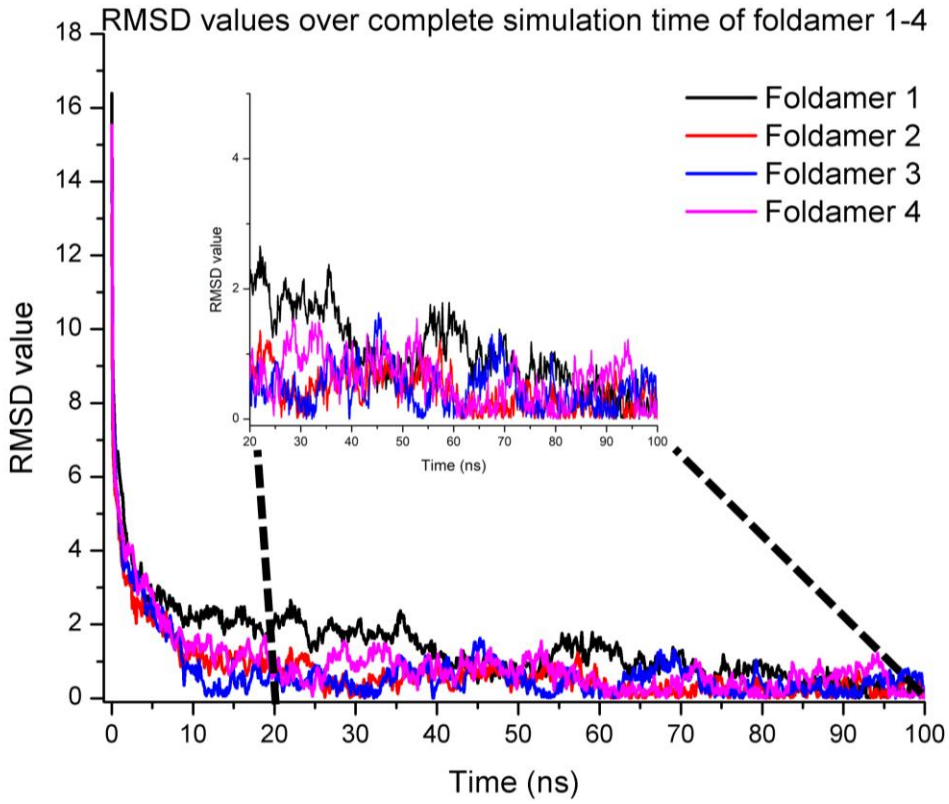

*Figure 13-5: RMSD value of molecular dynamics simulation over time of foldamer **1** - **4**. Note that the final frame is taken as the reference frame to calculate the RMSD values. A focus area is highlighted values between 20 ns to 100 ns of foldamer **1** - **4**.*

In this time range, it was possible to track the number of π-π stacking interactions, intramolecular hydrogen bonding interactions, and the average distance between helical turns. The output of this data is summarized in Figure 13-6. Utilizing the trends from Figure 13-6, a few deductions could be tentatively made about the system and the effect of introducing hydrogen bonds into the foldamer system. Firstly, from Figure 13-6a, it can be cautiously stated that all donors and acceptors that are introduced into the system will be involved in stabilizing it. Therefore, the distance of the hydrogen donors and acceptors (HBDA) from the aromatic backbone of the helix does not impact the HBDA's ability to provide stability to the foldamer system.

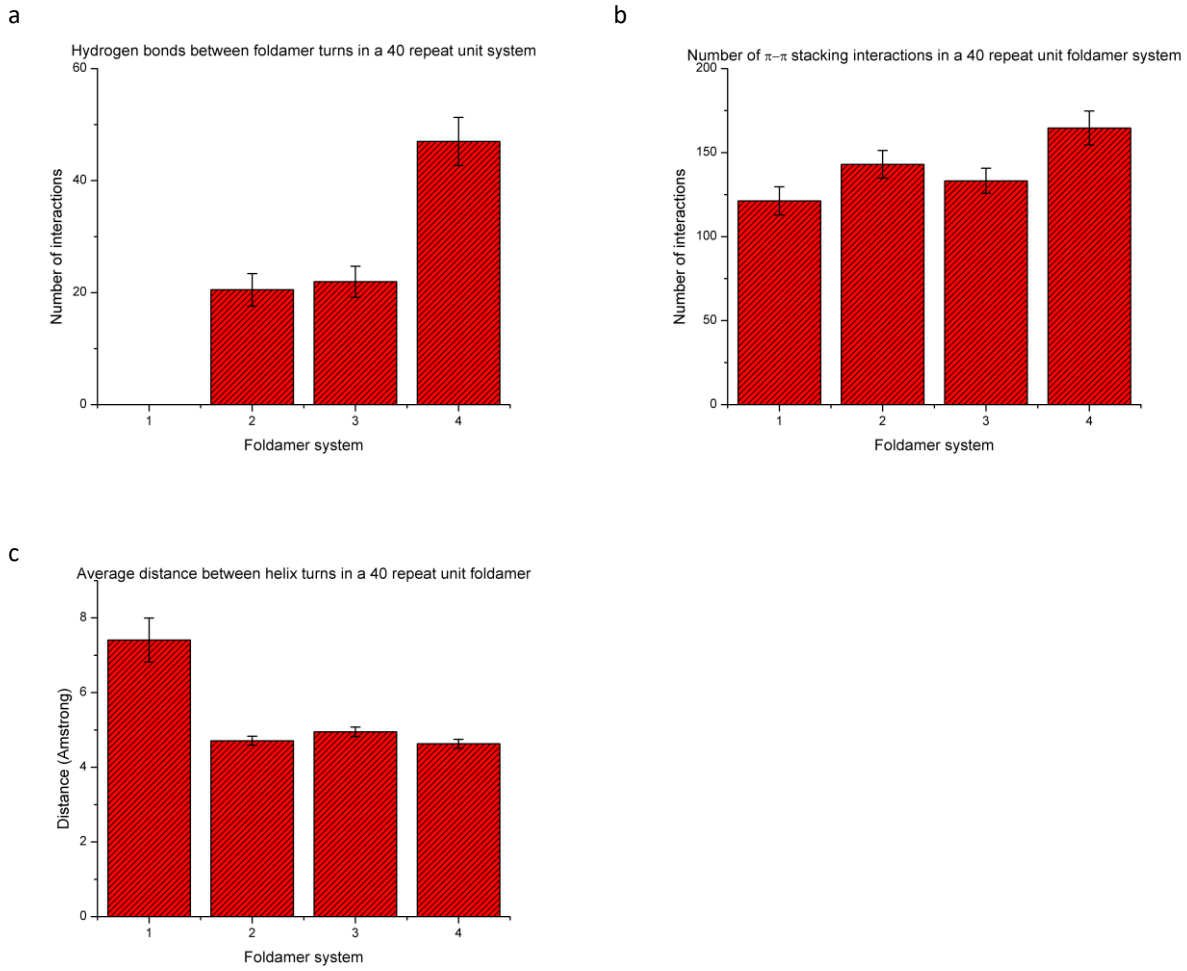

*Figure 13-6: Summary of data from molecular dynamics simulations of foldamers **1** - **4**. a) The number of hydrogen bonds within the foldamer system; b) the number of π-π stacking occurring within the foldamer system; c) the average distance (Å) between turns of the helix foldamer system.*

The output of the molecular dynamics calculation in Figure 13-6a alludes to the independence of the strength of the hydrogen bonding based on the distance of the functional groups from the aromatic ring as foldamer **4** in Figure 13-6a has close to double the number of hydrogen bonds present *in silico* to that of foldamer **2** and **3**. This matches that of the monomeric structures where foldamer **4** has twice as many HBDA as foldamers **2** and **3**. As a control, foldamer **1** which should not have internal hydrogen bonds, does not have any. In Figure 13-6b, it is depicted that the number of π-π stacking increases as the number of HBDA is increased within the system, this agrees with the results of Figure 13-6a. As the number of hydrogen bonds increases between the turns of the helix, the helix turns are pulled closer to one another, thus the number of π -π stacking interactions increases. This process could be described in Figure 13-7, which is a representation of what was often observed in the output of the simulations where hydrogen bonding occurs. It can be cautiously stated that as the number of HBDA increases so the extent of this effect increases where the helix 'tightens' and so the helix becomes more compact and the predominant 5 π - 5 π stacking and 6 π – 6 π stacking becomes predominantly 5 π - 6 π stacking.

Note that foldamer **1** has the least π -π stacking interactions present, this is most probably because of its disorderly glomeration process which it undergoes under high water content,[4,5] which results in limited ordered stacking (this is also evident from Figure 13-4a). Foldamer **1** would also have the least π -π stacking interactions because its helix turns to be the furthest apart as there is no added stabilization from hydrogen bonding present between the turns of the helix (as indicated in Figure 13-6a). Figure 13-6c further supports the proposed hypothesis that hydrogen bonding tightens the helix, as the distance between the helix turns decreases as the amount of HBDA increases in the system. Thus, the added hydrogen bonding tentatively shows to provide added stability to a helix structure as well as a tightening or compacting effect on the helical structure.

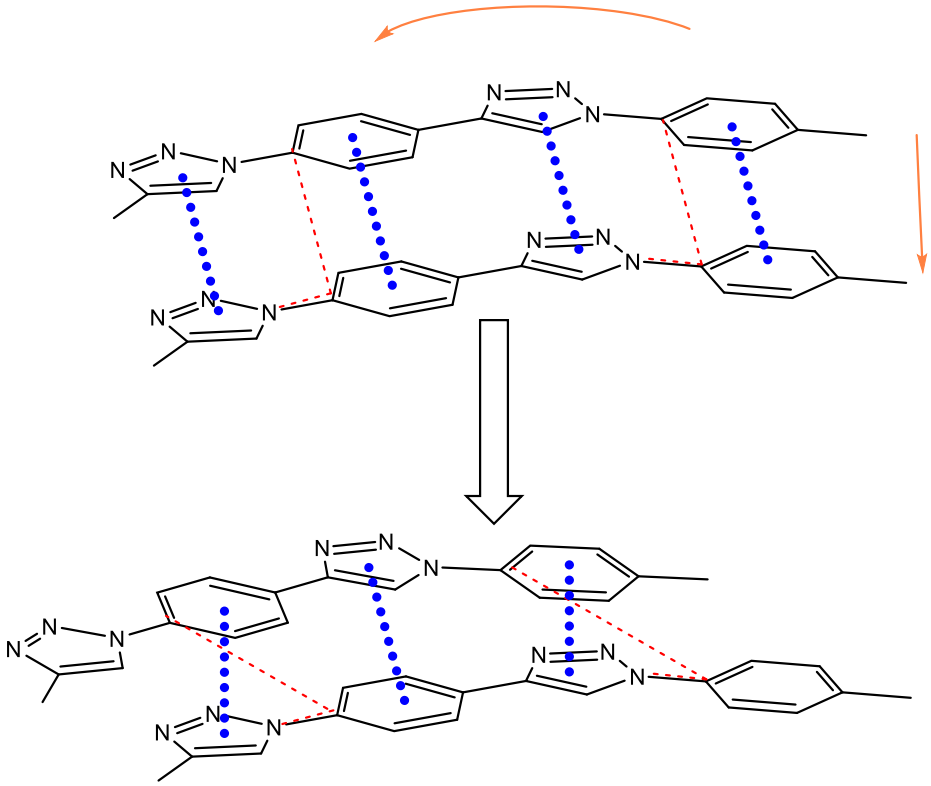

Figure 13-7: Observed in silico tightening effect that forms as a result of hydrogen bonding within the system. Where the effect becomes more pronounced as the number of HBDA increases within the foldamer system.

As there was sufficient *in silico* evidence which hinted toward the stability that may be provided by the incorporation of HBDA within the foldamer structure, the effects of hydrogen bonding on the foldamer system were investigated experimentally. As noted earlier the foldamers are comprised of monomers that have varying degrees of hydrogen bonding. Initially, the different pendant chains were synthesized, pendant chains R1 – R4 (Scheme 1). R1 was synthesized and used as a precursor to synthesize the remaining pendant chains. Once all the pendant chains were synthesized, the chains were coupled to an azido functionalized aromatic ring (c to d, Scheme 1) that would act as the backbone structure for the polymer. The aromatic ring was thereafter functionalized with an alkyne *para* relative to the azide

functional group (e, Scheme 1). This completed the monomer synthesis and thereafter the monomeric units would be polymerized *via* a 1,4- cycloaddition reaction.

13.2 Synthesis and characterization

The first hurdle presented in this project was that of the synthesis of hexa(ethylene glycol) monomethyl ether. Although this was conducted in previous work in our laboratory,[4] as well as in other laboratories,[30] it was found that the method utilized did not hold a lot of space for the synthesis of varying length oligomers. It was also found that the method produced several side-products. The side-products could be removed *via* column chromatography, but in so doing the yield would decrease dramatically (i.e., by 30 %). As a result, a new method was identified and adapted.[125] This new method was modified for the synthesis of ethylene glycol monomethyl ether oligomers as opposed to ethyl glycol oligomers.

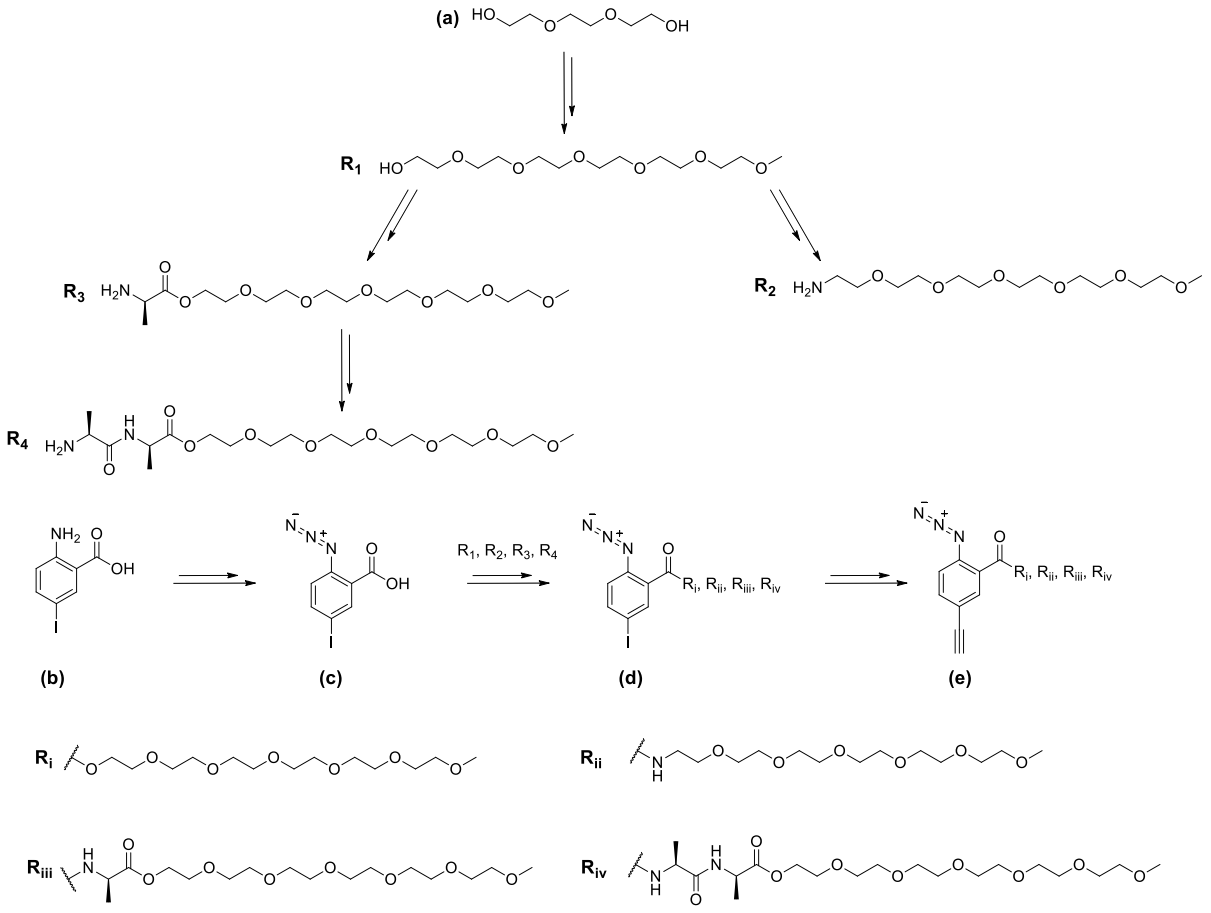

Scheme 1: General outline of monomer synthesis followed in this research project.

This method proves to be more beneficial as it allows for the synthesis of controlled length oligomers on a multigram scale (as far as a 25 g scale). [125] It is also ideal in that it does not rely on column chromatography, but instead makes use of conditions or reagents where minimal purification is needed. Where the procedure does produce side products, these products do not interfere with later synthetic steps. These side products can then be easily isolated after further reactions with column chromatography where the loss of the desired product on the silica column is not possible.

Firstly a protecting group is added to one of the alcohol groups on the tri(ethylene glycol) molecule. The addition of two trityl groups *via* addition to both alcohol groups is possible. This is avoided *via* the excess addition of tri(ethylene glycol).[125] Following the reaction, a workup is conducted (a wash with water and then brine, exact quantities in the experimental section) and the product, mono-tritylated product (compound **2**, Scheme 2), is isolated with little of the di-tritylated product.[125] This was confirmed *via* ^{1}H NMR spectroscopy with the appearance of ethylene glycol proton backbone signals between 3.67 ppm and 3.15 ppm (Figure 16-1). Mono-tritylation was further confirmed with the appearance of a singlet signal representing the OH signal in the ^{1}H NMR spectrum at 2.25 ppm, as per what is observed in the literature.[125]

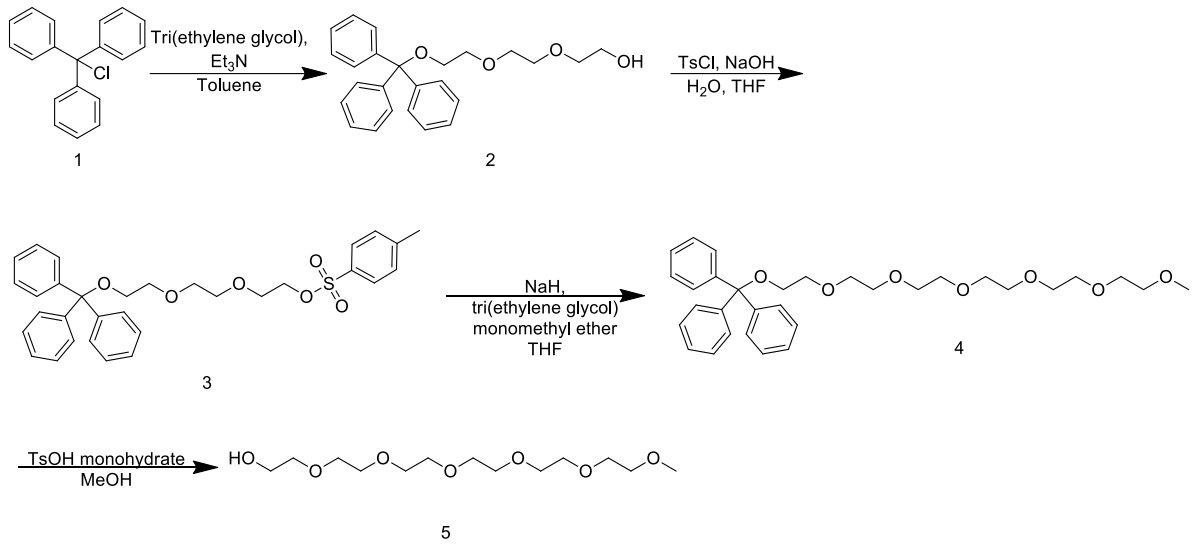

Scheme 2: Synthetic method to afford hexa(ethylene glycol) monomethyl ether.

This protecting group that has been added plays a pivotal role in the synthesis of controlled oligomer length. It limits the number of active functional groups in the tri(ethylene glycol) molecule, and thus in the next step where a tosylation reaction occurs, only a single oxygen atom can be tosylated. This is in contrast with the previous method,[4,30] where tosylation could occur on both alcohol groups (due to a lack of mono-protection) and thus longer oligomers would form as a by-product (Scheme 3). This was confirmed with ^{1}H NMR spectroscopy where the disappearance of the OH signal at 2.25 ppm was observed as well as the appearance of aromatic signals of the tosyl group which appeared between 7.71 ppm to 7.18 ppm (Figure 16-3).

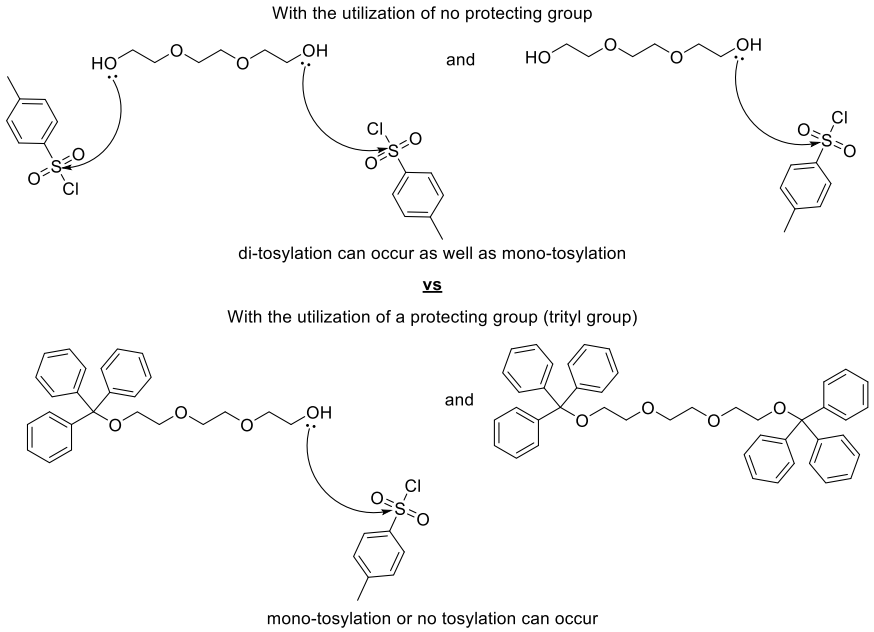

Scheme 3:The comparison of synthetic robustness of the previously utilized method(top); the newly identified method (bottom).

Compound **3**, the mono-tosylated product, was then reacted with tri(ethylene glycol) monomethyl ether under basic conditions. Only a single monomethyl ether is added *via* a substitution type reaction to afford compound **4**, which is the protected version of hexa(ethylene glycol) monomethyl ether. ^{1}H NMR spectroscopy was again utilized to confirm product formation with the disappearance of the aromatic proton signals from the tosyl group, as well as an increase in the integration value of the protons for the ethylene glycol backbone (Figure 16-5). Compound **4** was then deprotected under acidic conditions to afford the desired product, hexa(ethylene glycol) monomethyl ether (compound **5**, Scheme 2). This product was shown to be relatively pure (according to the mass spectrum) and could be utilized further without the need for any purification (Figure 13-8). ^{1}H NMR spectroscopy was utilized as further confirmation that the reaction had occurred with the disappearance of the aromatic signals of the trityl group of the starting material and the appearance of the now free OH group at 3.44 ppm (Figure 16-7) being important aspects of the spectrum. It is possible to see residual unbound trityl group present with this compound as column chromatography was not utilized to purify the final product.

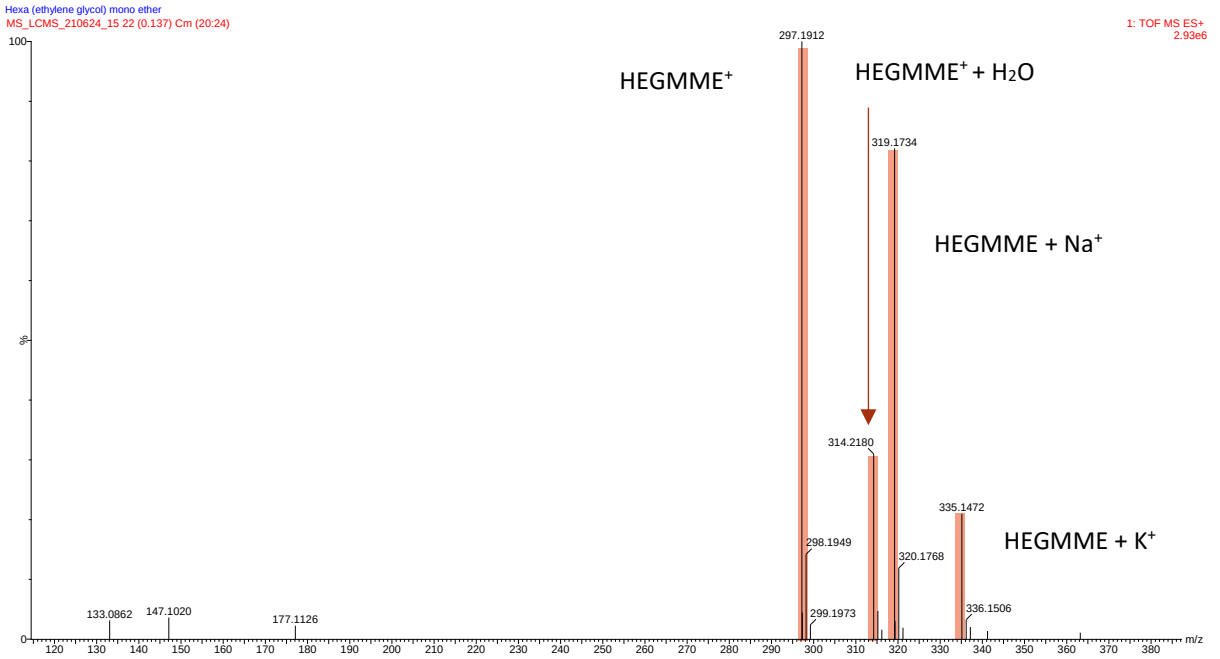

Figure 13-8: Mass spectrum of chromatography-free large scale hexa(ethylene glycol) monomethyl ether synthesis (25 g scale).

The described procedure that has been adapted from the literature,[125] can be further modified to afford any oligo(ethylene glycol) monomethyl ether oligomer length (Scheme 4).

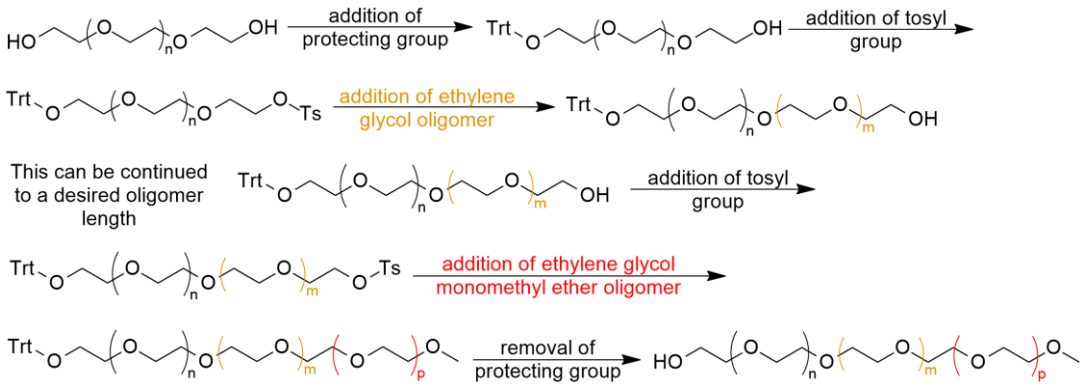

Scheme 4:General procedure for the synthesis of a particular ethylene glycol monomethyl ether oligomer chain length.

Following the successful synthesis of pendant group R1, the synthesis of the next pendant group (R2) could begin *via* another procedure identified in the literature.[126] This took place *via* the tosylation of the recently synthesized compound **5** to afford compound **6** (Scheme 5). This product was confirmed with ^{1}H NMR spectroscopy by the appearance of the aromatic signals of the tosyl group between 7.79 ppm and 7.33 ppm, as well as the disappearance of the alcohol groups signal at 3.44 ppm (Figure 16-10).

Thereafter a substitution type reaction could be conducted where sodium azide acted as the nucleophile under basic conditions to afford compound **7** (Scheme 5). Compound **7** could thereafter be purified *via* column chromatography and any impurities from the synthesis of the compound could be removed. The structure of this product was confirmed *via* a combination of NMR and FTIR spectroscopy. In the ^{13}C

NMR spectrum it was possible to confirm product formation based on a signal at 50.82 ppm which is indicative of the carbon atom connected to the azide functional group (Figure 16-13).[126] The FTIR spectrum provided further proof that the azide group had been added to the molecule with the appearance of the signal at 2099 cm^{-1}, which is a signal unique to azide functional groups (Figure 16-14).

A pure compound **7** could thereafter be reduced *via* palladium on carbon in a hydrogen atmosphere to afford the product in quantitative yield. The product could be easily isolated *via* filtration through Celite and without the need for purification *via* column chromatography. Column chromatography is also avoided at this step as it greatly reduces the yield (by about 20%). This is because of the product being retained on the column and therefore not eluting easily. This final reaction affords the desired pendant group R2 (compound **8**, Scheme 5). Product formation was confirmed *via* NMR spectroscopy and FTIR spectroscopy. Where in the ^{1}H NMR spectrum, the appearance of a singlet signal representing the primary amine group at 1.91 ppm was observed (Figure 16-16). In the ^{13}C NMR spectrum, it was possible to identify that all the azide groups had been converted into primary amines with the disappearance of the signal of 50.82 ppm and the appearance of a signal at 41.73 ppm which is indicative of the carbon atom connected to the primary amine (Figure 16-17).[125] It is also possible in the FTIR spectrum to see that the azide signal had completed disappeared and a signal between 3600 cm^{-1} to 3300 cm^{-1} representing a primary amine was now evident (Figure 16-18).

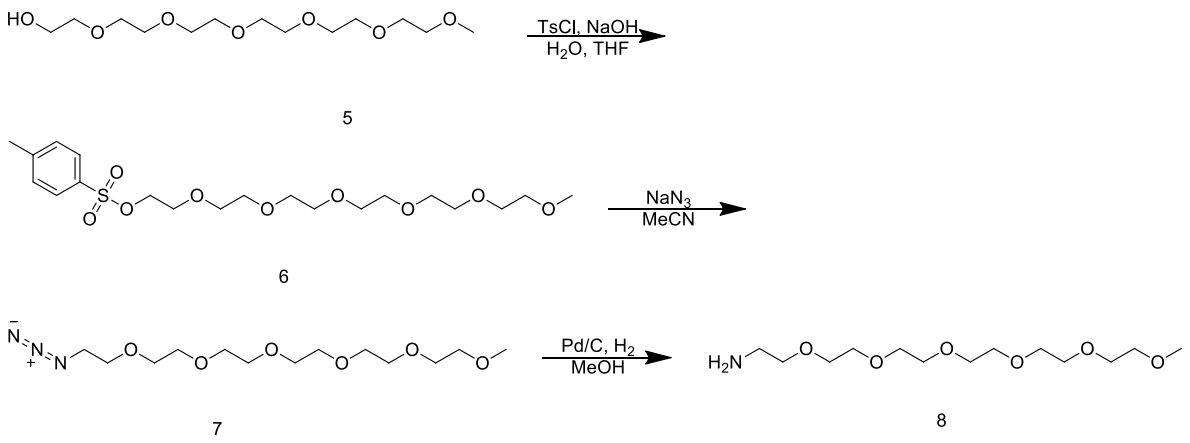

Scheme 5:Synthetic method to afford pendant group R2.

This method proves to be synthetically simpler in contrast to the more common method that makes use of PPh_3 as a reducing agent to conduct a Staudinger reduction. This is because this reaction produces triphenylphosphine oxide (TPPO), which is extremely difficult to remove from ethylene glycol and other reagents, (whole papers have been dedicated to the removal of such a side-product).[127,128] Instead this approach avoids this problem altogether, although being more expensive. The conversion of the azide to the amine is nicely illustrated *via* FTIR spectroscopy (Figure 13-9) where it is possible to see the removal of the azide signal at 2099 cm^{-1} and the appearance of the primary amine signal between 3600 cm^{-1} to 3300 cm^{-1}.

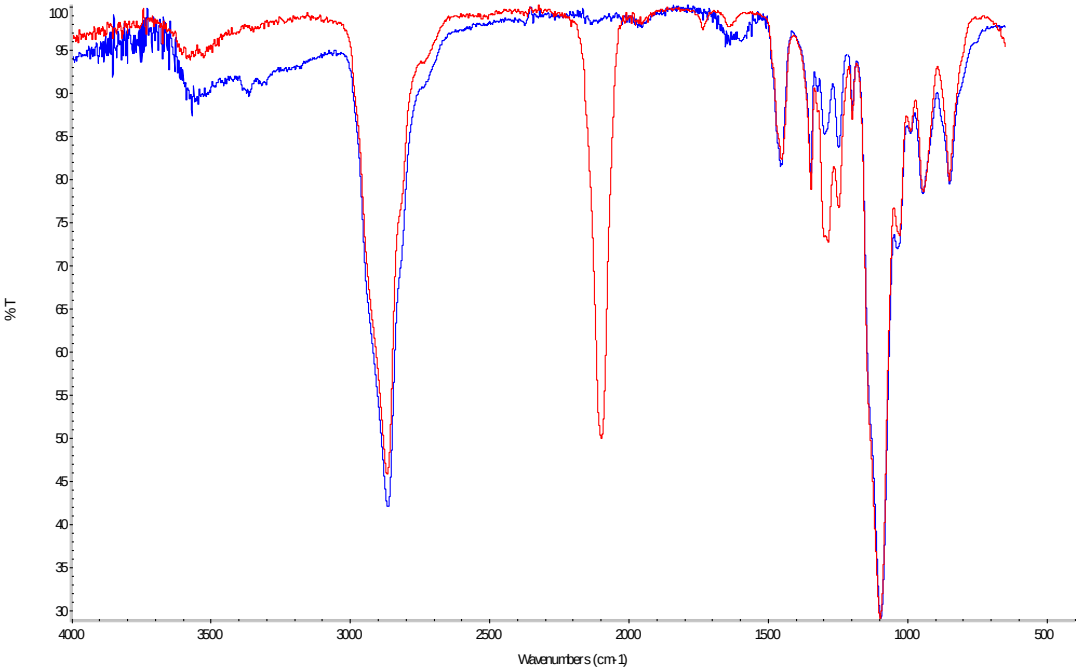

Figure 13-9: Fourier-transform infrared spectra of hexa(ethylene glycol) mono methylether with an azide end group (red) and with an amine end group (blue).

In addition, a mass spectrum was acquired from the final pendant group R2. This further confirms that R2 has been successfully synthesized (Figure 13-10).

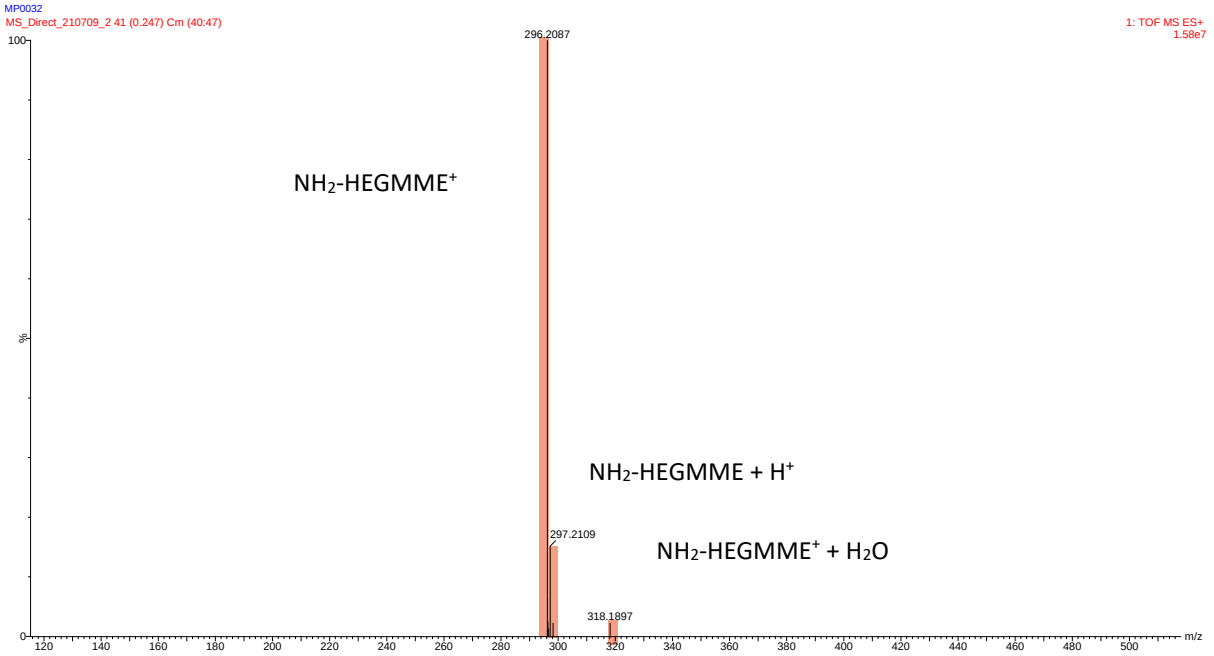

Figure 13-10: Mass spectrum of pendant group R2.

Thereafter pendant group R3 was synthesized *via* the procedure (Scheme 6).[129] In this approach, hexa(ethylene glycol) monomethyl ether (pendant group R1) was coupled to N-Boc-L-alanine and purified *via* column chromatography to afford compound **9**. Product formation was confirmed by the appearance of a singlet and a doublet in the ^{1}H NMR spectrum representing the $(CH_3)_3$ groups of the added Boc group at 1.40 ppm and the CH_3 at 1.35 ppm of the alanine methyl group respectively (Figure 16-20). FTIR spectroscopy also proved the formation of a secondary amide bond with a signal appearing at 1711 cm^{-1} (Figure 16-22). The final proof of product formation was by the inspection of the mass spectrum where the product is shown to be present with a molecular mass of 468.28 *m/z*, (calculated 468.27 for [M + H^{+}]) (Figure 16-23).

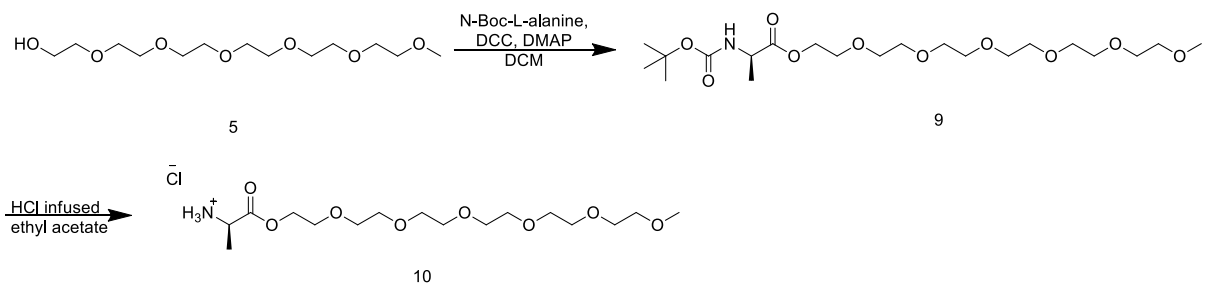

*Scheme 6: Synthetic scheme for the formation of compound **10**, R3.*

Thereafter the Boc protecting group was removed *via* an acid-mediated deprotection step without further purification to afford compound **10** (Scheme 6).[129] Compound **10** was confirmed to be obtained as an impure mixture as shown with the utilization of ^{1}H NMR spectroscopy which indicated the emergence of a singlet representing the three protons on the now deprotected amine at ~8.5 ppm (Figure 16-24). Additionally, mass spectrometry provided further proof with the appearance of the molecular ion at 368.23 *m/z*, (calculated 368.22 for [M + H^{+}]), and little to none of the molecular ion of compound being **9** present (Figure 13-11, and Figure 16-26).

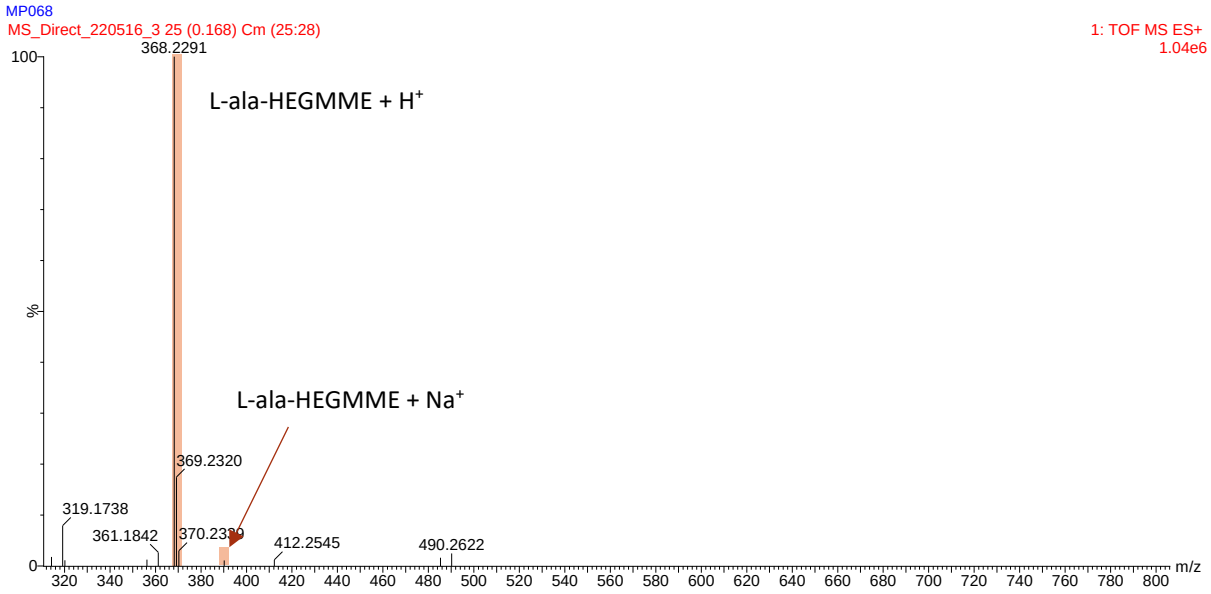

*Figure 13-11:Mass spectrum of compound **10**.*

The final pendant chain (pendant chain R4) was thereafter synthesized utilizing compound **10**, where compound **10** underwent another coupling reaction with *N*-Boc-D-alanine (Scheme 7). This crude compound was then purified *via* column chromatography to afford a pure compound **11**. This was confirmed with NMR spectroscopy, where in the ^{1}H NMR spectrum there is an appearance of the Boc $(CH_3)_3$ singlet at 1.44 ppm and there are two doublets present at 1.41 ppm and 1.34 ppm which are indicative of the two CH_3 groups of the two alanine methyl groups within compound **11** (Figure 16-27).[129]

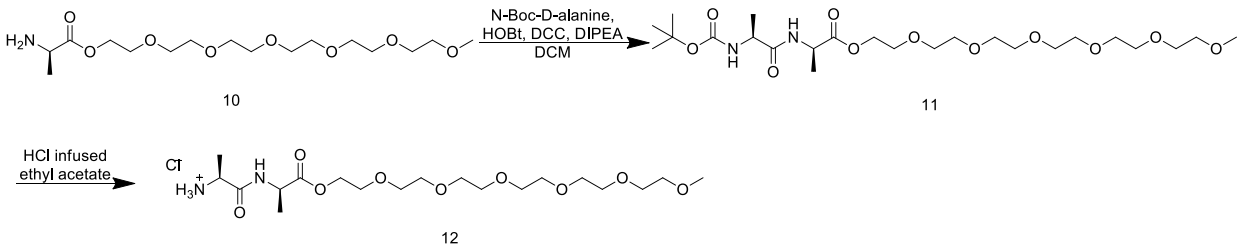

*Scheme 7: Formation of compound **12**.*

Compound **11** was then deprotected under acidic conditions to afford compound **12** and utilized later in the procedure without column purification.[129] This synthetic step was confirmed with ^{1}H NMR

spectroscopy, with the appearance of a singlet at ~ 7.7 ppm which integrates for three protons which is indicative of the deprotected primary amine group (Figure 16-29). In addition to this mass spectroscopy was utilized to confirm product formation with the molecular ion present at 439.27 m/z (calculated 439.64 for [M + H^+]), (Figure 13-12, and Figure 16-31) with little to none of the protected compound **11** present.

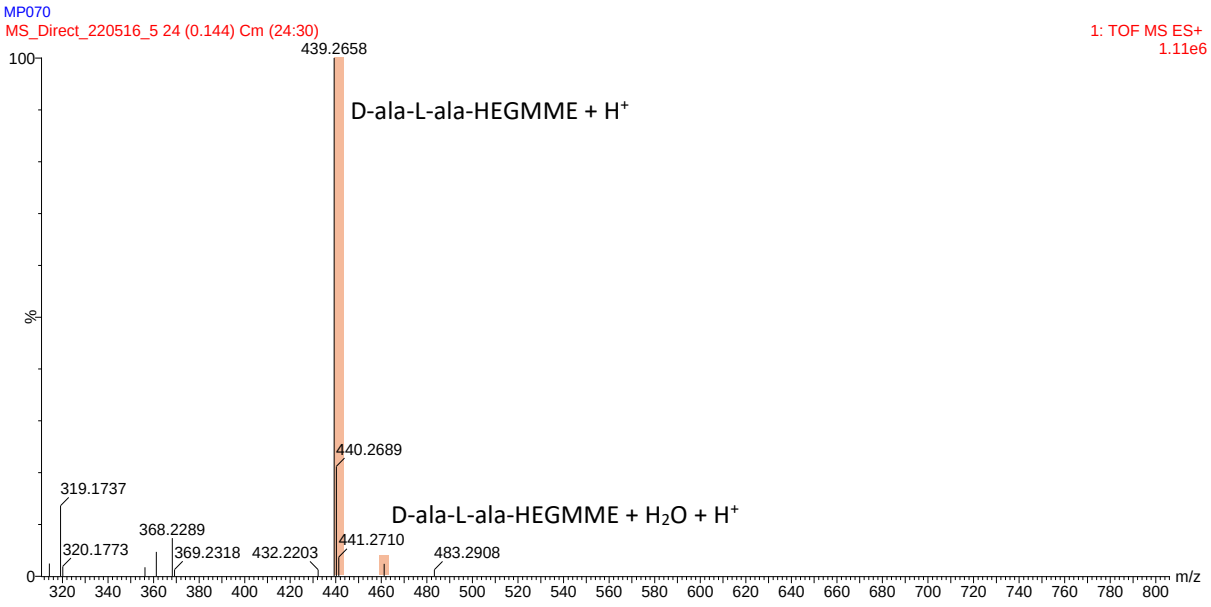

*Figure 13-12: Mass spectrum of compound **12**.*

As all the pendant chains were successfully synthesized, these pendant groups R1 (compound **5**), R2 (compound **8**), R3 (compound **10**), and R4 (compound **12**) could then be coupled to the azide functionalized aromatic backbone (compound **14**). Compound **14** was afforded by the conversion of an amine functional group to azide functionality *via* a method utilized by Klumperman and co-workers,[4] and was also upscaled to a 5.0 g reaction scale. Product formation was confirmed by ^{1}H NMR spectroscopy with the disappearance of the starting material amine proton signals, therefore the product spectrum only had three different proton signals which are those of the aromatic protons (Figure 16-32).

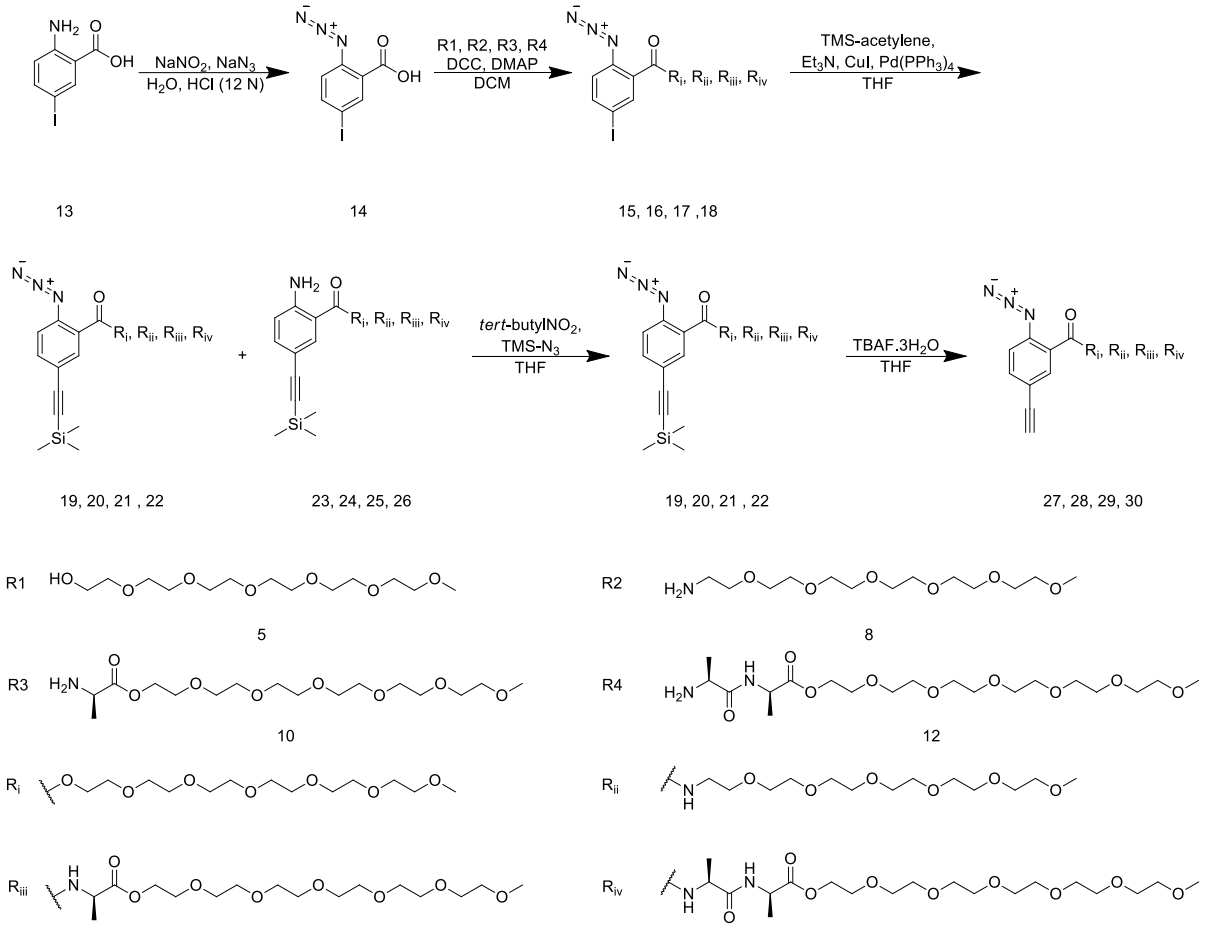

Scheme 8:Synthesis of final monomer structures.

Once compound **14** had been successfully synthesized, pendant chains R_1, R_2, R_3, and R_4 were coupled to the azide functionalized backbone *via* a coupling reaction utilizing DCC and DMAP. This afforded the coupled products (compounds **15** -**18**, Scheme 8). These compounds were purified *via* silica gel column chromatography and characterized by means of ^{1}H NMR spectroscopy (Figure 16-33, Figure 16-35 ,Figure 16-38, and Figure 16-41) and ^{13}C NMR spectroscopy (Figure 16-34, Figure 16-36, Figure 16-39, and Figure 16-42). For compounds **15**-**18**, it was possible to confirm product formation *via* the appearance of the respective R1-R4 backbone protons present in the ^{1}H NMR spectrum (Figure 16-33, Figure 16-35, Figure 16-38, and Figure 16-41). The success of the coupling could be further confirmed by the appearance of a signal at ~ 163 ppm in the ^{13}C NMR spectrum, which is indicative of the carbonyl carbon atom that is utilized in the formation of the ester or amide functional group in compound **15**-**18** during the coupling reaction (Table 1). This confirms that the coupling had taken place in each case and that the two compounds are chemically bound. Compounds **15** and **16** were readily isolated *via* column chromatography. Compound **15**'s spectra matched that which were found in the literature.[4] Compounds **17** and **18** proved to be harder to isolate due to the large molecular weight of each compound. This meant that the compound would often drag on the column and more polar solvent compositions were required to elute the compound from the silica gel.

*Table 1: ^{1}H and ^{13}C NMR spectroscopy signals that appear during the successful coupling reaction to form compounds **15-18** Relevant spectrum in addendum, Figure 16-33 – 36, 16-38 – 39, 16-41 – 42.*

Compound	^{1}H NMR spectroscopy pendant chain shifts (ppm)	^{13}C NMR spectroscopy Ester / Amide C=O carbon signal (ppm)
15	4.45–4.42 (m, 2H), 3.81–3.79 (m, 2H), 3.68–3.61 (m, 18H), 3.53–3.51 (m, 2H), **3.35 (s, 3H)**	163.73
16	3.65–3.61 (m, 22H), 3.54–3.52 (m, 2H), **3.36 (s, 3H)**	163.44
17	4.37 – 4.26 (m, 2H), 3.74 – 3.68 (m, 2H), 3.65 – 3.62 (m, 18H), 3.55 – 3.52 (m, 2H), **3.37 (s, 3H)**, 1.53 (d, *J* = 8.0 Hz, 3H)	162.59
18	4.75 – 4.56 (m, 2H), 4.31 – 4.27 (m, 2H), 3.69 – 3.62 (m, 18H), 3.55 – 3.53 (m, 2H), **3.37 (s, 3H)**, 1.48 (d, *J* = 4.0 Hz, 3H), 1.44 (d, *J* = 8.0 Hz, 3H)	163.28

Compounds **15-18** were then subjected to a Sonogashira-Hagihara cross coupling reaction (Scheme 8) to add a TMS-protected alkyne group *para* relative to the azide functional group (detailed procedure in supplementary information).[4] Previously in the work conducted by Klumperman and co-workers,[4] it was reported that this reaction produced a mixture of the desired product (compounds **19-22**, Scheme 8) and a side product (compounds **23-26**, Scheme 8). A singlet signal between 5.5 ppm and 6.0 ppm in the ^{1}H NMR spectrum is indicative of the side-product being present (NH_2 signal). In addition to this, the appearance of a ^{13}C signal in the ^{13}C NMR spectrum between 145 ppm and 155 ppm is indicative of the carbon atom connected to the amine functional group (Figure 13-13).[4]

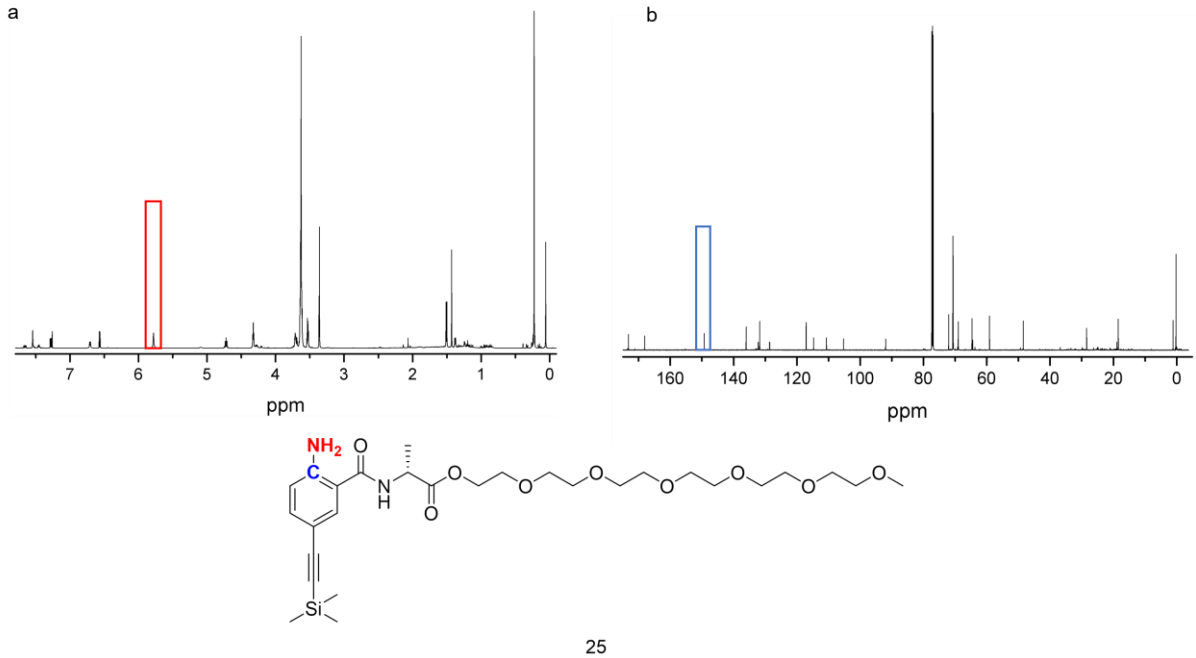

*Figure 13-13: Representative spectra of a mixture containing the amine side product (compound **25**). With the amine proton signals highlighted in red and the carbon atom connected to the amine functional group highlighted in blue of the side product. a) ^{1}H NMR spectrum, b) ^{13}C NMR spectrum*

This amine side product that is formed is detrimental during the cycloaddition-mediated polymerization as it acts as a chain end. Because of this, having the smallest amount (2% or less) of amine side product greatly impacts the achievable molecular weight of the polymer.[11] Side-product formation may take place as a result of a Staudinger reduction reaction taking place between PPh_3 and the azide functional group on the monomer (Scheme 9).[11] PPh_3 is present in the reaction as a consequence of the ligand leaving the catalyst, $Pd(PPh_3)_4$, once the catalyst had been utilized in the reaction or as a result of slow catalyst decomposition as it is exposed to oxygen as its container is opened and closed repeatedly.

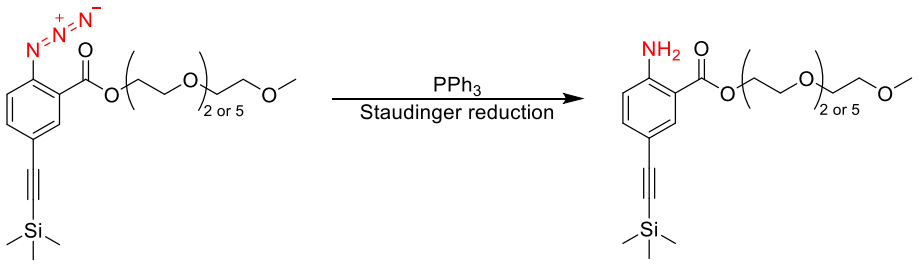

Scheme 9: A representation of the chemical side reaction, a Staudinger reduction, that takes place at the same time as the Sonagashira-Hagihara cross coupling reaction.

In prior work by Klumperman and co-workers it was possible to remove this side product easily *via* column chromatography.[4] The impurity could easily be removed as it eluted after the desired azide product. Thus compound **19** could be purified *via* column chromatography to remove the amine side product, although this did take a large amount of time to run a slow column. In contrast compound **20** - **22** could not be purified *via* column chromatography no matter the solvent combination. This is a result of the R_f values of the desired product (compounds **19-22**, Scheme 8) and the amine-containing impurity (compounds **23-26**, Scheme 8) being too similar (separated by an R_f value of 0.02-0.05) and thus the compounds could not be separated. The struggles with separation of the side product and the desired product may be due to the introduction of hydrogen bonding groups, as this was the only change other than the increase in molar mass to the different molecules. Column chromatography with a small quantity of triethylamine (1% – 3%) was also attempted, but this did not aid in the separation issue. Thus, instead of attempting to purify the azide impurity of the amine side product, the two compounds were collected (compounds **19-22** and compounds **23-26**, Scheme 8) and isolated together after the Sonagashira-Hagihara coupling step. Thereafter the mixture of the two were reacted in such a manner to convert all remaining amine functionalities (compounds **23-26**, Scheme 8) into the desired azide containing product (compound **19-22**, Scheme 8).[4] Formation of compounds **19-22** (with no amounts of compound **23-26**) were confirmed *via* full NMR characterization (^{1}H NMR, ^{13}C NMR, COSY, HSQC, and HMBC) and mass spectroscopy (full spectral assignment in supplementary information). The successful conversion of the amine to the azide functionality is indicated *via* the disappearance of the proton signals indicative of the amine group (red block, Figure 13-14a to Figure 13-14c). As well as shift of the signal of the carbon atom connected to the amine functional group (pink block, Figure

13-14b) of the side-product being transformed to a carbon atom connected to an azide functional group (movement of pink block to the orange block, Figure 13-14d).

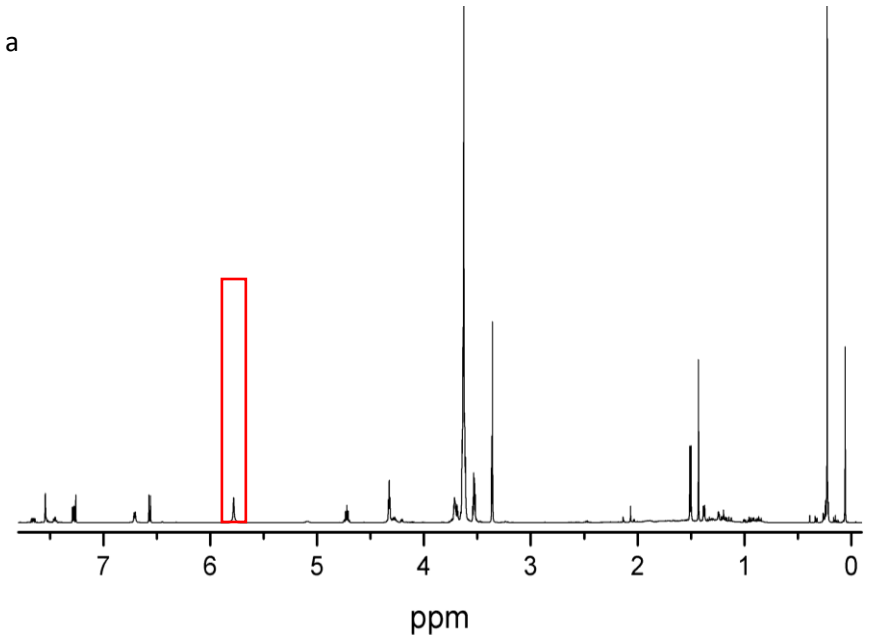

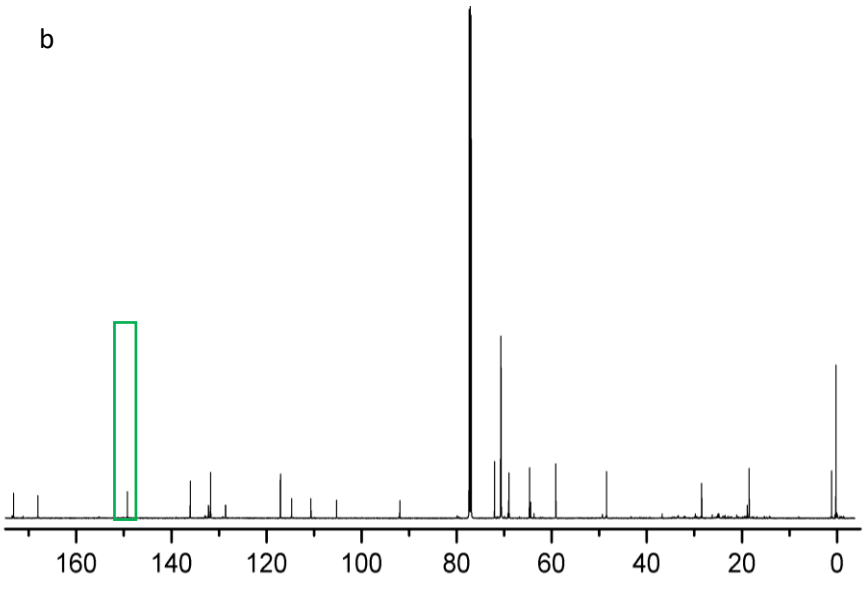

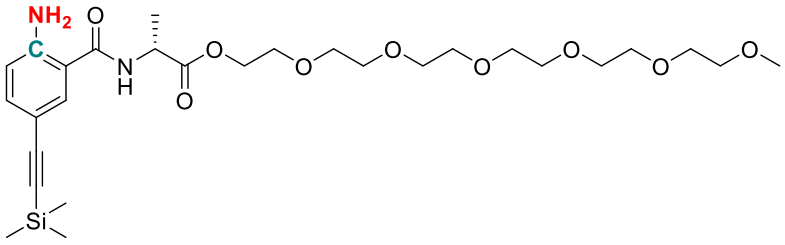

25

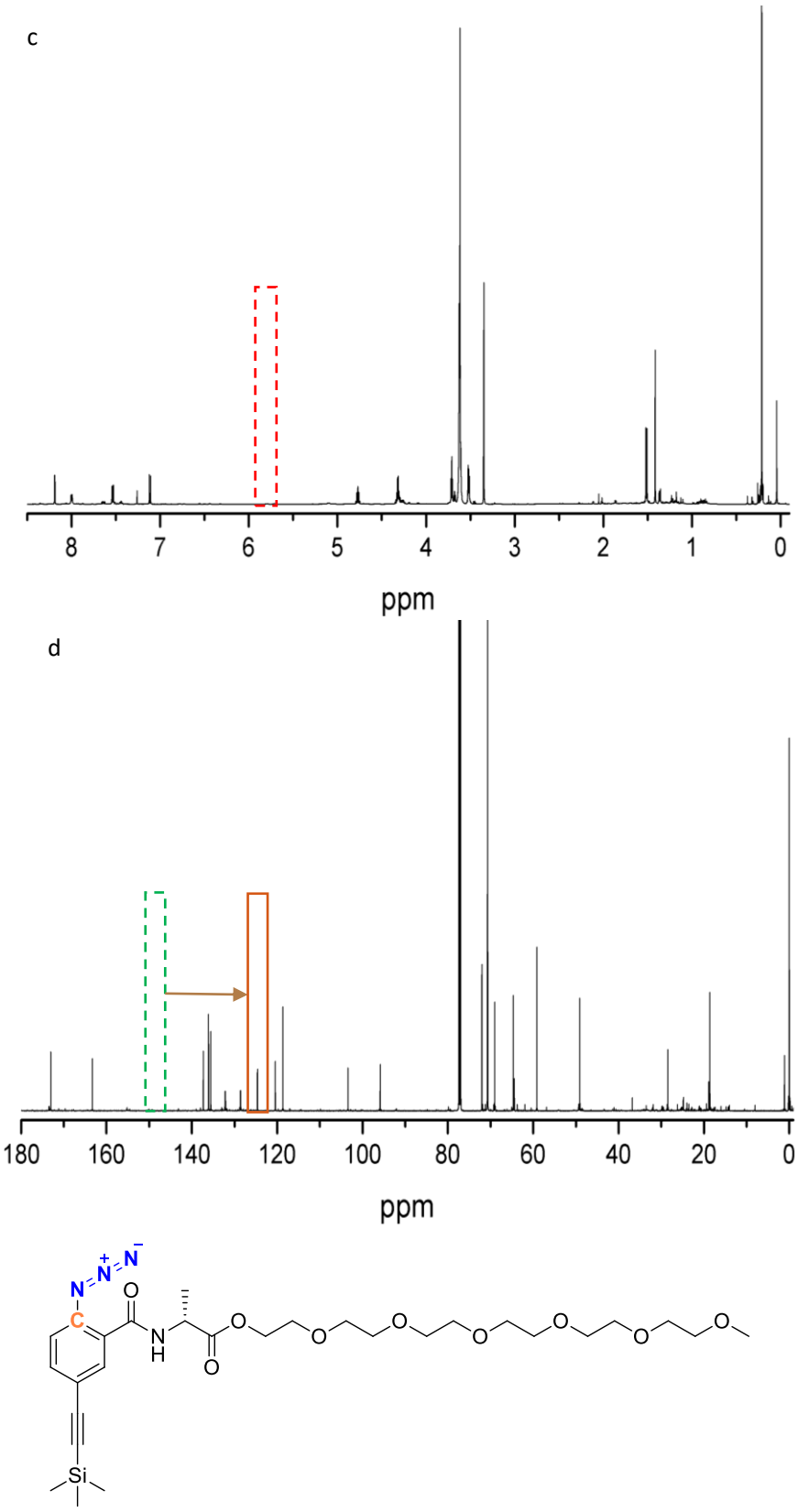

21

*Figure 13-14: NMR spectra of the amine side product (compound **25**), with focus on the amine protons in red in the ^{1}H NMR spectrum (a), the carbon atom connected to the amine functional group in the ^{13}C NMR spectrum, green block(b). The spectra of the desired product (compound **21**), with a focus on the disappearance of the amine functional group proton signals in the ^{1}H NMR spectrum(c), and the carbon atom shifting from the position where the amine carbon was present (dashed green block, d) to where it is once the amine functional group was converted to the azide functional group (solid orange block, d).*

Once full 2D NMR spectroscopic characterization was conducted on compounds **19**-**22**, it was possible to proceed with the deprotection step to afford compounds **27**-**30** (Scheme 8).[4] Compound **27** could be easily isolated after silica gel chromatography and could therefore be characterized *via* ^{1}H and ^{13}C NMR spectroscopy,[4] before the monomer could auto-react *via* an ambient non-selective Huisgen cycloaddition,[130] where the terminal alkyne and the aromatic azide would undergo non-selective cycloaddition reactions. This was not the case for compounds **28**-**30**, which were difficult to completely purify under the same time constraints (imposed by the possibility of the ambient non-selective Huisgen cycloaddition auto-reaction). This may be because of the incorporation of hydrogen bonding groups. Because of this, a highly polar mobile phase was required to elute the molecules from the silica gel (as well as the molecule dragging on the column). As a result of this, it was difficult to acquire a good/clean and dry NMR spectrum before the monomer started to react. Because of this, mass spectroscopy was utilized instead (which was conducted a mere 5 minutes after the reaction to confirm product formation) to confirm that the deprotection had taken place (supplementary information). This was confirmed *via* identifying the molecular ions/ variations of the molecular ions of the deprotected monomer in the mass spectra acquired. Once it was confirmed that the deprotection reaction was successful (Scheme 8), it was possible to progress to the polymerization. On the same day the deprotected reaction was conducted, the respective monomer was polymerized according to the general polymerization procedure (Scheme 10), (supplementary information section).

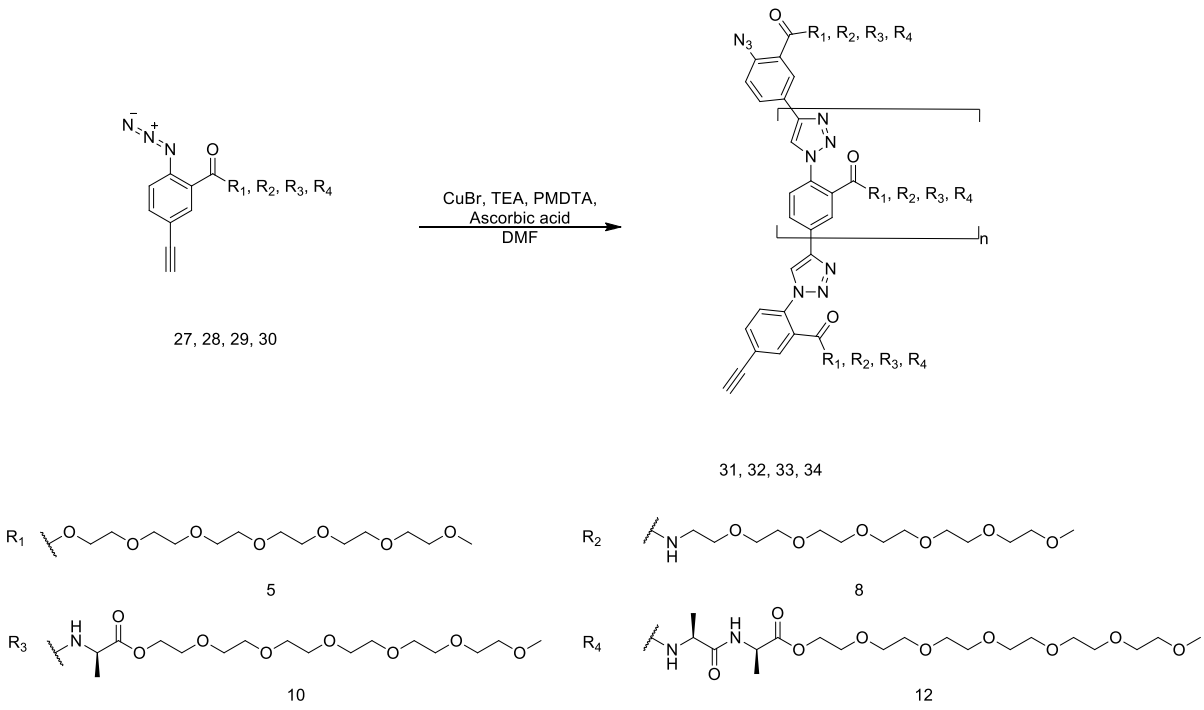

*Scheme 10: Generalized polymerization procedure to afford compounds **31**, **32**, **33**, **34**.*

After the polymerization procedure (supplementary information) was conducted, ^{1}H NMR spectroscopy was conducted to confirm polymer formation. This crude method of polymer formation had to be conducted as size exclusion chromatography (SEC) utilizing HFIP nor DMF could solubilize compounds **32**, **33**, and **34**. In addition to this, MALDI-ToF MS proved to be hampered by solubility problems that led to partial solubilization of the polymer and most likely to selective exclusion of the larger molecular weight polymers. The acquired data was therefore a misrepresentation of the (full) samples composition. It was therefore not possible to determine the average molecular weight nor molecular weight distribution of the polymers synthesized *via* conventional, readily available means. Developing a methodology to determine the molecular weight (*via* a modified SEC methodology, field flow fractionation, or a new MALDI-ToF MS solvent/matrix combination) would be possible, but this is beyond the scope and time constraints of this study. On inspection of the ^{1}H NMR spectra (Figure 13-15), it should be noted that the spectral signals are broad and undistinguishable, except for compound **31** which looks the same as per literature.[11]

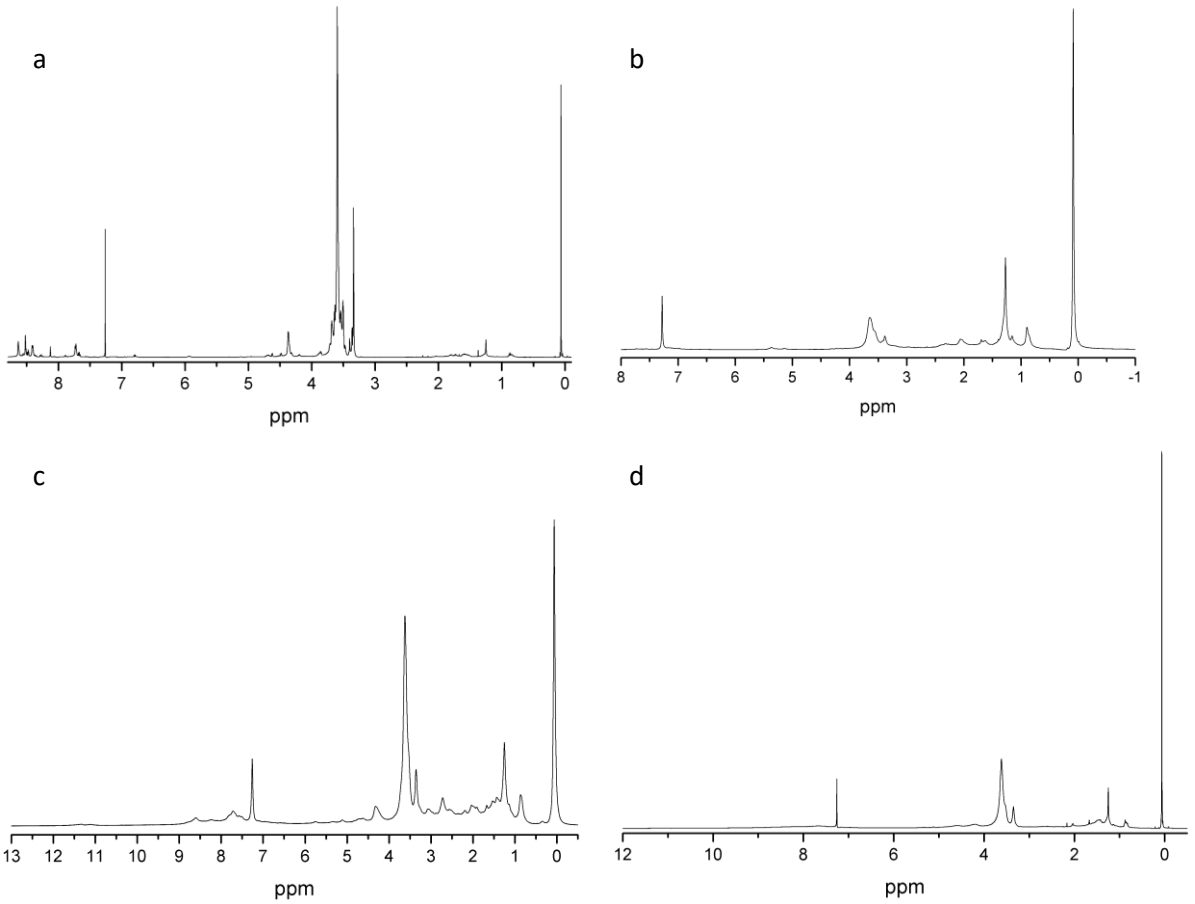

*Figure 13-15: ^{1}H NMR spectra of a) compound **31**, b) compound **32**, c) compound **33**, d) compound **34** in $CDCl_3$.*

The poor ^{1}H NMR spectra may arise due to two possible reasons. Firstly, the spectra may have poor resolution as a result of the formation of higher molecular weight polymers. Another field of thought to explain the poor resolution may be because of the formation of low molecular weight oligomers as opposed to polymer formation. The possible low molecular weights may be a result of side-reactions

that have been reported in literature,[131,132] for instance, where an aromatic azide functional group can be converted to an aromatic amine functional group in the presence of copper (similar conditions to the polymerization reaction). The rate and the extent of this reaction has been shown to be controlled based on several conditions, but the most relevant here is that of the electronic environment of the azide functional group within the molecule. If this side reaction were to occur to even the smallest extent while polymerization takes place, it would greatly impact the molecular weight as noted by Klumperman and co-workers.[11] This may hint as to why the polymers (compound **32**, **33**, and **34**) that have an amide functional group attached to the aromatic ring may struggle to reach high molecular weights, while compound **31**, which has an ester functional group (a different functional group with different electronic effects), does not struggle to polymerize, although this is for now hypothetical, since as noted earlier it was not possible to acquire molecular weight data.

If shorter oligomer chains did form due to reduction of the azide to amine it would not be possible to study the folding pattern of these polymers as the polymers require at least two turns in the helix to fold (i.e., 27 repeat units).[11] Thus, the samples were repolymerized (or chain-extended) according to the image outline in Figure 13-16. This was done to improve the likelihood that the samples to be tested were of larger molecular weights. Although as stated earlier this could not be confirmed *via* SEC (with DMF or HFIP) or MALDI-ToF MS.

Firstly, the possible oligomers acquired from the first polymerization were isolated (Figure 13-16a) and the amine functional groups were converted to azide functional groups *via* a method identified by Klumperman and co-workers (Figure 13-16b).[4] Once the reaction was complete, these azide and alkyne capped oligomers were immediately subjected to a subsequent polymerization to afford ideally longer polymer chains (Figure 13-16c). The resulting polymers from this polymerization were purified *via* dialysis with 10 kDa molecular weight cut-off snakeskin dialysis tubing (Figure 13-16d). This process removed any oligomer chains that were too short to fold into the desired foldamer helical structure as well as remove the copper metal utilized in the polymerization, thus removing the green colour of the polymer. The polymer left in the dialysis bag was then isolated and freeze dried (Figure 13-16e) and subsequently analysed *via* various analytical techniques. The polymerization procedure that was utilized in both cases was that which was developed by Klumperman and co-workers (Scheme 10).[4]

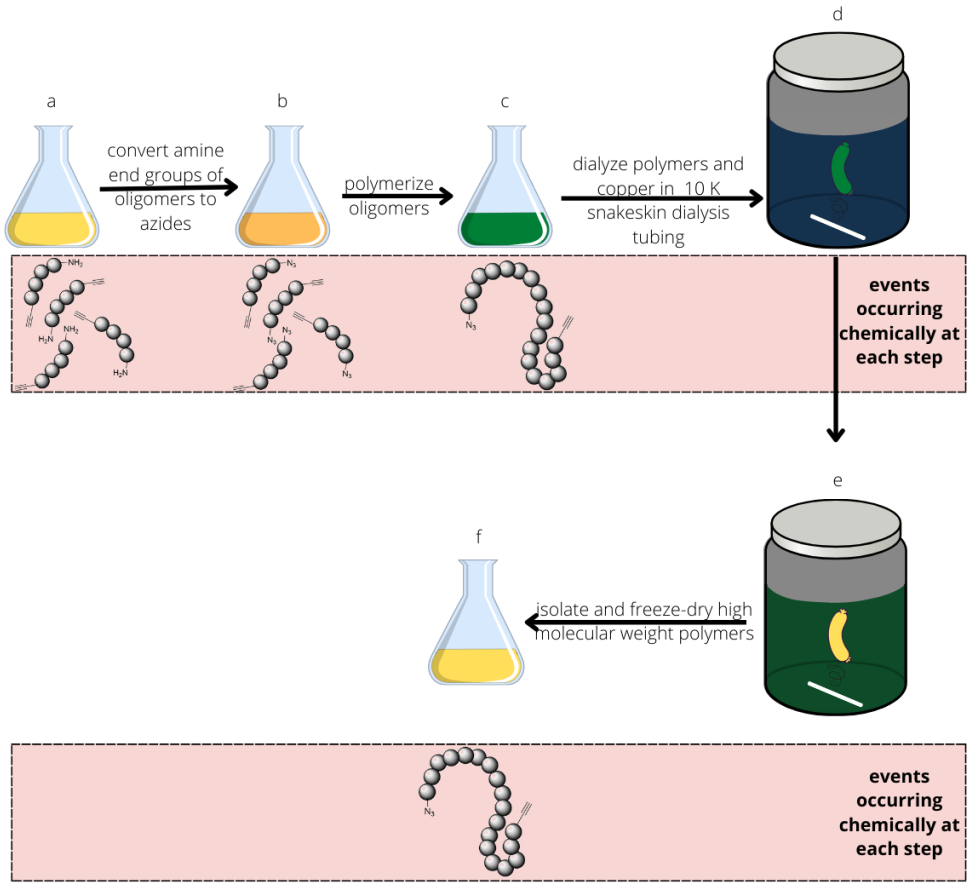

Figure 13-16: Methodology utilized to afford longer polymer chains from short oligomer chains.

^{1}H NMR spectroscopy, variable temperature ^{1}H NMR spectroscopy, ROESY NMR spectroscopy, and COSY NMR spectroscopy in conjunction with literature,[11] were utilized to assign the polymers' ^{1}H NMR spectra (found in supplementary information). The assigned signals are highlighted in Figure 13-17. Take note that most probably as a result of low molecular weight oligomers being present in large quantities, assignment of the NMR spectroscopy signals for compound **33** was not possible, although polymer formation can be confirmed by specific broad signals indicated in Figure 13-17 as well as the formation of a solid material that struggled to dissolve in solvents. Although again this could not be proved and is just a hypothesis until molecular weight of the polymer can be determined in the future.

A

Polymer 1

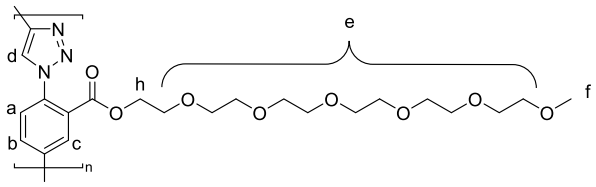

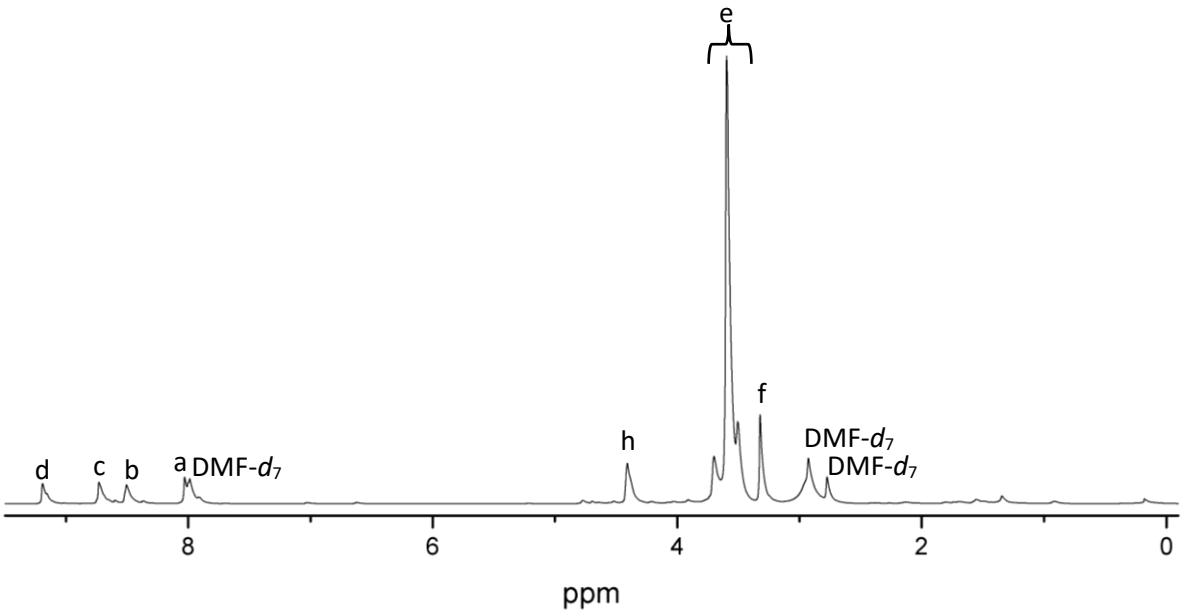

B

Polymer 2

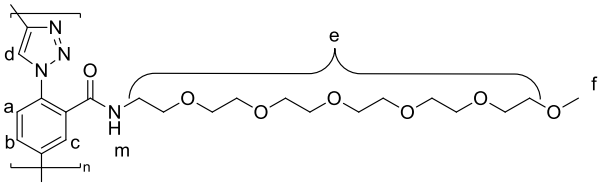

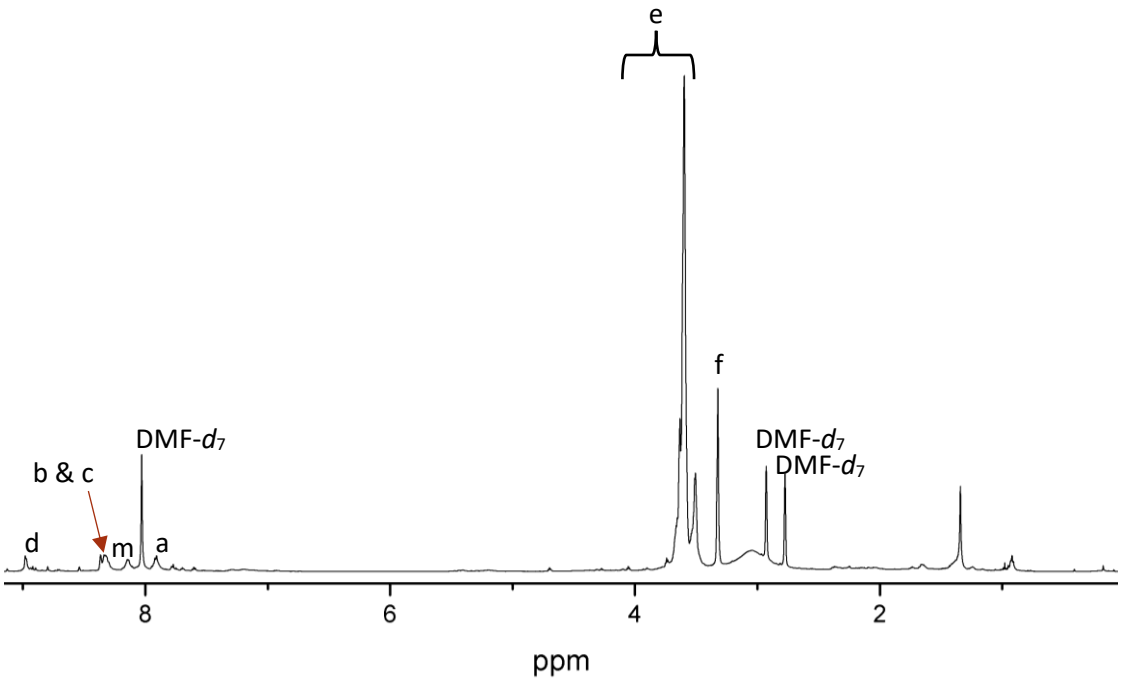

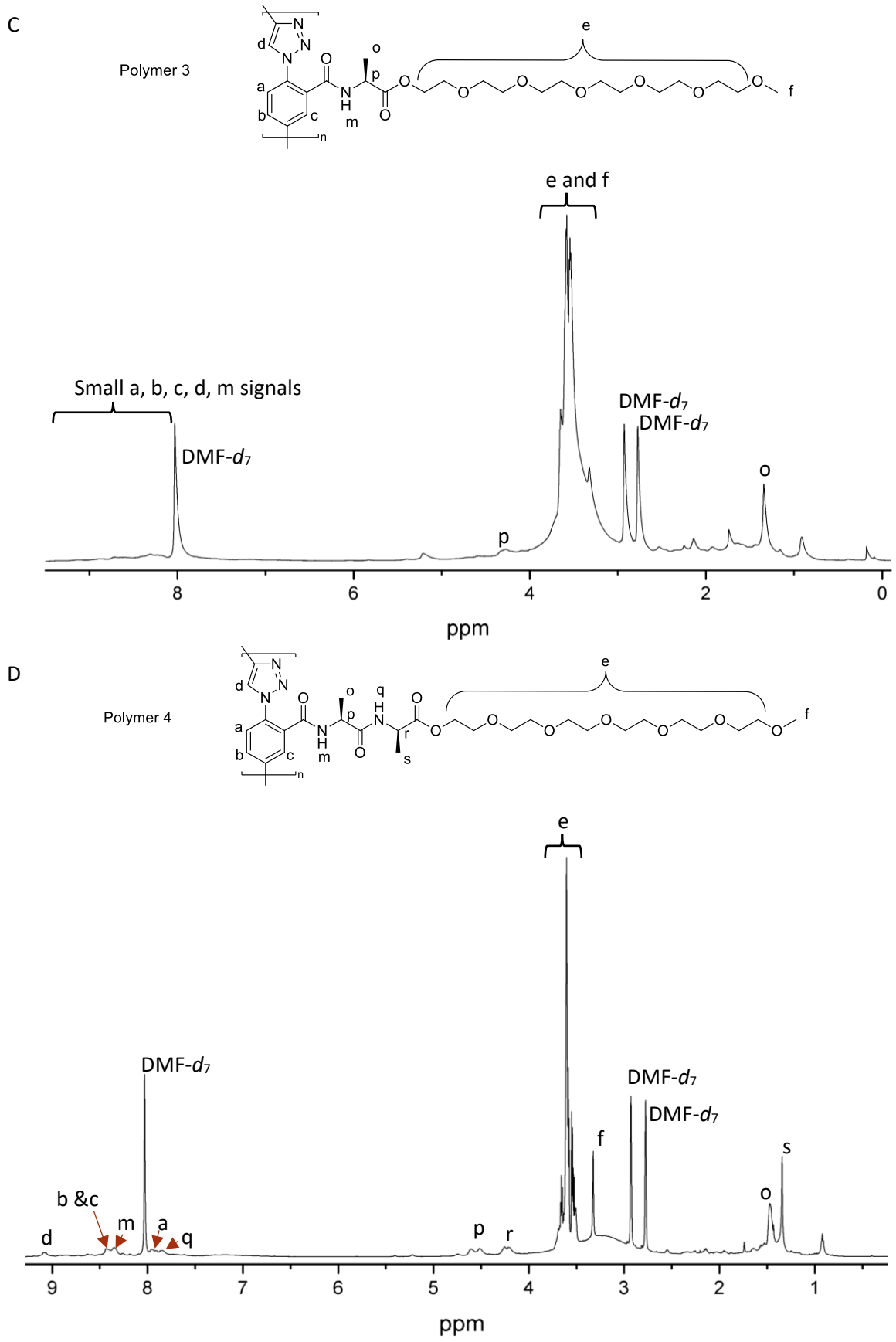

*Figure 13-17: ^{1}H NMR spectroscopy spectral assignment of A) polymer **1** or known as compound **31**, B) polymer **2** or known as compound **32**, C) polymer **3** or known as compound **33**, D) polymer **4** or known as compound **34**, at 105 °C in DMF-d_7.*

In Figure 13-17A it is noted that the spectrum of compound **31** matches that acquired by Klumperman and co-workers.[11] Because of this, confidence was gained in the ability to reproduce previously conducted work, which offered good prospects for the monomers with hydrogen bonding capabilities. This hints at the idea that there should be no reason as to why compounds **32**, **33**, and **34** should not form *via* the same polymerization procedure. And if they were not to form, that this may be a result of the polymer and not that of insufficient skill/ experience displayed.

It was then possible to confirm the introduction of hydrogen bonding moieties in compounds **31**, **32**, and **34** *via* variable temperature ^{1}H NMR spectroscopy in DMF-d_7 (Figure 13-18). It was not possible to achieve this with compound **33** as the signals could not be confidently assigned as a result of poor signal intensity and resolution. It can be noted in Figure 13-18 that all ^{1}H NMR signals that shift up-field with increasing temperatures (protons d, m, and q) are those of protons that are involved with hydrogen bonding, as the increase in temperature weakens the hydrogen bond strength.[11] It is also interesting to note that both q and p protons in compound **34** (1C and 2C in Figure 13-18) have the same gradient of shift (but the gradient is still larger than proton d). This suggests that the extent of hydrogen bonding capabilities of the amide units is not dependent on the local chemical environment of the proton within the monomeric unit. Figure 13-18 confirms that compounds **32**, **33**, and **34** should have added stability incorporated within the foldamer system itself because of added hydrogen bonding moieties. Where compound **34** should have the most added stability, this being evident by having the most hydrogen bonding moieties present within the monomer structure.

Following the characterization of compounds **31**, **32**, **33**, and **34**, the properties in solution were evaluated. This part of the study began with inspection of the polymers *via* dynamic light scattering (DLS). It is to be acknowledged that DLS is traditionally utilized to accurately determine the hydrodynamic radii (nm) of spherical nanoparticles and micelles in solution *via* the scattering of light that is achieved by particles in solution. For polymer systems such as the ones under inspection, that are not spherical in nature, DLS does allow for the determination of the presence of large molecules or supramolecular aggregates in solution (> 10 nm). DLS also makes it possible to determine if these molecules/ polymers change in hydrodynamic radius with a change in solvent composition. It should be noted that this method of analysis is by no means quantitative, but instead can act as a comparative test to detect patterns of peak shifts and shapes of peaks with changes in solvent composition. The results of this study are summarized in Figure 13-19, please note that the curves displayed are an average of 9 scans (of 9 runs) of the same sample. For all the analytical methods to follow, concentrations of polymer in solution were determined by a brief UV/Vis analysis and were kept constant unless otherwise stated, polymer **1** (interchangeably called compound **31**) repeat unit concentration of 0.04125 μM, polymer **2** (interchangeably called compound **32**) repeat unit concentration of 0.0825 μM , polymer **3** (interchangeably called compound **33**) repeat unit concentration of 0.1155 μM, and polymer **4** (interchangeably called compound **34**) repeat unit concentration of 0.0825 μM.

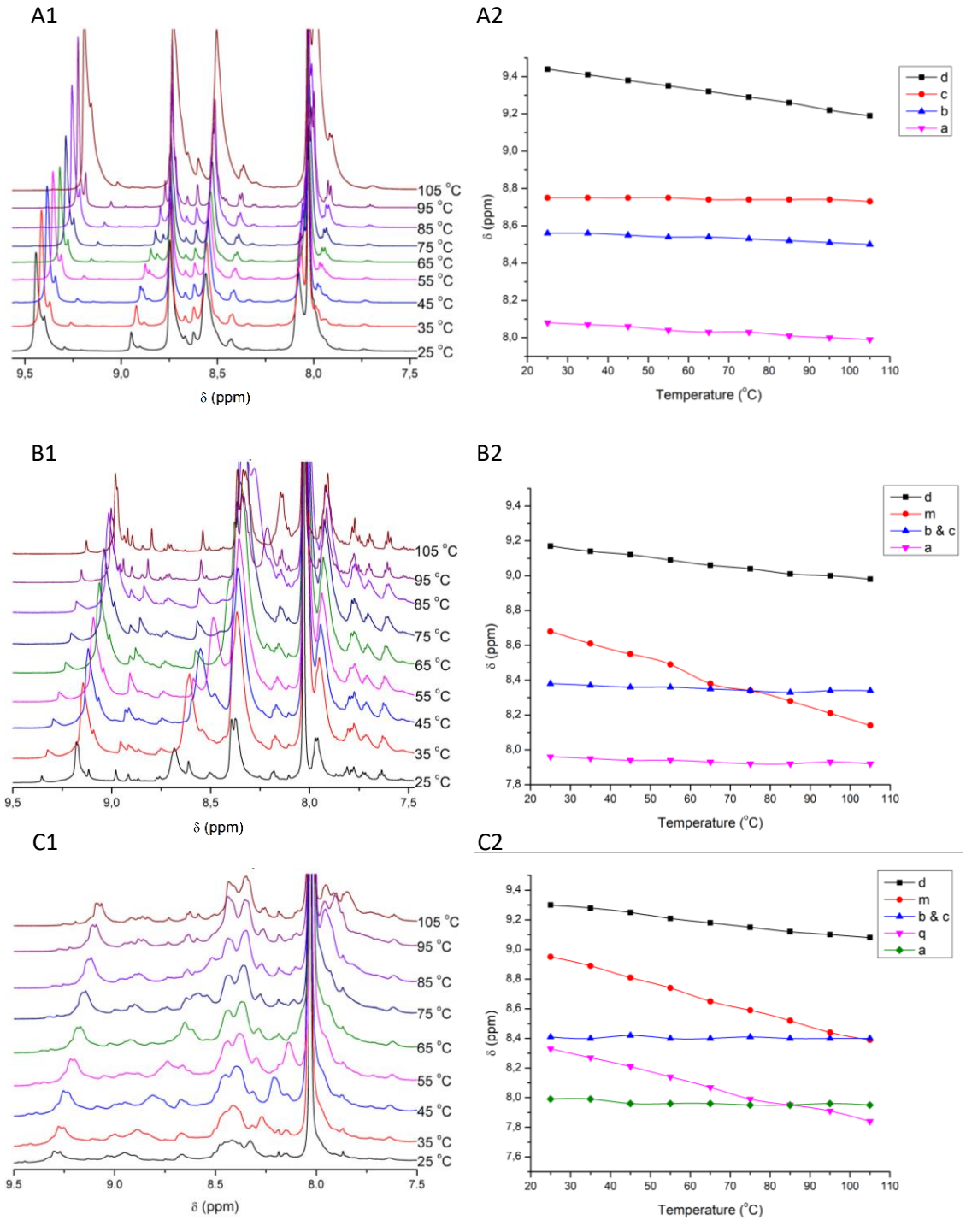

*Figure 13-18: Variable temperature (in degrees Celsius [°C]) ^{1}H NMR spectroscopy in DMF-d_7 of A1) polymer **1** or known as compound **31**, B1) polymer **2** or known as compound **32**, C1) polymer **4** or known as compound **34**. With respective signal tracking in A2, B2, and C2 at variable temperatures.*

In Figure 13-19A, the results of DLS conducted on compound **31** indicate that as the solvent composition changes to that of increasing amounts of water, so the peak's shift to smaller radii sizes. It is also worth noting the peak shape, that of narrow peaks initially only slightly widens upon an increase in water percentage in the solvent composition. On the other hand, compound **32**, **33**, and **34** in Figure 13-19B, Figure 13-19C, and Figure 13-19D respectively, behave slightly differently. Firstly, all the signals for these polymers progressively broaden (a lot more than polymer **1**) as the water content increases. This hints at the idea that polymers with hydrogen bonding moieties do not fold into ordered structures, but instead form large structures in solution (with a larger distribution in sizes present). Confirmation *via* several spectroscopic techniques (CD (circular dichroism), LD (linear dichroism), and UV/VIS (ultraviolet-visible spectroscopy)) will be discussed below. Secondly it should be noted that in comparison to compound **31** which follows a more linear path in change in size composition (a decrease in hydrodynamic radius with increased water content), compound's **32**, **33**, and **34**, do not. Instead, the polymers do not follow any pattern at all which again hints at the idea of agglomeration taking place as a result of solvent composition change as opposed to folding occurring. The exact reason for there being possibly no folding taking place is unknown as of present.

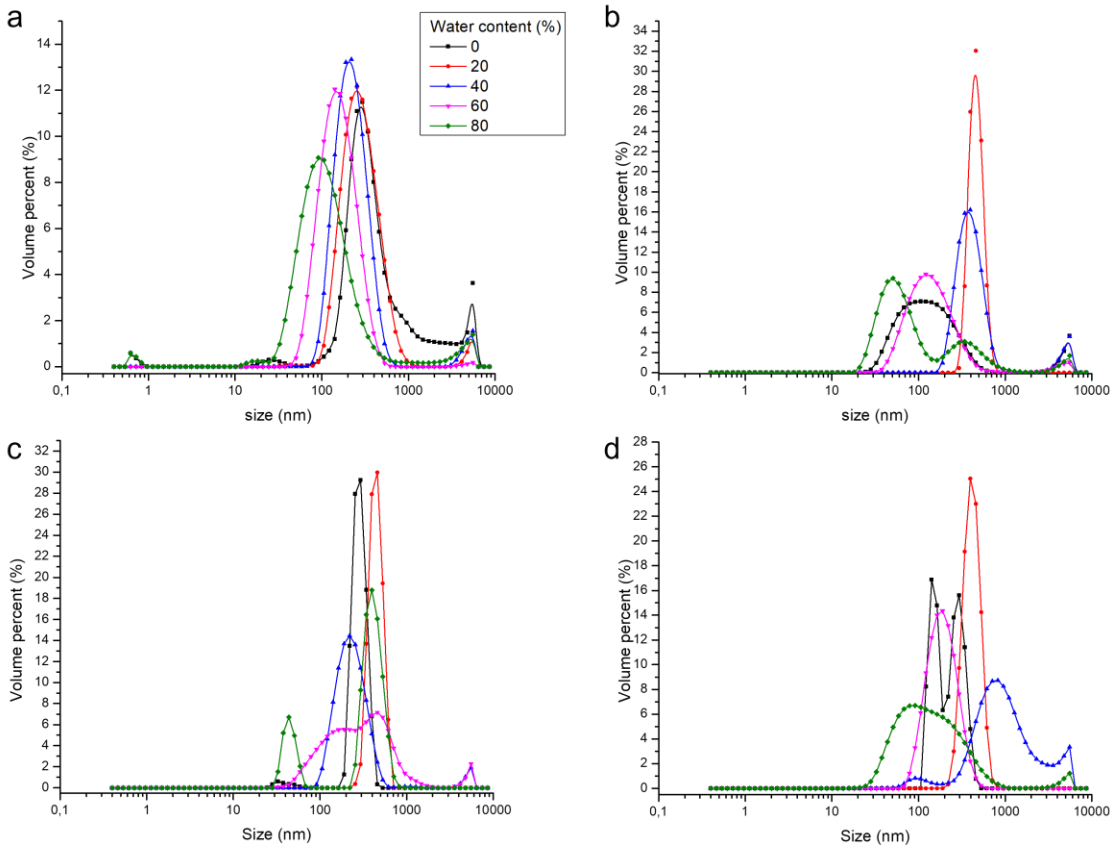

*Figure 13-19: DLS results of volume percent (%) at various solvent compositions of polymer **1** (A) or known as compound **31**, polymer **2** (B) or known as compound **32**, polymer **3** (C) or known as compound **33**, and polymer **4** (D) or known as compound **34**, at 25°C.*

As it has now been confirmed that i) polymers were formed (although the exact molecular weight could not be determined), and characterized and ii), that the hydrodynamic radii of the polymers change as a function of solvent composition. It made logical sense to investigate if the change in hydrodynamic radii was as a result of folding or glomeration of the polymer as a function of solvent composition. This would be conducted through a collection of different analytical techniques, namely, UV/Vis spectroscopy, CD, and LD. Each of these techniques imparting more information and giving a clue as to what may be occurring with these polymers in solution.

Firstly UV/Vis spectroscopy was conducted on each of the foldamer samples (Figure 13-20). The samples were prepared according to the procedure outlined in the supplementary information. In previous work conducted by Klumperman and co-workers,[11] it was determined that the folding of polymers with this backbone moiety (*para*-aryl triazole) can be tracked with UV/Vis spectroscopy. It was shown that a disordered/ unfolded polymer produces a signal at 284 nm as a result of the benzene rings not being stacked upon each other. As the solvent composition changes and the polymer forms an ordered foldamer helix (and the benzene rings stack atop one another), it was shown that there was a red shift in the signal to 310 nm. Utilizing this property, it is possible to generate a graph which indicates

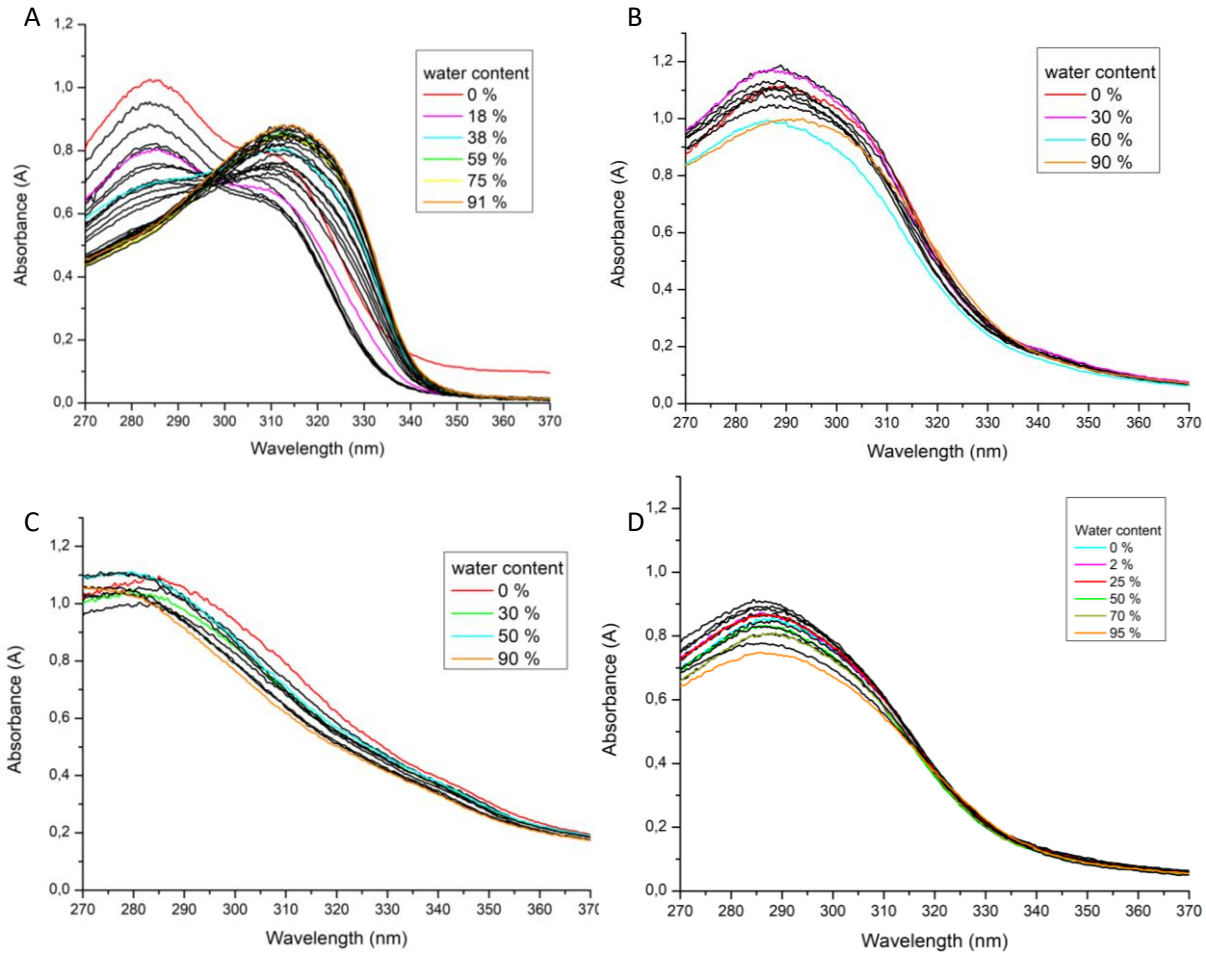

*Figure 13-20: UV/Vis spectroscopy spectra at varying solvent compositions of; A) polymer **1** or known as compound **31**, B) polymer **2** or known as compound **32**, C) polymer **3** or known as compound **33**, D) polymer **4** or known as compound **34**.*

the folding kinetics of the polymers. [11] Where the ratios of the intensities of absorbances at 310 nm and 284 nm represents the degree of folding into an ordered helical structure of the polymer in solution. [11] In previous literature it was indicated that the polymers would form ordered structures as the fraction of water increased in the DMF/water mixture (to a point). Thus during the folding process, the UV/Vis signal of the polymer at 284 nm should decrease in absorbance with increasing water content and increase in absorbance at 310 nm.[11] If this is compared to the results in Figure 13-20, it can be noticed that compound **31** (Figure 13-20A) is the only polymer that has such a trend. Compounds **32** (Figure 13-20B), **33** (Figure 13-20C), and **34** (Figure 13-20D) on the other hand do not show such a trend.

What can be noticed, is that in polymers **2** (compound **32**), **3** (compound **33**), and **4** (compound **34**) (Figure 13-20), although there is no appearance of a signal at 310 nm, there is a slight decrease in the absorbance value at 284 nm. This suggests that although there is no formation of ordered folded helixes, there is a decrease in free chains in solution. A hypothesized explanation for this, is that the polymers may be glomerating into a large mass instead of forming an ordered helix upon the introduction of increasingly polar solvents (water). During this glomeration process, the hydrophobic moieties (the benzene rings) would be 'hidden' or encapsulated within the hydrophilic moieties (ethylene glycol chains) from the increasingly polar solvent. Because of this, there would be less of a signal at 284 nm as the fraction of water in the solvent increased. Glomeration of the monomers would also explain why

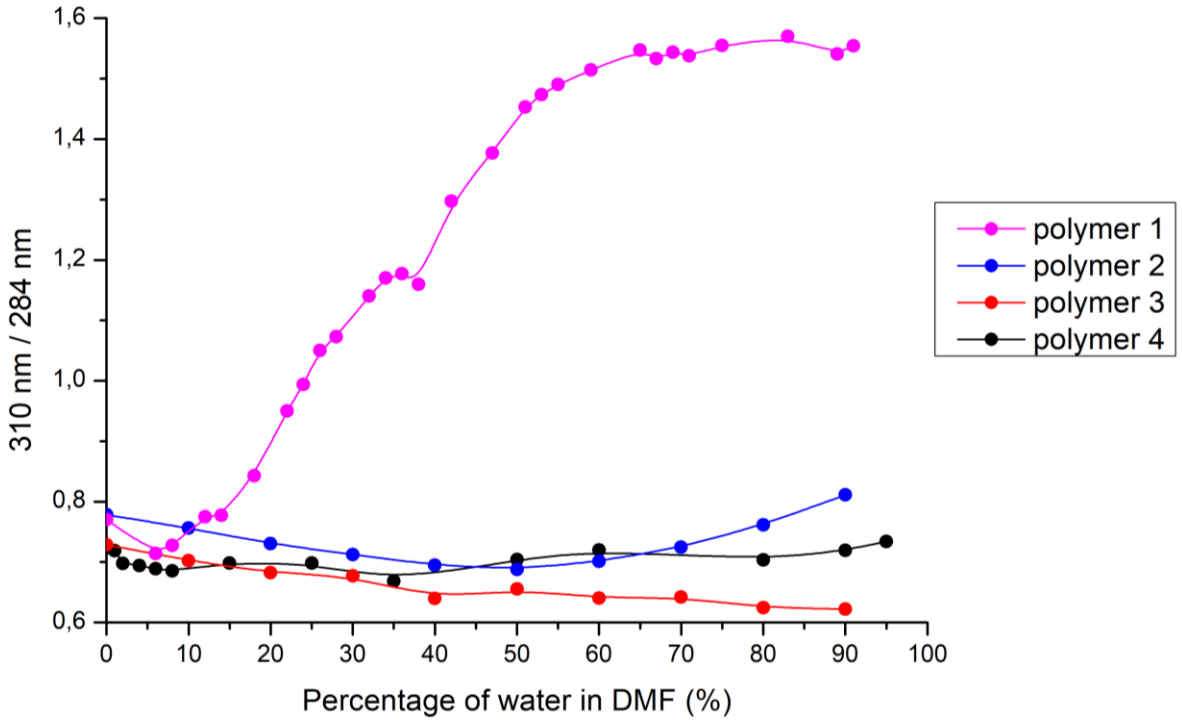

*Figure 13-21: A plot of 310 nm/284 nm as a function of increasing amounts of water in DMF for polymer **1** or known as compound **31**, polymer **2** or known as compound **32**, polymer **3** or known as compound **33**, polymer **4** or known as compound **34**.*

there is no increase in a signal at 310 nm as a function of solvent composition as there would be no stacking of the rings during the glomeration process as there would be no ordering of the polymer.

Utilizing the data from Figure 13-20, it was possible to generate Figure 13-21, which depicts the degree of folding as a function of solvent composition. Inspecting Figure 13-21, it further agrees with the deduction made regarding Figure 13-20, which is that compound **31** is the only polymer that folds as a function of solvent composition. The other polymers (compounds **32**, **33**, and **34**) give a consistently low ratio of 310 nm/284 nm. Thus, indicating that the polymers do not form an ordered structure as the water content increases but instead remain disordered independent of solvent composition. The result

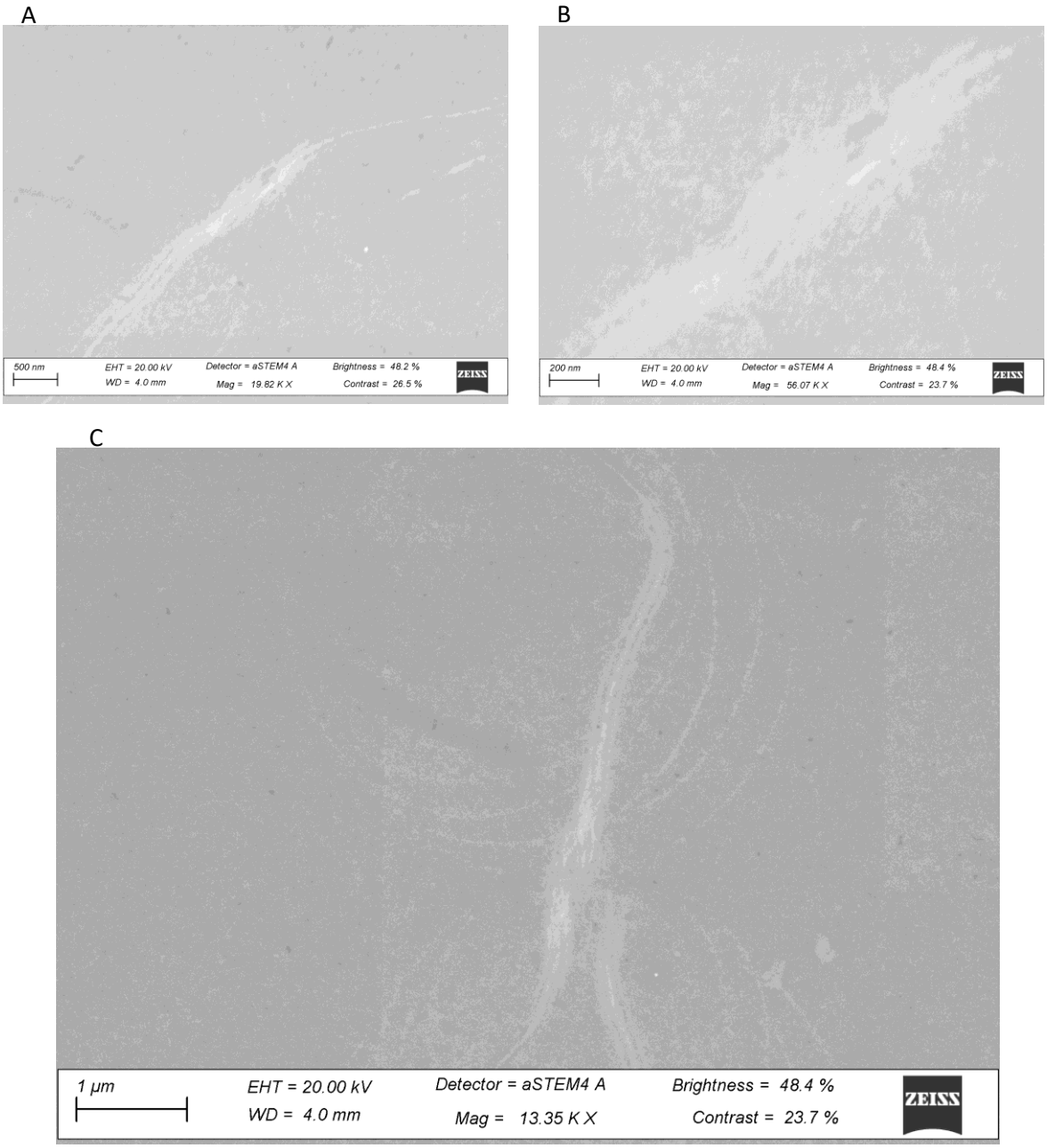

*Figure 13-22: Standing TEM images of compound **31** at a solvent composition of 80 % water in DMF. A) that of a loose polymer thread, B) a zoomed in image of A, C) image of large-scale helical thread-like structure in solution. The sample was prepared as stated in the supplementary section.*

also agrees with the deduction made on inspection of the DLS results. In Figure 13-21 it is also of interest to note that compound **31** has a same folding profile to that of other polymers synthesized by Klumperman and co-workers.[4] Previously in literature, it was indicated that polymer **1** would plateau in terms of its degree of folding at around 60 % water in DMF,[4] which is what is identified in polymer **1** (Figure 13-21). To further prove no glomeration was taking place and to observe the morphological structure of the polymer in solution, Standing TEM (Standing Transmission Electron Microscopy) was conducted on a sample of compound **31** (polymer **1**) in 80 % water in DMF (Figure 13-22). A solvent composition of 80 % water was chosen as it would ensure that if it were possible for polymer **1** to form ordered helical structures, that these structures would be visible in the Standing TEM images. The images in Figure 13-22 confirm that the helixes had not collapsed, but instead are large, thread-like, and homogenous in width throughout as in literature at this solvent composition.[4] Furthermore there were no conglomerates identified in solution during the analysis. The images displayed in Figure 13-22 aligns with what is observed in the UV/Vis spectra in Figure 13-20 and Figure 13-21. To confirm that there was no instance of folding or formation of ordered structures occurring in solution, both CD and LD analysis were conducted on all four of the polymer systems. Based on literature,[4] if there was folding present, there would be a CD signal (in the order of magnitude of ± 40 mdeg) for compounds **33**, and **34**. This would be because of the introduction of chiral centres within the monomeric unit. These chiral centres would aid in the biased formation of a specific handedness of the helix (left or right-handed helix based on the chirality of the chiral centre introduced). Compounds **31**, and **32** on the other hand should not provide a CD signal, since they do not contain a chiral substituent. A summary of the results is indicated in Figure 13-23.

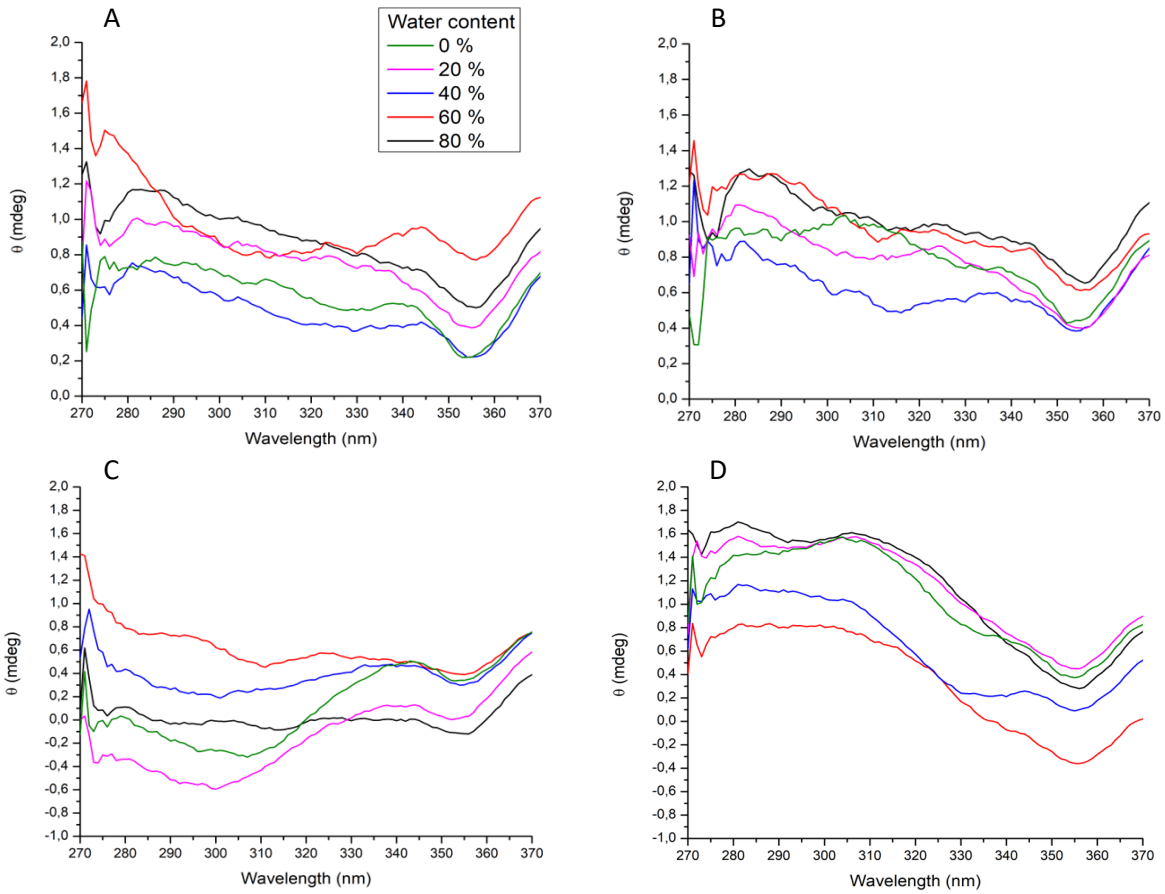

*Figure 13-23: CD spectra of A) polymer **1** or known as compound **31**, B) polymer **2** or known as compound **32**, C) polymer **3** or known as compound **33**, D) polymer **4** or known as compound **34**.*

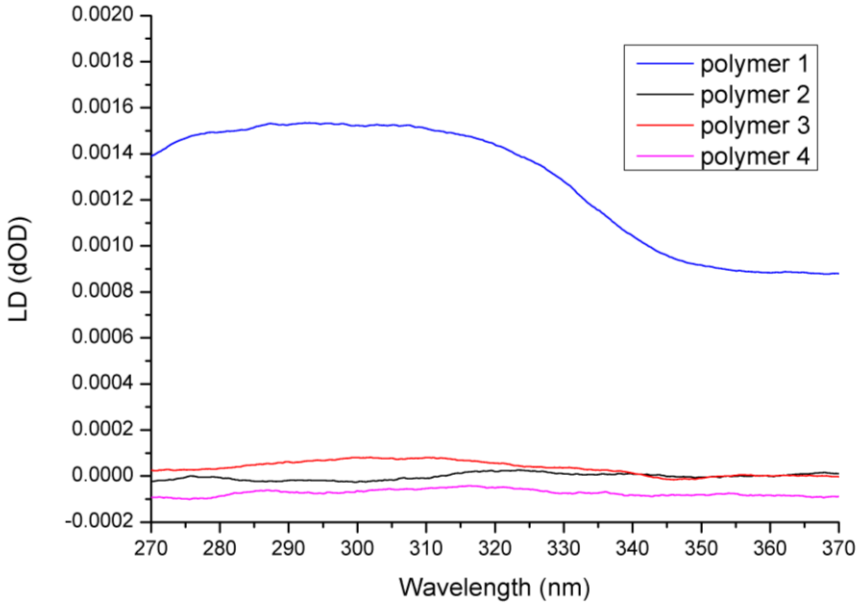

*Figure 13-24: LD spectra of all polymers (**1** (compound **31**), **2** (compound **32**), **3** (compound **33**), and **4** (compound **34**)) as indicated in the key at a solvent composition of 80% water in DMF.*

Based on Figure 13-23, it can be noted that neither compound **33** (Figure 13-23C), nor compound **34** (Figure 13-23D), show any signal near the magnitude (40 mdeg) identified in literature.[4] This indicates that the polymers do not form a chiral biased ordered structure, this contrasts with what would be expected of the folded polymer with the incorporated chiral centre.[4] It should be noted that there is a slight chiral bias, in compounds **33** (Figure 13-23C), and **34** (Figure 13-23D), but this is most likely due to the chiral centres themselves within the monomeric units and is too small a signal to be as a result of a bias in the higher ordered structure formation. For compounds **31** (Figure 13-23A), and **32** (Figure 13-23B), there should be no chiral bias as there is no introduction of a chiral centre within the monomer as well as what has been conducted in literature,[4] although it can be noted in Figure 13-23 that there is a small CD signal. This is most likely signal production as a result of aggregation as noted by Professor Alison Rodger of Macquarie University (Sydney Australia), a pioneer in the CD and LD arena. Thus, based on the CD results it can be concluded that none of the polymers show chiral bias as a function of solvent composition. For further investigation as to whether ordered structures can form as a function of solvent composition, LD was conducted on the samples. Linear dichroism is a technique which is measured in a Couette cell that makes it possible induce shear alignment of potential elongated structures. This is in contrast to circular dichroism which investigates the differential absorption of right- and left-handed polarized light based on chiral structures in solution. Based on previous work on a similar foldamer system, it would be possible to track higher ordered structure formation.[5] Initially samples were run at 80% water in DMF, these samples were utilized to determine if there was any self-organization in solution *via* the intensity of the signal at 310 nm, based on the same logic utilized in CD and UV/Vis spectroscopy (Figure 13-24). Again, a solvent composition of 80% water in DMF was chosen as to ensure that if it were possible for the polymers to form ordered helical structures, that these structures would be detected *via* the LD instrument.

Based on the LD spectrum (Figure 13-24), it is noticeable that compound **31** is the only polymer that displays a signal response at 310 nm of any magnitude. This is indicative that compound **31** is the only polymer that forms ordered structures (which is based on the alignment of chromaphores relative to the shear direction induced by the Couette cell) at 80 % water in DMF (where all polymers should be forming ordered structures), this confirms all prior results from other analytical techniques utilized. In addition to conducting standard LD, time dependant LD was conducted on each of the polymers. Polymers **2** (compound **32**), **3** (compound **33**), and **4** (compound **34**), showed no dependency of LD spectra on time, this indicating that there is no movement within the system towards an ordered state (i.e., if the system were to fold into a helical structure). This was not the case with compound **31** (polymer 1), which generated the below folding profile (Figure 13-25A). The LD response at 310 nm over time was plotted in Figure 13-25B. It is evident from Figure 13-25B that polymer **1** (compound **31**) does fold. It is interesting to note that this polymer takes a long time to plateau in terms of its degree of folding (about 600 minutes). This may be a result of the polymer possibly having a low molecular

weight (<40 kDa), where although it is high enough for the polymer to fold, it is not high enough to induce folding at a fast rate (possible around 15 kDa), since the driving force for folding is low. Based on previous literature, it was noted that the polymer could readily fold when the molecular weight was close 40 kDa.[11] According to molecular modelling conducted in the work, [11] this should account for approximately 6 helical turns. Where 15 kDa would only allow for approximately 2.5 helical turns, thus not affording much stabilization in terms of π- π stacking interactions. This logic would explain why polymer 1 is the only polymer to have a high resolution ^{1}H NMR spectrum, as a clearer NMR spectrum is generally indicative of a lower molecular weight polymer. Alternatively, it may be due to the polymer having an extremely large molecular weight and thus struggling to fold in solution due to steric constraints. These hypotheses, though, are given tentatively as none could be proved at current as no accurate molecular weight data could be acquired due to limited solubility.

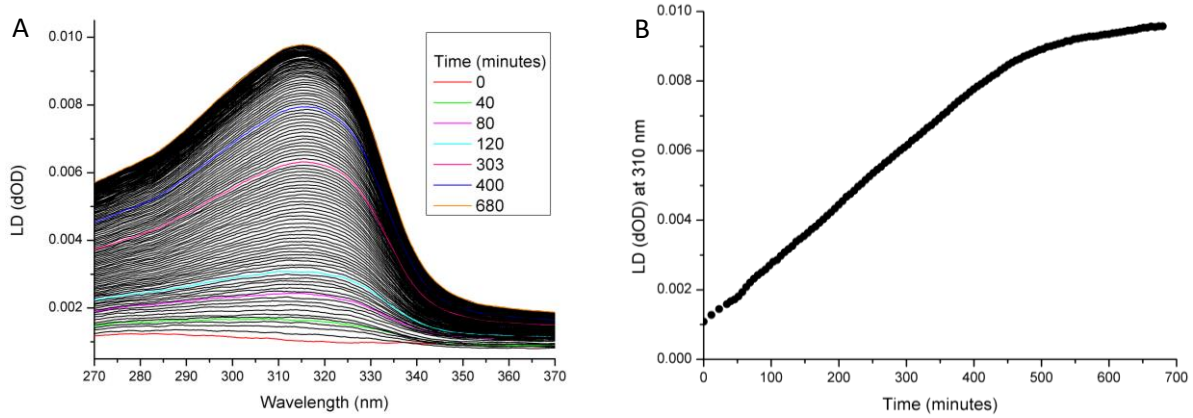

*Figure 13-25: A) LD response of polymer **1** as a function of time (minutes) at a solvent composition of 80 % water in DMF, B) the LD (dOD) response at 310 nm over time at a solvent composition of 80 % water in DMF.*

The time latency it takes to form an ordered structure suggests it would be possible to fold the polymer around a guest of adequate size i.e. poly (γ-benzyl-L-glutamate) (PBLG) as was conducted in previous literature.[11] The use of a host guest interaction could also be utilized to induce and guide folding in polymers **2** (compound **32**), **3** (compound **33**), and **4** (compound **34**), where no folding was observed (Figure 13-26). Thus, PBLG C was utilized as the guest molecule based on availability, the details of this guest can be found in previous works by Klumperman and co-workers. [11]

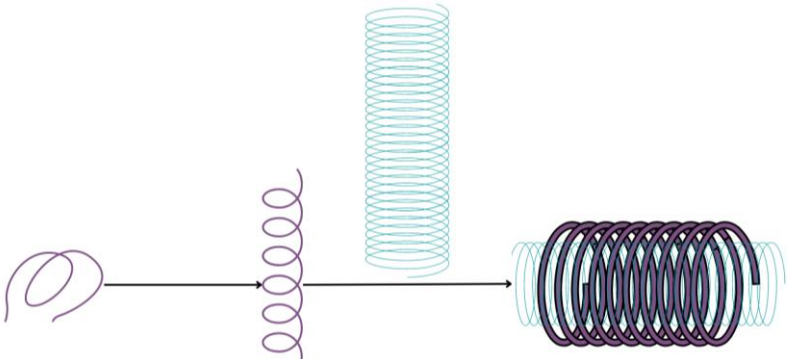

Figure 13-26: Representation of the templating process. Here the template is in blue, assisting with the folding process of the purple polymer. It assists in forming a more tightly ordered helix from a loose helix.

It should be noted that the templated polymers could only be detected when the template concentration was that of 2.00 µM and the polymer samples were of a concentration of 0.0825 µM, 0.165 µM, 0.23 µM, and 0.165 µM for polymers **1**, **2**, **3**, and **4** respectively. The host - guest interactions were measured at a solvent composition of 50 % water in DMF as opposed to 80% water in DMF to ensure that the polymer was in a transition folding state so that it could fold around the guest and not immediately stacking into ordered structures. Thus, the lower water percentage (50 % water compared to 80 % water) ensured that the polymer was both in a dynamic folding state as well as ensuring that the polymer would be in an ordered state to be detected by the LD spectrometer.

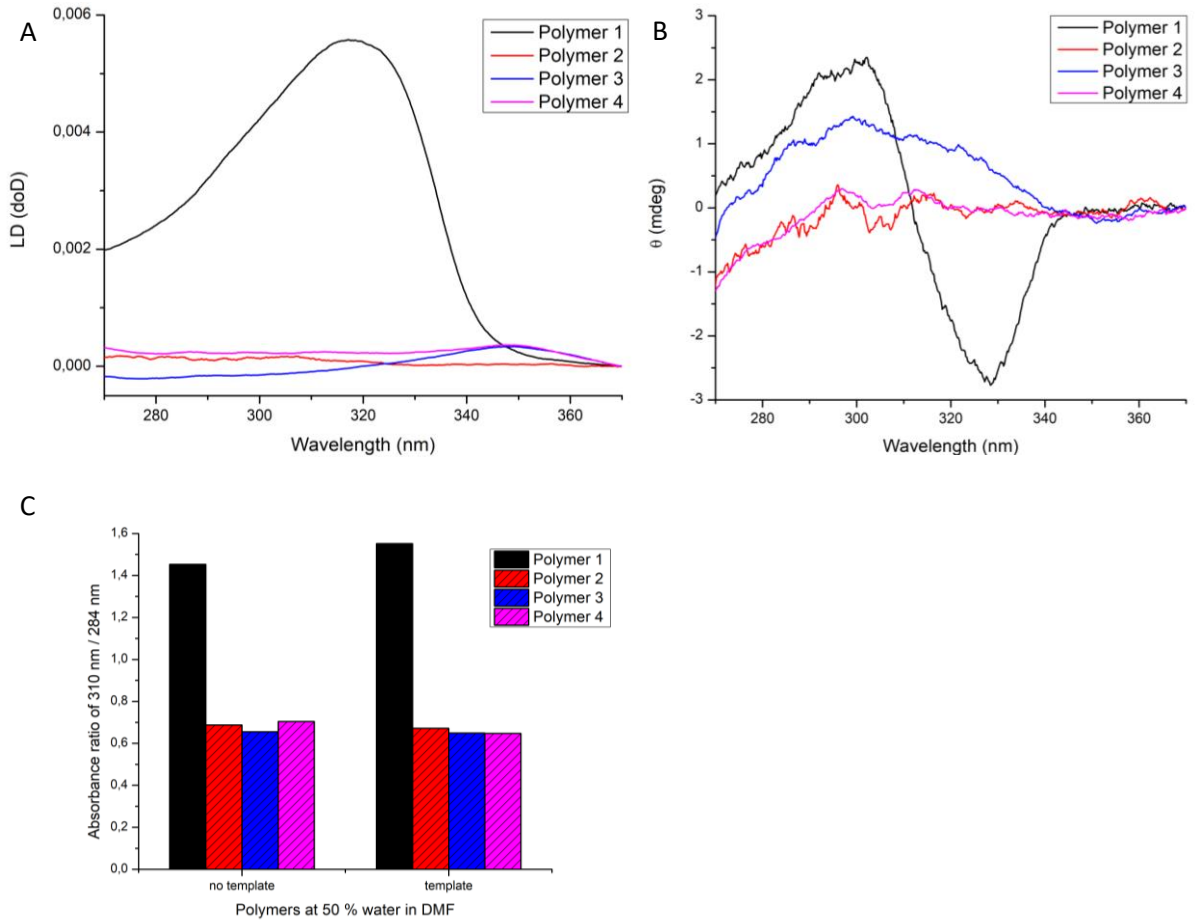

*Figure 13-27: A) LD spectra of polymers **1** (0.0825 µM), **2** (0.165 µM), **3** (0.23 µM), and **4** (0.165 µM), in the presence of a template (2.00 µM), PBLG, at a solvent composition of 50 % water in DMF,B) CD spectra of the same polymer and template samples, C) comparison of the UV/Vis data of the templated assisted to the non-templated assisted polymers at the ratio of 310 nm to 284 nm at a solvent composition of 50 % water in DMF.*

Inspecting Figure 13-27A, it is evident that the guest molecule did not induce folding in polymers **2** (compound **32**), and **4**(compound **34**), instead the guest only interacted with polymer **1** (compound **31**) and slightly with polymer **3**(compound **33**). This is evident *via* the signal present at 310 nm in polymer **1** and a very small signal in polymer **3** and no signal in polymers **2**, and **4**. To determine if the guest induced a chiral bias, CD spectra were acquired of the samples (Figure 13-27B). It can be noted that the chiral guest had successfully induced a chiral bias in a polymer that originally had none, that of polymer **1**. This is indicative through the now present signal in Figure 13-27B compared to Figure

13-23A. It can also be noted that polymer **3** has also acquired a chiral bias as a result of binding around the guest, although this bias is not as prominent as it does not have the same profile as that of polymer **1** or that of previous work conducted by Klumperman and co-workers. [11] Polymers **2** and **4** on the other hand have no chiral bias imparted onto the polymers from the guest. UV/Vis data was thereafter acquired of the templated samples, the data was used to acquire the ratio of 310 nm to 284 nm. This data was compared to that of the polymers that were not in the presence of the template. Ideally the template would assist and promote polymer folding and thus increase the ratio value (Figure 13-27C). Inspection of Figure 13-27C reveals that only polymer **1** increases in the ratio 310 nm/284 nm value, thus indicating that polymer **1** is the only polymer that significantly interacts with (and is stabilized by) the guest molecule. All other polymers are destabilized by the presence of the template, this is indicated by a decrease in the ratio value. Taking all the previously mentioned information it is possible to draw conclusions and produce a few educated and informed guesses based on the acquired data as to what may be occurring in the systems developed.

13.3 Discussion and summary of results

The investigation began with a molecular dynamics computational modelling of a library of four polymers to determine if the introduction of hydrogen bonding moieties (amide functional groups) within the pendant groups attached to a *para*-aryl triazole monomeric unit would stabilize the formed helical structure. It was determined that the amide groups stabilize the helix significantly and tighten the helical turns. It should be noted that the model does not take into account the formation of the helical structures (the folding process) and assumes the helix can form without being inhibited *via* the introduction of hydrogen bonding groups to the monomers.

The library of the four polymers was successfully synthesized and characterized with assistance of a number of different types of NMR spectroscopy (both one dimensional and two dimensional). Utilizing variable temperature ^{1}H NMR spectroscopy it was possible to identify hydrogen bonding moieties and compare the strength/ability of the moieties in the monomeric units to hydrogen bond. It was determined that the strength of the hydrogen bonds generated from amide groups is stronger than that from the triazole proton. This is based on the difference in the gradients of the hydrogen bond donor groups as a function of temperature (the triazole proton signal gradient as a function of temperature is a less steep than that of the amide protons). In cases where two amide groups were present in a monomer, the location of the amide group in the monomeric unit did not impact its ability to hydrogen bond. This was evident *via* the amide protons in polymer **4** having the same proton signal gradient as a function of temperature.

The information from DLS was more qualitative than quantitative and it hinted towards the idea that polymer **2**, **3**, and **4**, may possibly not be able to fold into ordered structures as a function of solvent composition. This is evident as the polymers have larger distributions in size as a function of solvent composition (increasing amounts of water in DMF) compared to polymer **1**. The UV/Vis spectroscopy

data indicated that polymer **1** was the only polymer that folded into an ordered structure. This conclusion was based on the comparison of the ratios of 310 nm to 284 nm as a function of solvent composition. Where polymers **2**, **3**, and **4**, did not have much variation in the value of this ratio, polymer **1** showed changes in its ratio values that matched that which was indicated in literature. [11] From the UV/Vis data it was evident that polymer **2**, **3**, and **4**, did not have an increase in the signal at 310 nm as should occur on ordered structure formation. Instead, what was identified was that as the water content increased, so the 284 nm signal decreased. This hints at the idea that as the water content increases so the hydrophobic groups (aromatic rings) become more shield by the more hydrophilic ethylene glycol pendant chains. This would account for the decreased signal at 284 nm. Standing TEM analysis of polymer **1** provided evidence that homogenous, ordered helical structures had formed at higher percentages of water in DMF (80 % water in DMF). The CD data acquired of the polymers (without a template) proved that polymers **3** and **4** had no chiral bias which should have been present (as a result of the chiral centres present on the monomeric units) if highly ordered structures had been formed as a function of solvent composition. The LD data further confirmed that polymers **2**, **3,** and **4** (all without the template present), do not form any ordered structures as a function of solvent composition. The LD data did indicate that polymer **1** does form ordered structures. The folding kinetics at 80 % water in DMF were tracked as a function of time for polymer **1** (as well as the other polymers but this gave no change with time). The folding kinetics indicate that the polymer takes a long time to completely fold (approximately 550 minutes). To further investigate if polymers **2**, **3,** and **4**, could be persuaded to fold, a template was added to the polymer samples, that of PBLG. The effect of the introduction of the template was investigated at a solvent composition of 50 % water in DMF. The samples were investigated *via* UV/Vis spectroscopy, CD spectroscopy, LD spectroscopy. The LD spectra indicated that polymer **1** formed a definite ordered structure with the assistance of the template. In addition to this, polymer **3** generated a small LD signal. The result for polymer **4** was interesting as there was no LD spectrum without the template. Investigation of the CD spectra in the presence of the template indicated that polymer **1** had generated an ordered structure with a definite chiral bias, while polymer **3** generated an ordered structure with a CD signal. The signal generated though did not follow the signature curve shape that is characteristic of this foldamer class. Polymers **2** and **4** did not generate a chiral bias at all. Finally comparison of the 310 nm/ 284 nm ratio of the template assisted and non-template assisted polymers indicated that only polymer **1** formed a more folded structure as a result of the presence of the template in solution. This was apparent *via* comparison of the ratios, where polymer **1** had a higher ratio value in the presence of the template.

Another final piece of important information is that the molecular weight of the polymers could not be reliably determined, various attempts were made to do this including DMF SEC, HFIP SEC, and MALDI-ToF MS. All of which suffered from poor solubility of the polymer in the respective solvents. As future work, it may be possible to determine the molecular weight *via* other methods like variable

temperature SEC, a form of DOSY-NMR, or field flow fractionation or even develop a more compatible matrix for MALDI-ToF MS. But due to time constraints these avenues were not explored.

Based on all the previously mentioned data it is possible to state that polymer **1** is the only polymer that folds as a function of solvent composition. Inspection of the LD kinetic folding data of polymer **1** suggests that the polymer molecular weight is not very high <40 kDa (as noted in a previous discussion, this was the molecular weight in previous work that was required to form a polymer that could fold.[11] This is most likely as at this molecular weight sufficient helical turns could form and thus added stabilization could be acquired *via* π-π stacking). This can be stated as it took a long time for the polymer to fold (approximately 550 minutes), this hints at the idea that the polymer consists of shorter chains than would have been ideal for the folding experiments (molecular weights of around 15 kDa), although this cannot be proved as no accurate molecular weight data could be acquired of the polymer.

It was also shown that polymer **1** was the only polymer to benefit from the introduction of a template structure (PBLG). All the other polymers (which all happened to contain hydrogen bonding moieties, amide functional groups), did not fold, or in the case of polymer **3**, did fold to some degree with the assistance of a template.

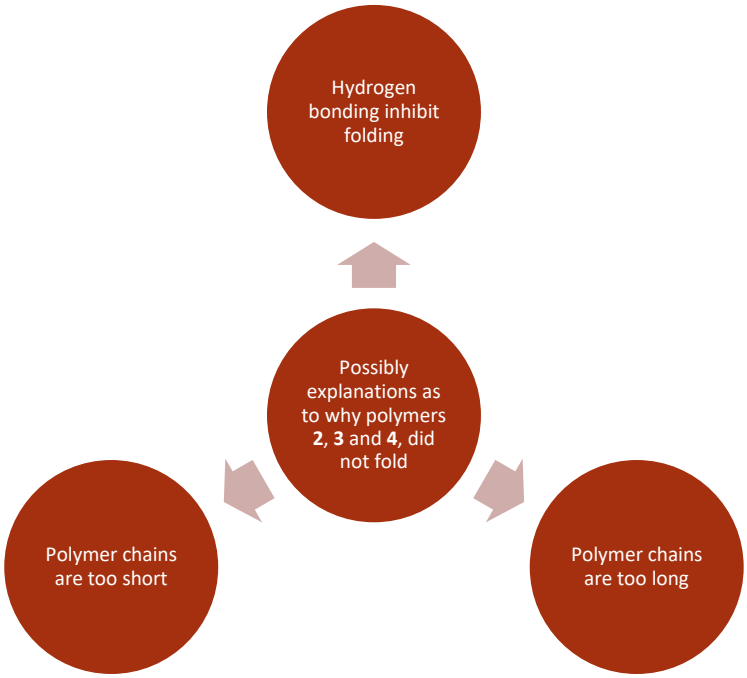

*Figure 13-28: Possible explanations as to why there is no folding occurring in polymers **2**, **3**, and **4**.*

As it was not possible to accurately determine the molecular weight of all the polymers synthesized, it is not possible to conclusively state why these amide containing polymers did not fold on their own, as polymer **1** did (although rather sluggishly). It is however possible to give several hypotheses as to why the events that occurred, did occur.

Firstly (Figure 13-28) it may be possible that polymers **2**, **3**, and **4**, were too short to fold i.e., the molecular weights of the polymers were too low. This is a possibility as the polymers showed little to no dependency on the solvent composition and showed no propensity to fold (based on the CD, LD, and UV/Vis data). During the introduction of the template, polymer 3 started to show signs of the formation of an ordered structure (LD and CD). This suggests that the polymers were too short to form a single turn of a helix and thus could not form ordered structures without the guidance of a template. What faults this hypothesis is that the polymers were only partially soluble where there was always solid residue that did not wish to dissolve. This may be as a result of the presence of very high molecular weight polymers.

The second hypothesis (Figure 13-28) as to why the polymers do not fold may be as a result of hydrogen bonding inhibiting the folding process. The model that was generated for this project was a rather rudimentary one, which did not account for the folding process. Instead, the model was only utilized to study if the introduction of amide groups within the pedant chains would have an impact on the polymer helixes (which it was shown to have a large impact based on the number of amide groups present in the monomer unit). The model did not consider the folding process. Therefore, it may be possible that the hydrogen bonding groups may be inhibiting the folding process. Thus, instead of the polymers folding into ordered structures as the water composition of the solvent increases, instead the hydrogen bonding groups could be promoting the formation of disordered conglomerates that may be packed together via hydrogen bonding groups. This hypothesis may explain the visible aggregates forming in solution and the limited solubility in solution. This again could not be proved and is merely a hypothesis.

The third and final hypothesis (Figure 13-28) as to why no folding occurred may be because of the polymers being too long. If the polymers had a large molecular weight (>70 kDa), it may be possible that the length of the polymer chains may be inhibiting the folding process. By this, it is meant that on the introduction of a large fraction of water to the solvent, the polymer does not fold, but instead forms stacks of intertwined sheets. Thus, the hydrogen bonding groups do not form a helix but form hydrogen bonded sheets of sorts. This would inhibit the folding process and would explain the limited solubility. Again, the large molecular weights cannot be proved as currently available methods could not be utilized to accurately determine the molecular weight of the polymers.

13.4 Chemicals and equipment utilized

13.4.1 Chemicals

$Pd(PPh_3)_4$ was synthesized according to a literature method.[133]

Hydrogen chloride infused ethyl acetate was prepared *via* the utilization of a gas infuser. Hydrogen chloride gas was slowly produced in a round bottom flask through the slow addition of concentrated H_2SO_4 to vigorously stirring sodium chloride. The gas was left to slowly infuse the ethyl acetate over 8 hours in the infuser. The pH of the ethyl acetate was determined *via* acid-base titration and adjusted to the required concentration via the addition of further ethyl acetate.

DCM, ethyl acetate, CuBr, tri(ethylene glycol), tri(ethylene glycol) monomethyl ether, TsCl, THF, methanol, $TsOH.H_2O$, acetonitrile, DCC, DMAP were purified according to literature.[134] All other chemicals were acquired from Sigma Life Science group.

13.4.2 Practices in the lab

Glassware was oven-dried before each reaction. Glassware utilized for inert reaction were dried at 150 °C and thereafter flushed with argon for three cycles. Note that all reactions were performed under an argon atmosphere. Column chromatography utilized 230 nm - 400 nm silica gel and thin layer chromatography utilized Macherey-Nagel DC-Fertigfolien ALUGRAM Xtra SIL G/UV254 TLC plates. Compounds were visualized on TLC using either an iodine in silica stain, UV light at 254 nm, or ninhydrin. Solvents utilized in various ratios for column chromatography include that of dichloromethane, methanol, hexane, and ethyl acetate.

13.4.3 Instruments utilized for analysis

- UV/Vis spectroscopy - UV-1800 spectrophotometer was utilized. Fast length scans were completed over a wavelength range of 270 nm – 380 nm.
- NMR – Bruker Ascend 400, a 400 MHz NMR spectrometer. Analysis of monomers and all precursors was conducted in $CDCl_3$, while polymers were characterized in DMF-d_7.
- Mass spectroscopy - Waters Synapt G2, ESI probe, ESI Pos, Cone Voltage 15 V at the Central Analytical Facility (CAF), Stellenbosch University.
- CD – Applied Photophysics, Chirascan Plus from CAF, Stellenbosch was utilized
- LD - Jasco J-1500 spectropolarimeter (Hachioji, Japan)
- IR - Thermo Nicolet Nexus FT-IR instrument using the ATR attachment.
- DLS - Zetasizer Nano Nano-S series instrument where the solvent composition range between different ratios of DMF and water
- Standing TEM - images were acquired on a Zeiss Merlin Fesem instrument at CAF, Stellenbosch.

The Schrodinger software utilized formed a part of the CHPC package provided to Professor WAL van Otterlo.

13.4.4 Experimental details for the various analytical equipment

- UV/Vis spectroscopy - Fast length scans were completed over a wavelength range of 270 nm – 380 nm. The scans had a bandwidth of 1 nm. Samples were allowed to equilibrate at 25 °C in the cuvette chamber for 3 minutes between each scan.
- NMR - Bruker Ascend 400, a 400 MHz NMR spectrometer. Analysis of monomers and all precursors was conducted in $CDCl_3$, while polymers were characterized in DMF-d_7. The number of scans required varied from 64 scans to 108 scans for the proton NMR spectra. All carbon NMR spectra were run overnight for 5000 to 10000 scans. The variable temperature proton NMR spectra were acquired *via* 1000 scans at each temperature, between each temperature there was a 10 minute equilibration time to ensure the sample was at the correct temperature.
- Mass spectroscopy - Waters Synapt G2, ESI probe, ESI Pos, Cone Voltage 15 V at the Central Analytical Facility (CAF), Stellenbosch University.
- CD - The scans were run to detect millidegrees and absorbance. The sample cuvette was set to 25 °C and each sample was allowed to equilibrate for 5 minutes before any scans were run. The bandwidth was that of 1 nm and ran between 270 nm to 400 nm in 1 nm increments.
- LD - Firstly data was measured at 2.9 V (~1000 rpm of the spinning cuvette) and then measured at 0 V. The scans were collected at a bandwidth of 1 nm between 200 nm and 800 nm. All runs were conducted at 25 °C in a temperature regulated spinning cell.
- IR - A fast scanning rate was conducted with 64 scans completed in total. No solvent was utilized in this scan and after each scan the spectrometers crystal was cleaned with acetone and thereafter methanol.
- DLS - Scans were conducted in the following manner. The cuvette was first loaded with the required sample *via* syringe. Once load the cuvette was allowed to equilibrate in the machine for 300 seconds at 25 °C. Thereafter 11 runs (10 seconds each) were conducted for 3 measurements. This procedure was then repeated in triplicate.
- Standing TEM - This was conducted *via* CAF staff, the exact conditions utilized to acquire each image is stated at the bottom of each image.

13.5 Computational supplementary information

Computational calculations were conducted in the Material Science program which is part of the Schrodinger Suite 2021-4. Each foldamer structure was determined according to the below procedure. A foldamer was generated with the polymer builder application, where 50 repeat units were utilized. The chain growth was conducted with all backbone dihedral angles set to 180 º. Once the foldamer was generated the structure was minimized according to the OPLS4 forcefield in a TIP4P water model to generate the most stable structure in vacuo. Once the most stable conformation was determined, a system builder application was run to build a water box to surround the foldamer system. This would be utilized for the later molecular dynamics and trajectory calculations. The box was chosen to be orthorhombic in shape with 1 Å buffer space between the foldamer and the edge of the box. The TIP4P solvent model was selected, utilizing the OPLS4 forcefield. Once the foldamer has been placed in the box filled with water (TIP4P solvent model), a molecular dynamics multistage workflow was setup. In this workflow, a Brownian minimization was first conducted (with a simulation time of 100 ps) and thereafter a molecular dynamics calculation was conducted. In this calculation the simulation time was determined to be 100 ns. With approximately 1000 frames being recorded. The temperature was set to a constant 300.0 K, as well a s a pressure of 1.01325 bar. The ensemble class was selected as NPT for the follow simulations. During this time the trajectory was also recorded.

13.6 Sample preparation for analyses reported in the supplementary information

This procedure was utilized for the preparation of samples to be tested *via* UV/Vis, CD, DLS, Standing TEM, and LD.

Polymer DMF stock solution.

An amount of polymer as indicated in Table 2 was dissolved in the below-indicated amount of anhydrous DMF to afford the dissolved polymer stock solutions.

Table 2: Amounts of polymer (mg) and volumes of DMF (mL) utilized to make stock solutions for each polymer.

Polymer	Amount of polymer	Amount of DMF	Repeat unit concentration
1	2.0 mg	1.30 mL	3.29 µM
2	2.0 mg	1.30 mL	3.30 µM
3	2.5 mg	1.40 mL	3.32 µM
4	2.5 mg	1.24 mL	3.31 µM

The sample solutions were then made utilizing the above stock solutions. Below is an example of how a sample was made. The final concentrations of the samples were determined *via* a quick UV analysis to determine the correct intensity of absorbance in solution (~ 1 Abs).

For a sample of polymer **1** dissolved in 40 % water in DMF

In an empty polytop, the required amount of stock solution (0.0125 mL) was added. Thereafter 0.7875 mL (this can be added normally, i.e., not dropwise) of anhydrous DMF was added to the polytop. The polytop was then given a swirl and left it to diffuse for one hour to make sure the solution was homogenous. Once homogenous, water was added dropwise (0.2000 mL) to the sample. With swirling done between each drop of water. The final sample was then left to sit for a further hour before taking the required measurements. When not working with the sample, the polytop was closed as DMF is hygroscopic.

This was then conducted for a number of samples for polymer **1** as stated below in Table 3.

*Table 3: Samples prepared for polymer **1**.*

experiment number	Titration percentage of DMF (%)	volume of stock solution (mL)	concentration of final vial (uM)	Total volume (mL)	volume of filler DMF (mL)	Volume of water (mL)
1	100	0.025	0.041	2.000	1.975	0.000
2	90	0.025	0.041	2.000	1.775	0.200

experiment number	Titration percentage of DMF (%)	volume of stock solution (mL)	concentration of final vial (uM)	Total volume (mL)	volume of filler DMF (mL)	Volume of water (mL)
3	80	0.025	0.041	2.000	1.575	0.400
4	70	0.025	0.041	2.000	1.375	0.600
5	60	0.025	0.041	2.000	1.175	0.800
6	50	0.025	0.041	2.000	0.975	1.000
7	40	0.025	0.041	2.000	0.775	1.200
8	30	0.025	0.041	2.000	0.575	1.400
9	20	0.025	0.041	2.000	0.375	1.600
10	10	0.025	0.041	2.000	0.175	1.800
11	98	0.013	0.041	1.000	0.968	0.020
12	96	0.013	0.041	1.000	0.948	0.040
13	94	0.013	0.041	1.000	0.928	0.060
14	92	0.013	0.041	1.000	0.908	0.080
15	85	0.013	0.041	1.000	0.838	0.150
16	75	0.013	0.041	1.000	0.738	0.250
17	65	0.013	0.041	1.000	0.638	0.350
18	55	0.013	0.041	1.000	0.538	0.450
19	53	0.013	0.041	1.000	0.518	0.470
20	51	0.013	0.041	1.000	0.498	0.490
21	49	0.013	0.041	1.000	0.478	0.510
22	47	0.013	0.041	1.000	0.458	0.530
23	45	0.013	0.041	1.000	0.438	0.550
24	43	0.013	0.041	1.000	0.418	0.570
25	41	0.013	0.041	1.000	0.398	0.590
26	39	0.013	0.041	1.000	0.378	0.610
27	37	0.013	0.041	1.000	0.358	0.630
28	35	0.013	0.041	1.000	0.338	0.650
29	33	0.013	0.041	1.000	0.318	0.670
30	31	0.013	0.041	1.000	0.298	0.690
31	29	0.013	0.041	1.000	0.278	0.710
32	27	0.013	0.041	1.000	0.258	0.730
33	25	0.013	0.041	1.000	0.238	0.750
34	23	0.013	0.041	1.000	0.218	0.770
35	21	0.013	0.041	1.000	0.198	0.790
36	19	0.013	0.041	1.000	0.178	0.810
37	17	0.013	0.041	1.000	0.158	0.830
38	15	0.013	0.041	1.000	0.138	0.850
39	13	0.013	0.041	1.000	0.118	0.870
40	11	0.013	0.041	1.000	0.098	0.890
41	9	0.013	0.041	1.000	0.078	0.910
42	7	0.013	0.041	1.000	0.058	0.930
43	5	0.013	0.041	1.000	0.038	0.950
44	13	0.013	0.041	1.000	0.118	0.870
45	3	0.013	0.041	1.000	0.018	0.970

experiment number	Titration percentage of DMF (%)	volume of stock solution (mL)	concentration of final vial (uM)	Total volume (mL)	volume of filler DMF (mL)	Volume of water (mL)
46	2	0.013	0.041	1.000	0.008	0.980
47	88	0.013	0.041	1.000	0.868	0.120
48	86	0.013	0.041	1.000	0.848	0.140
49	84	0.013	0.041	1.000	0.828	0.160
50	82	0.013	0.041	1.000	0.808	0.180
51	78	0.013	0.041	1.000	0.768	0.220
52	76	0.013	0.041	1.000	0.748	0.240
53	74	0.013	0.041	1.000	0.728	0.260
54	72	0.013	0.041	1.000	0.708	0.280
55	68	0.013	0.041	1.000	0.668	0.320
56	66	0.013	0.041	1.000	0.648	0.340
57	64	0.013	0.041	1.000	0.628	0.360
58	62	0.013	0.041	1.000	0.608	0.380
59	58	0.013	0.041	1.000	0.568	0.420
60	56	0.013	0.041	1.000	0.548	0.440

Final sample concentrations:

- Polymer **1** – 0.04125 µM
- Polymer **2** – 0.08250 µM
- Polymer **3** – 0.11550 µM
- Polymer **4** – 0.08250 µM

This was then similarly conducted on polymers **2**, **3**, and **4**.

Templating studies example with polymer **1**

A stock solution of the template was made where PBLG of a molecular weight of 162900 g/mol (4.07 mg) in 5 mL of DMF to achieve a stock solution with a concentration of 5.0 µM

The two stock solutions (of the template and the stock solution of the polymer from Table 2) were then added together (in varying quantities according to the percentage of DMF in water) and mixed to make a homogenous DMF mixture. Thereafter the required amount of water was added dropwise (amount depending on the ratio of water to DMF tested).

13.7 Synthetic supplementary information

13.7.1 Synthesis of compound **2**, 2-(2-(2-(trityloxy)ethoxy)ethoxy)ethan-1-ol

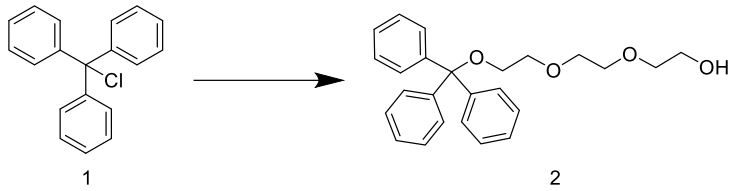

1 2

The synthetic procedure and signal assignment was based on work described in the literature.[125]

A two-necked, 500 mL round-bottomed flask was charged with dry tri(ethylene glycol) (17.238 g, 114.79 mmol, 6.4 eq.), an oval-shaped magnetic stir bar. and toluene (50 mL). The side-neck was equipped with an adaptor attached to the argon line. Thereafter, the flask was flushed with argon and triethylamine (3.20 mL, 2.32 g, 23.0 mmol, 1.3 eq.) was injected *via* a syringe in a single portion, followed by trityl chloride (5.000 g, 17.94 mmol, 1 eq.) was added over 10 minutes through the main neck against while there was argon flowing *via* the side neck. After the addition was completed, the flask was rinsed with toluene (15 mL) and the central neck equipped with a glass stopper. The adaptor connected to the argon line was disconnected and exchanged for a silicon oil bubbler, after which the flask was left to stir vigorously for 3 hours at room temperature. Ethyl acetate (50 mL) was subsequently added to the mixture, and it was stirred for an additional 10 minutes. The mixture was filtered through a sintered funnel and the solid washed with ethyl acetate (2 × 40 mL). The filtrate was then added to a 400 mL separation funnel and washed sequentially with water (3 × 75 mL), a saturated aqueous solution of ammonium chloride (2 × 40 mL) and thereafter brine (100 mL). The organic layer was then transferred to a 500 mL Erlenmeyer flask and dried over anhydrous sodium sulfate for 1 hour. The dried mixture was then filtered into a 250 mL round-bottomed flask and the solvent removed *via* rotary evaporation. A magnetic stir bar was then placed into the flask and the solution was left stirring under vacuum overnight to afford the crude product (compound **2**) as a viscous light-yellow oil (~7.22 g, yield difficult to determine as compound not completely dry). This compound was utilized in the next step without further purification as the NMR spectroscopic analysis proved satisfactory and compared well with that reported in the literature. [125]

^{1}H NMR (400 MHz, $CDCl_3$) δ: 7.40—7.37 (m, 5H), 7.23—7.13 (m, 10H), 3.67—3.59 (m, 8H), 3.55—3.53 (m, 2H), 3.19—3.15 (m, 2H), 2.25 (s, 1H, OH); ^{13}C NMR (100 MHz, $CDCl_3$) δ: 144.25, 128.84, 127.87, 127.02, 86.67, 72.72, 71.01, 70.88, 70.52, 63.42, 61.84.

13.7.2 Synthesis of compound **3**, 2-(2-(2-(trityloxy)ethoxy)ethoxy)ethyl 4-methylbenzenesulfonate

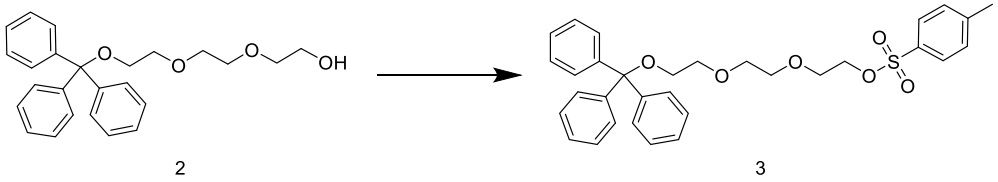

2 3

The synthetic procedure and signal assignment was based on work already described in the literature.[125]

Compound **2** (around 35.20 g as compound still has solvent present, around 89 mmol as starting material not completely dry) was added to a 500 mL round-bottomed flask. THF (140 mL) and a large oval-shaped magnetic stir bar was then added, and the mixture was stirred and cooled for 1 hour in an ice bath. Meanwhile, sodium hydroxide (14.35 g, 358.7 mmol, 4 eq.) was added to a 200 mL beaker and dissolved in distilled water (45 mL). This mixture was then left to cool to room temperature. The sodium hydroxide solution was next added in a single portion to the flask containing **2**, after which the mixture was stirred at 0 °C for 2 hours. The flask was thereafter equipped with a 300 mL dropping funnel (with a loosely attached stopper). At the same time *para*-toluenesulfonyl chloride (19.50 g, 102.2 mmol, 1.14 eq.) was added to a 200 mL beaker and dissolved in THF (45 mL), after which the solution was transferred to a dropping funnel. The solution was then added (at a rate of about 4 drops a second) to the stirring reaction mixture over the span of 20 minutes. Once all the components were added, the dropping funnel was exchanged for a stopper. The mixture was then vigorously stirred at 0 °C for 5 hours. Once completed, the ice bath was removed, and the mixture stirred at room temperature overnight (about 12 hours). Water (20 mL) and diethyl ether (120 mL) were then added to the flask and its contents were transferred to a 500 mL separating funnel. After separation, the aqueous phase was discarded, and the organic phase was washed with water (60 mL) and thereafter brine (2 × 60 mL). The organic layer was then transferred to a 400 mL Erlenmeyer flask and dried over anhydrous sodium sulfate for 2 hours. The resulting yellow liquid was filtered into a 1L round-bottomed flask and the solution was concentrated *via* rotary evaporation. An oval-shaped magnetic stir bar was placed into the flask and the solution was left to stir under vacuum overnight to afford compound **3** as a gum-like yellow liquid (50.6 g, 103.2% crude yield as no column chromatography was used to purify the product). Compound **3** was used in the following step without further purification as the NMR spectroscopic analysis proved satisfactory and compared well with that reported in the literature.[125]

^{1}H NMR (400 MHz, $CDCl_3$) δ: 7.71—7.69 (m, 2H), 7.39—7.37 (m, 7H), 7.23—7.18 (m, 10H), 4.09—4.07 (m, 2H), 3.65—3.53, (m, 8H), 3.16—3.13 (m, 2H), 2.33 (s, 3H); ^{13}C NMR (100 MHz, $CDCl_3$) δ: 144.86, 144.22, 129.92, 128.84, 128.11, 127.90, 127.08, 86.69, 71.01, 70.88, 69.40, 68.92, 63.43. The signal at 21.8 is missing according to literature.[125]

13.7.3 Synthesis of compound **4**, 1,1,1-triphenyl-2,5,8,11,14,17,20-heptaoxahenicosane

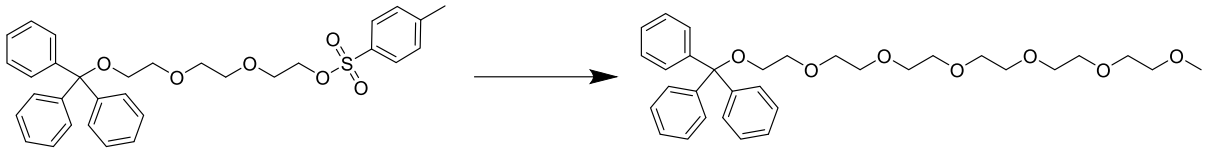

3 4

The synthetic procedure and signal assignment was based on work already described in the literature.[125]

An oven-dried, 500 mL two-necked round-bottomed flask was and an adaptor connected to an argon line. Once connected to the argon line, the flask was flushed with argon and equipped with an oval-shaped magnetic stir bar and a stopper. While the gas continued to flow through the side neck, sodium hydride (60% dispersion in paraffin, 5.610 g, 140.1 mmol, 1.5 eq.) was added through the main neck against the gas flow. The dispersion was then washed out with dry hexane (3 x 15 mL) leaving a grey solid behind. The flask was thereafter charged with dry THF (120 mL). The central neck was subsequently equipped with a 300 mL dropping funnel with a loosely attached stopper. The suspension was subsequently left to cool in an ice-water bath for 20 minutes. Dry tri(ethylene glycol) monomethyl ether (113.5 g, 691.5 mmol, 7.4 eq.) was added to the dropping funnel, the argon flow stopped and then added to the suspension of sodium hydride over 20 minutes. Subsequently the argon gas flow was re-introduced and a solution of compound **3** [(~50.6 g, ~93.4 mmol, unpurified from previous reaction) in dry THF (48 mL)] was added to the dropping funnel. The solution of compound **3** was then added to the reaction mixture over 10 minutes, after which the ice bath was removed. The dropping funnel was thereafter exchanged with a condenser fitted with a calcium chloride drying tube. The adaptor connecting the flask to the argon line was disconnected and exchanged for a stopper and the reaction mixture was heated in an oil bath (80 °C) under reflux for 6 hours. The oil bath was then removed, and the solution was left to cool to room temperature. Brine (100 mL) and water (100 mL) were added, and the solution was transferred to a 1 L separation funnel. The aqueous phase was discarded and the organic phase was washed sequentially with a water and brine mixture (1:1 v/v, 2 × 100 mL) and pure brine (100 mL). The solution was then transferred to a 1 L Erlenmeyer flask and dried over anhydrous sodium sulfate for 2 hours, after which it was filtered into a 1 L round-bottomed flask and concentrated *via* rotary evaporation. A magnetic stir bar was placed in the flask and the solution was left to stir under vacuum overnight (about 12 hours) to afford compound **4** as a yellow gum (54.28 g, crude yield of 107% without column chromatography), the compound was utilized in the following step without additional purification as the NMR spectroscopic analysis proved satisfactory and compared well with that reported in the literature.[125]

^{1}H NMR (400 MHz, $CDCl_3$) δ: 7.47—4.45 (m, 6H), 7.31—7.27 (m, 6H), 7.24—7.20 (m, 3H), 3.70—3.62 (m, 20H), 3.55—3.52 (m, 2H), 3.37 (s, 3H), 3.25—3.22 (m, 2H). ^{13}C NMR (100 MHz, $CDCl_3$) δ:

144.24, 128.83, 127.86, 127.02, 86.65, 72.04, 70.90, 70.81, 70.79, 70.68, 63.44, 59.14. It should be noted that the number of carbon atom signals is far from that of the number of carbon atoms in the molecule. This may be because of carbon signal overlap. Although it should be noted that the spectra match that as which was reported in literature. [125]

13.7.4 Synthesis of compound **5**, 2,5,8,11,14,17-hexaoxanonadecan-19-ol

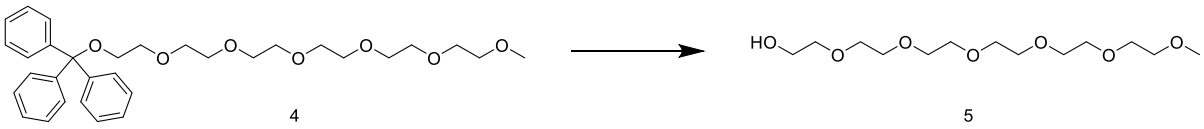

The synthetic procedure and signal assignment was based on work completed in the literature.[125]

Compound **4** (54.28 g, roughly 100.8 mmol as unpurified from previous reaction) was added to a single necked, 500 mL round-bottomed flask equipped with an oval-shaped magnetic stir bar and was dissolved in methanol (216 mL). *para*-Toluenesulfonic acid monohydrate (0.77 g, 4.03 mmol, 0.04 eq.) was thereafter added to the mixture and was stirred overnight (around 12 hours) at 25 °C. Once completed, ice was slowly added to the mixture to induce precipitation. This addition continued until no more precipitate formed. Water (150 mL) was thereafter slowly added to the mixture over 10 minutes and the mixture was then cooled in an ice bath. The mixture was then filtered and the solid rinsed with water (5 × 50 mL). The filtrate was then concentrated *via* rotary evaporation. A magnetic stir bar was then placed into the flask and the product was left stirring under vacuum overnight (about 18 hours) to afford a dry compound **5** as a yellow oil (29.9 g, impossible to determine percentage yield as no purification method was utilized), the compound was utilized in the following steps without additional purification as the NMR spectroscopic analysis proved satisfactory and compared well with that reported in the literature.[125]

^{1}H NMR (400 MHz, $CDCl_3$) δ: 3.73—3.71 (m, 2H), 3.67—3.59 (m, 20H), 3.55—3.52 (m, 2H), 3.44 (s, 1H, OH), 3.37 (s, 3H). ^{13}C NMR (100 MHz, $CDCl_3$) δ: 71.99, 70.61, 70.58, 70.54, 70.52, 70.33, 61.74, 59.11; It should be noted that the number of carbon atom signals is far from that of the number of carbon atoms in the molecule. This may be because of carbon signal overlap. Although it should be noted that the spectra match that as which was reported in literature. [125] MS (ESI): *m/z* = 297.17 (calculated 297.36 for [M + H^+]), 314.21 (calculated 314.36 for [M + NH_4^+]), 319.17 (calculated 319.36 for [M + Na^+]), 335.14 (calculated 335.36 for [M + K^+]).

13.7.5 Synthesis of compound **6**, 2,5,8,11,14,17-hexaoxanonadecan-19-yl 4-methylbenzenesulfonate

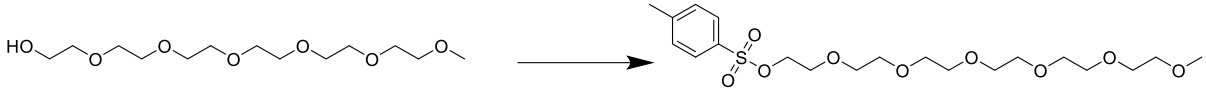

5 6

The synthetic procedure and signal assignment was based on work completed in the literature.[125]

Compound **5** (6.00 g, 20.2 mmol) was placed into a 150 mL, two-necked, round-bottomed flask equipped with an oval-shaped magnetic stir bar and was dissolved in dry THF (42 mL). An adaptor connected to an argon line was connected to the side neck of the flask and argon was flushed into the flask. The solution was then stirred and cooled for 30 minutes on an sodium chloride ice bath. At the same time sodium hydroxide (3.65 g, 91.105 mmol, 4.5 eq.) was added to a 50 mL beaker. Distilled water (12 mL) was thereafter added to the beaker, and it was then left to cool to room temperature. Once at room temperature the sodium hydroxide solution was added in a single portion to the 150 mL flask. The mixture was stirred at 0 °C for 1 hour. The flask was then equipped with a 300 mL dropping funnel with a loosely attached stopper. *para*-Toluenesulfonyl chloride (4.90 g, 25.7 mmol, 1.27 eq.) was then added to a 200 mL beaker and dissolved in THF (12 mL). The solution was then added to the dropping funnel. The solution was subsequently slowly added (5 drops a second) to the reaction mixture over 30 minutes. Thereafter the dropping funnel was removed and replaced with a loosely attached stopper. The mixture was subsequently stirred at 0 °C for 2 hours. The ice bath was then removed, and the mixture was left to stir at 25 °C overnight (about 12 hours). Once completed, the solution was diluted with water (40 mL) and diethyl ether (60 mL) and transferred to a 500 mL separatory funnel. The aqueous layer was then discarded, and the organic layer was washed with water (50 mL) and brine (2 x 60 mL). The organic layer was thereafter transferred to a 1 L round-bottomed flask and dried over anhydrous sodium sulfate over 3 hours. The resulting yellow liquid was filtered into a 1 L round-bottomed flask and the solution was concentrated *via* rotary evaporation. A magnetic stir bar was then placed into the flask and the product was left stirring under vacuum for one hour to afford the compound **6** as a yellow gum-consistency (6.38 g, 69% yield, the product was not isolated *via* column chromatography and was utilized as a light-yellow oil).

^{1}H NMR (400 MHz, $CDCl_3$) δ: 7.79 (d, J = 8.0 Hz, 2H), 7.33 (d, J = 8.0, 2H), 4.16—4.14 (m, 2H), 3.69—3.57 (m, 20H), 3.55—3.51 (m, 2H), 2.72 (s, 3H), 2.44 (s, 3H); ^{13}C NMR (100 MHz, $CDCl_3$) δ: 144.89, 133.15, 129.93, 128.09, 72.05, 70.87, 70.73, 70.68, 70.63, 69.36, 68.80, 59.15, 21.76. These signals match what is found in literature. [125]

13.7.6 Synthesis of compound **7**, 19-azido-2,5,8,11,14,17-hexaoxanonadecane

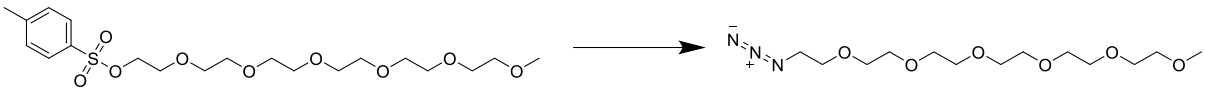

6 7

The synthetic procedure and signal assignment was based on work completed in the literature.[126]

A 150 mL oven-dried, two-necked, round-bottomed flask equipped with an oval-shaped magnetic stir bar was flush with argon *via* an adaptor connected to the side neck of the flask. Once the flask was purged, both compound **6** (3.0 g, 6.7 mmol) and acetonitrile (50 mL) was added to the flask *via* the central neck of the flask. Sodium azide (0.80 g, 12.3 mmol, 1.85 eq.) was then added and a stopper was then loosely fitted to the central neck of the flask. The mixture was then stirred at 78 °C for 24 hours. Subsequently the mixture was left to cool to room temperature and the contents were filtered into a round-bottomed flask. The filtrate was then concentrated *via* rotary evaporation and the residue was thereafter purified by column chromatography on silica (MeOH-DCM, 5:95) to give compound **7** as a green oil (1.2586 g, 59%).

^{1}H NMR (400 MHz, $CDCl_3$) δ: 3.66—3.61 (m, 20H), 3.53—3.52 (m, 2H), 3.37—3.36 (m, 2H), 3.36 (s, 3H); ^{13}C NMR (100 MHz, $CDCl_3$) δ: 72.06, 70.83, 70.80, 70.76, 70.73, 70.69, 70.64, 70.15, 59.15, 50.82; IR: 2869, 2099, 1452, 1348, 1285, 1247, 1099, 1030, 943, 851; MS (ESI): *m/z* = 322.20 (calculated 322.37 for $[M + H^+]$), 339.22 (calculated 339.37 for $[M + NH_4^+]$), 344.18 (calculated 344.37 for $[M + Na^+]$), 360.15 (calculated 360.37 for $[M + K^+]$). The spectra match that as was found in literature. [126]

13.7.7 Synthesis of compound **8**, 2,5,8,11,14,17-hexaoxanonadecan-19-amine

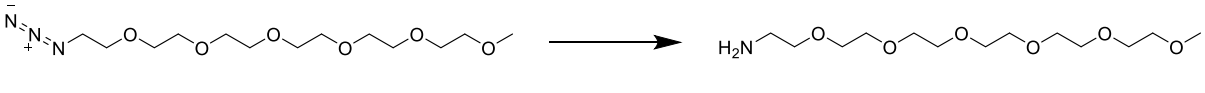

7 8

The synthetic procedure and signal assignment was based on work completed in the literature.[126]

A 150 mL oven-dried, three-necked, round-bottomed flask equipped with an oval-shaped magnetic stir bar was flushed with argon *via* an adaptor connected to one of the side necks of the flask. Once the flask was purged, compound **7** (0.62 g, 1.93 mmol), and 10 % palladium carbon (0.0263 g) were added to the flask and dissolved in methanol (12 mL). A hydrogen environment was then generated within the flask. This was conducted *via* the sealing of the top neck of the flask with a greased glass stopper. Then

replacing the argon line adaptor with a vacuum line adaptor on the side neck of the flask. A hydrogen filled balloon was then connected to the other side neck of the flask. Following this the flask was evacuated *via* utilisation of a vacuum pump and subsequently the flask was filled with hydrogen gas. This cycle was repeated three time. After the last cycle the balloon was left connected to the flask to ensure there was sufficient hydrogen gas to drive the reaction. The reaction was left to stir at 25 °C overnight (about 12 hours). Subsequently the mixture was filtered through Celite and concentrated *via* rotary evaporation to give compound **8** as a dark green oil (0.5649 g, quantitative yield).

^{1}H NMR (400 MHz, $CDCl_3$) δ: 3.60—3.658 (m, 18H), 3.53—3.45 (m, 4H), 3.32 (s, 3H), 2.82— 2.74 (m, 2H), 1.91(s, 2H, NH_2); ^{13}C NMR (100 MHz, $CDCl_3$) δ: 73.19, 71.93, 71.91, 70.73, 70.60, 70.57, 70.54, 70.53, 70.51, 70.49, 70.35, 70.28, 58.99, 41.73; IR: 2867, 1458, 1349, 1298, 1248, 1199, 1098, 946, 850; MS (ESI): *m/z* = 296.20 (calculated 296.20 for [M + H^+]), 318.19 (calculated 318.20 for [M + Na^+]). The spectra matches that found in literature. [126]

13.7.8 Synthesis of compound **9**, 2,5,8,11,14,17-hexaoxanonadecan-19-yl (tert-butoxycarbonyl)- D-alaninate

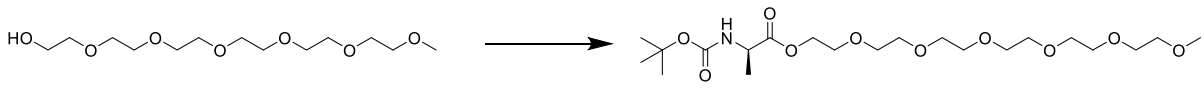

5 9

The synthetic procedure and signal assignment was based on work completed in the literature.[129]

A 150 mL oven-dried, two-necked, round-bottomed flask equipped with an oval-shaped magnetic stir bar was flush with argon *via* an adaptor connected to the side neck of the flask. The reaction flask was then cooled to 0 °C. Once the flask was purged, compound **5** (3.00 g, 10.1 mmol), N-Boc-(L)-alanine (1.92 g, 10.1 mmol, 1.00 eq), DMAP (0.15 g, 1.22, 0.12 eq), and freshly distilled DCM (18 mL) were added to the flask *via* the top neck of the flask. Once the contents of the flask had become homogenous, DCC (2.09 g, 10.1 mmol, 1.00 eq.) was added portion-wise over the span of 5 minutes. The mixture was then left to stir for 1 hour at 0 °C, followed by stirring at room temperature for 12 hours. Subsequently the reaction mixture was filtered into a round-bottomed flask, thereafter the precipitate was washed with ethyl acetate (3 x 30 mL). The filtrate was then concentrated *via* rotary evaporation and the residue was purified by column chromatography on silica (MeOH-DCM, 5:95) to give compound **9** as an orange oil (4.062 g, 94%).

^{1}H NMR (400 MHz, $CDCl_3$) δ: 5.09 (s, 1H, NH), 4.27—4.23 (m, 2H), 3.65 (t, J = 8.0 Hz, 2H) , 3.59—3.51 (m, 18H), 3.51—3.49 (m, 2H), 3.33 (s, 3H), 1.40 (s, 9H), 1.35 (d, J= 8.0 Hz, 3H); ^{13}C NMR (100 MHz, $CDCl_3$) δ: 173.35, 155.12, 79.76, 71.98, 70.67, 70.65, 70.62, 70.61, 70.55, 68.97, 64.33, 64.27,

59.06, 53.51, 28.38, 18.74; IR: 3550.71, 2976.04, 2872.54, 1743.57, 1711.72, 1519.22, 1453.87, 1390.54, 1365.51, 1348.18, 1297.96, 1248.37, 1163.87, 1102.69, 1067.88, 948.94, 854.74, 732.57; MS (ESI): *m/z* = 468.28 (calculated 468.27 for [M + H^+]), 485.30 (calculated 485.27 for [M + NH_4^+], 490.26 (calculated 490.27 for [M + Na^+]), 506.23 (calculated for 506.27 for [M + K^+]). The spectra acquired match that in literature. [129]

13.7.9 Synthesis of compound **10**, 2,5,8,11,14,17-hexaoxanonadecan-19-yl D-alaninate

9 10

A 100 mL oven-dried, two-necked, round-bottomed flask equipped with an oval-shaped magnetic stir bar was flush with argon *via* an adaptor connected to the side neck of the flask. Compound **9** (2.40 g, 5.14 mmol) was added through the central neck against argon flow. Thereafter HCl infused ethyl acetate (1 M, 30 mL) was added through the central neck with the aid of a glass syringe. The reaction was stirred for 5 hours at room temperature. Once the reaction had taken place the solvent was evaporated under vacuum and the excess HCl was removed *via* the addition of DCM (26 mL) and *n*-BuOH (1 mL). This was followed by evaporation overnight. The residual *n*-BuOH was then removed *via* azeotropic distillation with DCM (3 x 50 mL). The end product was not purified and utilized as crude material in the next step. Reaction conversion was confirmed *via* TLC and ^{1}H NMR with the emergence of a baseline peak ~ 8.5 ppm which represents the NH_2 of the deprotected amine group. Further confirmation was the emergence of mass spectrum signals indicative of the product. MS (ESI): *m/z* = 368.23 (calculated 368.22 for [M + H^+]), 390.21 (calculated 390.22 for [M + Na^+]).

13.7.10 Synthesis of compound **11**, 2,5,8,11,14,17-hexaoxanonadecan-19-yl (tert-butoxycarbonyl)- D-alanyl- L-alaninate

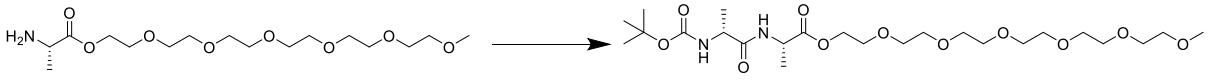

10 11

The synthetic procedure and signal assignment was based on work completed in the literature.[129]

An oven dried 100 mL, two necked, round-bottomed flask was filled with argon *via* the side neck and a magnetic stirrer bar was added. This flask was then charged *via* the central neck against argon flow

with compound **10** (1.886 g, 5.136 mmol), N-Boc-D-alanine (1.264, 6.677 mmol, 1.300 eq.) and HOBt monohydrate (0.79 g, 5.14 mmol, 1.00 eq.). Thereafter the contents of the flask were dissolved in distilled DCM (20 mL). Once the contents were fully dissolved, DIPEA (0.90 mL, 5.13 mmol, 1.00 eq.) was added dropwise. The mixture was then left to stir for 10 minutes. The flask was then cooled in an ice bath to 0 °C. Once cool then DCC (1.06 g, 5.14 mmol, 1.00 eq.) was added portion-wise to the flask against argon flow. Once the DCC was completely added to the flask, the contents were left to stir for 2 hours at 0 °C and thereafter stirred at room temperature for 6 hours. The precipitate that formed during the reaction was then filtered off and washed with ethyl acetate (3 x 10 mL). The excess solvent was then removed under reduced pressure. The crude product was the purified *via* column chromatography (gradient elution 10 % MeOH in DCM). The desired product was a runny yellow oil (1.4807 g, 54%).

^{1}H NMR (400 MHz, $CDCl_3$) δ: 6.83 (s, 1H, NH), 5.14 (d, *J*= 8.0 Hz, 1H, N*H*), 4.61— 4.54 (m, 1H), 4.33—4.24 (m, 2H), 4.20 (s, 1H), 3.70 – 3.62 (m, 20H), 3.55—3.53 (m, 2H), 3.37 (s, 3H), 1.44 (s, 9H), 1.41 (d, *J*= 8.0 Hz, 3H), 1.34 (d, *J*= 8.0 Hz, 3H), ^{13}C NMR (100 MHz, $CDCl_3$) δ: 172.87, 172.43, 155.73, 72.04, 70.72, 70.69, 70.67, 70.66, 70.61, 69.01, 64.58, 59.14, 48.22, 28.48, 28.45, 18.36, 18.27. The spectra acquired matches that found in literature. [129]

13.7.11 Synthesis of compound **12**, 2,5,8,11,14,17-hexaoxanonadecan-19-yl D-alanyl- L-alaninate

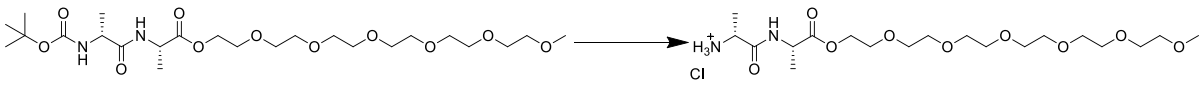

11 12

The synthetic procedure and signal assignment was based on work completed in the literature.[129]

An oven dried, two-necked, round-bottomed flask was charged with argon through the side neck of the flask. A magnetic stirrer bar was then added to the flask. Compound **11** (1.48 g, 2.75 mmol) was then added followed by the addition of HCl infused ethyl acetate (1 M, 16 mL). This reaction was then stirred at room temperature for 3 hours. Once the reaction had been completed, the solvent was removed under reduced pressure. Thereafter the excess HCl was removed *via* the addition of DCM (10 mL) and *n*-BuOH (1 mL) and slow evaporation overnight. The residual *n*-BuOH was then removed *via* azeotropic distillation with DCM (3 x 20 mL). The product was utilized in the following reactions without further purification. Product formation was confirmed with TLC, ^{1}H NMR with the appearance of the amine proton signal at ~ 7.7 ppm. As well as the further confirmation *via* mass spectrometry. MS (ESI): *m/z* = 439.26 (calculated 439.64 for [M + H^+]), 461.60 (calculated 461.64 for [M + Na^+]).

13.7.12Synthesis of compound **14**, 2-azido-5-iodobenzoic acid

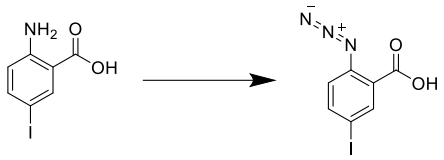

13 14

The synthetic procedure and signal assignment was based on work completed in the literature.[4]

An oven-dried, 100 mL, three-necked round-bottomed flask was charged with argon *via* one of the side necks of the flask. Thereafter a stir bar was added and compound **13** (0.20 g, 0.85 mmol) was added against argon flow. The contents of the flask were then dissolved in HCl (12 N, 2.3 mL). To this mixture $NaNO_2$ (0.175 g, 2.54 mmol, 3.00 eq.) dissolved in water (3 mL) was added. The resulting mixture was then stirred for 30 minutes. Once completed then NaN_3 (0.276 g, 4.23 mmol, 5.00 eq.) dissolved in distilled water (1.2 mL) was added to the mixture dropwise. The mixture was left to stir overnight. Once the reaction was completed the contents of the flask was poured over ice and the contents left in the freezer for 4 hours to assist with product precipitation. The solid was filtered off, collected, and dried under reduced pressure to afford compound **14** as a brown powder (0.15 g, 62%).

^{1}H NMR (400 MHz, $CDCl_3$) δ: 8.40 (d, J = 4.0 Hz, 1H), 7.89 (dd, J = 8.0 Hz, 4.0 Hz, 1H), 7.02 (d, J = 8.0 Hz, 1H). The spectrum matches that which is found in literature. [4]

13.7.13Synthesis of compound **15**, 2,5,8,11,14,17-hexaoxanonadecan-19-yl 2-azido-5-iodobenzoate

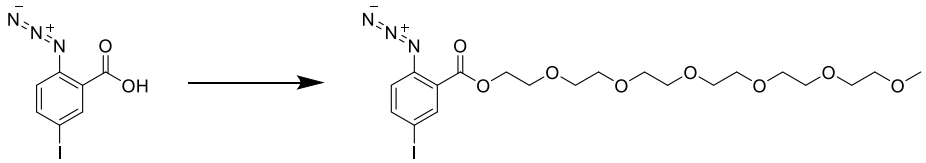

14 15

The synthetic procedure and signal assignment was based on work completed in literature.[4]

An oven dried, 150 mL three necked, round-bottomed flask was charged with compound **14** (1.0 g, 3.46 mmol). The compound was dissolved in dry DCM (45mL) and stirred with a magnetic stirrer bar till the mixture was homogenous. To this mixture compound **5** (1.128 g, 3.806 mmol, 1.100 eq.) was added, followed by the addition of DMAP (0.047 g, 0.381 mmol, 0.110 eq.). This mixture was then cooled to 0 °C for 30 minutes. DCC (0.785 g, 3.81 mmol, 1.1 eq.) was then added portion-wise and the reaction

was allowed to run for 2 hours at 0 °C before being allowed to run at room temperature for a further 18 hours. Once the reaction had taken place, the mixture was cooled and filtered. The filtrate was thereafter concentrated under vacuum and purified *via* column chromatography (gradient elution of 0 % to 10 % MeOH in DCM). The product was afforded as a pale-yellow oil (1.3736 g, 73%).

^{1}H NMR (400 MHz, $CDCl_3$) δ: 8.13 (d, *J* = 2.0 Hz, 1H), 7.78 (dd, *J* = 12.0 Hz, 4.0 Hz, 1H), 6.96 (d, *J* = 8.0 Hz, 1H), 4.45—4.42 (m, 2H), 3.81—3.79 (m, 2H), 3.68—3.61 (m, 18H), 3.53—3.51 (m, 2H), 3.35(s,3H). ^{13}C NMR (100 MHz, $CDCl_3$) δ: 163.73, 141.93, 140.45, 140.14, 124.36, 121.81, 87.42, 72.02, 70.66, 70.60, 69.03, 64.73, 59.11. The spectra matches that which is found in literature. [4]

13.7.14Synthesis of compound **16**, 2-azido-5-iodo-*N*-(2,5,8,11,14,17-hexaoxanonadecan-19-yl)benzamide

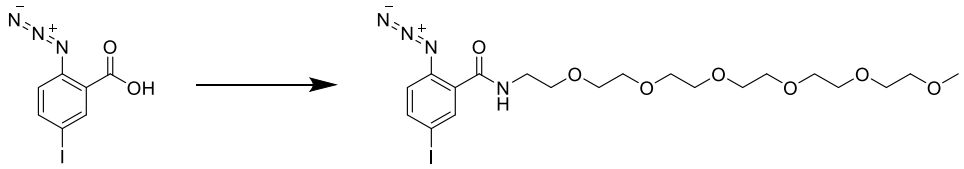

The synthetic procedure and signal assignment was based on work completed in the literature.[4]

Compound **16** was synthesized according to the same procedure and same reaction times as compound **15** with the below quantities of reagents. Compound **14** (2.85 g, 9.86 mmol), compound **8** (3.202 g, 10.85 mmol, 1.1 eq.), DMAP (0.133 g, 1.085 mmol, 0.11 eq.), DCC (2.238 g, 10.85 mmol, 1.1 eq.), DCM (132 mL). The product was afforded as an orange oil (4.3836 g, 78%)

^{1}H NMR (400 MHz, $CDCl_3$) δ: 8.37 (d, *J* = 2.0 Hz, 1H), 7.76 (dd, *J*= 12.0 Hz, 4.0 Hz, 1H), 7.73 (bs, 1H, N*H*), 6.93 (d, *J*= 8.0 Hz, 1H), 3.65—3.61 (m, 22H), 3.54—3.52 (m, 2H), 3.36(s, 3H); ^{13}C NMR (100 MHz, $CDCl_3$) δ: 163.44, 140.90, 140.78, 137.13, 127.16, 120.48, 88.64, 72.03, 70.69, 70.48, 69.75, 59.14, 40.05. MS (ESI): *m/z* = 567.13 (calculated 567.39 for [M + H^+]), 584.15 (calculated 584.39 for [M + NH_4^+]), 589.11 (calculated 589.39 for [M + Na^+]), 605.08 (calculated 605.39 for [M + K^+]). The spectra matches that which is found in literature. [4]

13.7.15Synthesis of compound **17**, 2,5,8,11,14,17-hexaoxanonadecan-19-yl (2-azido-5-iodobenzoyl)- D-alaninate

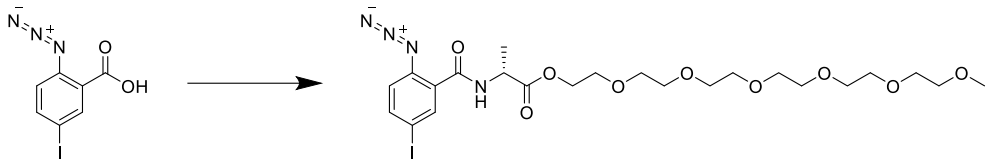

14 17

The synthetic procedure and signal assignment was based on work completed in literature.[4]

Compound **17** was synthesized according to the same procedure and reaction times as compound **15** with the below quantities of reagents. Compound **14** (0.939 g, 3.25 mmol), crude compound **10** (1.79 g, 4.87 mmol, 1.50 eq.), DMAP (0.044 g, 0.358 mmol, 0.11 eq.), DCC (0.7375 g, 3.574 mmol, 1.1 eq.), DCM (45 mL). To afford the product as an orange oil (1.2842 g, 62%).

^{1}H NMR (400 MHz, $CDCl_3$) δ: 8.43 (d, *J* = 4.0 Hz, 1H), 8.07 (d, *J* = 8.0 Hz, 1H, N*H*), 7.78 (dd, *J*= 8.0 Hz, 4.0 Hz, 1H), 6.95 (d, *J* = 8.0 Hz, 1H), 4.80 — 4.75 (m, 1H), 4.37 – 4.26 (m, 2H), 3.74 – 3.68 (m, 2H), 3.65 – 3.62 (m, 18H), 3.55 – 3.52 (m, 2H), 3.37 (s, 3H), 1.53 (d, *J* = 8.0 Hz, 3H); ^{13}C NMR (100 MHz, CDCl3) δ: 172.98, 162.59, 141.32, 141.12, 137.40, 126.13, 120.42, 88.68, 72.06, 70.77, 70.75, 70.73, 70.70, 70.64, 69.06, 69.03, 64.71, 59.15, 49.14, 18.59; MS (ESI): *m/z* = 639.15 (calculated 638.03 for [M + H^+]), 656.17 (calculated 656.03 for [M + NH_4^+]), 657.18 (calculated 657.03 for [M + H_3O^+]), 661.13 (calculated 661.03 for [M + Na^+]), 677.10 (calculated 677.03 for [M + K^+]), 485.30 (calculated for 485.36 as compound **9** + NH_4^+). The spectra matches that which is found in literature.[4,129]

13.7.16Synthesis of compound **18**, 2,5,8,11,14,17-hexaoxanonadecan-19-yl (2-azido-5-iodobenzoyl)- D-alanyl- L-alaninate

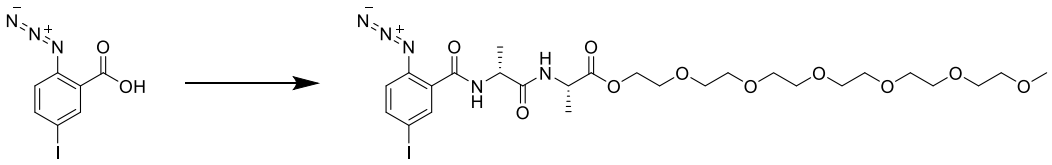

14 18

The synthetic procedure and signal assignment was based on work completed in the literature.[4]

Compound **18** was synthesized according to the same procedure as compound **15** with the below quantities of reagents. Compound **14** (0.723 g, 2.499 mmol), crude compound **12** (2.75 mmol, 1.1 eq.), DMAP (0.034 g, 0.275 mmol, 0.11 eq.), DCC (0.568 g, 2.75 mmol, 1.1 eq.), DCM (35 mL). To afford the product as an orange oil (1.24 g, 70%).

^{1}H NMR (400 MHz, $CDCl_3$) δ: 8.38 (d, *J* = 4.0 Hz, 1H), 7.92 (d, *J* = 8.0 Hz, 1H, NH), 7.78 (dd, *J*= 8.0 Hz, 4.0 Hz, 1H), 7.04 (d, *J* = 4.0 Hz, 1H, N*H*), 6.96 (d, *J* = 12.0 Hz, 1H), 4.75 — 4.56 (m, 2H), 4.31 – 4.27 (m, 2H), 3.69 – 3.62 (m, 18H), 3.55 – 3.53 (m, 2H), 3.37 (s, 3H), 1.48 (d, *J* = 4.0 Hz, 3H), 1.44 (d, *J* = 8.0 Hz, 3H); ^{13}C NMR (100 MHz, CDCl3) δ: 172.74, 171.62, 163.28, 141.30, 140.83, 137.46, 126.47, 120.41, 88.63, 72.05, 70.72, 70.70, 70.67, 70.63, 69.01, 59.16, 49.58, 48.43, 18.40, 18.33. MS (ESI): *m/z* = 710.18 (calculated 710.53 for [M + H^+]), 727.21 (calculated 727.53 for [M + NH_4^+]), 728.21 (calculated 728.21 for [M + H_3O^+]), 732.17 (calculated 732.21 for [M + Na^+]), 748.14 (calculated 748.21 for [M + K^+]), 485.30 (calculated for 485.36 as compound **9** + NH_4^+), 556.34 (calculated for 538.64 as compound 11 + NH_4^+). The spectra matches that which is found in literature.[4,129]

13.7.17 Synthesis of compound **19**, 2,5,8,11,14,17-hexaoxanonadecan-19-yl 2-azido-5-((trimethylsilyl)ethynyl)benzoate

*13.7.17.1 Synthesis of a mixture of compound **19**, 2,5,8,11,14,17-hexaoxanonadecan-19-yl 2-azido-5-((trimethylsilyl)ethynyl)benzoate, and **23**, 2,5,8,11,14,17-hexaoxanonadecan-19-yl 2-amino-5-((trimethylsilyl)ethynyl)benzoate*

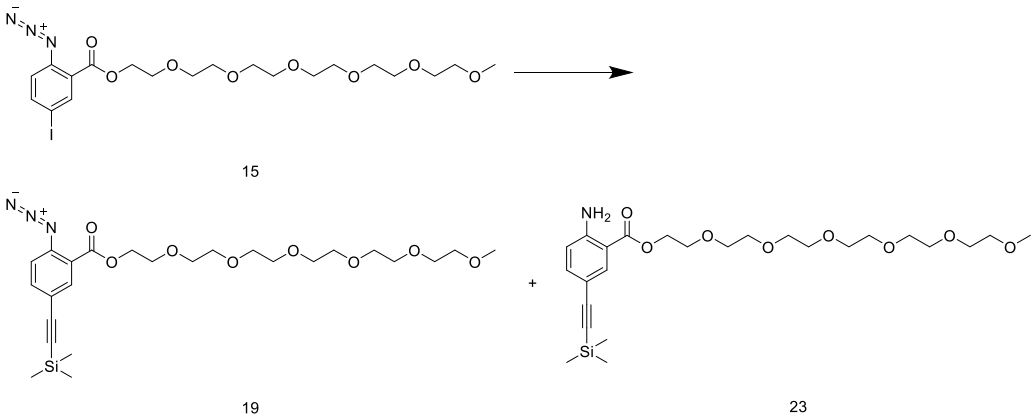

The synthetic procedure and signal assignment was based on work completed in literature.[4]

An oven dried, 50 mL, Schlenk flask was charged with compound **15** (3.59 g, 6.33 mmol), TEA (11.48 mL, 82.26 mmol, 13.0 eq.), trimethylsilyl acetylene (1.00 mL, 6.96 mmol, 1.1 eq.) and THF (18 mL). The mixture was then subjected to two freeze pump thaw cycles. After the final cycle the schlenk flask was backfilled with argon. The flask was thereafter quickly opened and $Pd(PPh_3)_4$ (0.0731, 0.0633 mmol, 0.01eq.) and CuI (0.0121 g, 0.0633 mmol, 0.01 eq.) were added. The schlenk flask was then immediately closed and evacuated before another four freeze pump thaw cycles were conducted. Once the final cycle was complete, the flask was filled with argon and the schlenk flask was immersed in a preheated 30 °C oil bath. The reaction was then allowed to run till the reaction mixture changed from a orange-yellow solution to a dark brown solution. This took between 30 to 60 minutes. Immediately when this occurred the reaction was quenched with the addition of ethyl acetate in excess and then introduction of air into the schlenk flask. The white precipitate that had been formed during the reaction was filtered off and was washed with ethyl acetate (2 x 10 mL). The filtrate was thereafter concentrated, and a single spot was isolated *via* column chromatography (gradient elution from 0 % ethyl acetate in hexane to 80% ethyl acetate in hexane). This spot was not pure and contained a mixture of a detrimental impurity (compound **23**) and the desired product (compound **19**). The impure fraction was an orange gum once dried (1.899 g crude mass).

*13.7.17.2 Isolation of compound **19**, 2,5,8,11,14,17-hexaoxanonadecan-19-yl 2-azido-5-((trimethylsilyl)ethynyl)benzoate*

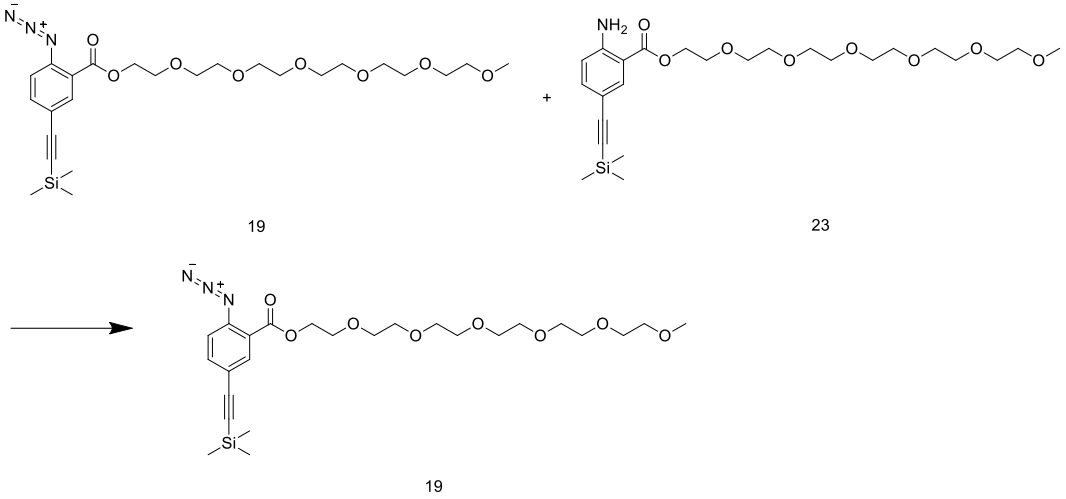

The synthetic procedure and signal assignment was based on work completed in the literature.[4]

The mixture of compound **19** and **23** (0.86 g, ~1.68 mmol as it is a mixture) was added to an oven dried, 50 mL, one-necked flask equipped with an oval-stir bar. THF (23.6 mL) was thereafter added, and the flask was sealed with a rubber septum. The sealed flask was sparged with argon and allowed to cool to 0 °C in a sodium chloride ice bath. Once the mixture had been sparged for 15 minutes, *tert*-$BuNO_2$ (1.2 mL, 9.5 mmol, ~ 5.65 eq.) was added dropwise *via* a syringe. The mixture was then left to stir for 30 minutes before TMS-N_3 (0.52 mL, 3.87 mmol, ~2.3 eq.) was added dropwise *via* a syringe. The mixture was left to stir at 0 °C for one hour and thereafter left to stir at room temperature for three hours. Once the reaction had occurred the product was concentrated on a rotary evaporator. The desired product was then isolated *via* column chromatography (gradient elution from 0 % ethyl acetate in hexane to 80% ethyl acetate in hexane). The desired product was concentrated and dried under vacuum. The product once dried was that of a yellow gum (0.863 g, percentage yield is hard to determine as the starting material was a mixture of the desired product and the impurity).

^{1}H NMR (400 MHz, $CDCl_3$) δ: 7.95 (d, J = 2.0 Hz, 1H), 7.58 (dd, J = 8.0, 4.0 Hz, 1H), 7.15 (d, J = 8.0 Hz, 1H), 4.46 – 4.44 (m, 2H), 3.83 – 3.80 (m, 2H), 3.68 – 3.61 (m, 18H), 3.54 – 3.52 (m, 2H), 3.36 (s, 3H), 0.24 (s, 9H); ^{13}C NMR (100 MHz, $CDCl_3$) δ: 164.49, 140.13, 136.39, 135.56, 122.59, 119.94, 119.71, 103.21, 95.91, 72.06, 70.77, 70.74, 70.73, 70.69, 70.64, 70.59, 69.14, 64.60, 59.15, 1.14; MS (ESI): *m/z* = 555.28 (calculated 555.28 for [M + NH_4^+]), 556.29 (calculated 556.27 for [M + H_3O^+]), 560.24 (calculated: 560.24 for [M + Na^+]). These signals match which is found in literature. [4]

13.7.18 Synthesis of compound **20**, 2-azido-*N*-(2,5,8,11,14,17-hexaoxanonadecan-19-yl)-5-((trimethylsilyl)ethynyl)benzamide

*13.7.18.1 Synthesis of a mixture of compound **20**, 2-azido-N-(2,5,8,11,14,17-hexaoxanonadecan-19-yl)-5-((trimethylsilyl)ethynyl)benzamide, and **24**, 2-amino-N-(2,5,8,11,14,17-hexaoxanonadecan-19-yl)-5-((trimethylsilyl)ethynyl)benzamide*

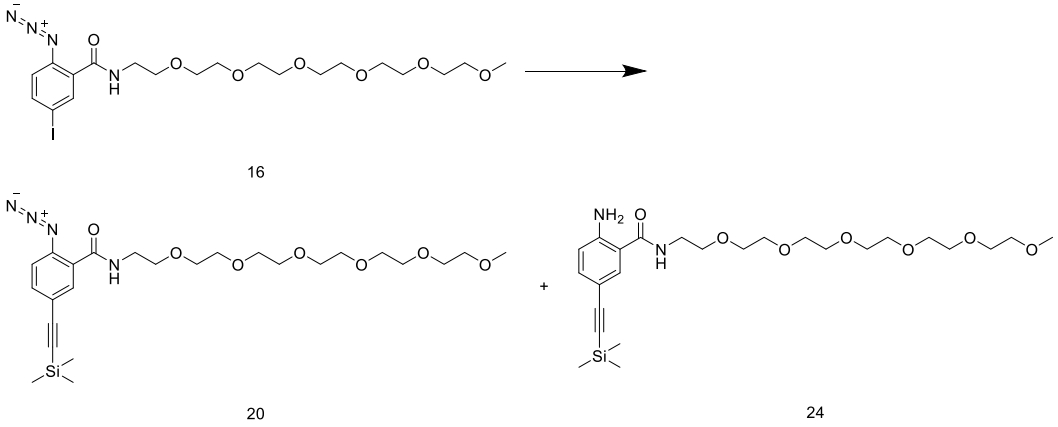

The synthetic procedure and signal assignment was based on work completed in the literature.[4]

The procedure for this step is the same as that which was conducted for the step "Synthesis of a mixture of compound **19** and **23**" with the following changes in terms of the masses of reagents utilized. Compound **16** (1.00 g, 1.77 mmol), TEA (3.20 mL, 22.9 mmol, 13.0 eq.), trimethylsilyl acetylene (0.28 mL, 1.94 mmol, 1.10), THF (5.5 mL), $Pd(PPh_3)_4$ (0.021 g, 0.018 mmol, 0.01 eq.), and CuI (3.37×10^{-3} g, 0.018 mmol, 0.01 eq.) were added at these specific masses/volumes in order to isolate single spot *via* column chromatography (gradient elution from 0 % MeOH in DCM to 5% MeOH in DCM). This spot was impure and contained a mixture of an impurity (compound **24**) and the desired product (compound **20**). The impure fraction was an orange oil once dried (0.6241 g crude mass).

*13.7.18.2 Isolation of compound **20**, 2-azido-N-(2,5,8,11,14,17-hexaoxanonadecan-19-yl)-5-((trimethylsilyl)ethynyl)benzamide*

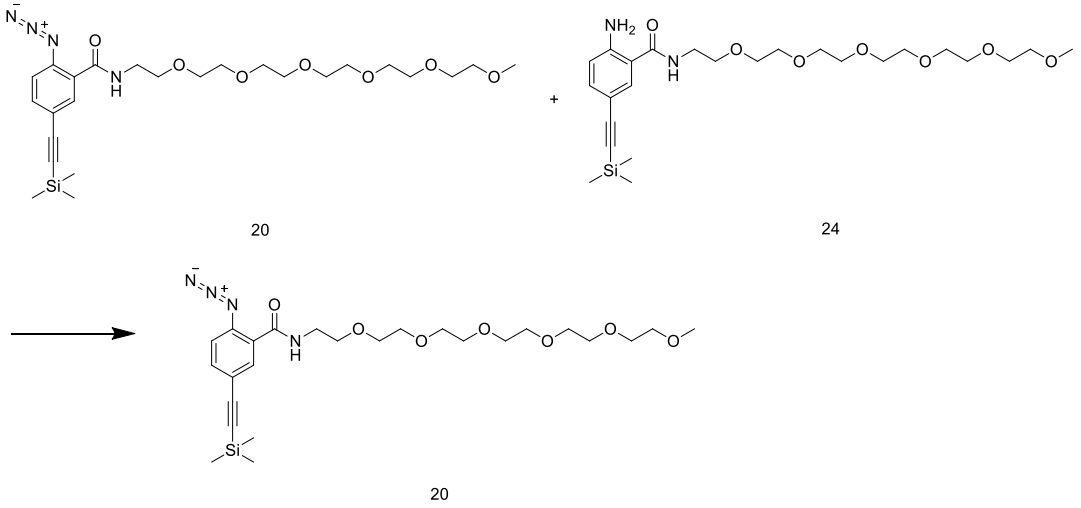

20 + 24 → 20

The synthetic procedure and signal assignment was based on work completed in the literature.[4]

This synthetic procedure is the same as the procedure for 'Isolation of compound **19**' except there were differences in the volumes and masses utilized. Namely with the mixture of compound **20** and **24** (0.313 g, ~0.613 mmol as it was a mixture), THF (8.8 mL), *tert*-$BuNO_2$ (0.44 mL, 3.68 mmol, ~ 6.0 eq.), and TMS-N_3 (0.21 mL,1.54 mmol, ~2.5 eq.). The desired product (compound 20) was then isolated *via* column chromatography (gradient elution from 0 % methanol in DCM to 5% methanol in DCM). The desired product was thereafter concentrated and dried under vacuum. The product was that of a yellow oil (0.3104 g, percentage yield is hard to determine as the starting material was a mixture of the desired product and the impurity).

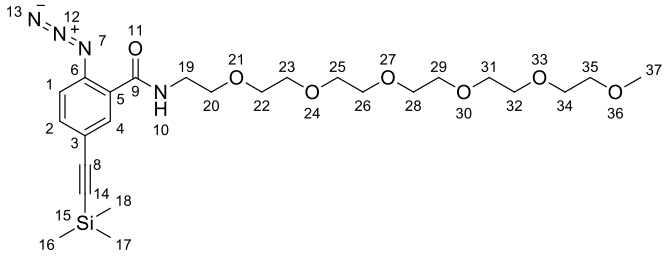

20

^{1}H NMR (400 MHz, $CDCl_3$) δ: 8.16 (d, *J* = 4.0 Hz, 1H, ArH_4),7.69 (s, 1H, NH_{10}), 7.54 (dd, *J* = 8.0, 4.0 Hz, 1H, ArH_2), 7.12 (d, *J* = 8.0 Hz, 1H, ArH_1), 3.66—3.62 (m, 22H, C$H_{19\text{-}34}$), 3.55 – 3.53 (m, 2H, CH_{35}), 3.37 (s, 3H, CH_{37}), 0.24 (s, 8H but should be 9H, C$H_{16\text{-}18}$); ^{13}C NMR (100 MHz, $CDCl_3$) δ: 164.19 (C_9), 137.10 (C_4), 135.82 (C_3), 135.24 (C_2), 125.64 (C_6), 120.39 (C_5), 118.70 (C_1), 103.53 (C_8), 95.81 (C_{14}), 72.08 (C_{35}), 70.75($C_{19\text{-}34}$), 70.73 ($C_{19\text{-}34}$), 70.71 ($C_{19\text{-}34}$), 70.66 ($C_{19\text{-}34}$), 70.52 ($C_{19\text{-}34}$), 69.86 ($C_{19\text{-}34}$), 59.18 (CH_{37}), 40.03 ($C_{19\text{-}34}$), 0.02 ($C_{16\text{-}18}$); ^{1}H,^{1}H GCOSY (400/400 MHz, $CDCl_3$) δ: ^{1}H /δ ^{1}H ppm 8.16/7.54 (ArH_4/ ArH_2),7.69/3.66—3.62 (NH_{10}, C$H_{19\text{-}34}$), 7.54/7.12 (ArH_2/ ArH_1); ^{1}H,^{13}C GHSQC

(400/400 MHz, $CDCl_3$) δ: ^1H/δ ^{13}C ppm 8.16/137.10 (ArH_4/ C_4), 7.54/ 135.24(ArH_2/ C_2), 7.12/118.70 (ArH_1/ C_1), 3.66—3.62/70.75, 40.03 (C$H_{19\text{-}34}$/ $C_{19\text{-}34}$), 3.55—5.53/ 72.08 (CH_{35}/ C_{35}), 3.37/59.18 (CH_{37}/ C_{37}), 0.24/0.02 (C$H_{15\text{-}18}$/$C_{16\text{-}18}$); ^1H,^{13}C GHMBC (400/400 MHz, $CDCl_3$): δ ^1H/δ ^{13}C ppm 8.16/164.19, 135.82, 118.70, 103.53 (ArH_4/ C_9, C_3, C_1, C_8), 7.54/135.82, 103.53 (ArH_2/ C_3, C_8), 7.12/164.19, 135.82, 125.64, 120.39 (ArH_1/ C_9, C_3, C_6, C_5), 3.66 – 3.62/164.19, 70.52, 40.03 (C$H_{19\text{-}34}$/ C_9, $C_{19\text{-}34}$, $C_{19\text{-}34}$), 3.55 – 3.53/70.66, 59.18 (CH_{35}/ $C_{19\text{-}34}$, C_{37}), 3.37/72.08 (CH_{37}/ C_{35}), 0.21/103.53, 95.81, 0.02 (C$H_{15\text{-}18}$/ C_8, C_{14}, $C_{16\text{-}18}$); MS (ESI): *m/z* = 537.27 (calculated 537.69 for [M + H^+]), 559.25 (calculated 559.69 for [M + Na^+]).

13.7.19 Synthesis of compound **21**, 2,5,8,11,14,17-hexaoxanonadecan-19-yl (2-azido-5-((trimethylsilyl)ethynyl)benzoyl)- D-alaninate

*13.7.19.1 Synthesis of a mixture of compound **21**, 2,5,8,11,14,17-hexaoxanonadecan-19-yl (2-azido-5-((trimethylsilyl)ethynyl)benzoyl)- D-alaninate, and **25**, 2,5,8,11,14,17-hexaoxanonadecan-19-yl (2-amino-5-((trimethylsilyl)ethynyl)benzoyl)- D-alaninate*

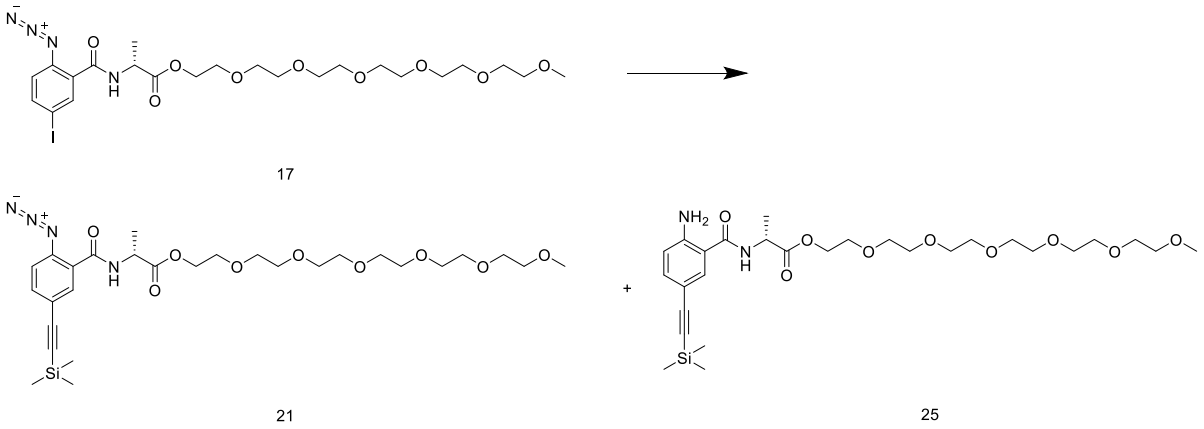

The synthetic procedure and signal assignment was based off work completed in literature.[4]

The procedure for this synthetic procedure is the same as was conducted for the step "Synthesis of a mixture of compound **19** and **23**" with the following changes in terms of masses and volumes of reagents utilized. Compound **17** (3.05 g, 4.78 mmol), TEA (8.70 mL, 62.1 mmol, 13.0 eq.), trimethylsilyl acetylene (0.75 mL, 5.26 mmol, 1.10 eq.), THF (13.6 mL), $Pd(PPh_3)_4$ (0.056 g, 0.048 mmol, 0.01 eq.), and CuI (9.2×10^{-3} g, 0.05 mmol, 0.01 eq.) were added in order to isolate single spot *via* column chromatography (gradient elution from 0 % methanol in DCM to 15% methanol in DCM). This spot was impure and contained a mixture of an impurity (compound **25**) and the desired product (compound **21**). The impure fraction was a dark brown, orange oil once dried (3.058 g crude mass).

*13.7.19.2 Isolation of compound **21**, 2,5,8,11,14,17-hexaoxanonadecan-19-yl (2-azido-5-((trimethylsilyl)ethynyl)benzoyl)- D-alaninate*

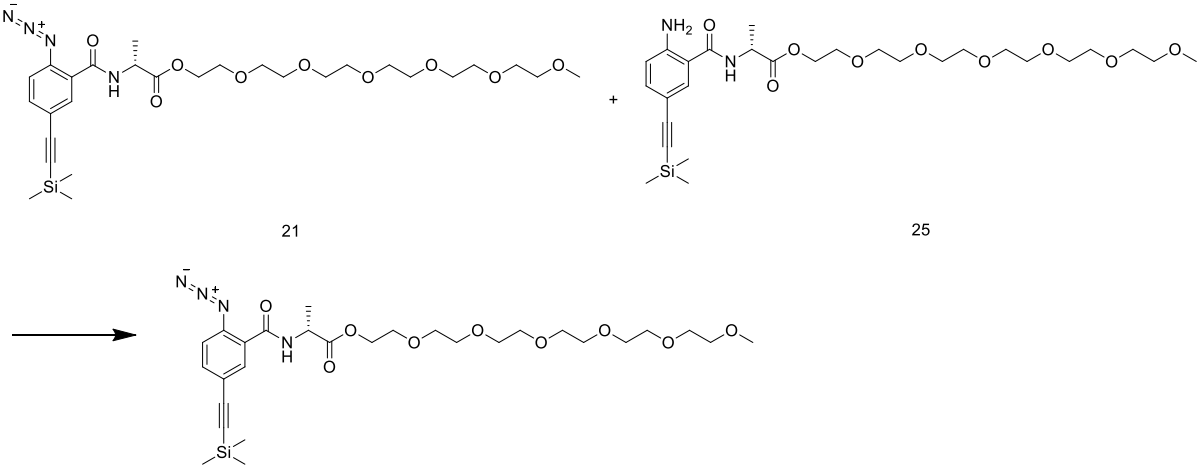

21 + 25 → 21

The synthetic procedure and signal assignment was based off work completed in the literature.[4]

This synthetic procedure is identical to that of the procedure titled 'Isolation of compound **19**' except there were differences in term of the volumes and masses utilized. Namely with the mixture of compound **21** and **25** (3.0 g, ~5.15 mmol as it is a mixture), THF (74 mL), *tert*-$BuNO_2$ (3.5 mL, 29.1 mmol, ~ 5.65 eq.), and TMS-N_3 (1.56 mL, 11.9 mmol, ~2.3 eq.). The desired product (compound **21**) was then isolated *via* column chromatography (gradient elution from 0 % methanol in DCM to 15% methanol in DCM). The desired product was thereafter concentrated and dried under vacuum. The product was that of a yellow oil (2.205 g, percentage yield is hard to determine as the starting material was a mixture of the desired product and the impurity).

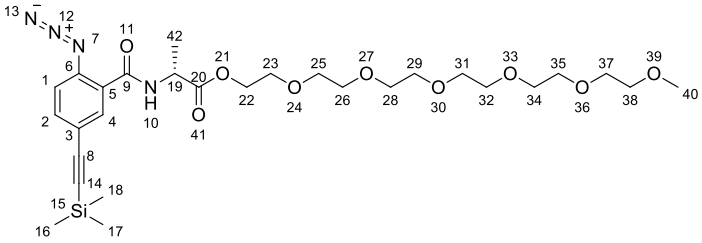

21

^{1}H NMR (400 MHz, $CDCl_3$) δ: 8.19 (d, *J* = 2.0 Hz, 1H, ArH_4), 7.99 (bs, 1H, NH_{10}), 7.54 (dd, *J* = 4.0, 2.0 Hz, 1H, ArH_2), 7.11 (d, *J* = 4.0 Hz, 1H, ArH_1), 4.77 (p, *J* = 8.0 Hz, 1H, CH_{19}), 4.34— 4.29(m, 2H, CH_{22}), 3.72—3.70 (m, 2H, CH_{23}), 3.64 – 3.61 (m, 18H, C$H_{25\text{-}37}$), 3.53 – 3.51(m, 2H, CH_{38}), 3.35 (s, 3H,CH_{40}), 1.51 (d, *J*= 4.0 Hz, 3H, CH_{42}), 0.21 (s, 8H, C$H_{16\text{-}18}$); ^{13}C NMR (100 MHz, $CDCl_3$) δ: 173.07 (C_{20}), 163.30 (C_9), 137.32 (C_4), 136.09 (C_3), 135.56 (C_2), 124.63(C_6), 120.43(C_5), 118.67(C_1), 103.41(C_8), 95.88 (C_{14}),72.05 (C_{38}), 70.77($C_{25\text{-}37}$), 70.75 ($C_{25\text{-}37}$), 70.72($C_{25\text{-}37}$), 70.69($C_{25\text{-}37}$), 70.68($C_{25\text{-}37}$), 70.63($C_{25\text{-}37}$), 69.06 (C_{23}), 64.69 (C_{22}), 59.16 (C_{40}), 49.09 (C_{19}), 18.63(C_{42}), 1.16 ($C_{16\text{-}18}$), ^{1}H,^{1}H

GCOSY (400/400 MHz, $CDCl_3$) δ: ^1H /δ ^1H ppm 8.19/7.54 (ArH_4/ ArH_2),7.99/4.77 (NH_{10}, CH_{19}), 7.54/7.11 (ArH_2/ ArH_1), 4.77/1.52 (CH_{19}/ CH_{42}), 4.34—4.29/ 3.72—3.70 (CH_{22}/CH_{23}), 1.51/4.77 (CH_{42}/ CH_{19}), 0.21/8.21 (C$H_{16\text{-}18}$/ ArH_4); ^1H,^{13}C GHSQC (400/400 MHz, $CDCl_3$) δ: ^1H/δ ^{13}C ppm 8.19/137.32 (ArH_4/ C_4), 7.54/ 135.56(ArH_2/ C_2), 7.11/118.67(ArH_1/ C_1), 4.77/49.09(CH_{19}/ C_{19}), 4.32/64.69(CH_{22}/ C_{22}), 3.72—3.70/ 69.06 (CH_{23}/ C_{23}), 3.64—3.61/70.60(C$H_{25\text{-}37}$/ $C_{25\text{-}37}$), 3.53—5.51/ 72.05 (CH_{38}/ C_{38}), 3.35/59.16 (CH_{40}/ C_{40}), 1.52/18.63 (CH_{42}/ C_{42}), 0.21/1.16 (C$H_{15\text{-}18}$/$C_{16\text{-}18}$); ^1H,^{13}C GHMBC (400/400 MHz, $CDCl_3$): δ ^1H/δ ^{13}C ppm 8.19/163.30, 136.09, 118.67, 103.41 (ArH_4/ C_9, C_3, C_1, C_8), 7.99/173.07, 163.30, 49.09 (NH_{10}/ C_{20}, C_9, C_{19}), 7.54/136.09, 124.63, 103.41 (ArH_2/ C_3, C_6,C_8), 7.11/163.30, 135.56, 124.63, 120.43(ArH_1/ C_9, C_2, C_6, C_5), 4.77/ 173.07, 163.30, 18.63 (CH_{19}/C_{20}, C_9, C_{42}), 4.34—4.29/173.07, 69.06(CH_{22}/ C_{20}, C_{23}), 3.72—3.70/69.06, 64.69 (CH_{23}/ C_{23}, C_{22}), 3.64 – 3.61/69.54 (C$H_{25\text{-}37}$/ C_{23}), 3.53 – 3.51/69.06, 59.16 (CH_{38}/ C_{23}, C_{40}), 3.35/70.77 (CH_{40}/ $C_{25\text{-}37}$), 1.51/173.07, 49.09 (CH_{42}/ C_{20}, C_{19}), 0.21/98.88, 1.16 (C$H_{15\text{-}18}$/ C_{14}, $C_{16\text{-}18}$); MS (ESI): *m/z* = 608.30 (calculated 608.76 for [M + H^+]), 626.32 (calculated 626.76 for [M + NH_4^+]), 627.32 (calculated 627.76 for [M + H_3O^+]), 631.28 (calculated 631.76 for [M + Na^+]), 647.25 (647.76 calculated for [M + K^+]).

13.7.20 Synthesis of compound **22**, 2,5,8,11,14,17-hexaoxanonadecan-19-yl (2-azido-5-((trimethylsilyl)ethynyl)benzoyl)- D-alanyl-L-alaninate

*13.7.20.1 Synthesis of a mixture of compound **22**, 2,5,8,11,14,17-hexaoxanonadecan-19-yl (2-azido-5-((trimethylsilyl)ethynyl)benzoyl)- D-alanyl-L-alaninate, and **26**, 2,5,8,11,14,17-hexaoxanonadecan-19-yl (2-amino-5-((trimethylsilyl)ethynyl)benzoyl)- D-alanyl-L-alaninate*

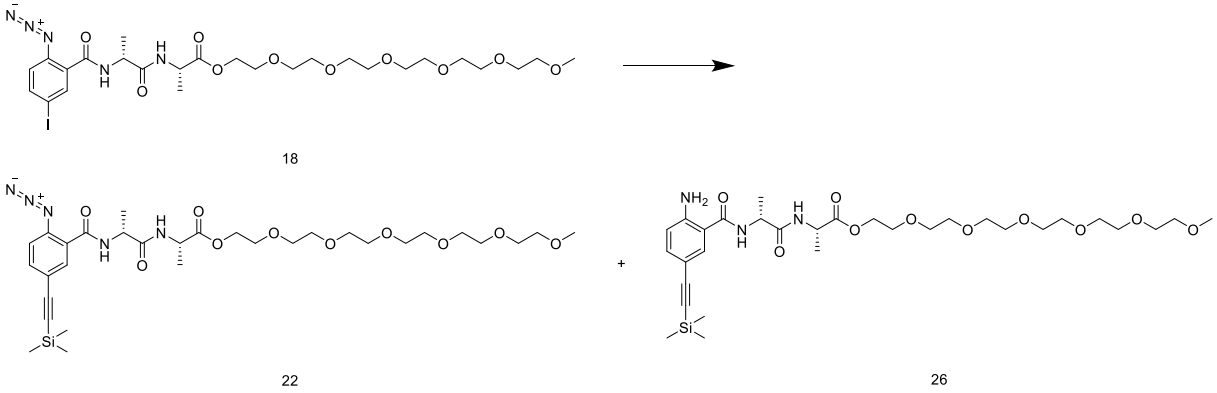

18

22 + 26

The synthetic procedure and signal assignment was based off work completed in the literature.[4]

The procedure for this synthetic procedure is the same as that which was conducted for the step named "Synthesis of a mixture of compound **19** and **23**" with the following changes in terms of masses and volumes of reagents utilized. Compound **18** (1.23 g, 1.73 mmol), TEA (3.2 mL, 2.3 mmol, 13.0 eq.), trimethylsilyl acetylene (0.3 mL, 1.9 mmol, 1.10 eq.), THF (5 mL), $Pd(PPh_3)_4$ (0.021 g, 0.018 mmol, 0.01 eq.), and CuI (3.43 x 10^{-3} g, 0.018 g, 0.01 eq.) were added in order to isolate single spot *via* column chromatography (gradient elution from 0 % methanol in DCM to 15% methanol in DCM). This spot

was impure and contained a mixture of an impurity (compound **26**) and the desired product (compound **22**). The impure fraction was a brown, orange oil once dried (0.67 g crude mass).

*13.7.20.2 Isolation of compound **22**, 2,5,8,11,14,17-hexaoxanonadecan-19-yl (2-azido-5-((trimethylsilyl)ethynyl)benzoyl)- D-alanyl-L-alaninate*

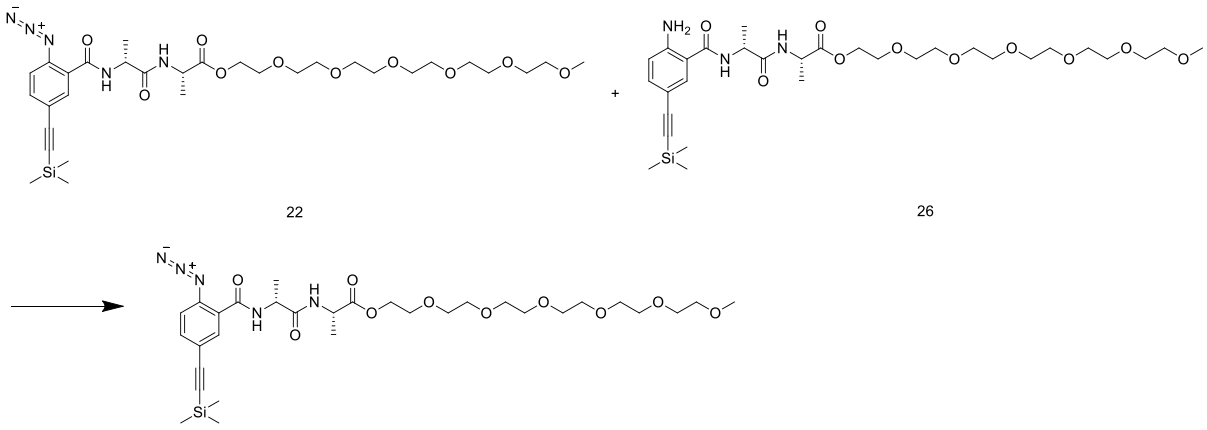

22 + 26

22

The synthetic procedure and signal assignment was based off work completed in the literature.[4]

This synthetic procedure is identical to that of the procedure titled 'Isolation of compound **19**' except there were differences in the volumes utilized. Namely with the mixture of compound **22** and **26** (0.6 g, ~0.9 mmol as it is a mixture), THF (13 mL), *tert*-$BuNO_2$ (0.62 mL, 5.19 mmol, ~ 5.65 eq.), and TMS-N_3 (0.28 mL, 2.12 mmol, ~2.3 eq.). The desired product (compound **22**) was thereafter isolated *via* column chromatography (gradient elution from 0 % methanol in DCM to 15% methanol in DCM). The desired product was then concentrated and dried under vacuum. The product was that of a dark orange oil (0.56 g, percentage yield is hard to determine as the starting material was a mixture of the desired product and the impurity).

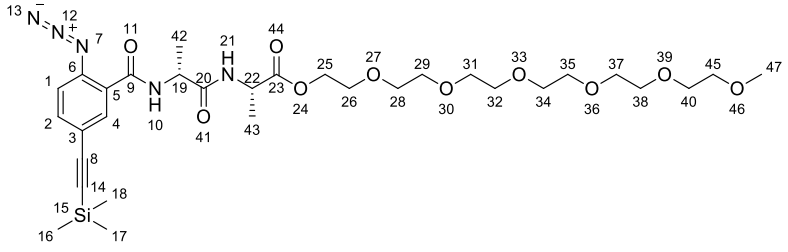

22

^{1}H NMR (400 MHz, $CDCl_3$) δ: 8.16 (d, *J* = 4.0 Hz, 1H, ArH_4), 7.84 (d, *J* = 8.0 Hz, 1H, NH_{10}), 7.55 (dd, *J* = 8.0, 4.0 Hz, 1H, ArH_2), 7.13 (d, *J* = 8.0 Hz, 1H, ArH_1), 7.06 (d, *J* = 8.0 Hz, NH_{21}), 4.73 (p, *J*= 8.0 Hz, 1H, CH_{19}), 4.60 (p, *J*= 8.0 Hz, 1H, CH_{22}), 4.35 – 4.20 (m, 2H, CH_{25}), 3.73 – 3.61 (m, 20H, C$H_{26\text{-}40}$), 3.54 – 3.52 (m, 2H, CH_{45}), 3.36 (s, 3H, CH_{47}), 1.48 (d, *J*= 4.0 Hz, 3H, CH_{42}), 1.43 (d, *J*= 8.0 Hz,

3H, CH_{43}) 0.23 (s, 9H, C$H_{16\text{-}18}$); ^{13}C NMR (100 MHz, $CDCl_3$) δ: 172.75 (C_{23}), 171.69 (C_{20}), 163.99 (C_9), 137.35 (C_4), 135.84 (C_3), 135.58 (C_2), 124.87 (C_6), 120.44 (C_5), 118.62 (C_1), 103.34 (C_8), 95.96 (C_{14}), 72.05 (C_{45}), 70.71 ($C_{26\text{-}40}$), 70.68 ($C_{26\text{-}40}$), 70.65 ($C_{26\text{-}40}$), 70.62 ($C_{26\text{-}40}$), 69.01 ($C_{26\text{-}40}$), 64.59 (C_{25}), 59.15(C_{47}) , 49.52 (C_{19}) , 48.41 (C_{22}), 18.39(C_{43}), 18.27 (C_{42}), 1.15 ($C_{16\text{-}18}$); ^{1}H,^{1}H GCOSY (400/400 MHz, $CDCl_3$) δ: ^{1}H /δ ^{1}H ppm 8.16/7.55 (ArH_4/ ArH_2), 7.55/7.13 (ArH_2/ ArH_1), 7.84/4.73 (NH_{10}/CH_{19}), 4.60/7.06 (CH_{22}/ NH_{21}), 4.35—4.20/3.73—3.61 (CH_{25}/C$H_{26\text{-}40}$), 1.48/4.73 (CH_{42}/ CH_{19}), 1.43, 4.60 (CH_{43}/ CH_{22}); 1H,13C GHSQC (400/400 MHz, $CDCl_3$) δ: 1H/δ 13C ppm 8.16/ 137.35 (ArH_4/C_4), 7.55/135.58 (ArH_2/C_2), 7.13/118.62 (ArH_1/C_1), 4.73/49.52 (CH_{19}/ C_{19}), 4.60/48.41 (CH_{22}/ C_{22}), 4.35 – 4.20/ 64.59 (CH_{25}/ C_{25}), 3.73 – 3.61/ 70.71, 70.68, 70.65, 70.62, 69.01 (C$H_{26\text{-}40}$ / $C_{26\text{-}40}$), 3.54 – 3.52/ 72.05 (CH_{45}/ C_{25}), 3.36/ 59.15 (CH_{47}/ C_{47}), 1.48/ 18.27 (CH_{42}/ C_{42}), 1.43/18.39 (CH_{43}/ C_{43}) 0.23/ 1.15 (C$H_{16\text{-}18}$/ $C_{16\text{-}18}$); ^{1}H,^{13}C GHMBC (400/400 MHz, $CDCl_3$): δ ^{1}H/δ ^{13}C ppm 8.16/163.99, 137.35, 103.34, (ArH_4/ C_9, C_4, C_8), 7.84/ 163.99 (NH_{10}/ C_9), 7.55/ 135.84, 103.34(ArH_2/ C_3, C_8), 7.13/ 163.99, 137.35, 124.87, 120.44 (ArH_1/ C_9, C_4, C_6, C_5), 7.06/ 171.69 (NH_{21}/ C_{20}), 4.73/ 171.69, 163.99, 18.27 (CH_{19}/ C_{20}, C_9,C_{42}), 4.60/ 172.75, 18.39 (CH_{22}/ C_{23}, C_{43}), 4.35 – 4.20/ 172.75,69.01 (CH_{25} / C_{23}, $C_{26\text{-}40}$), 3.73 – 3.61/70.70 (C$H_{26\text{-}40}$/ C$H_{26\text{-}40}$), 3.54 – 3.52/70.65, 59.15 (CH_{45}/ C$H_{26\text{-}40}$, C_{47}), 3.36/72.05 (CH_{47}/ C_{45}), 1.48/ 171.69, 49.52 (CH_{42}/ C_{20}, C_{19}), 1.43/172.75, 48.41 (CH_{43}/ C_{23}, C_{22}) 0.23/95.96, 1.15 (C$H_{16\text{-}18}$/ C_{14}, $C_{16\text{-}18}$); MS (ESI): *m/z* = 680.33 (calculated 680.83 for [M + H^+]),697.36 (calculated 697.83 for [M + NH_4^+]), 698.36 (calculated for 698.83 [M + H_3O^+]), 702.31(calculated: 702.83 for [M + Na^+]), 718.29 (calculated for 718.83 for [M + K^+]).

13.7.21Synthesis of compound **27**, 2,5,8,11,14,17-hexaoxanonadecan-19-yl 2-azido-5-ethynylbenzoate

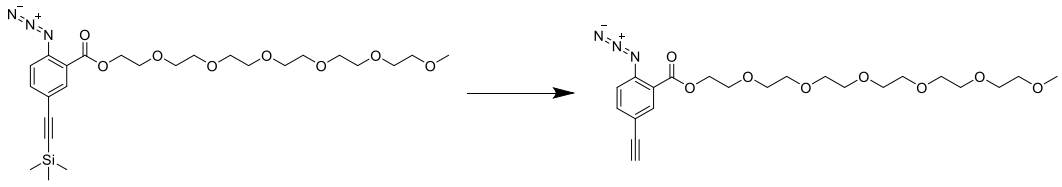

19 27

The synthetic procedure and signal assignment was based off work completed in the literature.[4]

Compound **19** (0.86 g, 1.60 mmol) was added to a 100 mL, oven-dried, one-necked flask equipped with an oval-shaped magnetic stir bar. THF (32.5 mL) was then added to flask and the mixture was stirred for 1 minute. Once stirred, TBAF.H_2O (0.935 g, 2.962 mmol, 1.85 eq.) was added in one portion and the reaction was left to run for 15 minutes. During the reaction, the mixture changed from a yellow to dark brown colour. Once the mixture had been complete, the contents of the flask was concentrated *via* rotary evaporation and then purified *via* column chromatography plug (gradient elusion from 0 % methanol in DCM to 2 % methanol in DCM) to remove the residual TBAF.H_2O. The product was

thereafter dried under reduced pressure for 1 hour to afford a yellow oil (0.7 g, percentage yield is not possible to determine as the product was not dried sufficiently due to time constraints as a results of compound auto-reaction). The product was then immediately utilized in the generalized polymerization procedure (procedure to follow).

^{1}H NMR (400 MHz, $CDCl_3$) δ: 7.99 (d, J = 2.0 Hz, 1H), 7.61 (dd, J = 8.0, 4.0 Hz, 1H), 7.19 (d, J = 8.0 Hz, 1H), 4.47 – 4.45 (m, 2H), 3.83 – 3.81 (m, 2H), 3.71 – 3.62 (m, 18H); 3.55 – 3.53 (m, 2H), 3.37 (s, 3H), 3.13 (s, 1H). ^{13}C NMR (100 MHz, $CDCl_3$) δ: 164.39, 140.61, 136.58, 135.75, 122.73, 120.10, 118.65, 81.99, 78.66, 72.05, 70.68, 69.13, 64.68, 59.17. The spectra aligns with what is found in literature. [4]

13.7.22Synthesis of compound **28**, 2-azido-5-ethynyl-*N*-(2,5,8,11,14,17-hexaoxanonadecan-19-yl)benzamide

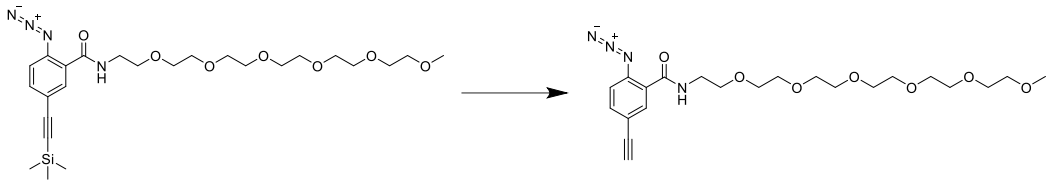

20 28

The synthetic procedure and signal assignment was based off work completed in the literature.[4]

This procedure is the same as that as the 'Synthesis of compound **27**', with the only difference being in the quantities utilized as follows; compound **20** (0.311 g, 0.578 mmol), TBAF.H_2O (0.338 g, 1.07 mmol, 1.85 eq.), THF (12 mL). The product acquired was that of a dark orange oil (0.26 g, percentage yield is not possible to determine as the product was not dried sufficiently due to time constraints as a results of compound auto-reaction). The product was then immediately utilized in the generalized polymerization procedure (procedure to follow).

MS (ESI): m/z = 465.24 (calculated 465.50 for [M + H^+]), 466.24 (calculated 466.50 for [M + $2H^+$]), 482.26 (calculated 482.50 for [M + NH_4^+]), 487.22 (calculated 487.50 for [M + Na^+]).

13.7.23Synthesis of compound **29**, 2,5,8,11,14,17-hexaoxanonadecan-19-yl (2-azido-5-ethynylbenzoyl)- D-alaninate

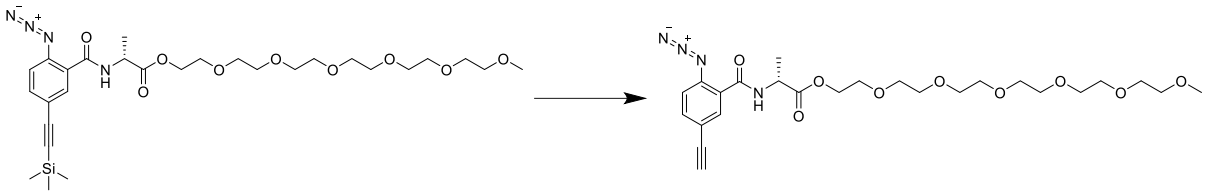

21 29

The synthetic procedure and signal assignment was based off work completed in the literature.[4]

The procedure for this step was conducted in the same manner as the 'Synthesis of compound **27**', with the only difference being in the quantities utilized as follows; compound **21** (1.946 g, 3.197 mmol), TBAF.H_2O (1.87 g, 5.92 mmol, 1.85 eq.), THF (64 mL). The product acquired was that of a bright orange oil (1.6 g, percentage yield is not possible to determine as the product was not dried due to time constraints as a results of compound auto-reaction). The product was then immediately utilized in the generalized polymerization procedure.

MS (ESI): *m/z* = 537.25 (calculated 537.58 for [M + H^+]), 554.28 (calculated 554.58 for [M + NH_4^+]), 555.29 (calculated 555.58 for [M + H_3O^+]), 559.24 (calculated 555.58 for [M + Na^+]), 575.21 (calculated 575.58 for [M + K^+]). Tetra(butyl) ammonium = 242.28 (calculated 242.20 for [M^+]), 243.28 (calculated 243.20 for [M^+ + H^+]). Compound 10 = 368.23 (calculated 368.25 for [M + H^+]), 369.23 (calculated 369.25 for [M + 2H^+]).

13.7.24Synthesis of compound **30**, 2,5,8,11,14,17-hexaoxanonadecan-19-yl (2-azido-5-ethynylbenzoyl)- D-alanyl- L-alaninate

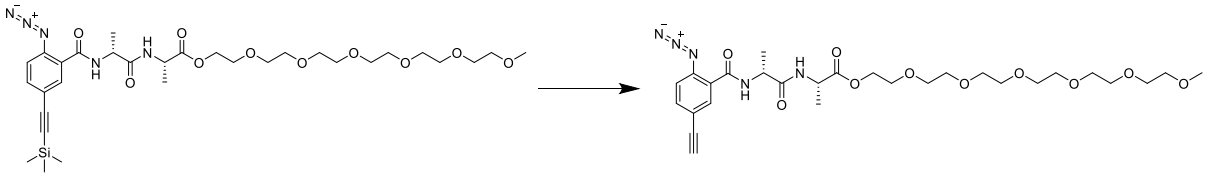

22 30

The synthetic procedure and signal assignment was based off work completed in the literature.[4]

The procedure for this synthesis was performed in the same manner as the 'Synthesis of compound **27**', with the differences being in the quantities of components utilized; compound **22** (0.56 g, 0.82 mmol), TBAF.H_2O (0.481 g, 1.523 mmol, 1.85 eq.), and THF (16 mL). The product acquired was that of a dark orange oil (0.5 g, percentage yield is not possible to determine as the product was not dried due to time

constraints as a results of compound auto-reaction). The product was then immediately utilized in the generalized polymerization procedure.

MS (ESI): *m/z* = 608.29 (calculated 608.66 for [M + H^+]), 609.29 (calculated 609.66 for [M + $2H^+$]), 625.32 (calculated 625.66 for [M + NH_4^+]), 626.32 (calculated 626.66 for [M + H_3O^+]). Tetra(butyl) ammonium = 242.28 (calculated 242.20 for [M^+]), 243.28 (calculated 243.20 for [$M^+ + H^+$]). Compound 10 = 368.23 (calculated 368.23 for [M + H^+]), 369.23 (calculated 369.23 for [M + $2H^+$]).

13.7.25Generalized polymerization procedure utilized for all monomers

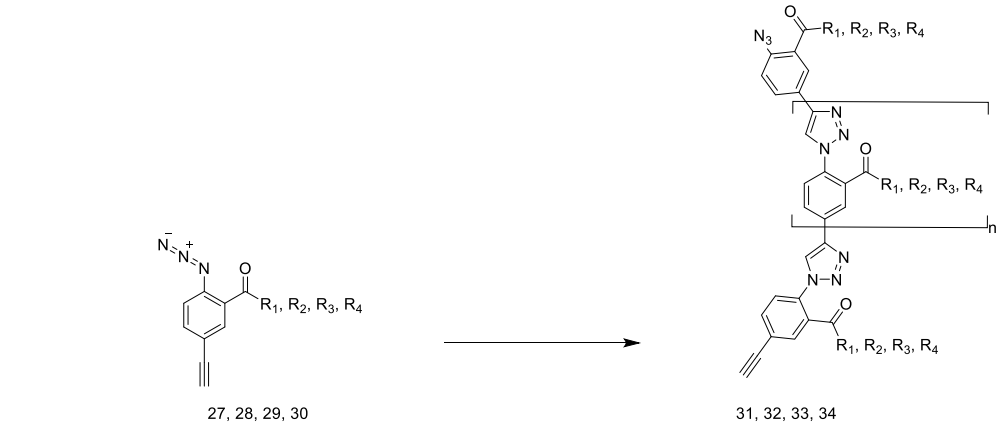

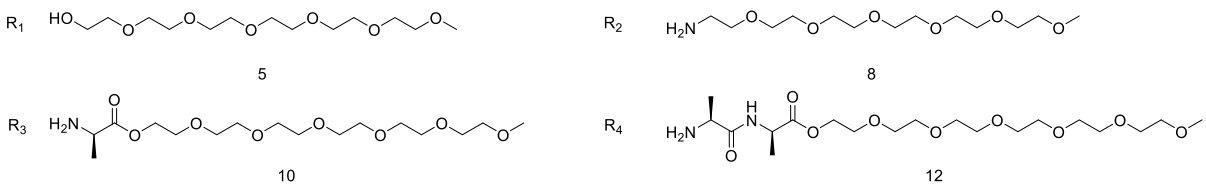

The synthetic procedure and signal assignment was based off work completed in the literature.[4]

A 50 mL, oven-dried schlenk flask was initially flushed with argon for 15 minutes. Once completed, the flask was charged with either compound **27**, **28**, **29**, or **30** (1.0 eq.) and an oval-shaped stir bar. PMDTA (0.11 eq.), ascorbic acid (0.05 eq.), DMF (0.65 mL per mmol of monomer), and TEA (0.11 eq.) were added to the schlenk flask. The flask was mixed for 30 seconds to make the contents homogenous. Once completed then the reaction flask was subjected to three freeze-pump-thaw cycles, where each time the flask was backfilled with argon. Once the cycles had been completed, the flask was opened and CuBr (0.11 eq.) was added quickly, and the flask was again sealed and subjected to three more freeze-pump-thaw cycles where again after each cycle the flask was backfilled with argon. After the last cycle the flask was added to a preheated 30 °C oil bath. The polymerization was then left to react for 1 day under an argon atmosphere. Over the course of the reaction, the colour of the mixture changed from dark yellow to dark green. After a day, the polymerization was considered finished, excess DMF

(approximately 3 mL) was added to the flask and the mixture was exposed to oxygen. Water was then added to the flask (10 mL water per 1 mL DMF in the flask). The contents of the flask were then transferred to a dialysis tubing with a 3.5 kDa cut-off. The dialysis tubing was left to dialyse for 1 week, with the dialysis water being changed twice a day to ensure low molecular weight compounds are removed as well as the copper from the reaction. Once the dialysis was complete, the contents were freeze dried and the redissolved in DMF (less than 1 mL per 0.5 g of sample). The sample was then diluted with $CHCl_3$ and dialyzed again for 1 day in $CHCl_3$ to ensure any low molecular weight compounds were removed.

Polymer **1**

Polymer 1

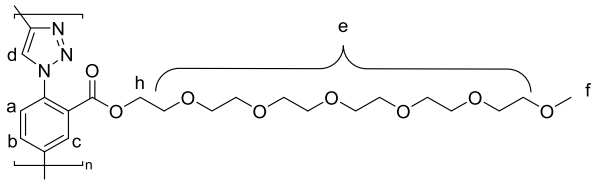

^{1}H NMR (400 MHz, DMF-d_7) δ: 9.45(s, **d**), 8.75 (s, **c**), 8.56 (s, **b**), 8.08 (s, **a**), 4.39 (s, **h**), 3.64 – 3.46 (m, **e**), 3.27 (s, **f**); ^{1}H,^{1}H GCOSY (400/400 MHz, DMF-d_7) δ: ^{1}H /δ ^{1}H ppm 8.09/ 8.54 (**a**/ **b**), 4.39/3.64 (**h** /**e**); ^{1}H,^{1}H ROESY (400/400 MHz, DMF-d_7) δ: ^{1}H /δ ^{1}H ppm 8.75/9.44 (**c**/**d**), 8.57/9.42, 8.08 (**b**/ **d**, **a**), 4.39/3.63 (**h** /**e**). The signals acquired match that which is identified in literature. [4,11]

Polymer **2**

Polymer 2

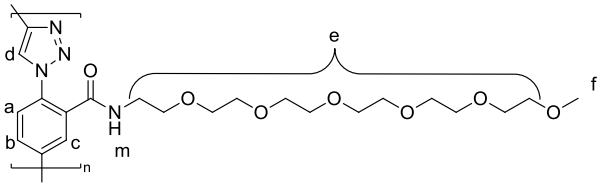

^{1}H NMR (400 MHz, DMF-d_7) δ: 9.17(s, **d**), 8.68 (s, **m**), 8.37 (s, **b** & **c**), 7.96 (m, **a**), 3.55 – 3.47 (m, **e**), 3.28 (s, **f**); ^{1}H,^{1}H GCOSY (400/400 MHz, DMF-d_7) δ: ^{1}H /δ ^{1}H ppm 8.67/ 3.52 (**m**/ **e**), 8.39/7.94 (**b** & **c** /**a**); ^{1}H,^{1}H ROESY (400/400 MHz, DMF-d_7) δ: ^{1}H /δ ^{1}H ppm 8.69/3.49 (**m**/**e**), 8.40, 8.39/9.17, 8.67 (**b** & **c**/ **d**, **m**). The tentative spectral assignment was made with the assistance of previously reported literature.[4,11]

Polymer **3**

Polymer 3

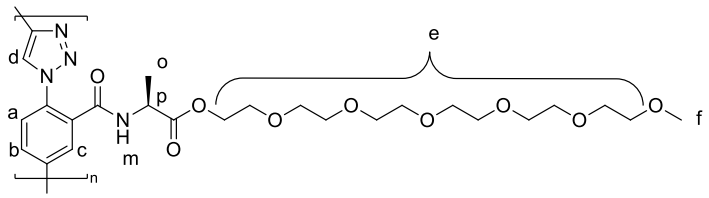

Due to the nature of the spectra acquired, it was not possible to assign many of the proton signals. It is possible to tentatively confirm polymer formation based on the below assignment. Considering that there are signals in the aromatic region, although these signals could not be confidently assigned, but it should be acknowledged that there are signals in this region. ^{1}H NMR (400 MHz, DMF-d_7) δ: 4.56 – 4.40 (m, **p**), 3.62 – 3.47 (m, **e**), 3.28 (s, **f**), 1.28 (s, **o**); ^{1}H,^{1}H GCOSY (400/400 MHz, DMF-d_7) δ: ^{1}H /δ ^{1}H ppm 3.49/ 1.22 (**e**/ **o**); ^{1}H,^{1}H ROESY (400/400 MHz, DMF-d_7) δ: ^{1}H /δ ^{1}H ppm, no signals. The tentative spectral assignment was made with the assistance of previously reported literature.[4,11]

Polymer **4**

Polymer 4

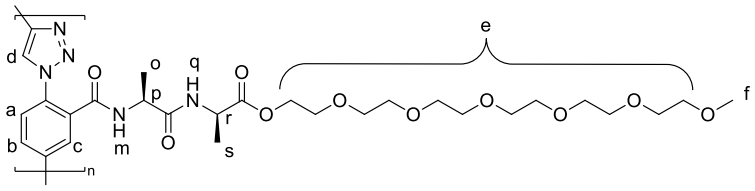

^{1}H NMR (400 MHz, DMF-d_7) δ: 9.35 – 9.23(m, **d**), 9.05 – 8.89 (m, **m**), 8.51 – 8.38 (m, **b** & **c**), 8.33 (s, **q**), 7.98 – 7.87 (m, **a**), 4.59 – 4.48 (m, **p**), 4.20 – 4.12 (m, **r**), 3.62 – 3.47 (m, **e**), 3.28 (s, **f**), 1.46 (s, **o**), 1.28 (s, **s**); ^{1}H,^{1}H GCOSY (400/400 MHz, DMF-d_7) δ: ^{1}H /δ ^{1}H ppm 8.41/ 8.01 (**b** & **c**/ **a**), 3.61/4.15 (**e**/**r**), 1.48/4.47 (**o**/**p**), 1.21/4.11 (**s**/ **r**); ^{1}H,^{1}H ROESY (400/400 MHz, DMF-d_7) δ: ^{1}H /δ ^{1}H ppm 9.30/8.45 (**d**/**b** & **c**), 8.47/8.93 (**b** & **c**/ **m**), 8.42/8.01 (**b** & **c**/ **a**), 8.33/4.59 (**q**/ **p**), 4.51/1.44 (**p**/**o**), 4.12/3.57 (**r**/ **e**), 1.46/4.52, 3.55 (**o**/ **p**, **e**). The tentative spectral assignment was made with the assistance of previously reported literature.[4,11]

14 Chapter 4- Future Work and Conclusions

14.1 Conclusions

During this study a library of polymers was modelled with the aid of molecular dynamics. It was determined *via* this brief computational study that incorporation of hydrogen bonding moieties within the repeat unit of these polymers would be beneficial and provide added stability within the helical supramolecular structures that would form. The computational model developed was a simplified representation of the actual structure and did not take into account the folding process, but instead only focused on the stability provided to the helix (that was assumed to have already folded into the correct conformation).

After the computational study, a library of polymers were synthesized, where the intermediates to afford the final monomeric units were characterized *via* a combination of NMR spectroscopy, mass spectrometry, and FTIR spectroscopy. The various polymers were characterized *via* NMR spectroscopy, FTIR spectroscopy, UV/Vis spectroscopy, LD, CD, DLS, and Standing TEM. Due to poor solubility of the polymers, it was not possible to accurately determine the molecular weight of the samples with the aid of readily available methods (DMF-SEC, HFIP-SEC, MALDI-ToF MS). Based on the various analytical methods, it was possible to determine that only polymer **1** folds. As it was not possible to accurately determine the molecular weights of the polymers, it is not possible to reach a final conclusion as to why polymer **2**, **3**, and **4**, do not fold. Three hypotheses have been made as to what may be inhibiting the folding of these polymers.

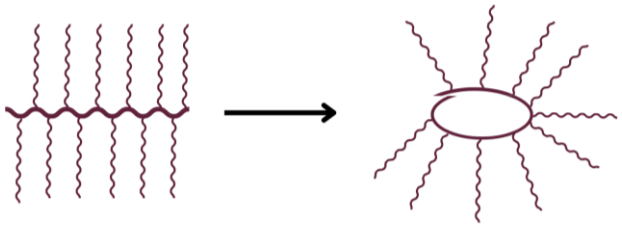

Figure 14-1: Hypotheses regarding the inhibition of folding of too short polymers.

The first hypothesis as to why polymers **2**, **3,** and **4**, do not fold related to the polymers having too low molecular weight, i.e. the polymer chains are too short to fold into a helix (Figure 14-1). The data acquired (by CD, LD, and UV/Vis spectroscopy) indicated that the polymers' ability to fold was independent of the solvent composition. In addition to this, the introduction of the template (PBLG) to polymer **3** resulted in signs of ordered structure formation (LD and CD). This suggests that the polymers

may be too short to form a single turn of a helix without the assistance of a template. In contrast, it was found that the polymers were only partially soluble where there was always solid residue that did not wish to dissolve. As it is known that polymer solubility is to some extent dependant on the molar mass, this insoluble fraction may be as a result of the presence of (very) high molecular weight polymers. Therefore leading into the second hypothesis, the polymers may be too long. If the polymers had a large molecular weight (>70 kDa) i.e. a very long polymer chain, it may be possible that the length of the polymer chains may be inhibiting the folding process *via* steric interactions among chains. These steric interactions would interrupt and inhibit the folding process, the polymers may not fold but may even instead form stacks of intertwined sheets. Thus, the hydrogen bonding groups do not form a helix but form hydrogen-bonded conglomerated sheets of sorts. This would inhibit the folding process and would explain the limited solubility. Again the large molecular weights cannot be proved as currently available methods could not be utilized to accurately determine the molecular weight of the polymers. The third hypothesis, is that that folding does not occur as a result of hydrogen bonding inhibiting the folding process. It may be possible that the hydrogen bonding groups may be inhibiting the folding process, thus instead of folding into ordered structures, the hydrogen bonding groups could be promoting the formation of disordered conglomerates that may be packed together *via* hydrogen bonding groups. This hypothesis may explain the visible aggregates forming in solution and the limited solubility in solution.

14.2 Future work

14.2.1 Future work on hydrogen bonding *para*-aryl triazole system

Although work has been conducted to characterize the novel polymer library developed in this work, the system still proves to be unresponsive to changes in solvent composition (without the presence of a template). This may be as a result of one of the noted hypotheses for this system mentioned in Section 4.1. Therefore, the first step towards further developing this system would be to be able to fully characterize it. This would entail the development of a methodology to determine the molecular weight of this polymer system. A number of systems could be used in this regard, namely field flow fractionation, DOESY NMR spectroscopy, or the usage of a custom matrix in MALDI-ToF MS.

Another aspect worth investigating is the development of a novel method of polymerization that ensures higher molecular weights of the polymer systems that include an amide moiety on the aromatic ring. This is because the moiety is hypothesized to impact the electronics of the system, to the extent where side reactions that inhibit polymerization occur at a greater extent/rate than is the case for aromatic rings with ester moieties present.[131,132] If it is found that the degree of hydrogen bonding actually inhibits the folding (one of the stated hypotheses) then this method would allow for the incorporation of hydrogen bonding moieties in every second or third monomeric unit, thus lessening the amount of hydrogen bonding occurring and maybe allowing the system to fold. The hydrogen bonding moieties would be

added to the system *via* post-polymerization coupling reactions to varying degrees of modification (Figure 14-2).

14.2.2 Applications and future work for the *para*-aryl triazole backbone

Although progress has been made, there is still a large amount of effort that needs to be made towards the further understanding of the *para*-aryl triazole system. Such a foldamer system has great potential

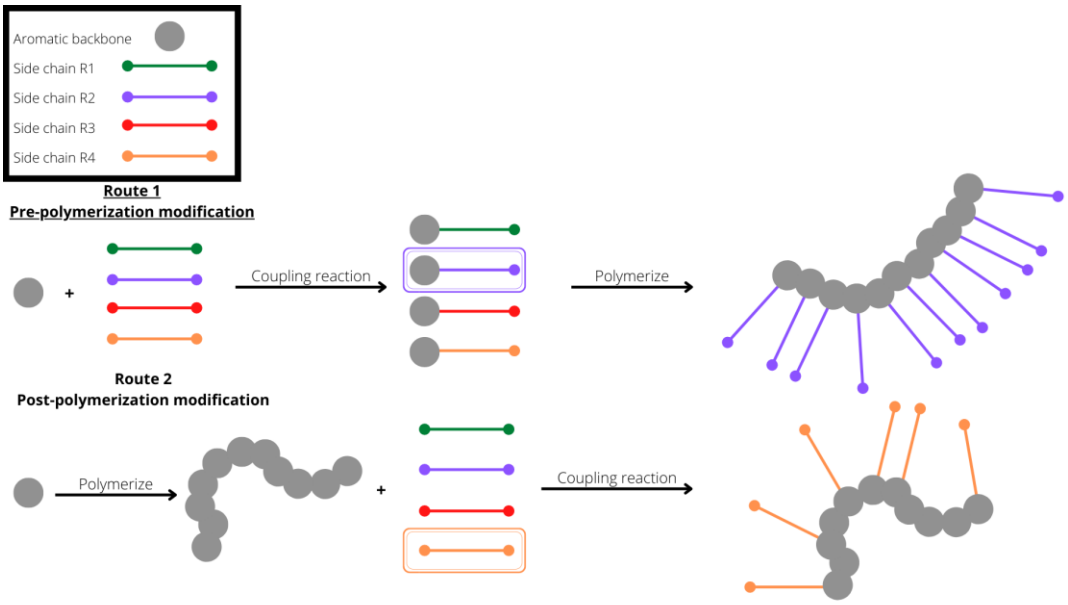

Figure 14-2: Comparison of methods to synthesize hydrogen bonding containing polymers. Route 1 was utilized in this thesis. Route 2 is a hypothesized procedure for future works.

in several applications. One such application would involve host-guest binding, where the foldamer would wrap around a suitably sized guest. This was previously conducted by Klumperman and co-workers,[11] In this previous work poly(γ-benzyl- L-glutamate) was utilized as a guest in the host-guest complex. The future work would thus build upon this host-guest ability of the foldamer system but will instead have a focus on the binding of anionic species in an aqueous environment. This has been conducted in the literature, but on smaller diameter foldamer systems.[32,135–137] The foldamer could be screened with a library of different sized anions, the binding efficiencies of the foldamer system to these anions could be studied and extraction studies could be conducted. This would both serve as an application of the foldamer system as well as provide insight as to the exact size of the foldamer system (Figure 14-3). The information on the dimensions of the foldamer system would greatly benefit later projects. The binding studies could be conducted *via* NMR spectroscopy.[138]

Another potential application that would be ideal for this foldamer system is that of the formation of a catalytic helix. The catalytic helix could afford the formation of enantiomerically pure organic compounds, which are highly sought after by pharmaceutical companies as well as other researchers. This enantiomerically pure product would be formed *via* the chirality that is imparted from the helical structure of the foldamer system. This helical system has inherent chirality due to the helix itself either

being a left-handed or a right-handed helix. The handedness of the helix could be biased based on the chirality of the monomeric unit utilized in the foldamer system.[4] The catalysis of reactions with helical polymers is not a new idea and can be found in literature.[2,139–142] It has also been conducted on other foldamer systems, although these foldamer systems are much smaller in diameter and this, in turn, limits the types of reagents that can be utilized, and thus limiting the scope of reactions that can be investigated.[143–149]

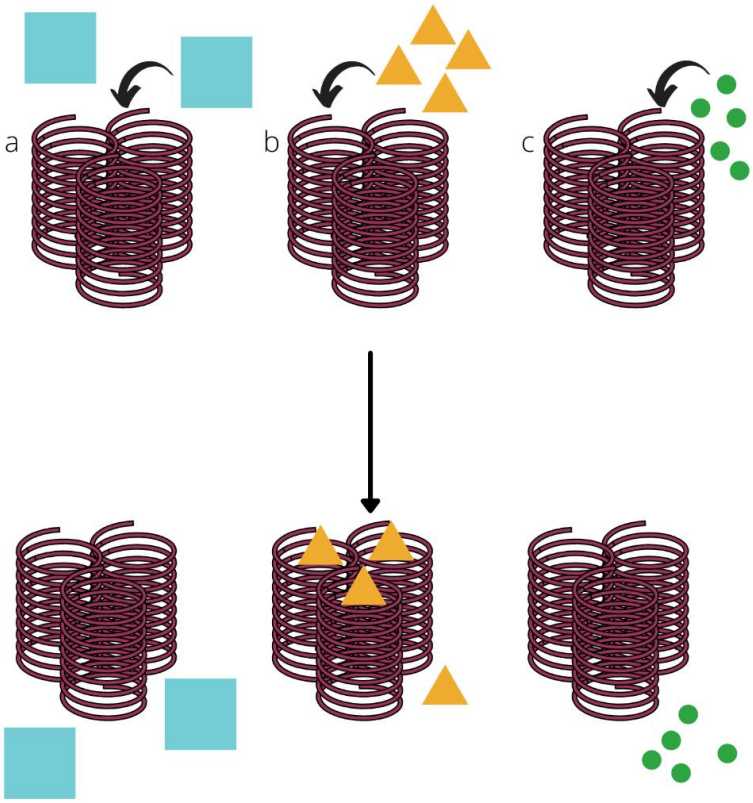

Figure 14-3: Representation of the binding of anions to the foldamer system. Scenario a) where the substrate is too large for the cavity of the foldamer system. Scenario b) where there is a high binding affinity to the foldamer system and the substrate fits in the cavity of the helix and c) where the substrate does fit in the cavity but has a low binding affinity to the foldamer system.

To achieve this final application several small research endeavours would need to be conducted. Starting with the investigation of the ability of the foldamer system to undergo a process called threading. This is a scenario where a substrate is threaded through a macrocyclic ring. This has been previously conducted by Deutman et al,[150] where a polymer was threaded through a macrocycle. This type of experiment would be utilized to determine whether the substrate could physically enter and pass through the cavity of the helix. This could confirm whether the foldamer system could indeed be utilized as a catalytic helix. Thus, a similar experiment could be conducted on the folded foldamer system where varyingly sized fluorescent substrates could be added to the foldamer system. Fluorescence microscopy could be used to analyse if the substrates can enter the cavity of the helix. This experiment could also be used to determine the maximum-sized substrate that can be used in conjunction with this catalytic foldamer system.

It is worth noting that there are preliminary, unpublished results from our lab, which indicate that it is possible to introduce a novel active centre on the foldamer system. This active centre could be used to introduce specific chemical groups on the inner surface of the helix. This modification could afford the foldamer system to act as a recyclable catalyst for various organic reactions depending on the chemical group that is introduced at this active site. Further research will be needed to confirm these preliminary results. Following this further investigation, it would be worthwhile investigating the number of these sites in one foldamer system, this can be conducted by binding fluorescent groups to the active centres. These fluorescent groups would thus act as chemical tags, the tags could then be visualized *via* fluorescence microscopy. This experiment would prove without question that these active sites are present on the foldamer system, and it would further prove the threading hypothesis discussed earlier. This final set of results would involve catalysis studies with various substrates based on the chemical groups that are added to the active site (Figure 14-4). In addition to this, catalysis studies could also be conducted with the foldamer system without modification or active sites. These experiments would prove that the incorporation of these active sites within the helix is beneficial and acts as a catalyst in chemical reactions, this type of experiment is often conducted in smaller (shorter internal diameter) foldamer systems in literature.[144,146–149]

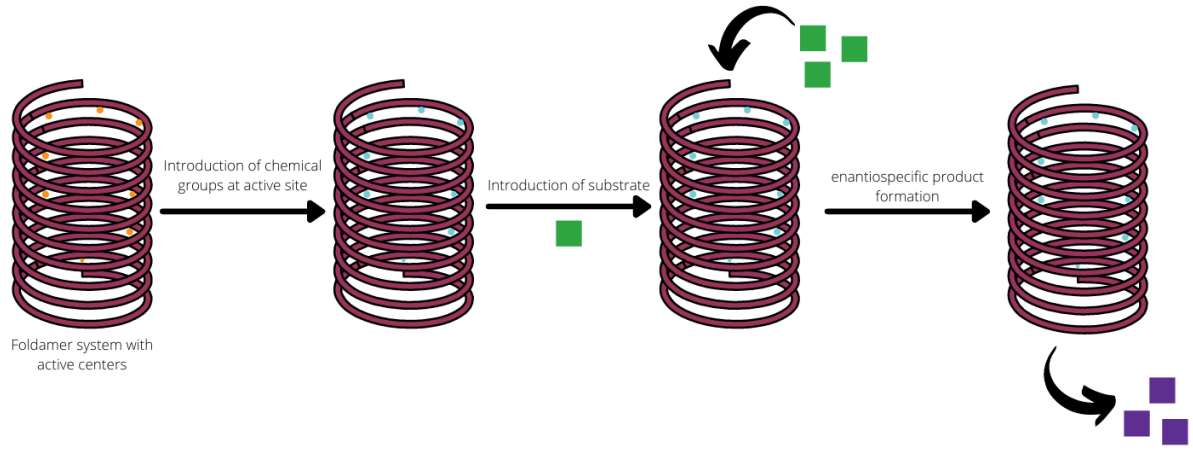

Figure 14-4: Mechanism for the formation of the foldamer-based catalytic helix. Where the active centre containing foldamer will be modified with a specific chemical group. The substrate will then be added to the foldamer system, and the reaction will occur. Once complete the polymer can be reacquired and recycled for another reaction.

15 Reference list

1 M. Toya, H. Ito and K. Itami, *Polym. Chem.*, 2021, **12**, 3290–3298.

2 R. P. Megens and G. Roelfes, *Chem. – Eur. J.*, 2011, **17**, 8514–8523.

3 T. Leigh and P. Fernandez-Trillo, *Nat. Rev. Chem.*, 2020, **4**, 291–310.

4 R. Pfukwa, P. H. J. Kouwer, A. E. Rowan and B. Klumperman, *Angew. Chem., Int. Ed. Engl.*, 2013, **52**, 11040–11044.

5 J. G. Carter, R. Pfukwa, L. Riley, J. H. R. Tucker, A. Rodger, T. R. Dafforn and B. Klumperman, *ACS Omega*, 2021, **6**, 33231–33237.

6 F. J. Vernerey, S. Lalitha Sridhar, A. Muralidharan and S. J. Bryant, *Chem. Rev.*, 2021, **18**, 11085-11148.

7 M. W. Tibbitt and K. S. Anseth, *Biotechnol. Bioeng.*, 2009, **103**, 655–663.

8 D. Jhala and R. Vasita, *Polym. Rev.*, 2015, **55**, 561–595.

9 K. A. Kyburz and K. S. Anseth, *Ann. Biomed. Eng.*, 2015, **43**, 489–500.

10 H. Yuan, J. Xu, E. P. van Dam, G. Giubertoni, Y. L. A. Rezus, R. Hammink, H. J. Bakker, Y. Zhan, A. E. Rowan, C. Xing and P. H. J. Kouwer, *Macromolecules*, 2017, **50**, 9058–9065.

11 R. Pfukwa, PhD thesis, University of Stellenbosch. 2012.

12 J. B. Reece, L. A. Urry, M. L. Cain, S. A. Wasserman, P. v. Minorsky and R. B. Jackson, *Campbell Biology 10th edition*, 2014, **1**, 66–91.

13 C. M. Runnels, K. A. Lanier, J. K. Williams, J. C. Bowman, A. S. Petrov, N. v. Hud and L. D. Williams, *J. Mol. Evol.*, 2018, **86**, 598–610.

14 D. J. Hill, M. J. Mio, R. B. Prince, T. S. Hughes and J. S. Moore, *Chem. Rev.*, 2001, **101**, 3893–4011.

15 Z. C. Girvin and S. H. Gellman, *J. Am. Chem. Soc.*, 2020, **142**, 17211–17223.

16 A. Said Stålsmeden, A. J. Paterson, I. C. Szigyártó, L. Thunberg, J. R. Johansson, T. Beke-Somfai and N. Kann, *Org. Biomol. Chem.*, 2020, **18**, 1957–1967.

17 A. J. Nicoll, D. J. Miller, K. Fütterer, R. Ravelli and R. K. Allemann, *J. Am. Chem. Soc.*, 2006, **128**, 9187–9193.

18 T. Umeno, A. Ueda, M. Doi, T. Kato, M. Oba and M. Tanaka, *Tetrahedron Lett.*, 2019, **60**, 151301.

19 A. J. Nicoll, C. J. Weston, C. Cureton, C. Ludwig, F. Dancea, N. Spencer, O. S. Smart, U. L. Günther and R. K. Allemann, *Org. Biomol. Chem.*, 2005, **3**, 4310–4315.

20 W. S. Horne, J. L. Price, J. L. Keck and S. H. Gellman, *J. Am. Chem. Soc.*, 2007, **129**, 4178–4180.

21 E. F. Lee, J. D. Sadowsky, B. J. Smith, P. E. Czabotar, K. J. Peterson-Kaufman, P. M. Colman, S. H. Gellman and W. D. Fairlie, *Angew. Chem., Int. Ed. Engl.*, 2009, **48**, 4318–4322.

22 P. Teng, N. Ma, D. C. Cerrato, F. She, T. Odom, X. Wang, L. J. Ming, A. van der Vaart, L. Wojtas, H. Xu and J. Cai, *J. Am. Chem. Soc.*, 2017, **139**, 7363–7369.

23 B. F. Fisher, L. Guo, B. S. Dolinar, I. A. Guzei and S. H. Gellman, *J. Am. Chem. Soc.*, 2015, **137**, 6484–6487.

24 W. S. Horne and S. H. Gellman, *Acc. Chem. Res.*, 2008, **41**, 1399–1408.

25 D. Bécart, V. Diemer, A. Salaün, M. Oiarbide, Y. R. Nelli, B. Kauffmann, L. Fischer, C. Palomo and G. Guichard, *J. Am. Chem. Soc.*, 2017, **139**, 12524–12532.

26 J. Fremaux, L. Mauran, K. Pulka-Ziach, B. Kauffmann, B. Odaert and G. Guichard, *Antew. Chem., Int. Ed. Engl.*, 2015, **54**, 9816–9820.

27 G. W. Collie, K. Pulka-Ziach, C. M. Lombardo, J. Fremaux, F. Rosu, M. Decossas, L. Mauran, O. Lambert, V. Gabelica, C. D. Mackereth and G. Guichard, *Nat. Chem.*, 2015, **7**, 871–878.

28 G. W. Collie, R. Bailly, K. Pulka-Ziach, C. M. Lombardo, L. Mauran, N. Taib-Maamar, J. Dessolin, C. D. Mackereth and G. Guichard, *J. Am. Chem. Soc.*, 2017, **139**, 6128–6137.

29 Y. Zhong, B. Kauffmann, W. Xu, Z. L. Lu, Y. Ferrand, I. Huc, X. C. Zeng, R. Liu and B. Gong, *Org. Lett.*, 2020, **22**, 6938–6942.

30 M. T. Stone and J. S. Moore, *Org. Lett.*, 2004, **6**, 469–472.

31 S. Kumar, M. Birol, D. E. Schlamadinger, S. P. Wojcik, E. Rhoades and A. D. Miranker, *Nat. Commun.*, 2016, **7**, 11412.

32 A. Borissov, I. Marques, J. Y. C. Lim, V. Félix, M. D. Smith and P. D. Beer, *J. Am. Chem. Soc.*, 2019, **141**, 4119–4129.

33 A. Tanatani, T. S. Hughes and J. S. Moore, *Angew. Chem., Int. Ed. Engl.*, 2002, **41**, 325-328.

34 Y. Liu, F. C. Parks, W. Zhao and A. H. Flood, *J. Am. Chem. Soc.*, 2018, **140**, 15477–15486.

35 P. Prabhakaran, G. Priya and G. J. Sanjayan, *Antew. Chem., Int. Ed. Engl.*, 2012, **51**, 4006–4008.

36 Y. Ferrand, Q. Gan, B. Kauffmann, H. Jiang and I. Huc, *Antew. Chem., Int. Ed. Engl.*, 2011, **50**, 7572–7575.

37 S. Hecht and I. Huc, *Foldamers: Structure, Properties, and Applications*, Weinheim, 2007.

38 H. Makida, H. Abe and M. Inouye, *Org. Biomol. Chem.*, 2015, **13**, 1700–1707.

39 D. W. Zhang, X. Zhao, J. L. Hou and Z. T. Li, *Chem. Rev.*, 2012, **112**, 5271–5316.

40 J. M. Cary and J. S. Moore, *Org. Lett.*, 2002, **4**, 4663–4666.

41 Y. Zhao, A. L. Connor, T. A. Sobiech and B. Gong, *Org. Lett.*, 2018, **20**, 5486–5489.

42 B. A. Ikkanda and B. L. Iverson, *Chem. Commun.*, 2016, **52**, 7752–7759.

43 Y. Ferrand and I. Huc, *Acc. Chem. Res.*, 2018, **51**, 970–977.

44 C. Kübel, M. J. Mio, J. S. Moore and D. C. Martin, *J. Am. Chem. Soc.*, 2002, **124**, 8605–8610.

45 Z. Luo, N. Zhu and D. Zhao, *Chem. – Eur. J.*, 2016, **22**, 11028–11034.

46 T. Beránek, J. Žádný, T. Strašák, J. Karban, I. Císařová, J. Sýkora and J. Storch, *ACS Omega*, 2020, **5**, 882–892.

47 W. Cai, G. T. Wang, P. Du, R. X. Wang, X. K. Jiang and Z. T. Li, *J. Am. Chem. Soc.*, 2008, **130**, 13450–13459.

48 Y. Hua, Y. Liu, C. H. Chen and A. H. Flood, *J. Am. Chem. Soc.*, 2013, **135**, 14401–14412.

49 S. Lee, Y. Hua and A. H. Flood, *J. Org. Chem.*, 2014, **79**, 8383–8396.

50 K. A. Dill, *Biochemistry*, 1990, **29**, 7133-7155.

51 W. Blokzijl and J. B. F. N. Engberts, *Angew. Chem., Int. Ed. Engl.*, 1993, **32**, 1545-1579.

52 D. Chandler, *Nature*, 2005, **437**, 640–647.

53 N. T. Southall and K. A. Dill, *J. Phys. Chem. B*, 2000, **104**, 1326–1331.

54 G. Haran, *Curr. Opin. Struct. Biol.*, 2012, **22**, 14–20.

55 M. Knott and H. S. Chan, *Chem. Phys.*, 2004, **307**, 187–199.

56 C. F. Wu, Z. M. Li, X. N. Xu, Z. X. Zhao, X. Zhao, R. X. Wang and Z. T. Li, *Chem. – Eur. J.*, 2014, **20**, 1418–1426.

57 R. B. Prince, S. A. Barnes and J. S. Moore, *J. Am. Chem. Soc.*, 2000, **122**, 2758–2762.

58 P. Zhang, L. Zhang, Z. K. Wang, Y. C. Zhang, R. Guo, H. Wang, D. W. Zhang and Z. T. Li, *Chem. Asian J.*, 2016, **11**, 1725–1730.

59 J. J. L. M. Cornelissen, J. J. J. M. Donners, R. de Gelder, W. S. Graswinckel, G. A. Metselaar, A. E. Rowan, N. A. J. M. Sommerdijk and R. J. M. Nolte, *Sci.*, 2001, **293**, 676-680.

60 W. Zhao, Y. Wang, J. Shang, Y. Che and H. Jiang, *Chem. – Eur. J.*, 2015, **21**, 7731–7735.

61 Y. Wang, F. Bie and H. Jiang, *Org. Lett.*, 2010, **12**, 3630–3633.

62 H. G. Jeon, H. B. Jang, P. Kang, Y. R. Choi, J. Kim, J. H. Lee, M. G. Choi and K. S. Jeong, *Org. Lett.*, 2016, **18**, 4404–4407.

63 C. Adam, L. Faour, V. Bonnin, T. Breton, E. Levillain, M. Sallé, C. Gautier and D. Canevet, *Chem. Commun.*, 2019, **55**, 8426–8429.

64 R. Hein, A. Borissov, M. D. Smith, P. D. Beer and J. J. Davis, *Chem. Commun.*, 2019, **55**, 4849–4852.

65 Y. Wang, J. Xiang and H. Jiang, *Chem. – Eur. J.*, 2011, **17**, 613–619.

66 L. Y. You, S. G. Chen, X. Zhao, Y. Liu, W. X. Lan, Y. Zhang, H. J. Lu, C. Y. Cao and Z. T. Li, *Antew. Chem., Int. Ed. Engl.*, 2012, **51**, 1657–1661.

67 H. Juwarker, J. M. Suk and K. S. Jeong, *Chem. Soc. Rev.*, 2009, **38**, 3316–3325.

68 S. Qi, C. Zhang, H. Yu, J. Zhang, T. Yan, Z. Lin, B. Yang and Z. Dong, *J. Am. Chem. Soc.*, 2021, **143**, 3284–3288.

69 F. Chen, J. Shen, N. Li, A. Roy, R. Ye, C. Ren and H. Zeng, *Antew. Chem., Int. Ed. Engl.*, 2020, **132**, 1456–1460.

70 J. M. Suk, V. R. Naidu, X. Liu, M. S. Lah and K. S. Jeong, *J. Am. Chem. Soc.*, 2011, **133**, 13938–13941.

71 J. Y. Hwang, H. G. Jeon, Y. R. Choi, J. Kim, P. Kang, S. Lee and K. S. Jeong, *Org. Lett.*, 2017, **19**, 5625–5628.

72 J. M. Suk and K. S. Jeong, *J. Am. Chem. Soc.*, 2008, **130**, 11868–11869.

73 H. B. Jang, Y. R. Choi and K. S. Jeong, *J. Org. Chem.*, 2018, **83**, 5123–5131.

74 H. G. Jeon, J. Y. Jung, P. Kang, M. G. Choi and K. S. Jeong, *J. Am. Chem. Soc.*, 2016, **138**, 92–95.

75 Z. Yu, S. Weidner, T. Risse and S. Hecht, *Chem. Sci.*, 2013, **4**, 4156–4167.

76 R. A. Smaldone and J. S. Moore, *J. Am. Chem. Soc.*, 2007, **129**, 5444–5450.

77 K. Ghosh and J. S. Moore, *J. Am. Chem. Soc.*, 2011, **133**, 19650–19652.

78 H. H. Nguyen, J. H. McAliley, W. R. Batson and D. A. Bruce, *Macromolecules*, 2010, **43**, 5932–5942.

79 A. Tanatani, M. J. Mio and J. S. Moore, *J. Am. Chem. Soc.*, 2001, **123**, 1792–1793.

80 P. K. Mandal, B. Benoît, B. Langlois d'Estaintot, B. Kauffmann and I. Huc, *ChemBioChem*, 2016, **17**, 1911–1914.

81 C. Bao, Q. Gan, B. Kauffmann, H. Jiang and I. Huc, *Chem. – Eur. J.*, 2009, **15**, 11530–11536.

82 L. Zheng, C. Yu, Y. Zhan, X. Deng, Y. Wang and H. Jiang, *Chem. – Eur. J.*, 2017, **23**, 5361–5367.

83 L. Zheng, D. Zheng, Y. Wang, C. Yu, K. Zhang and H. Jiang, *Org. Biomol. Chem.*, 2019, **17**, 9573–9577.

84 H. Y. Hu, J. F. Xiang, Y. Yang and C. F. Chen, *Org. Lett.*, 2008, **10**, 1275–1278.

85 N. Chandramouli, Y. Ferrand, B. Kauffmann and I. Huc, *Chem. Commun.*, 2016, **52**, 3939–3942.

86 A. Méndez-Ardoy, N. Markandeya, X. Li, Y. T. Tsai, G. Pecastaings, T. Buffeteau, V. Maurizot, L. Muccioli, F. Castet, I. Huc and D. M. Bassani, *Chem. Sci.*, 2017, **8**, 7251–7257.

87 Y. Zhao, Z. Zhong and E. H. Ryu, *J. Am. Chem. Soc.*, 2007, **129**, 218–225.

88 Y. Zhao and Z. Zhong, *J. Am. Chem. Soc.*, 2006, **128**, 9988–9989.

89 Y. Zhao and Z. Zhong, *J. Am. Chem. Soc.*, 2005, **127**, 17894–17901.

90 Z. Zhong and Y. Zhao, *Org. Lett.*, 2007, **9**, 2891–2894.

91 X. Pan and Y. Zhao, *Org. Lett.*, 2009, **11**, 69–72.

92 Y. Zhao and Z. Zhong, *Org. Lett.*, 2006, **8**, 4715–4717.

93 Z. Zhong and Y. Zhao, *J. Org. Chem.*, 2008, **73**, 5498–5505.

94 D. Dziubak, K. Pułka-Ziach and S. Sęk, *J. Phys. Chem. C*, 2020, **124**, 17916–17923.

95 K. Pulka-Ziach, A. K. Puszko, J. Juhaniewicz-Debinska and S. Sek, *J. Phys. Chem. C*, 2019, **123**, 1136–1141.

96 J. M. Rodriguez and A. D. Hamilton, *Angew. Chem., Int. Ed. Engl.*, 2007, **46**, 8614–8617.

97 B. Wu, C. Jia, X. Wang, S. Li, X. Huang and X. J. Yang, *Org. Lett.*, 2012, **14**, 684–687.

98 R. Wechsel, J. Raftery, D. Cavagnat, G. Guichard and J. Clayden, *Angew. Chem., Int. Ed. Engl.*, 2016, **128**, 9809–9813.

99 S. Liu, P. Y. Zavalij, Y. F. Lam and L. Isaacs, *J. Am. Chem. Soc.*, 2007, **129**, 11232–11241.

100 D. W. Zhang, W. K. Wang and Z. T. Li, *Chem. Rec.*, 2015, **15**, 233–251.

101 R. P. Cheng, *Curr. Opin. Struct. Biol.*, 2004, **14**, 512–520.

102 H. Juwarker and K. S. Jeong, *Chem. Soc. Rev.*, 2010, **39**, 3664–3674.

103 I. Huc and H. Jiang, *Supramolecular Chemistry*, John Wiley & Sons, Ltd, 2012.

104 E. A. John, C. J. Massena and O. B. Berryman, *Chem. Rev.*, 2020, **120**, 2759–2782.

105 S. Rinaldi, *Molecules*, 2020, **25**, 3276.

106 D. W. Zhang, X. Zhao and Z. T. Li, *Acc. Chem. Res.*, 2014, **47**, 1961–1970.

107 D. W. Zhang, X. Zhao, J. L. Hou and Z. T. Li, *Chem. Rev.*, 2012, **112**, 5271–5316.

108 Y. Hua and A. H. Flood, *Chem. Soc. Rev.*, 2010, **39**, 1262–1271.

109 M. Juríek, P. H. J. Kouwer and A. E. Rowan, *Chem. Commun.*, 2011, **47**, 8740–8749.

110 V. Haridas, S. Sahu, P. P. Praveen Kumar and A. R. Sapala, *RSC Adv.*, 2012, **2**, 12594–12605.

111 J. Shang, W. Zhao, X. Li, Y. Wang and H. Jiang, *Chem. Commun.*, 2016, **52**, 4505–4508.

112 Y. Wang, W. Zhao, F. Bie, L. Wu, X. Li and H. Jiang, *Chem. – Eur. J.*, 2016, **22**, 5233–5242.

113 Y. Hua and A. H. Flood, *J. Am. Chem. Soc.*, 2010, **132**, 12838–12840.

114 D. Mondal, M. Ahmad, P. Panwaria, A. Upadhyay and P. Talukdar, *J. Org. Chem.*, 2022, **87**, 10–17.

115 J. Shang, N. M. Gallagher, F. Bie, Q. Li, Y. Che, Y. Wang and H. Jiang, *J. Org. Chem.*, 2014, **79**, 5134–5144.

116 J. Shang, W. Si, W. Zhao, Y. Che, J. L. Hou and H. Jiang, *Org. Lett.*, 2014, **16**, 4008–4011.

117 F. C. Parks, E. G. Sheetz, S. R. Stutsman, A. Lutolli, S. Debnath, K. Raghavachari and A. H. Flood, *J. Am. Chem. Soc.*, 2022, **144**, 1274–1287.

118 Y. Liu, F. C. Parks, E. G. Sheetz, C. H. Chen and A. H. Flood, *J. Am. Chem. Soc.*, 2021, **143**, 3191–3204.

119 M. Jaspers, A. C. H. Pape, I. K. Voets, A. E. Rowan, G. Portale and P. H. J. Kouwer, *Biomacromolecules*, 2016, **17**, 2642–2649.

120 M. Banno, T. Yamaguchi, K. Nagai, C. Kaiser, S. Hecht and E. Yashima, *J. Am. Chem. Soc.*, 2012, **134**, 8718–8728.

121 A. Kargaard, MSc thesis, University of Stellenbosch, 2014.

122 C. Lu, C. Wu, D. Ghoreishi, W. Chen, L. Wang, W. Damm, G. A. Ross, M. K. Dahlgren, E. Russell, C. D. von Bargen, R. Abel, R. A. Friesner and E. D. Harder, *J. Chem. Theory Comput.*, 2021, **17**, 4291–4300.

123 M. W. Mahoney and W. L. Jorgensen, *J. Chem. Phys.*, 2000, **112**, 8910–8922.

124 K. Sargsyan, C. Grauffel and C. Lim, *J. Chem. Theory Comput.*, 2017, **13**, 1518–1524.

125 A. M. Wawro, T. Muraoka, M. Kato and K. Kinbara, *Org. Chem. Front.*, 2016, **3**, 1524–1534.

126 A. M. Wawro, T. Muraoka and K. Kinbara, *Polym. Chem.*, 2016, **7**, 2389–2394.

127 D. C. Batesky, M. J. Goldfogel and D. J. Weix, *J. Org. Chem.*, 2017, **82**, 9931–9936.

128 Y. Tamboli, B. B. Kashid, R. P. Yadav, M. Rafeeq, R. Yeole and A. Y. Merwade, *ACS Omega*, 2021, **6**, 13940–13945.

129 S. Mandal, Z. H. Eksteen-Akeroyd, M. J. Jacobs, R. Hammink, M. Koepf, A. J. A. Lambeck, J. C. M. van Hest, C. J. Wilson, K. Blank, C. G. Figdor and A. E. Rowan, *Chem. Sci*, 2013, **4**, 4168-4174.

130 M. Breugst and H. U. Reissig, *Angew. Chem., Int. Ed. Engl.*, 2020, **59**, 12293–12307.

131 M. Roemer, I. Luck and N. Proschogo, *Adv. Synth. Catal.*, 2022, **59**, 12293-12307.

132 H. Kwart and A. A. Kahn, *J. Am. Chem. Soc.*, 1967, **89**, 1950–1951.

133 F. A. Cotton, *Inorganic Syntheses*, 1972, **13**.

134 W. L. F. Armarego and D. D. Perrin, *Purification of laboratory chemicals*, Butterworth Heinemann, 1997.

135 É. M. Foyle and N. G. White, *Chem. Asian J.*, 2021, **16**, 575–587.

136 J. Cai and J. L. Sessler, *Chem. Soc. Rev.*, 2014, **43**, 6198–6213.

137 W. Zhao, F. Huang, Y. Wang, Q. Li, J. Shang, Y. Che and H. Jiang, *Tetrahedron Lett.*, 2016, **57**, 1691–1694.

138 D. von der Heiden, A. Vanderkooy and M. Erdélyi, *Coord. Chem. Rev.*, 2020, **407**, 213147.

139 L. Shen, L. Xu, X. H. Hou, N. Liu and Z. Q. Wu, *Macromolecules*, 2018, **51**, 9547–9554.

140 J. Deng, J. Deng and B. Zhao, *Ind. Eng. Chem. Res.*, 2016, **55**, 7328–7337.

141 T. Yamamoto, T. Yamada, Y. Nagata and M. Suginome, *J. Am. Chem. Soc.*, 2010, **132**, 7899–7901.

142 Y. Akai, L. Konnert, T. Yamamoto and M. Suginome, *Chem. Commun.*, 2015, **51**, 7211–7214.

143 Q. N. Duong, L. Schifferer and O. García Mancheño, *Eur. J. Org. Chem.*, 2019, **2019**, 5452–5461.

144 M. Zurro and O. G. Mancheño, *Chem. Rec.,* 2017, **17**, 485–498.

145 D. G. Piekarski, P. Steinforth, M. Gómez-Martínez, J. Bamberger, F. Ostler, M. Schönhoff and O. García Mancheño, *Chem. – Eur. J.*, 2020, **26**, 17598–17603.

146 M. Zurro, S. Asmus, J. Bamberger, S. Beckendorf and O. García Mancheño, *Chem. – Eur. J.*, 2016, **22**, 3785–3793.

147 T. Fischer, Q. N. Duong and O. García Mancheño, *Chem. – Eur. J.*, 2017, **23**, 5983–5987.

148 M. Zurro, S. Asmus, S. Beckendorf, C. Mück-Lichtenfeld and O. G. Mancheño, *J. Am. Chem. Soc.*, 2014, **136**, 13999–14002.

149 T. Fischer, J. Bamberger and O. G. Mancheño, *Org. Biomol. Chem.*, 2016, **14**, 5794–5802.

150 A. B. C. Deutman, S. Cantekin, J. A. A. W. Elemans, A. E. Rowan and R. J. M. Nolte, *J. Am. Chem. Soc.*, 2014, **136**, 9165–9172.

151 A. M. Abramyan, Z. Liu and V. Pophristic, *Phys. Chem. Chem. Phys.*, 2014, **16**, 20406–20410.

16 Addendum A

16.1 Spectral data

16.1.1 Compound 2

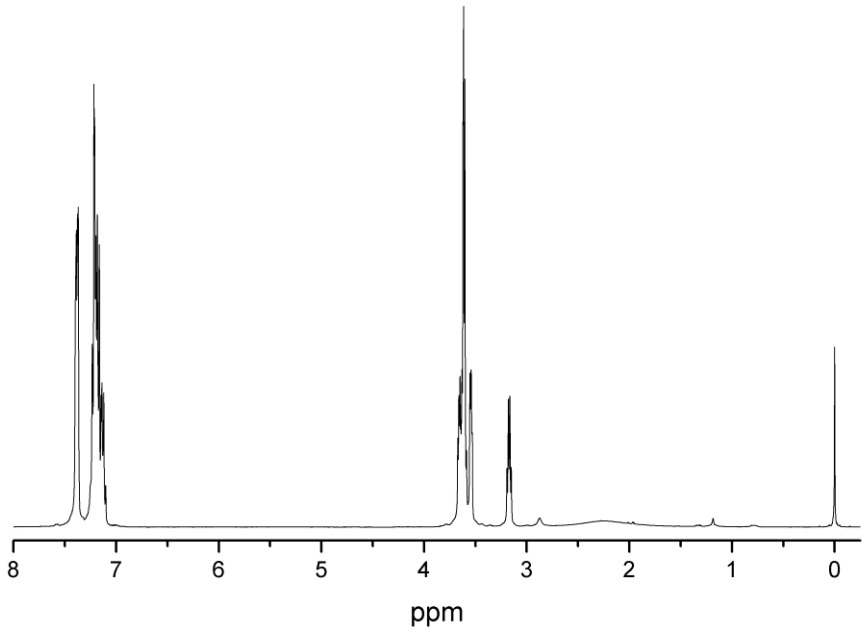

Figure 16-1: ^{1}H NMR spectrum of compound 2.

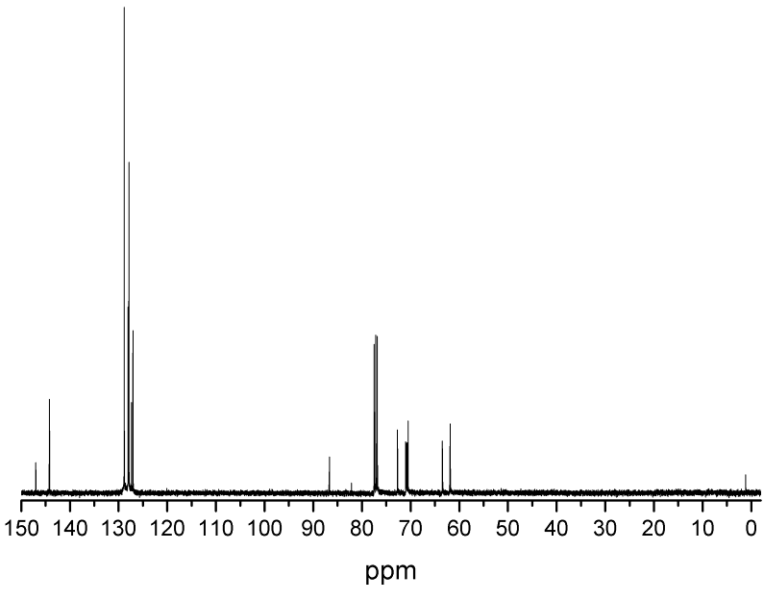

Figure 16-2: ^{13}C NMR of compound 2.

16.1.2 Compound 3

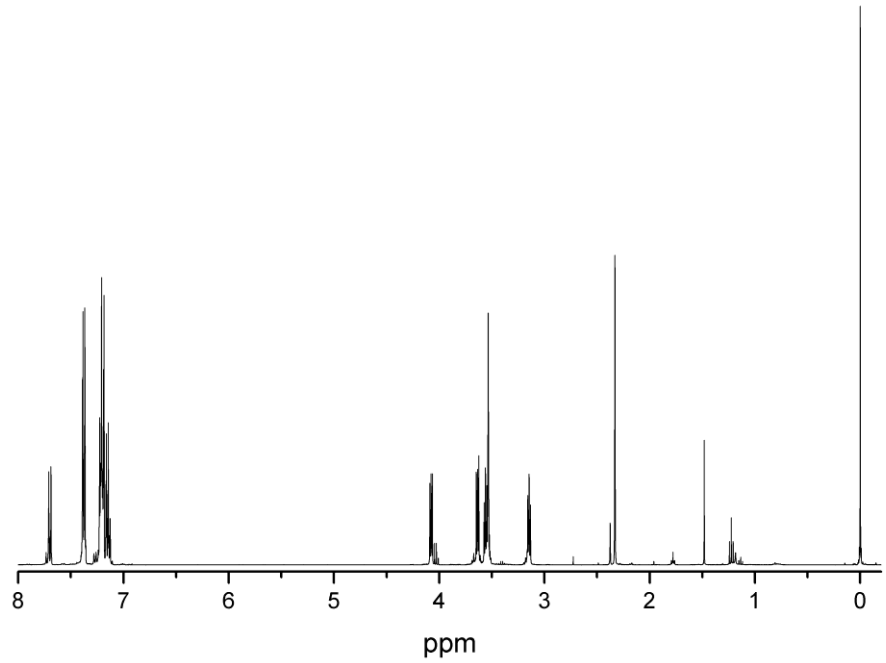

Figure 16-3: ^{1}H NMR of compound 3.

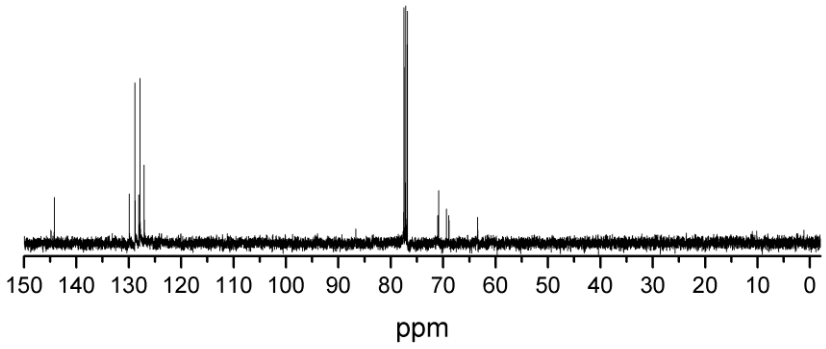

Figure 16-4: ^{13}C NMR of compound 3.

16.1.3 Compound 4

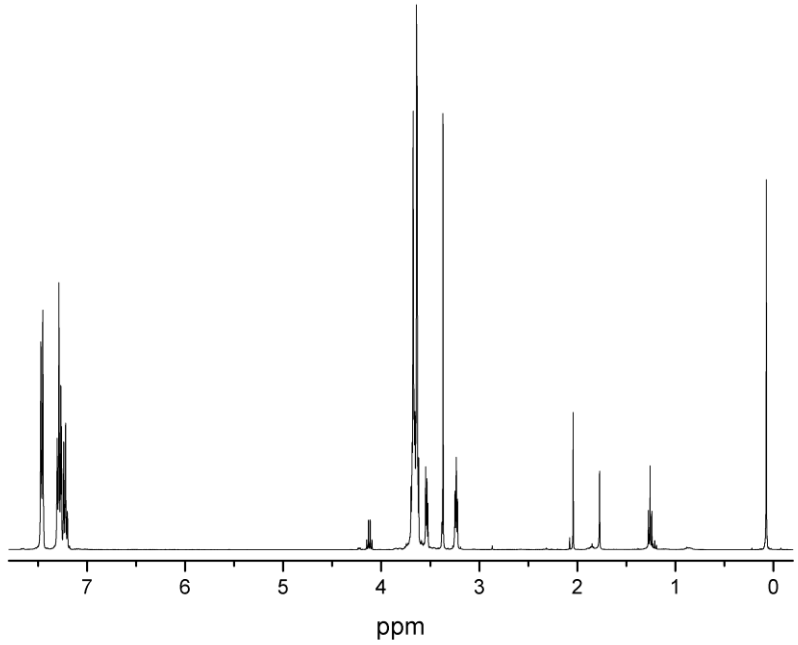

Figure 16-5: ^{1}H NMR of compound 4.

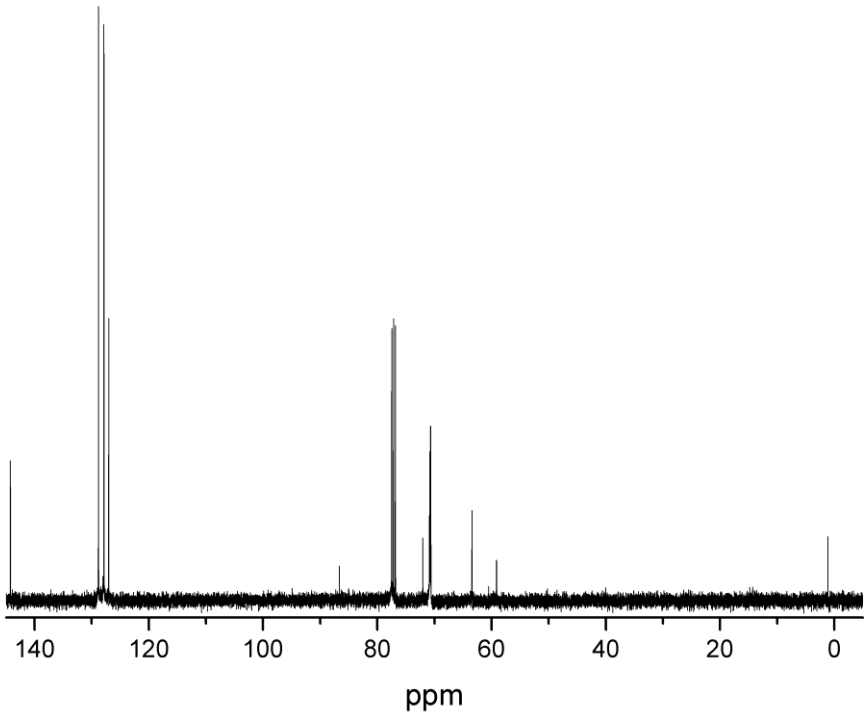

Figure 16-6: ^{13}C NMR of compound 4.

16.1.4 Compound 5

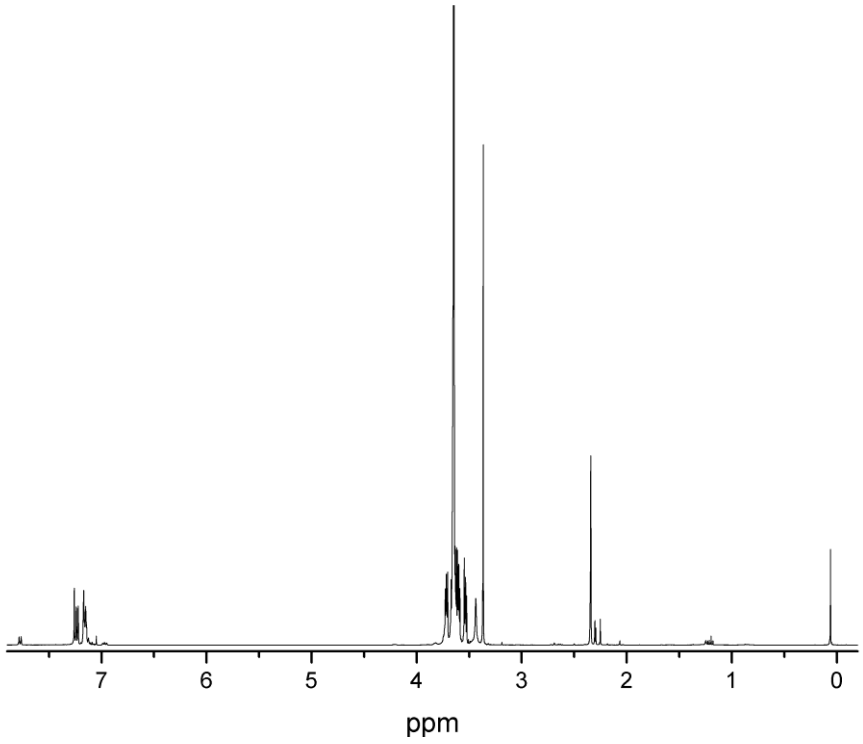

Figure 16-7: ^{1}H NMR of compound 5.

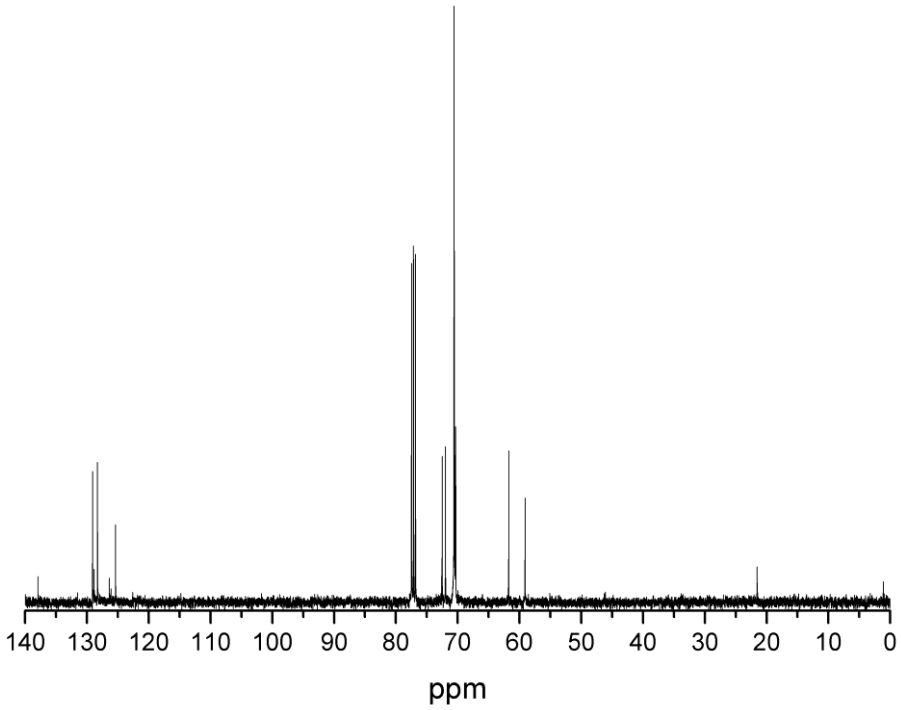

Figure 16-8: ^{13}C NMR of compound 5.

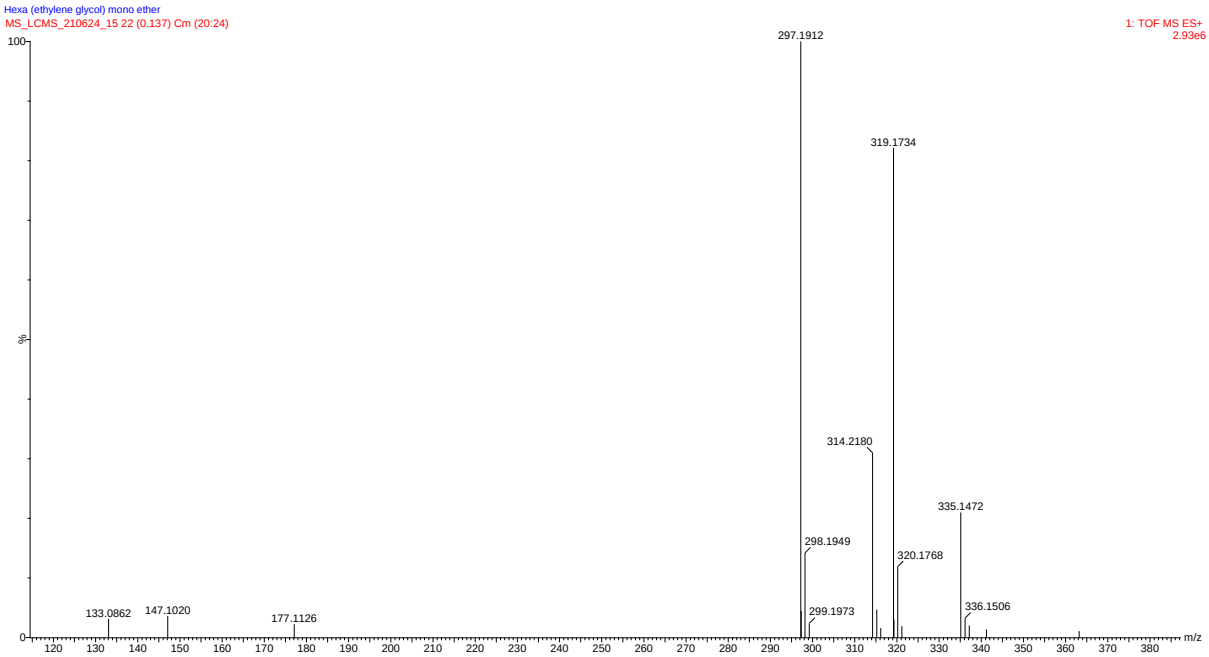

Figure 16-9: Mass spectrum of compound 5.

16.1.5 Compound 6

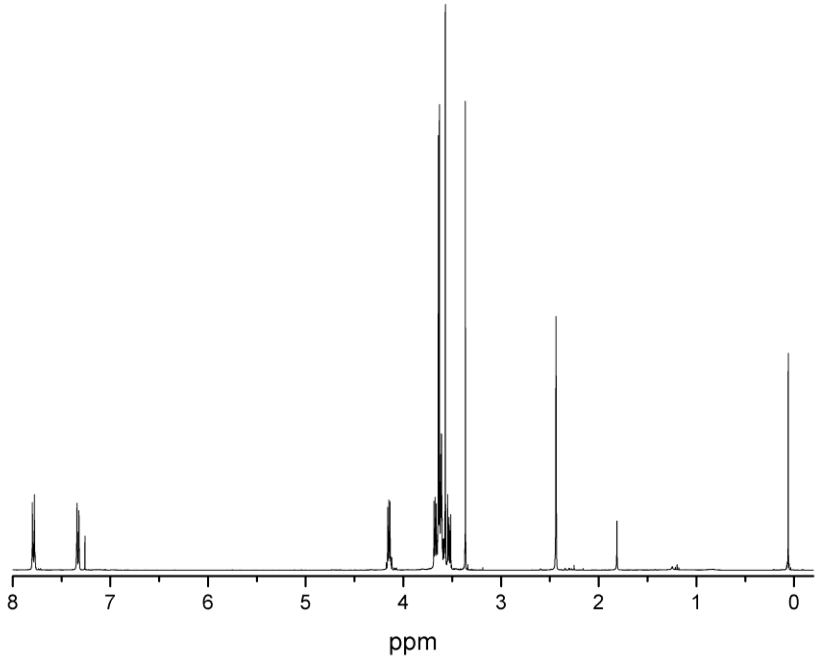

Figure 16-10: ^{1}H NMR of compound 6.

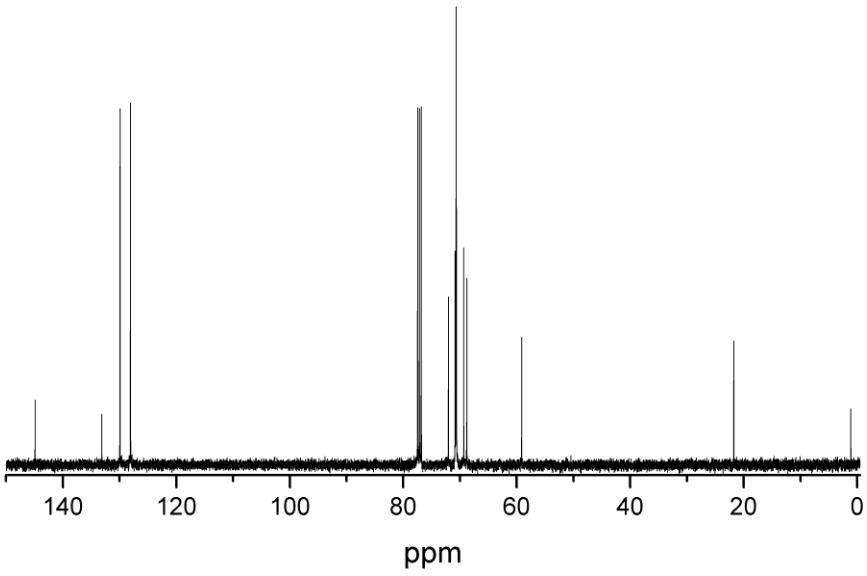

Figure 16-11: ^{13}C NMR of compound 6.

16.1.6 Compound 7

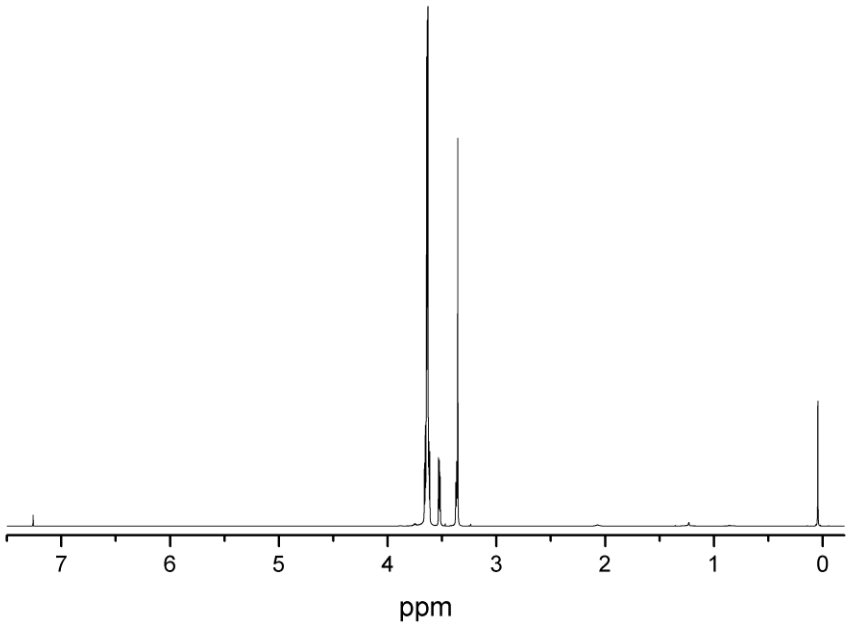

Figure 16-12: ^{1}H NMR of compound 7.

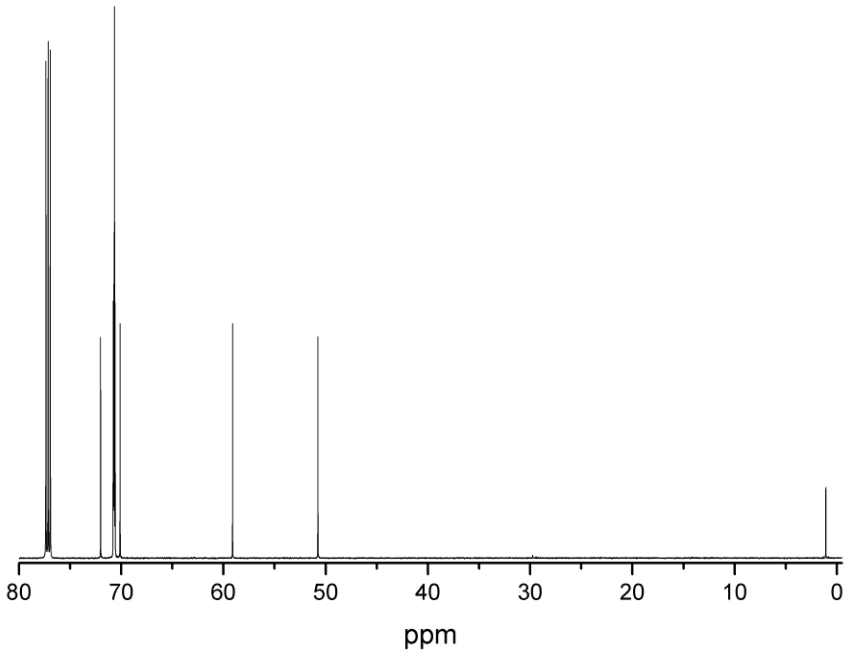

Figure 16-13: ^{13}C NMR of compound 7.

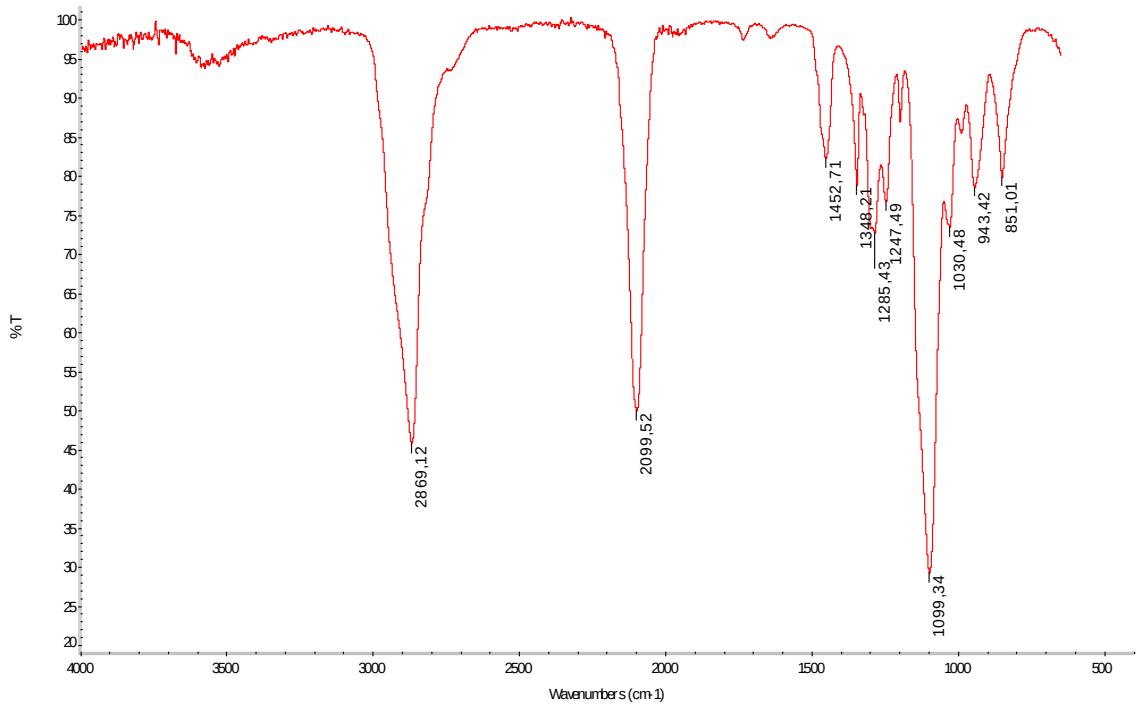

Figure 16-14: IR spectrum of compound 7.

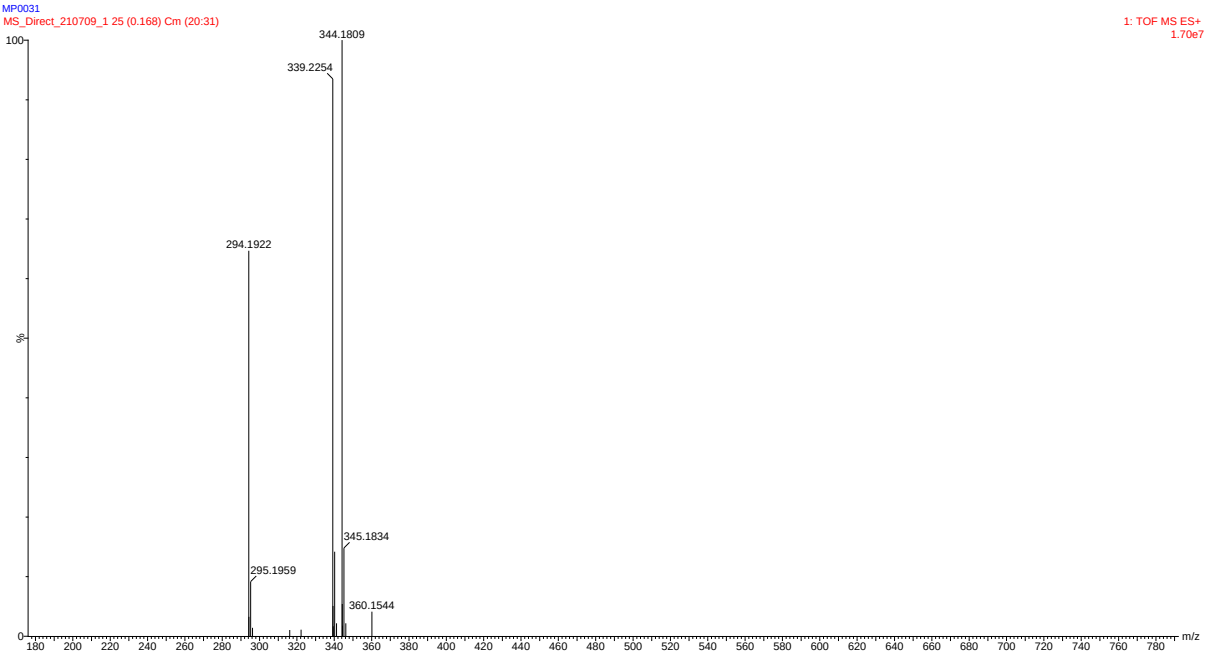

Figure 16-15: Mass spectrum of compound 7.

16.1.7 Compound 8

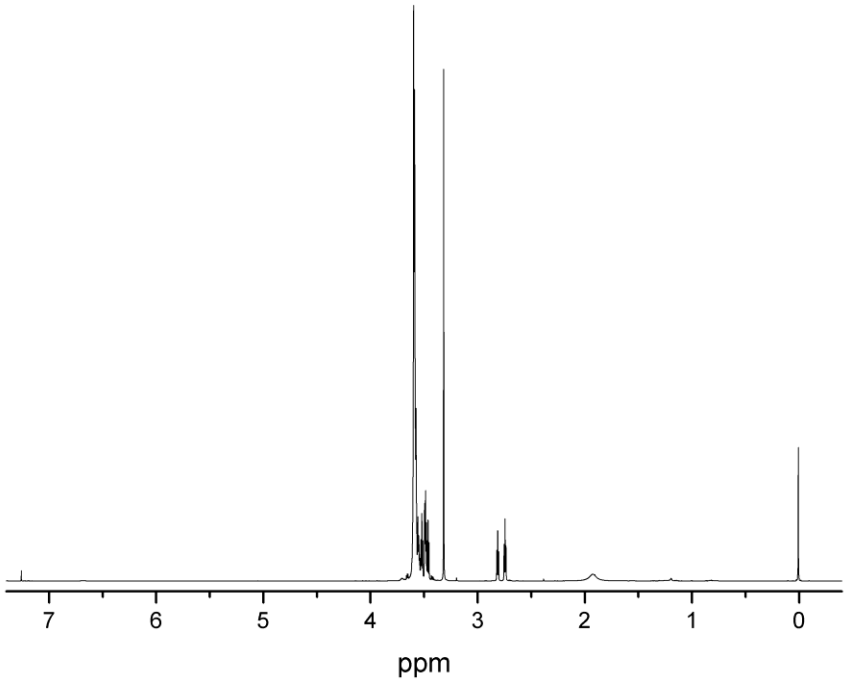

Figure 16-16: ^{1}H NMR of compound 8.

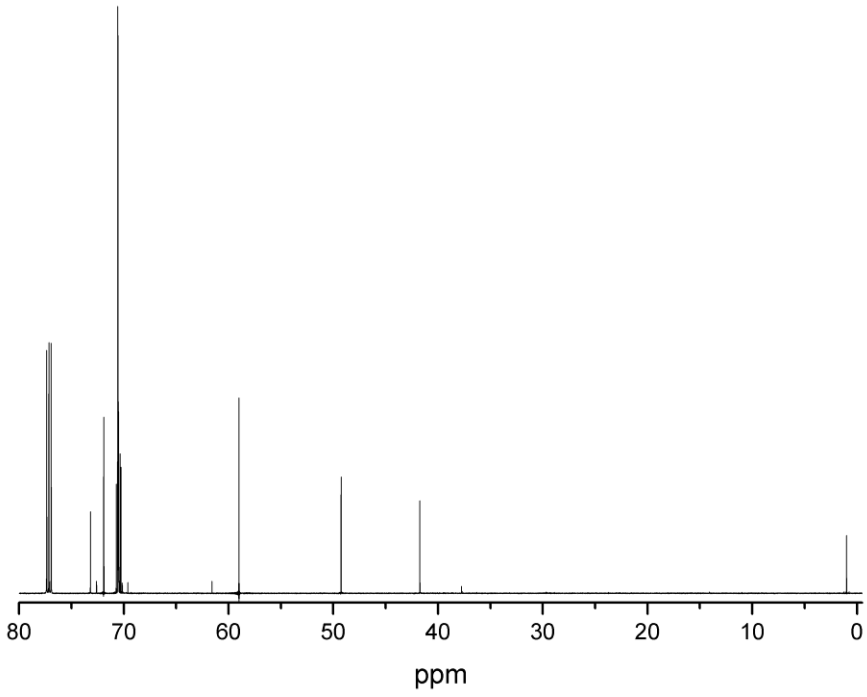

Figure 16-17: ^{13}C NMR of compound 8.

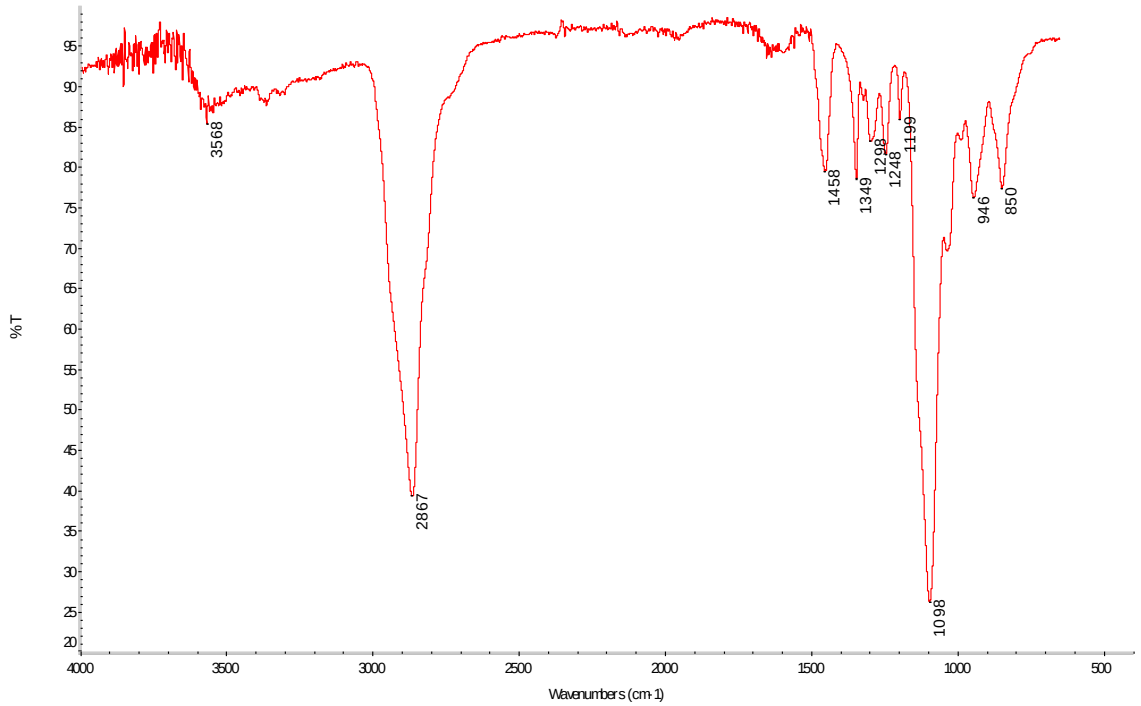

Figure 16-18: IR spectrum of compound 8.

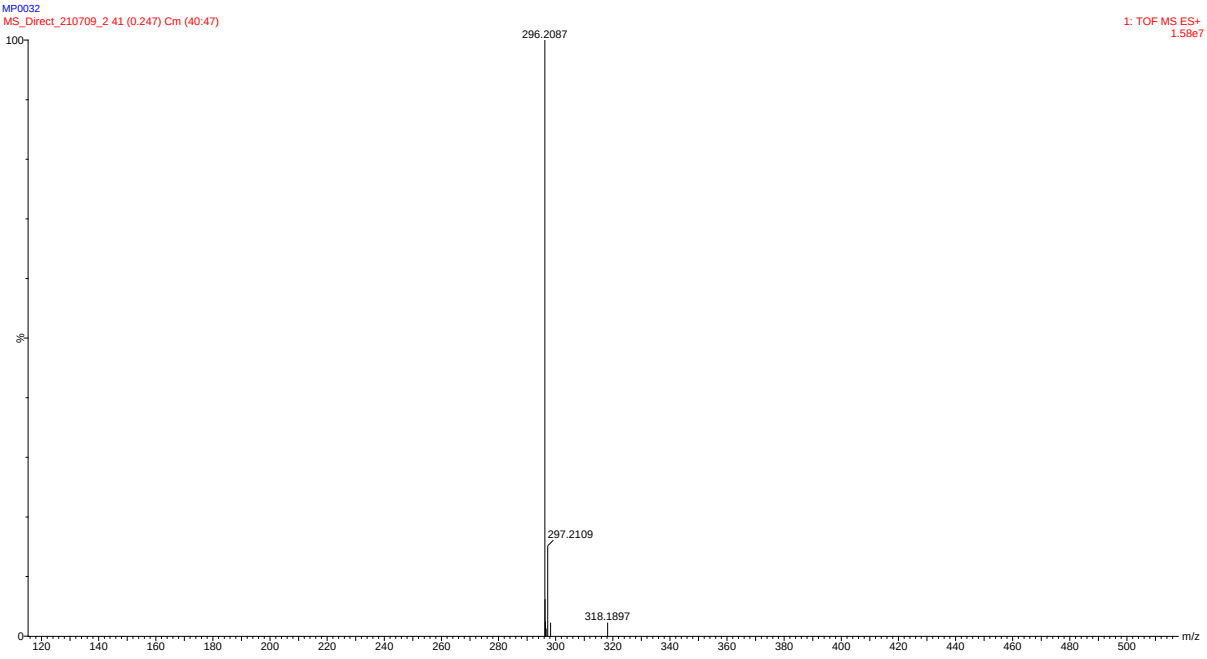

Figure 16-19: Mass spectrum of compound 8.

16.1.8 Compound 9

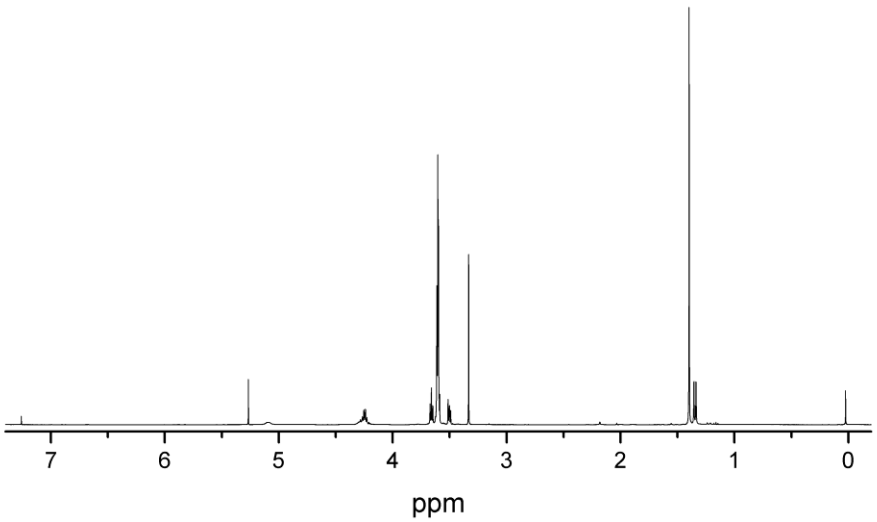

Figure 16-20: ^{1}H NMR of compound 9.

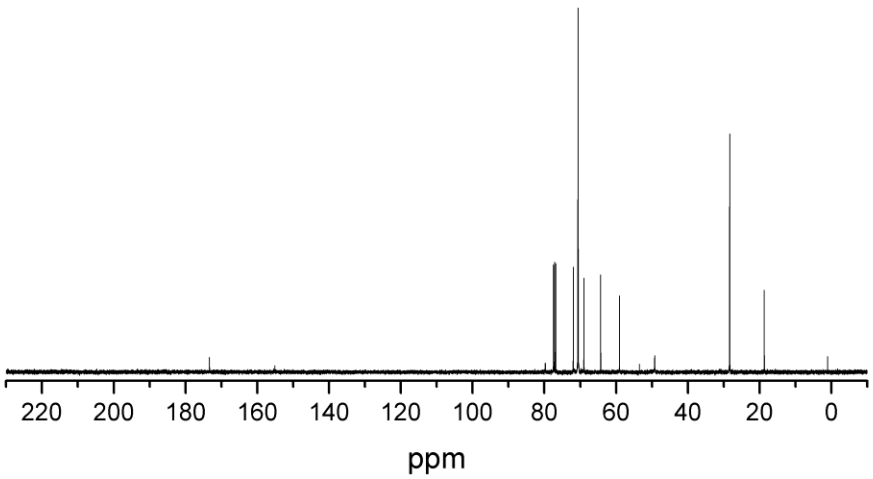

Figure 16-21:^{13}C NMR of compound 9.

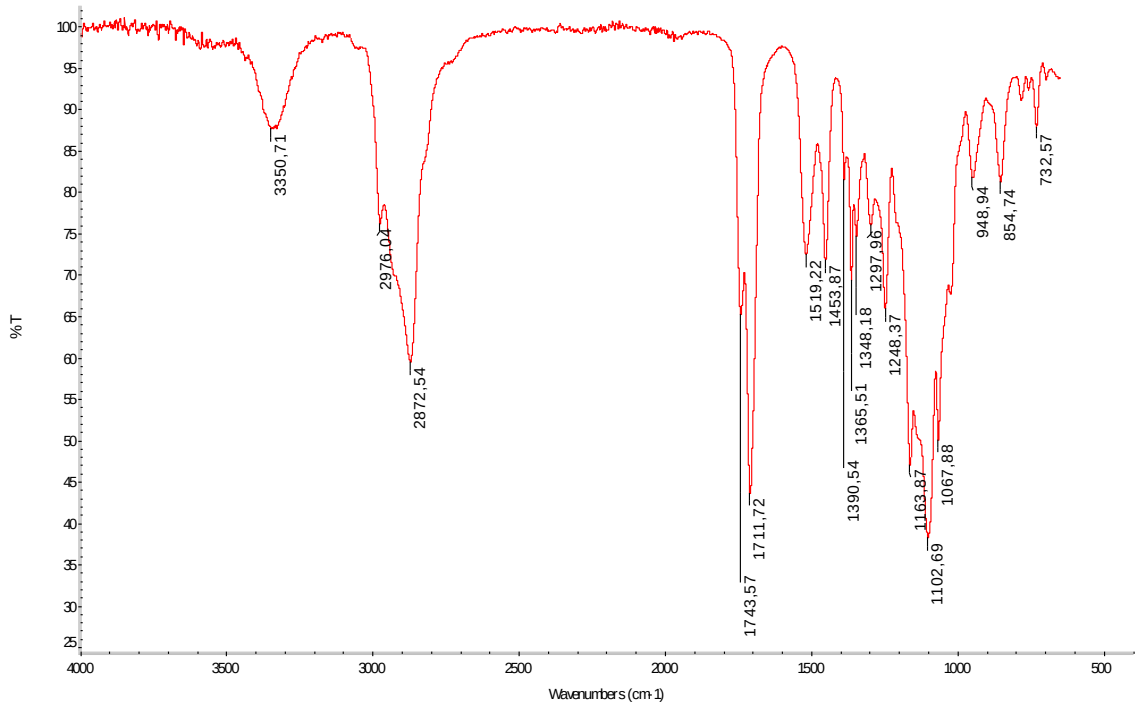

Figure 16-22: IR of compound 9.

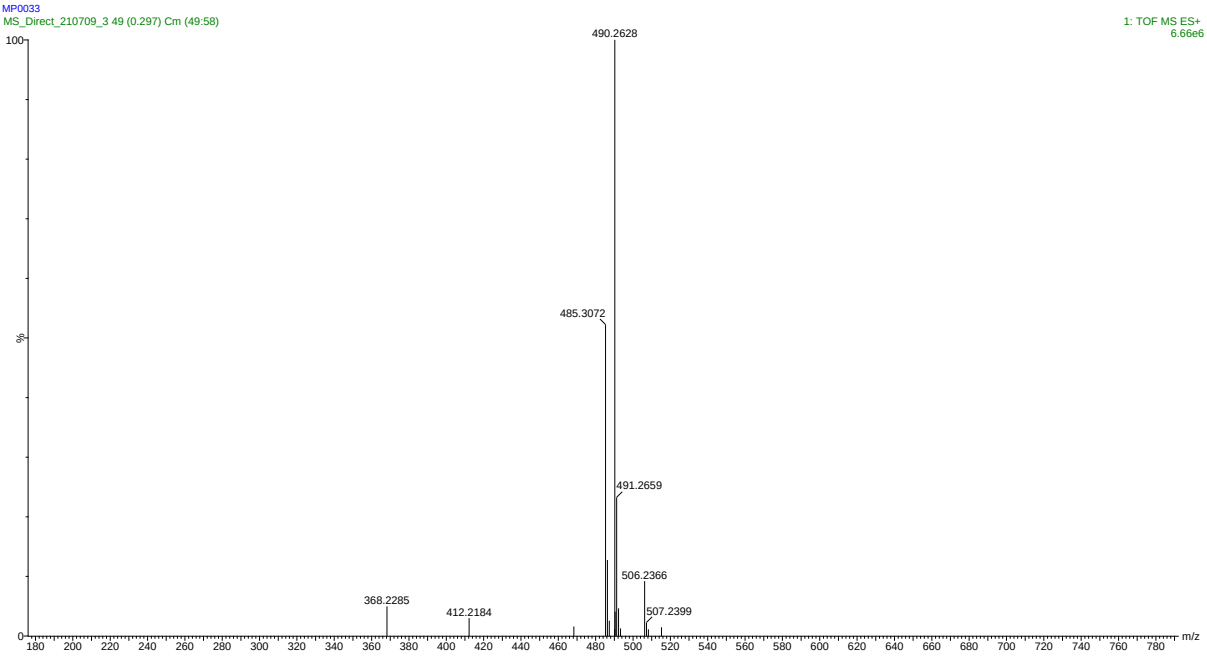

Figure 16-23: Mass spectrum of compound 9.

16.1.9 Compound 10

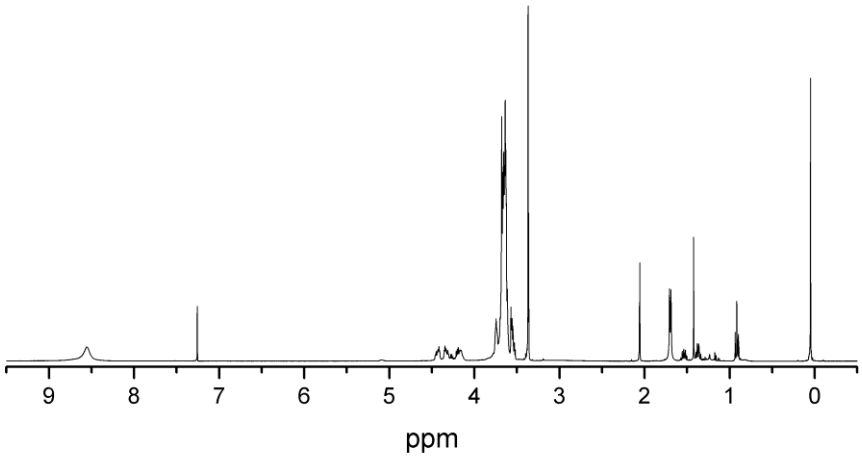

Figure 16-24: ^{1}H NMR of compound 10.

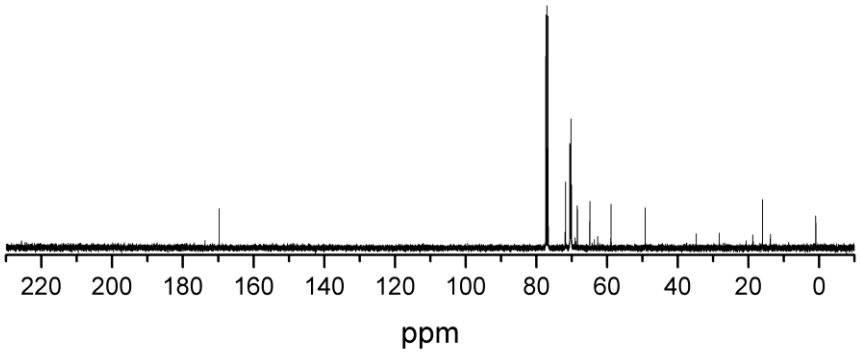

Figure 16-25: ^{13}C NMR of compound 10.

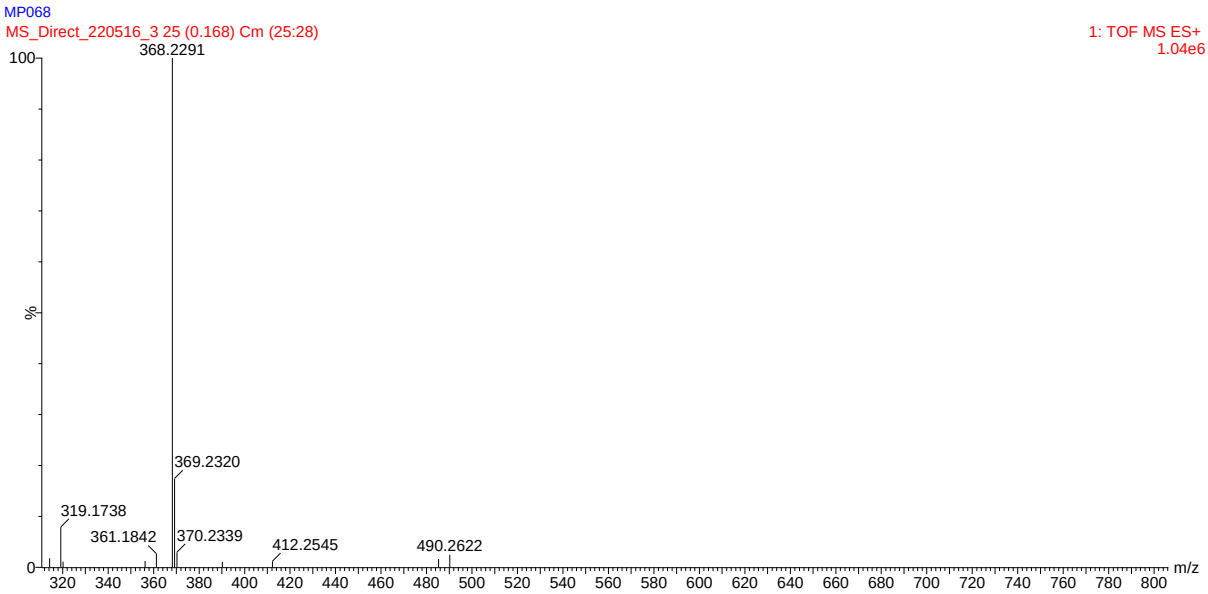

Figure 16-26: Mass spectrum of compound 10.

16.1.10Compound 11

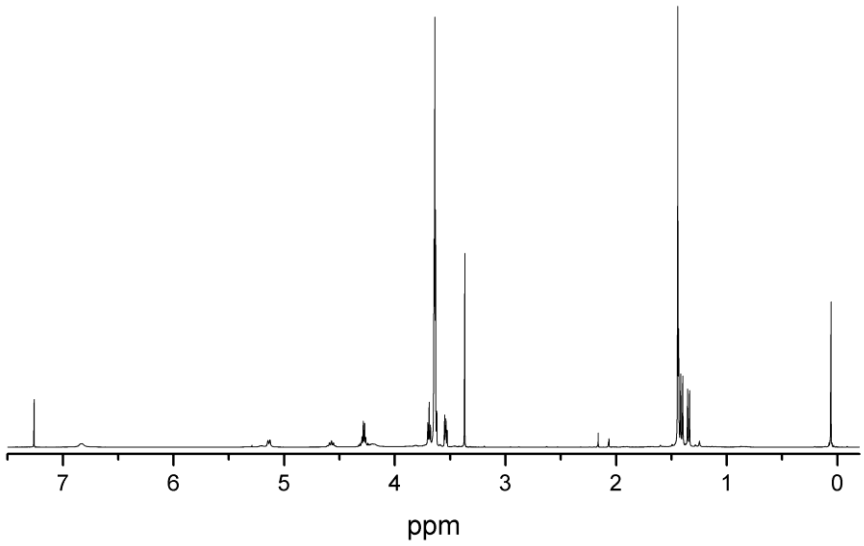

Figure 16-27: ^{1}H NMR of compound 11.

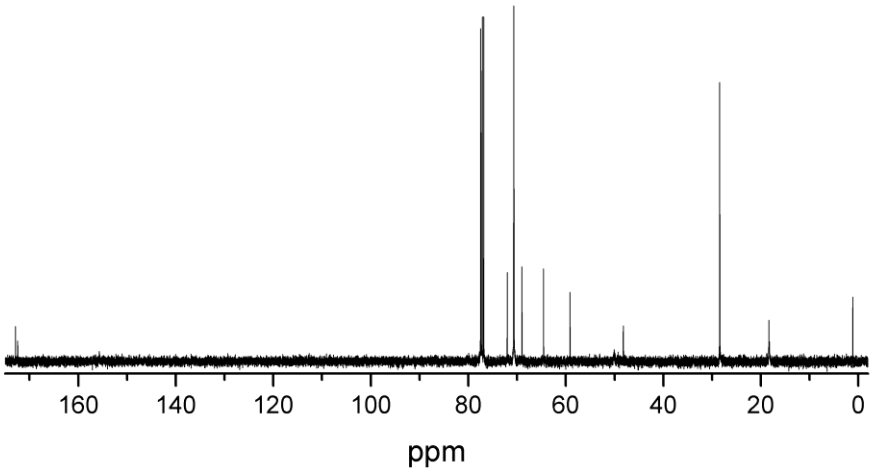

Figure 16-28:^{13}C NMR of compound 11.

16.1.11Compound 12

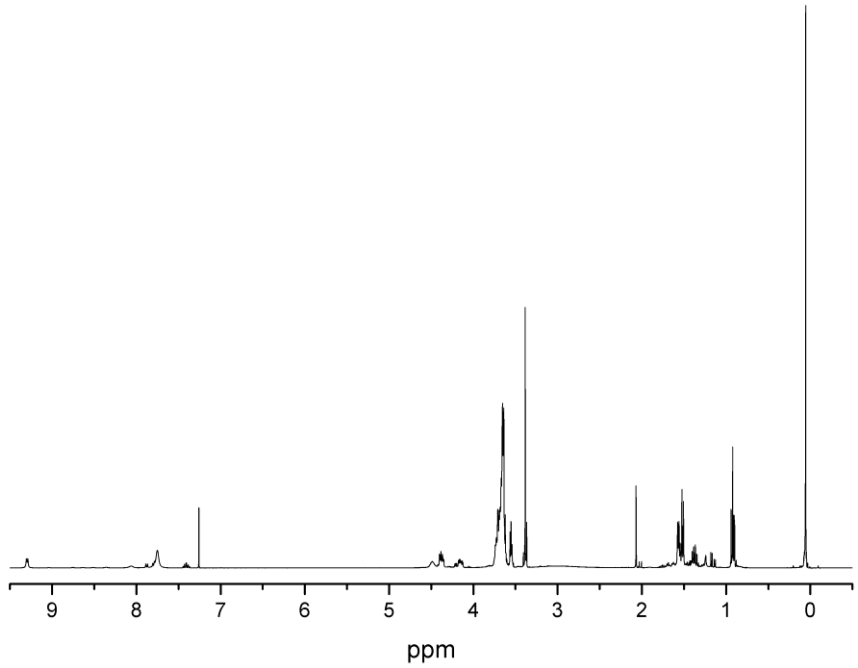

Figure 16-29:[1]H NMR of compound 12.

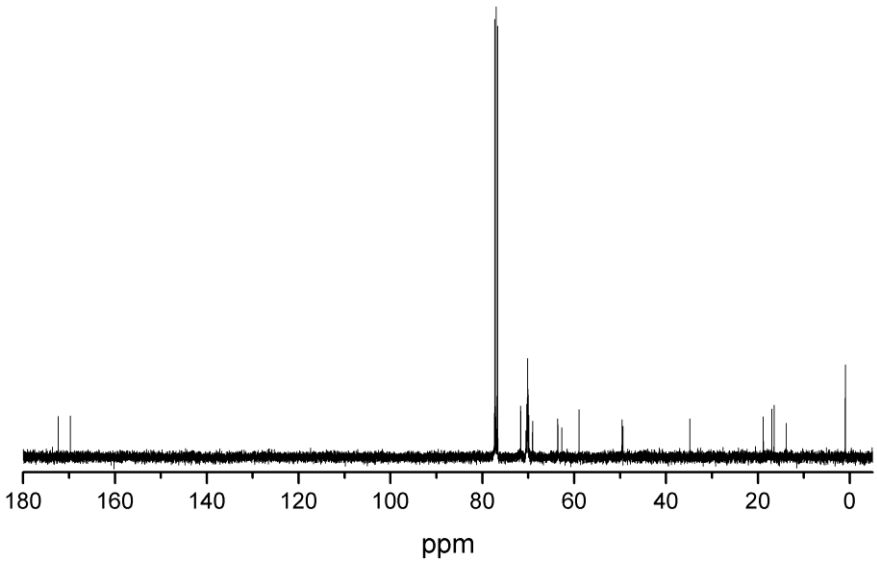

Figure 16-30: [13]C NMR of compound 12.

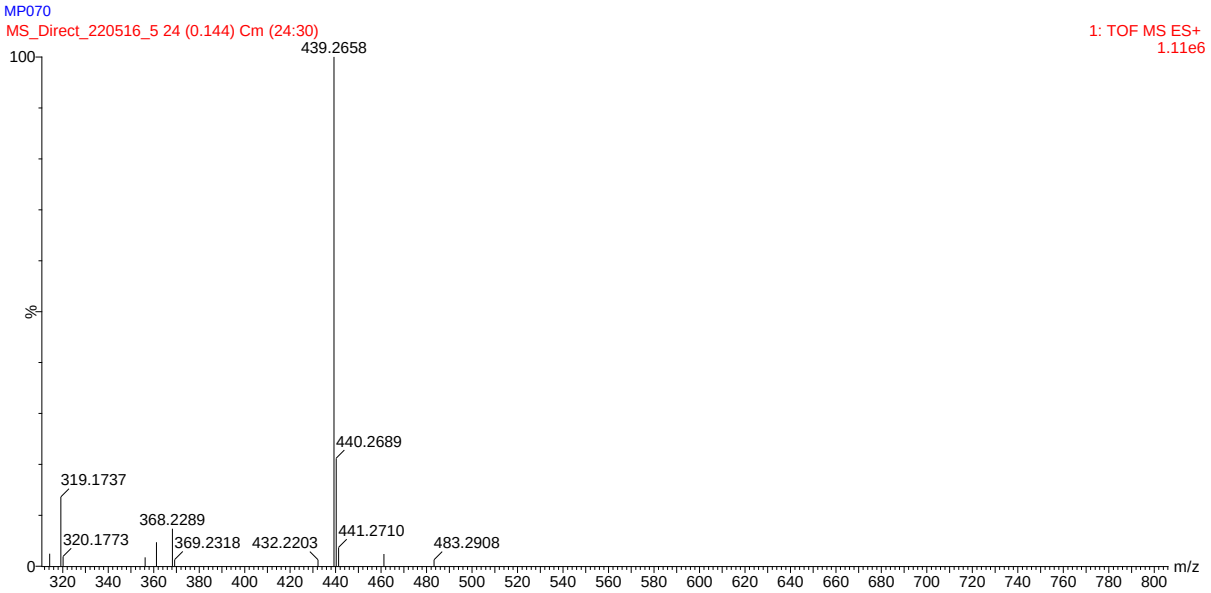

Figure 16-31: Mass spectrum of compound 12.

16.1.12Compound 14

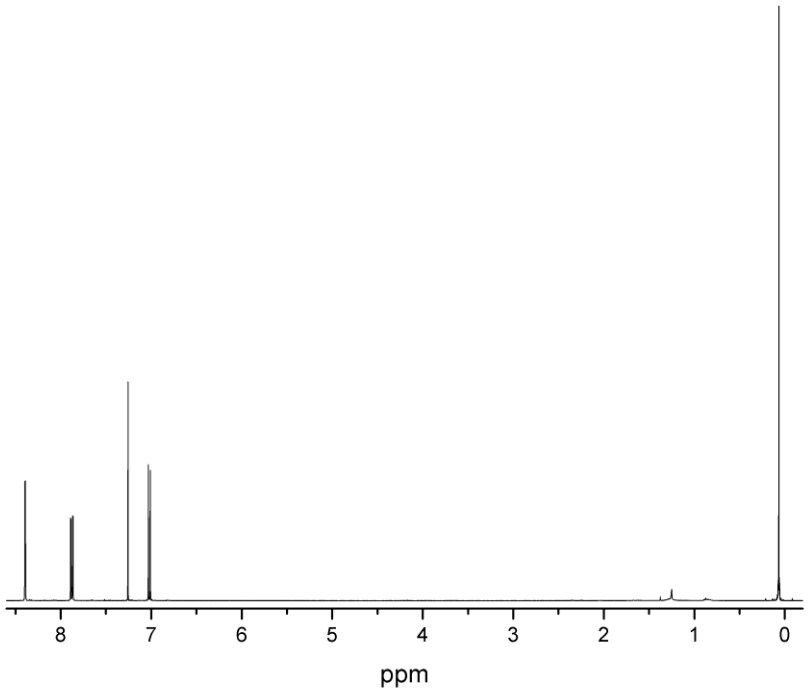

Figure 16-32: ^{1}H NMR of compound 14.

16.1.13Compound 15

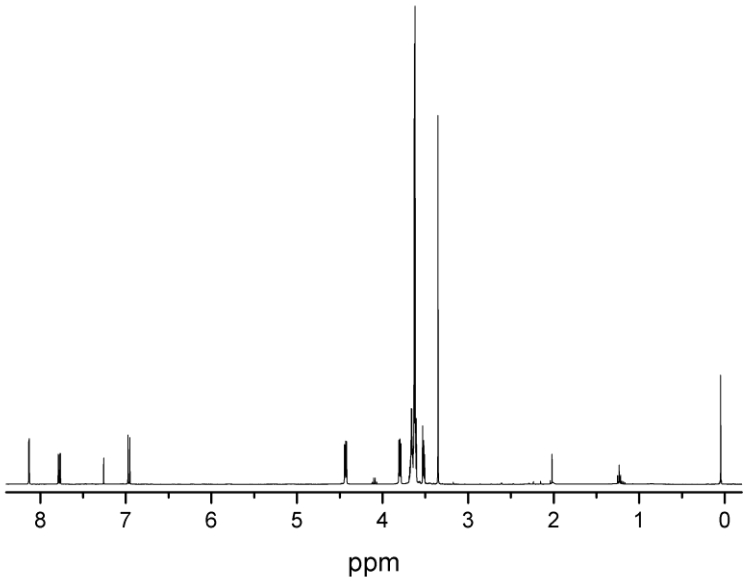

Figure 16-33: ^{1}H NMR of Compound 15.

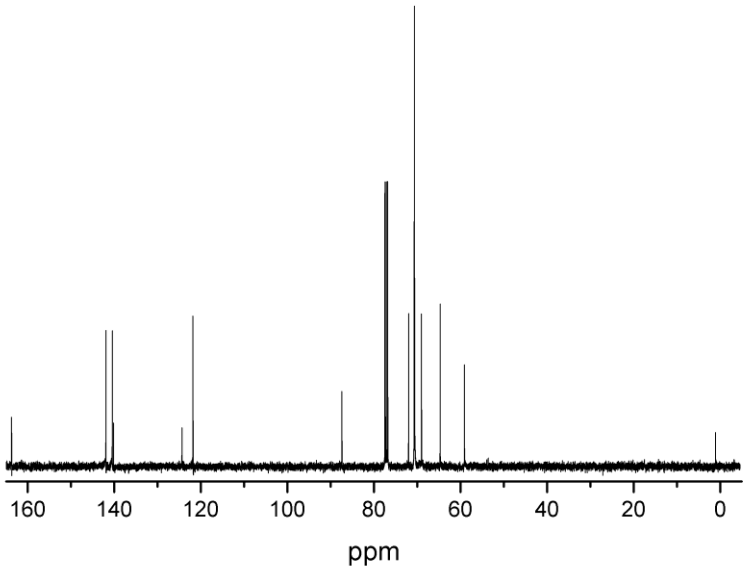

Figure 16-34: ^{13}C NMR of Compound 15.

16.1.14Compound 16

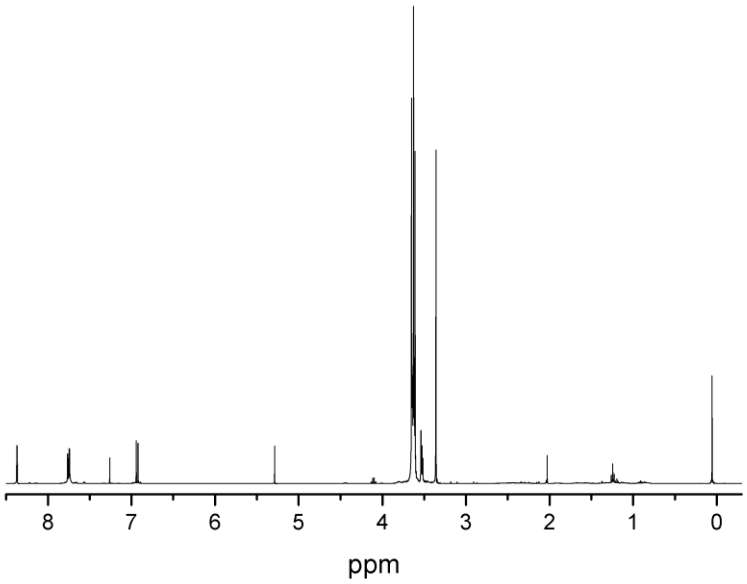

Figure 16-35: ^{1}H NMR of Compound 16.

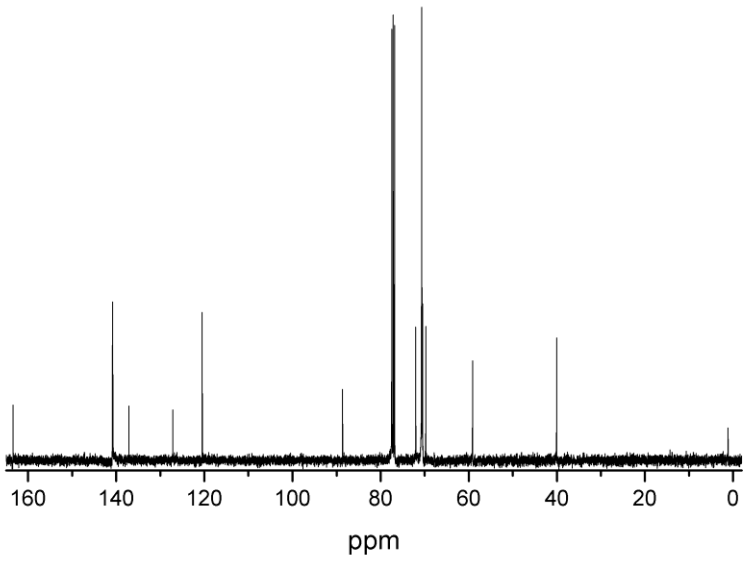

Figure 16-36: ^{13}C NMR of Compound 16.

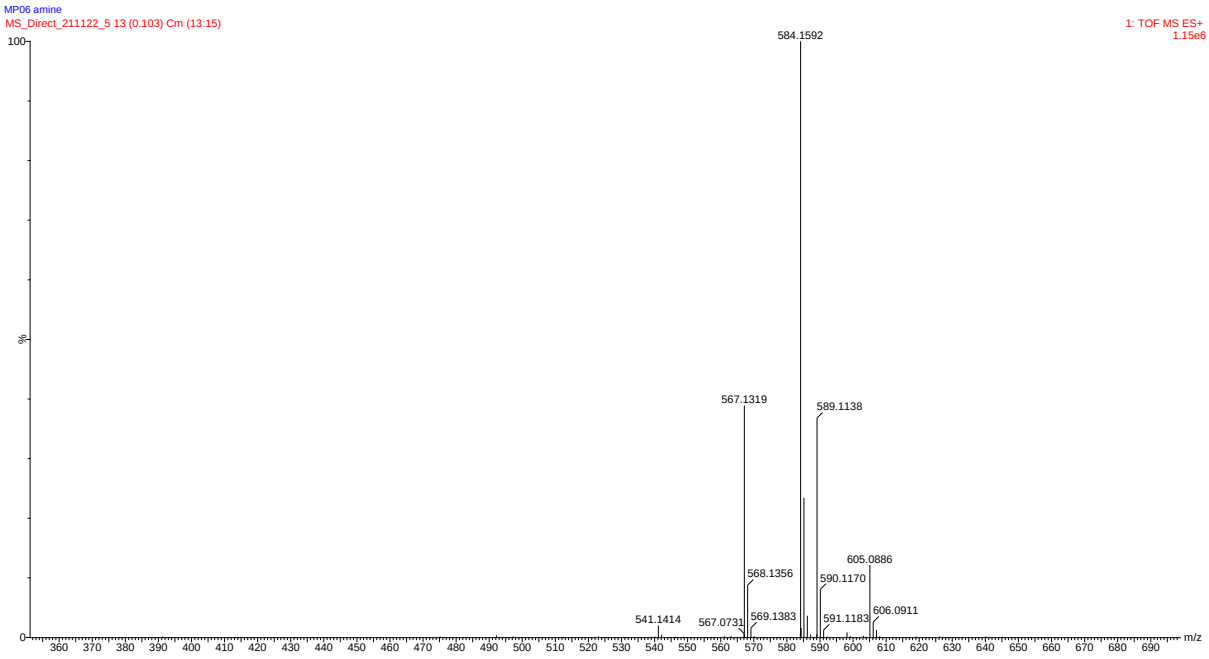

Figure 16-37: Mass spectrum of compound 16.

16.1.15Compound 17

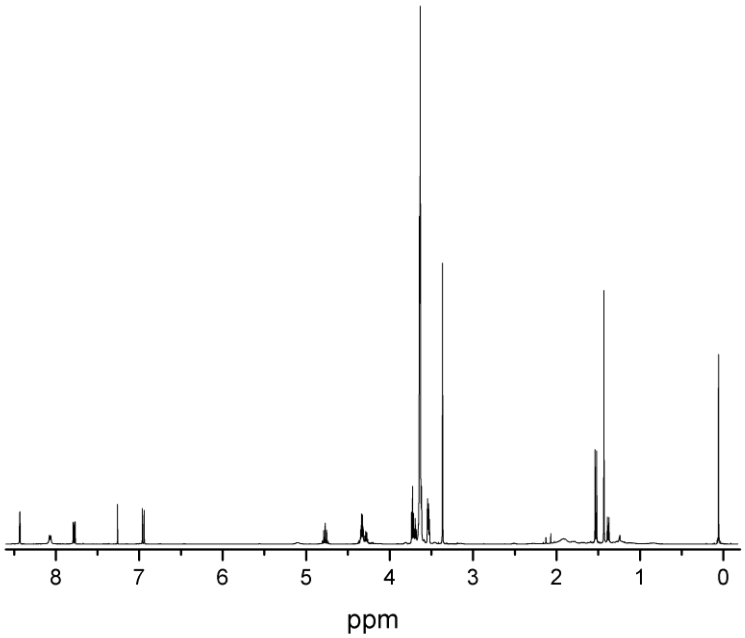

Figure 16-38: ^{1}H NMR of Compound 17.

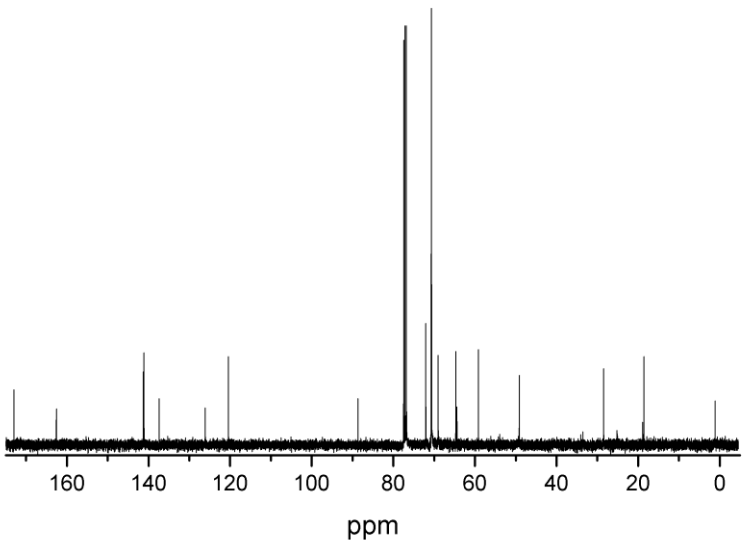

Figure 16-39: ^{13}C NMR of Compound 17.

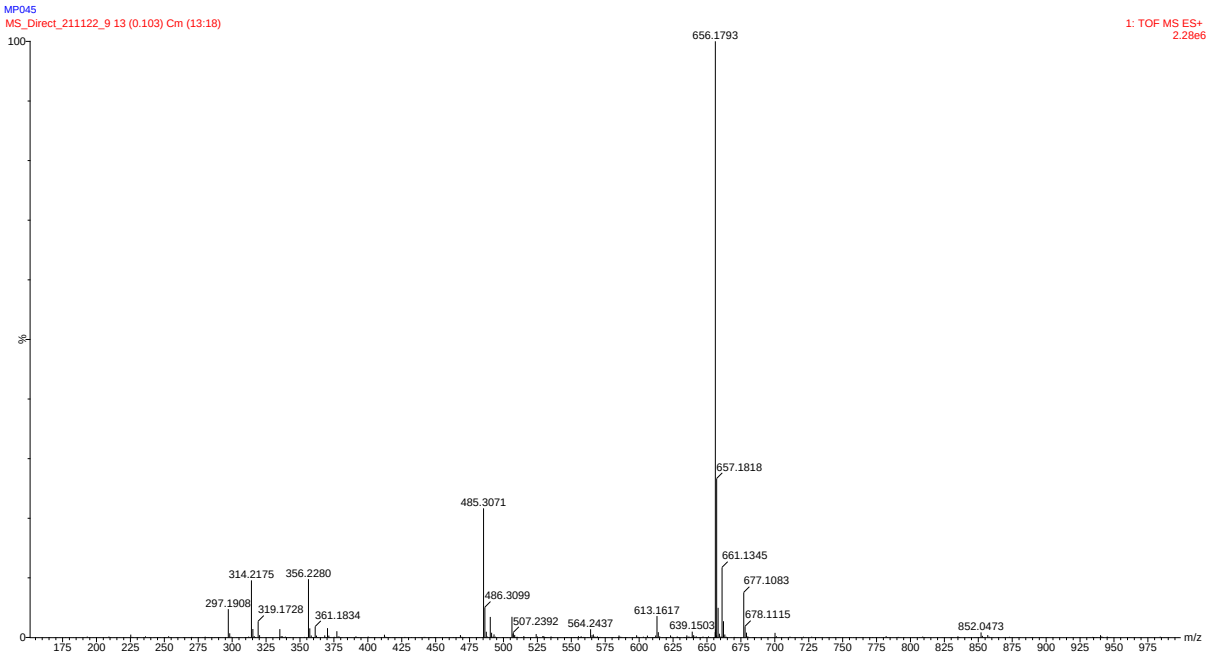

Figure 16-40: Mass spectrum of compound 17.

16.1.16Compound 18

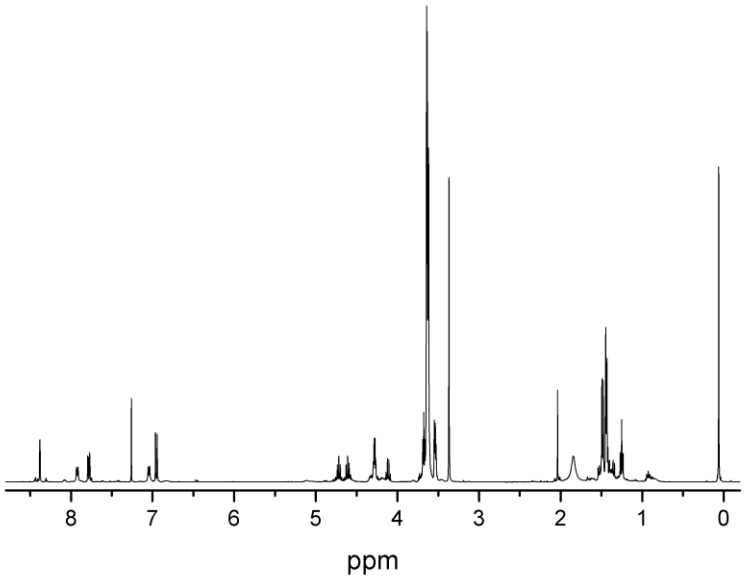

Figure 16-41: ^{1}H NMR of compound 18.

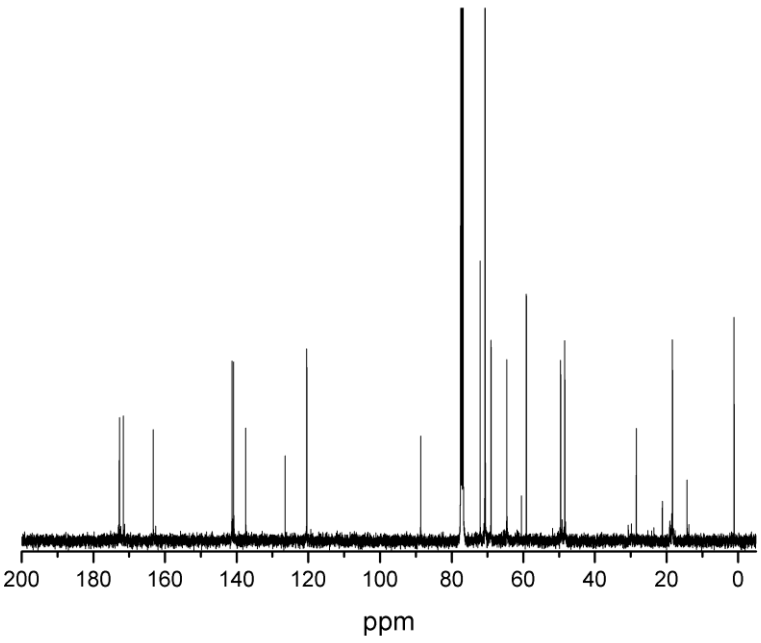

Figure 16-42: ^{13}C NMR of compound 18.

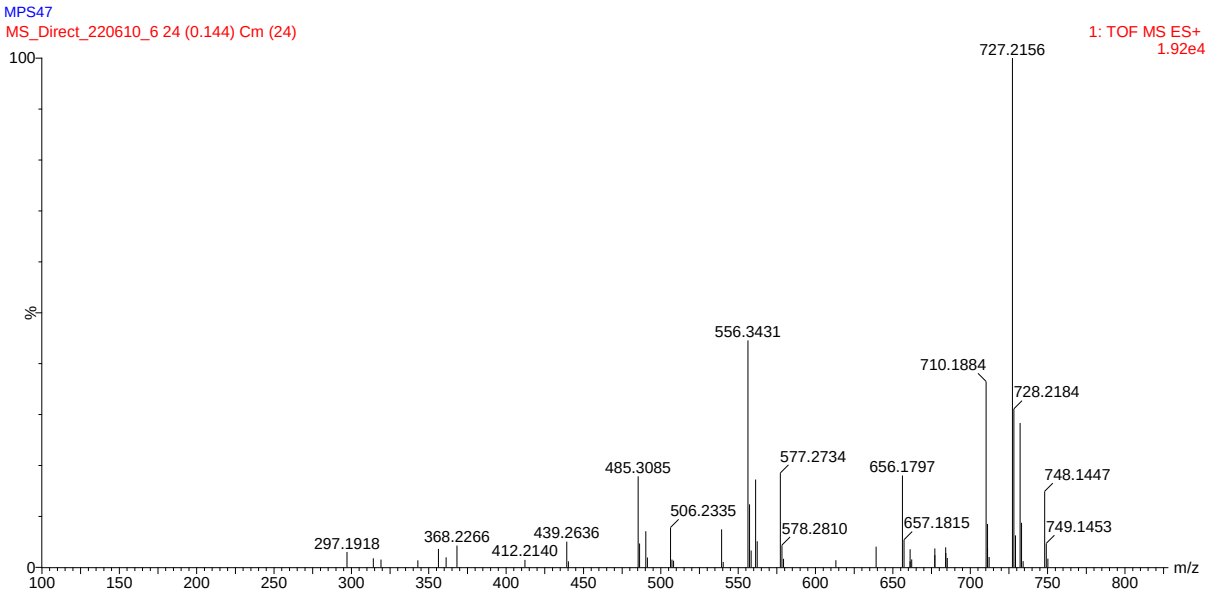

Figure 16-43: Mass spectrum of compound 18.

16.1.17Mixture of Compound 19 and 23

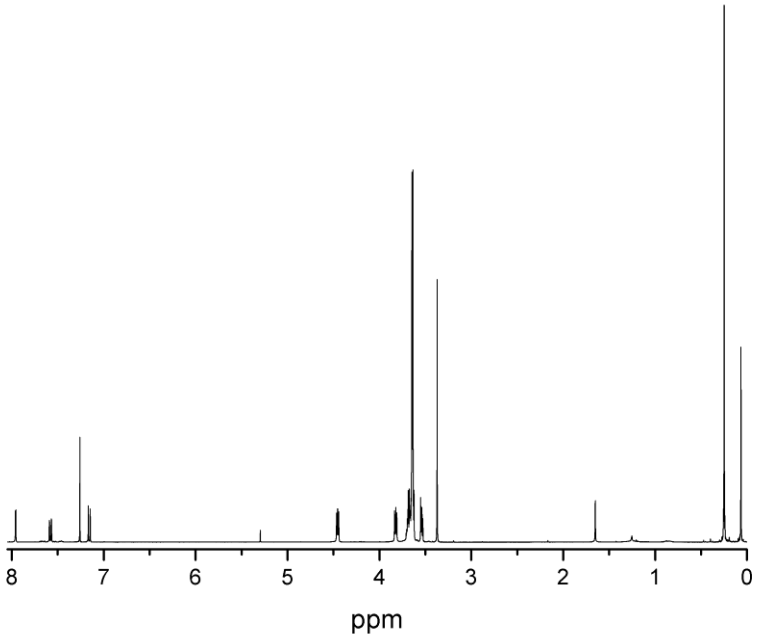

Figure 16-44: ^{1}H NMR of a mixture of compound 19 and 23.

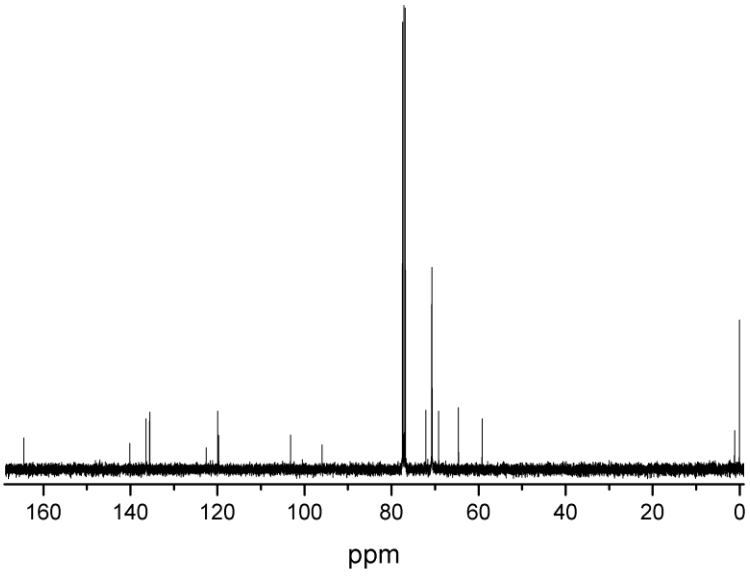

Figure 16-45:^{13}C NMR of a mixture of compound 19 and 23.

16.1.18Compound 19

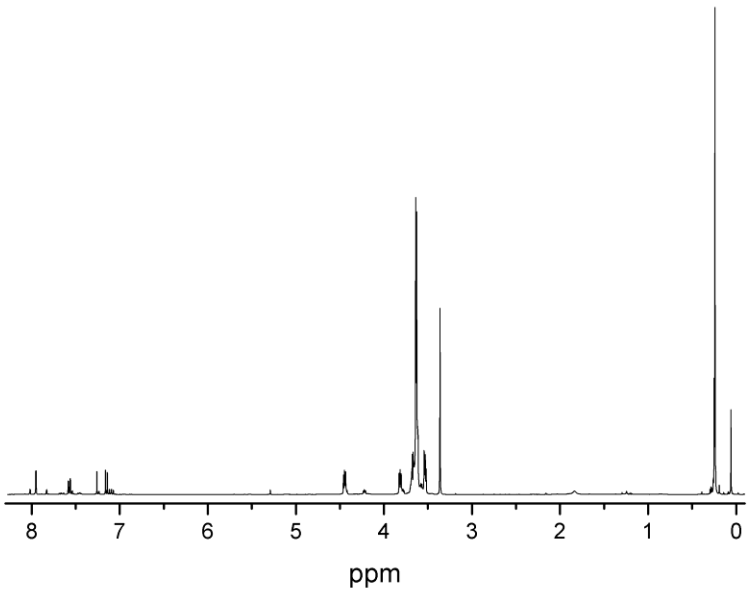

Figure 16-46: ^{1}H NMR of compound 19.

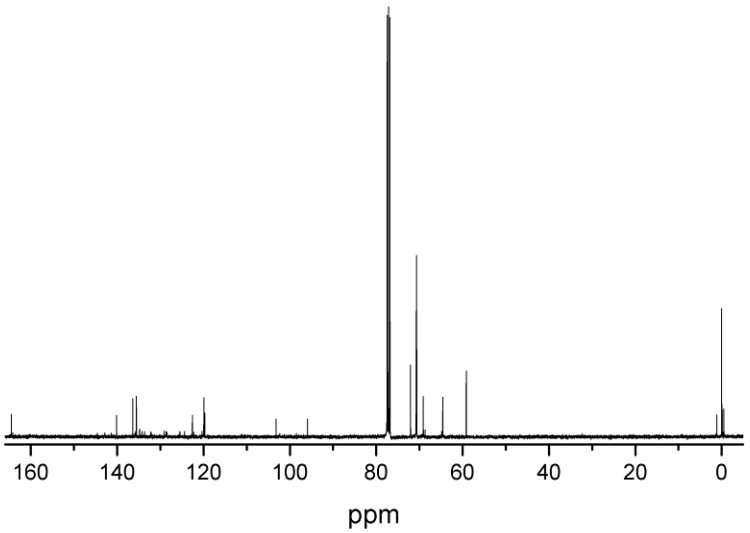

Figure 16-47: ^{13}C NMR of compound 19.

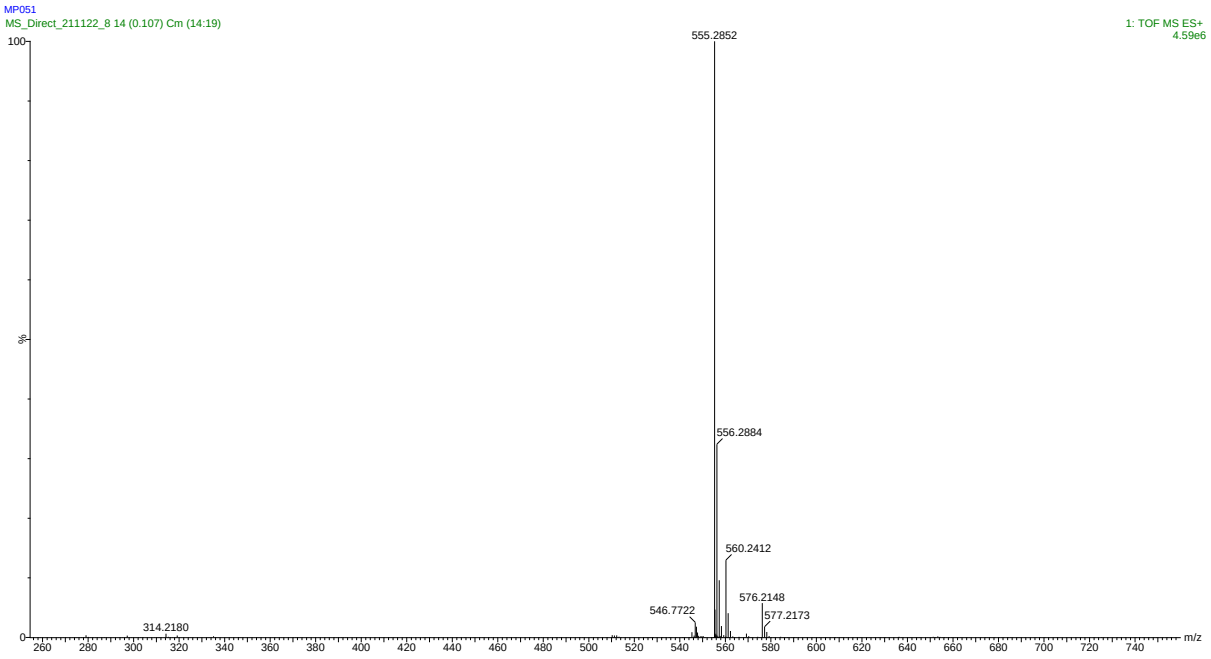

Figure 16-48: Mass spectrum of compound 19.

16.1.19Mixture of Compound 20 and 24

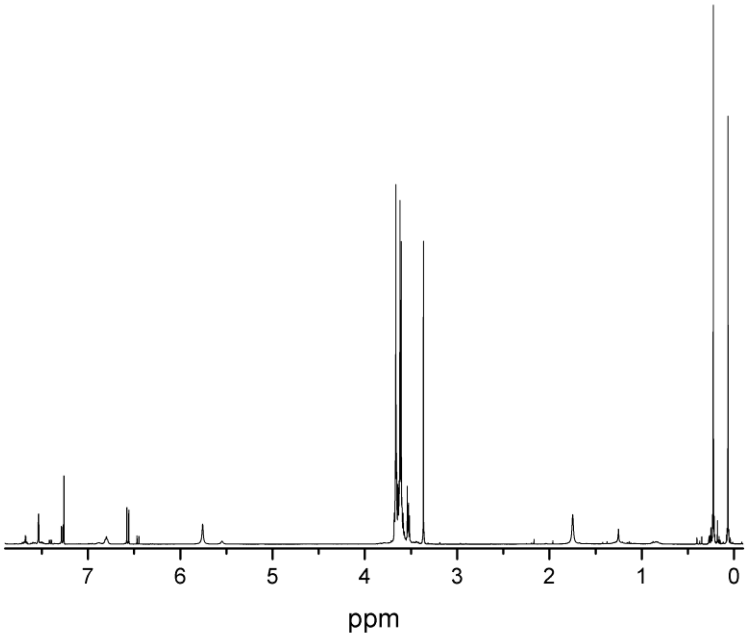

Figure 16-50: ^{1}H NMR of a mixture of compound 20 and 24.

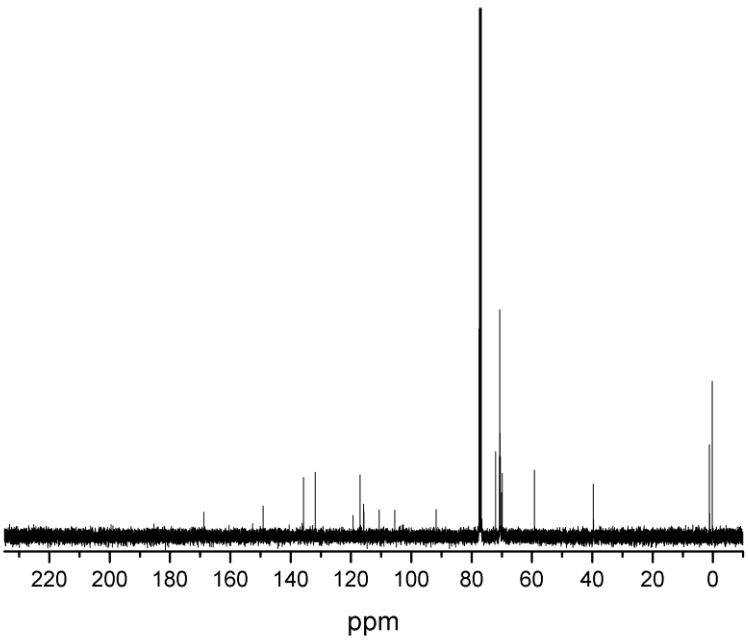

Figure 16-49: ^{13}C NMR of a mixture of compound 20 and 24.

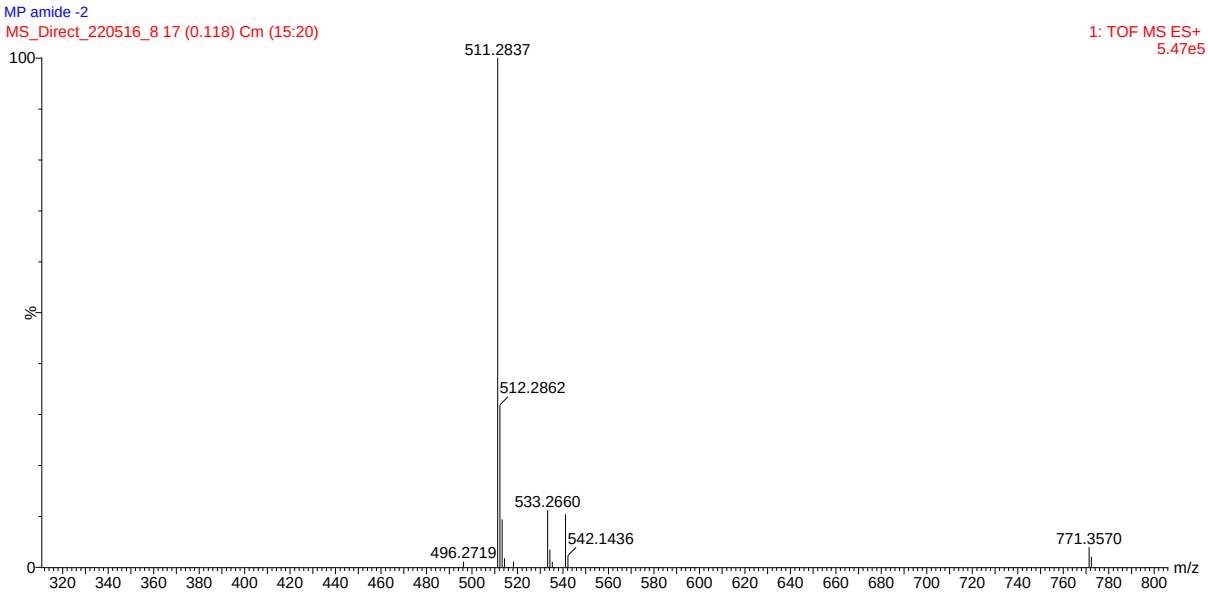

Figure 16-51: Mass spectrum of a mixture of compound 20 and 24.

16.1.20Compound 20

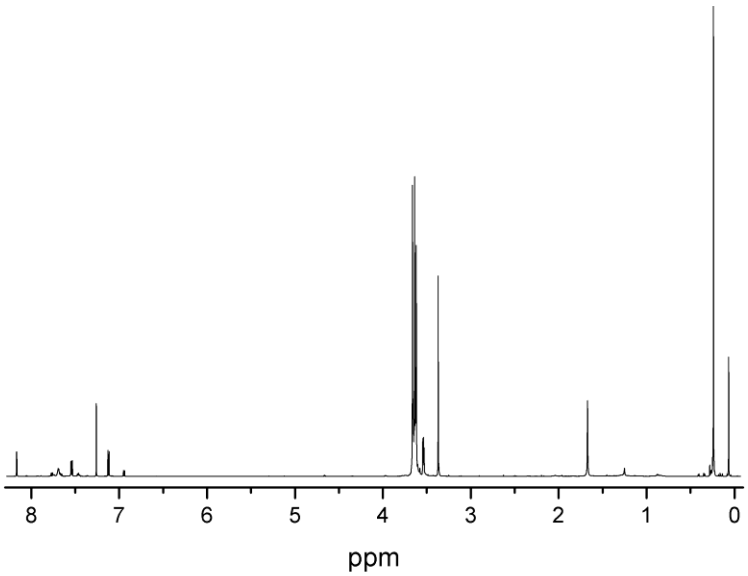

Figure 16-52: ^{1}H NMR of compound 20.

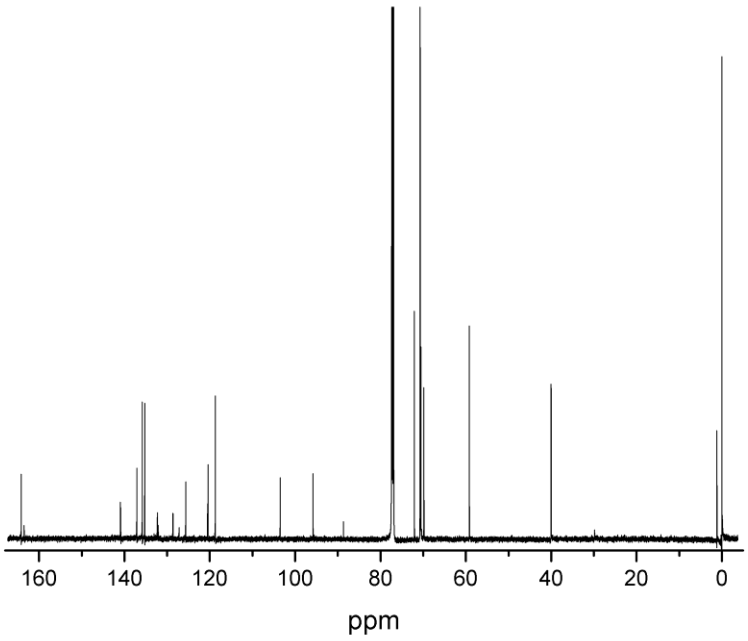

Figure 16-53: ^{13}C NMR of compound 20.

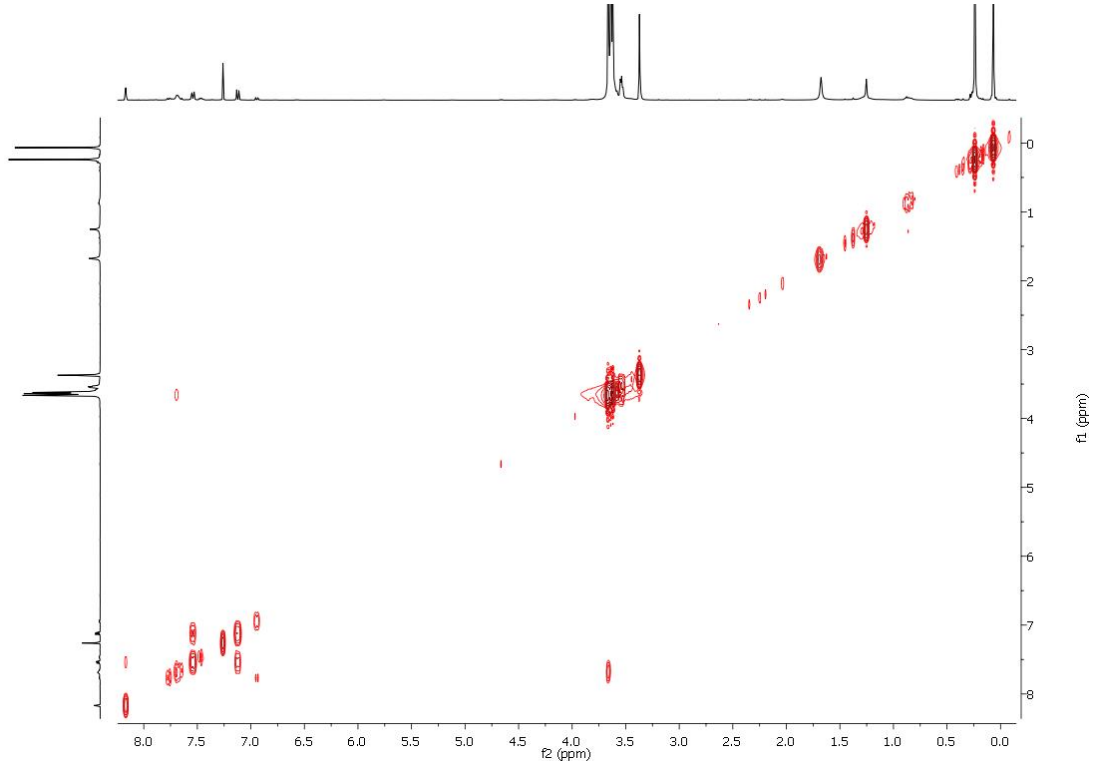

Figure 16-55: COSY of compound 20.

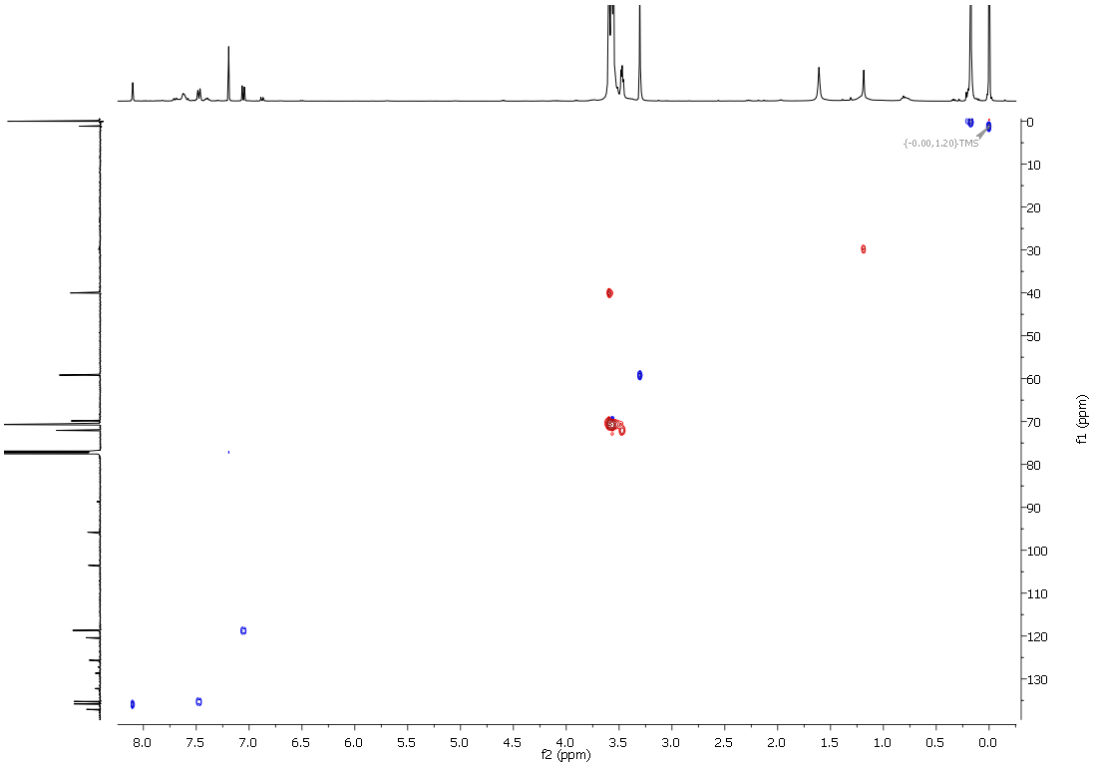

Figure 16-54: HSQC of compound 20.

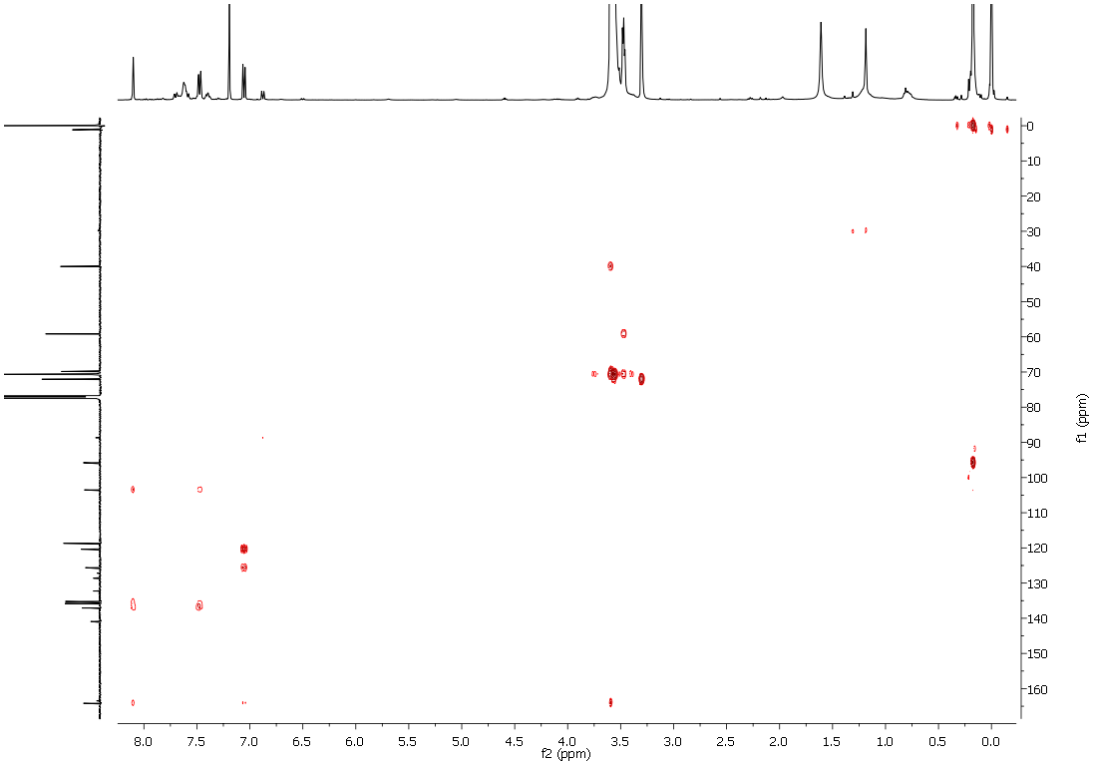

Figure 16-56: HMBC of compound 20.

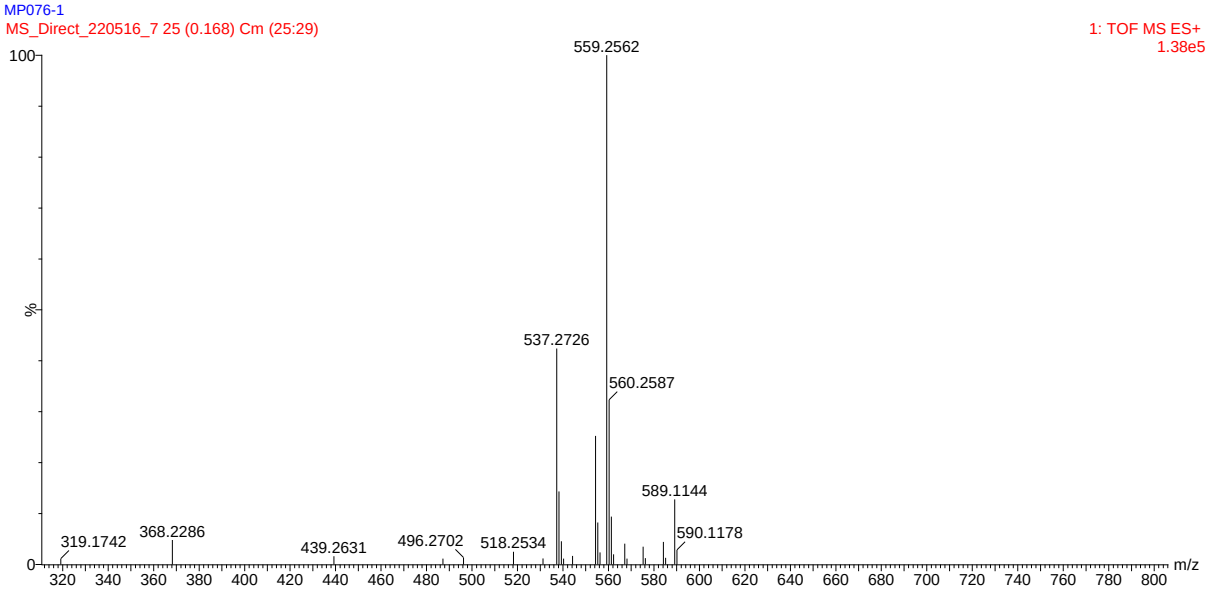

Figure 16-57: Mass spectrum of compound 20.

16.1.21Mixture of Compound 21 and 25

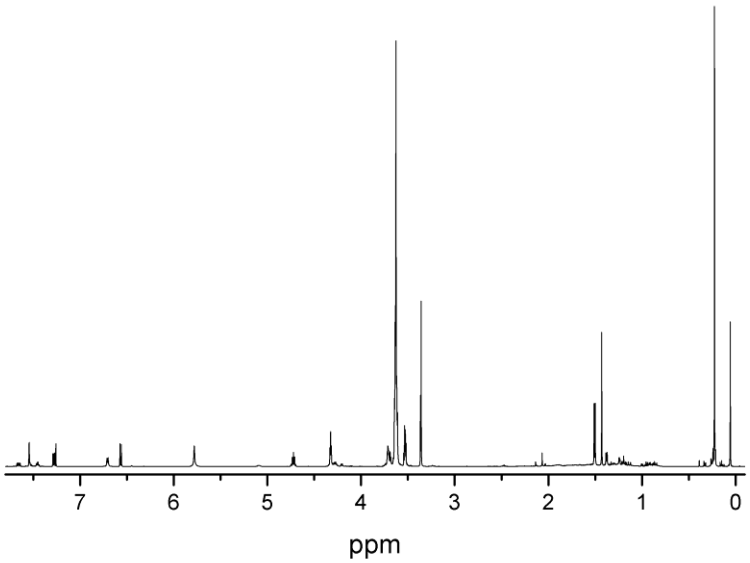

Figure 16-58: ^{1}H NMR of a mixture of compound 21 and 25.

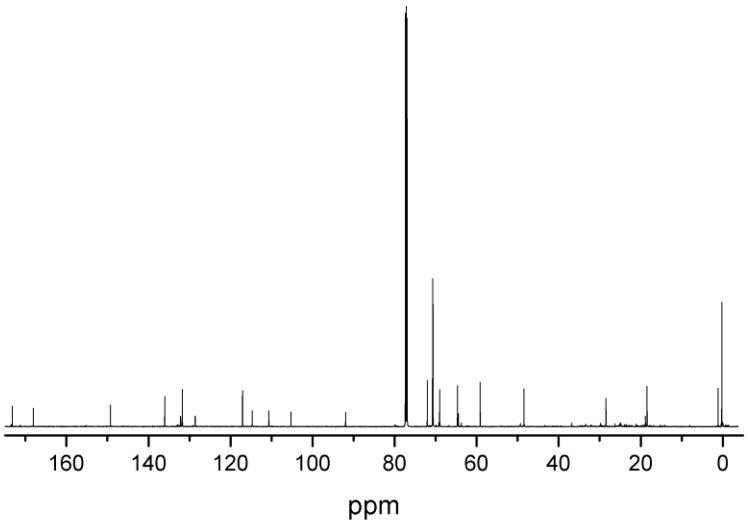

Figure 16-59: ^{13}C NMR of a mixture of compound 21 and 25.

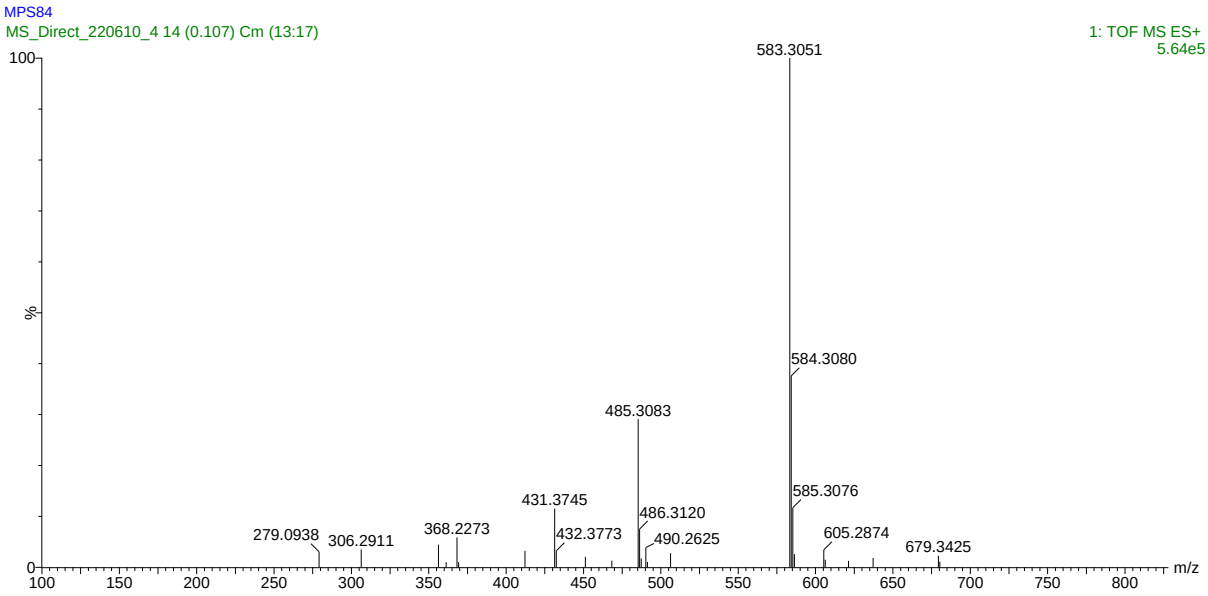

Figure 16-60: Mass spectrum of a mixture of compound 21 and 25.

16.1.22Compound 21

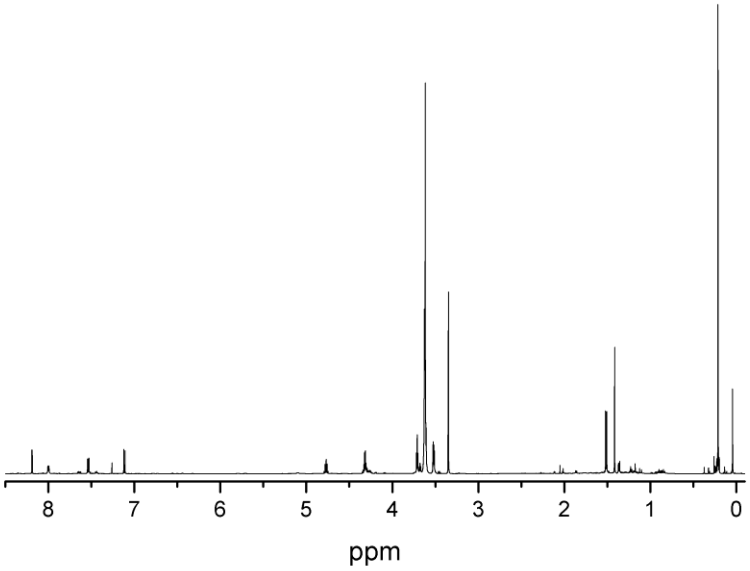

Figure 16-61: ^{1}H NMR of compound 21.

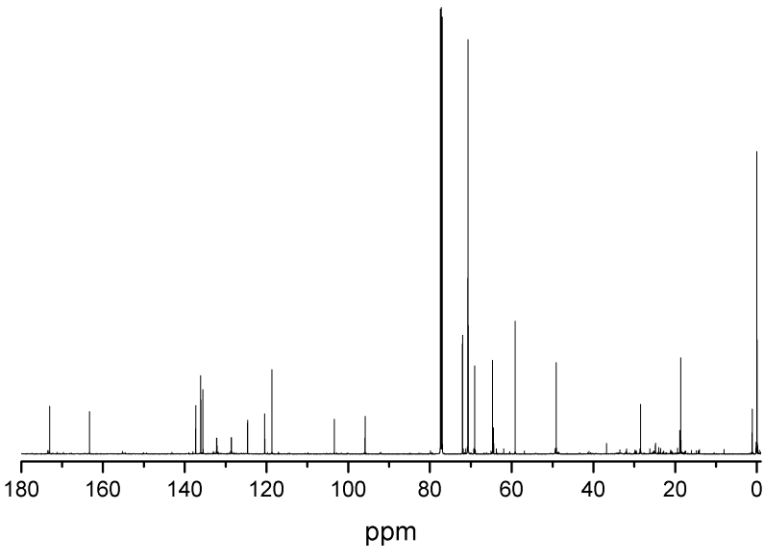

Figure 16-62: ^{13}C NMR of compound 21.

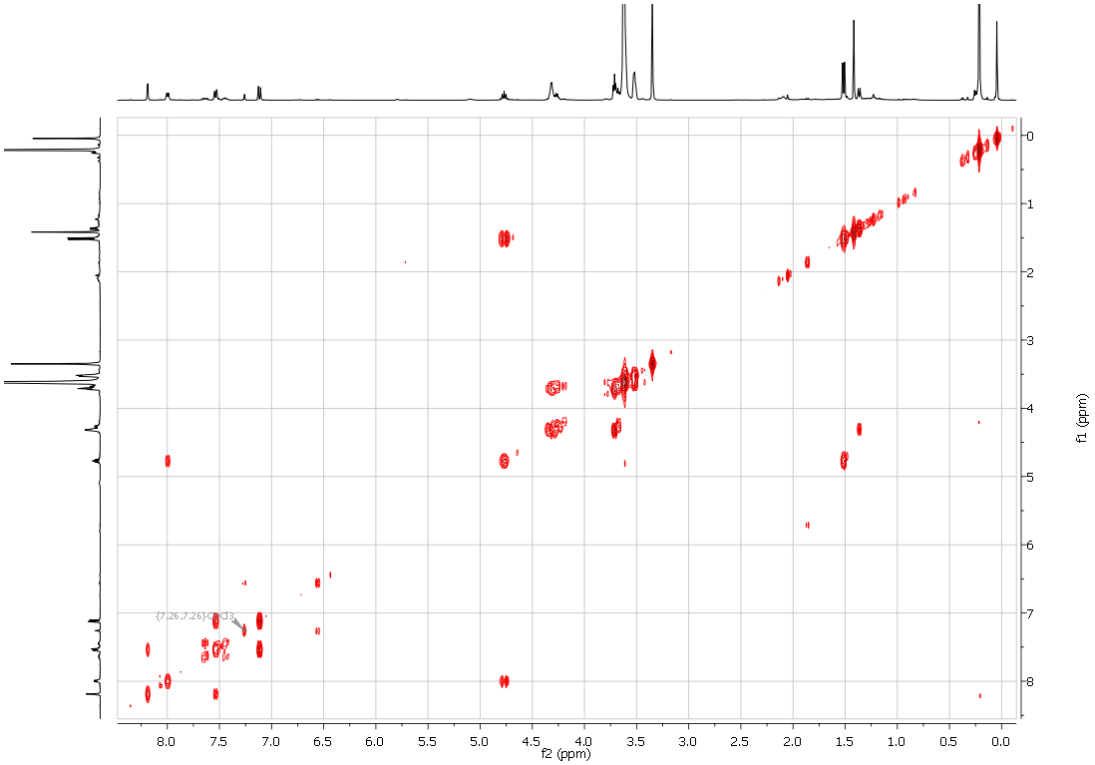

Figure 16-63: COSY of compound 21.

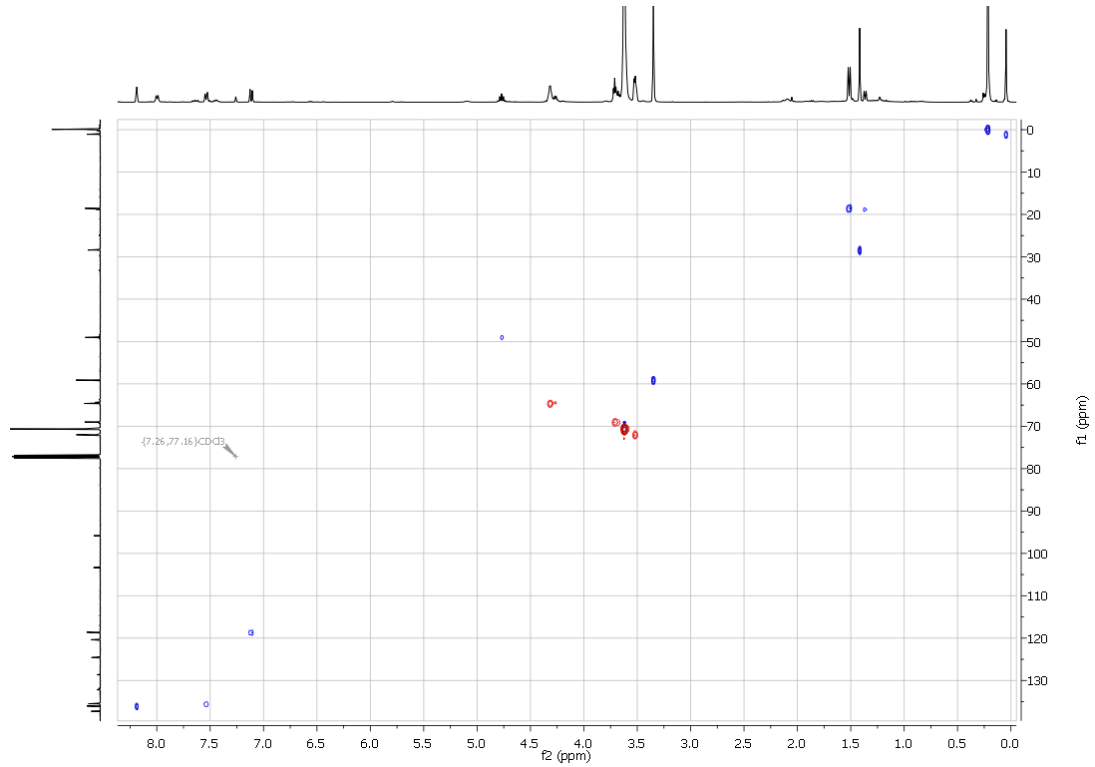

Figure 16-64: HSQC of compound 21.

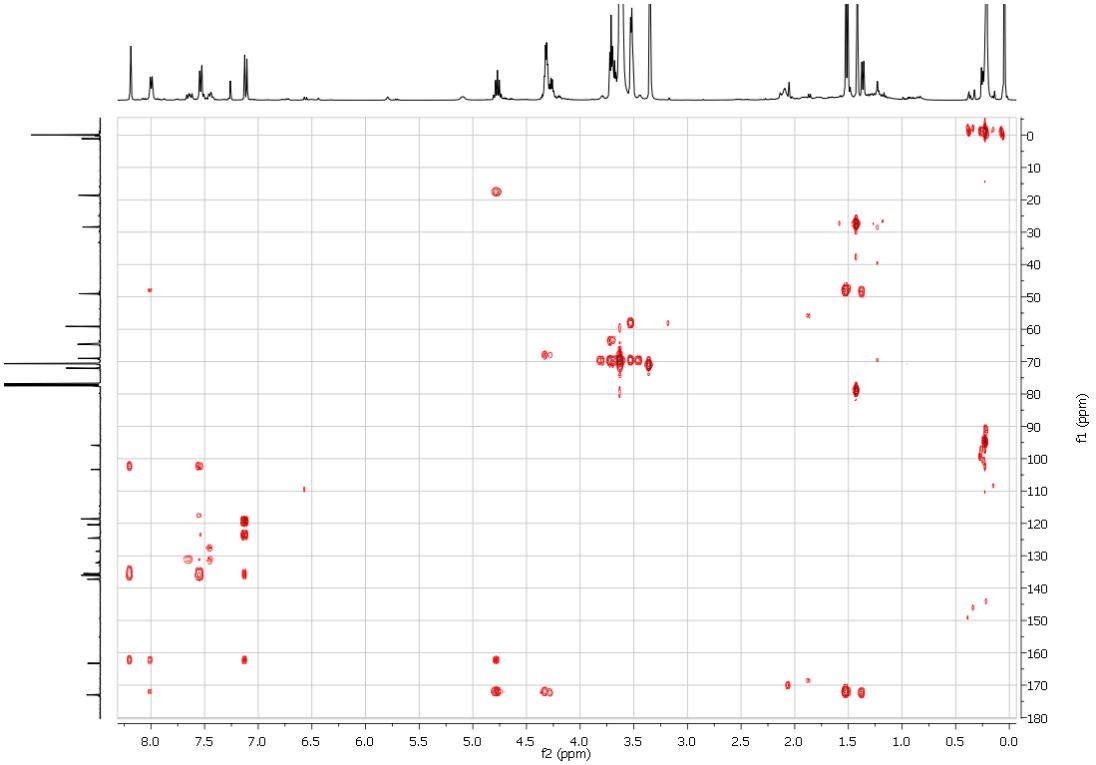

Figure 16-65: HMBC of compound 21.

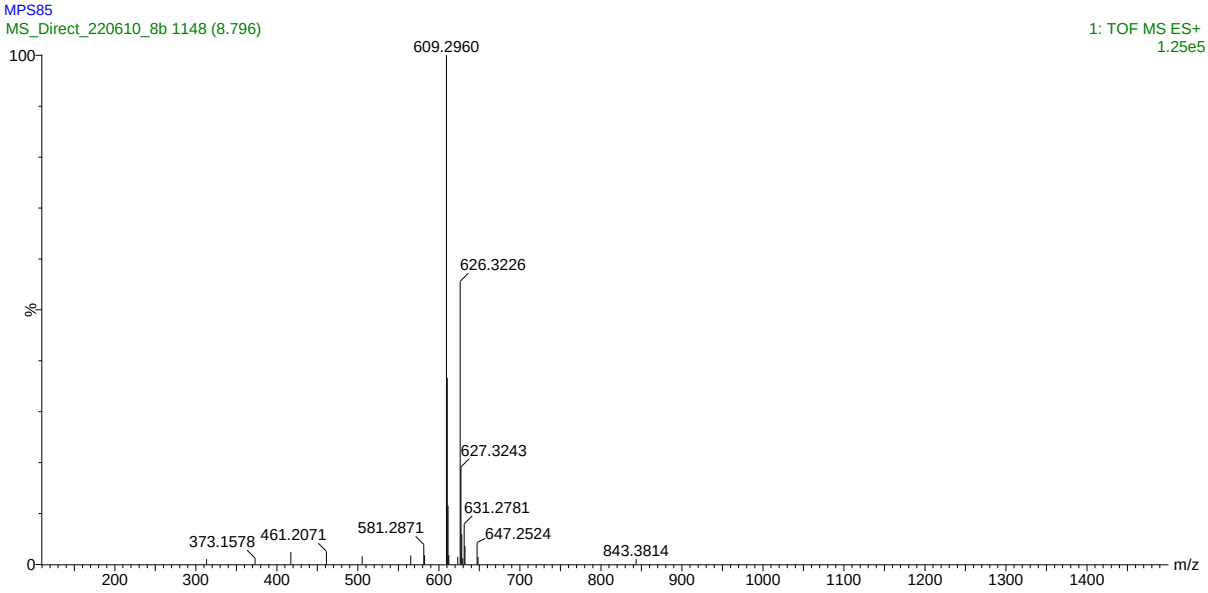

Figure 16-66: Mass spectrum of compound 21.

16.1.23Mixture of Compound 22 and 26

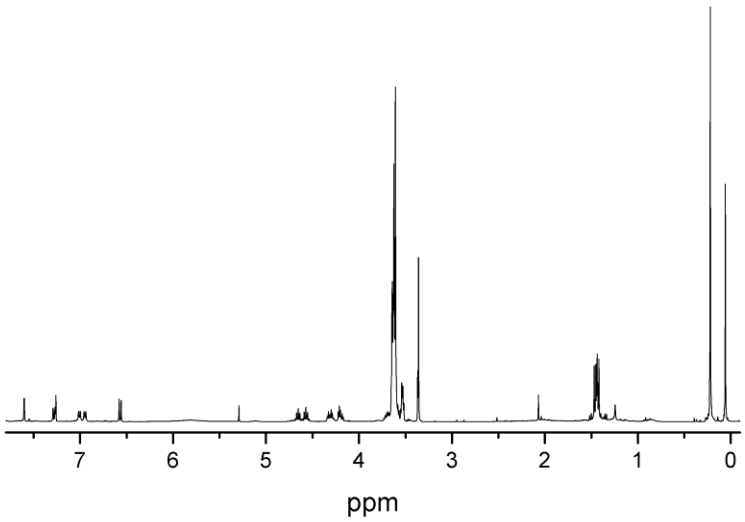

Figure 16-68: ^{1}H NMR of a mixture of Compound 22 and 26.

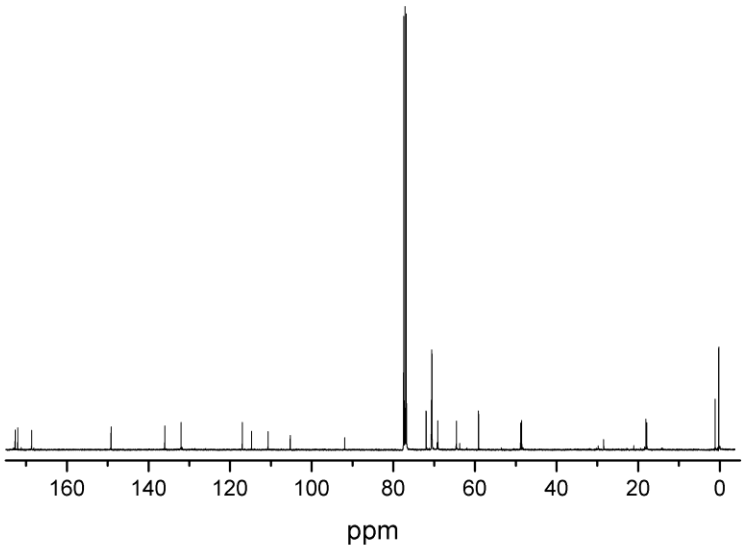

Figure 16-67: ^{13}C NMR of a mixture of Compound 22 and 26.

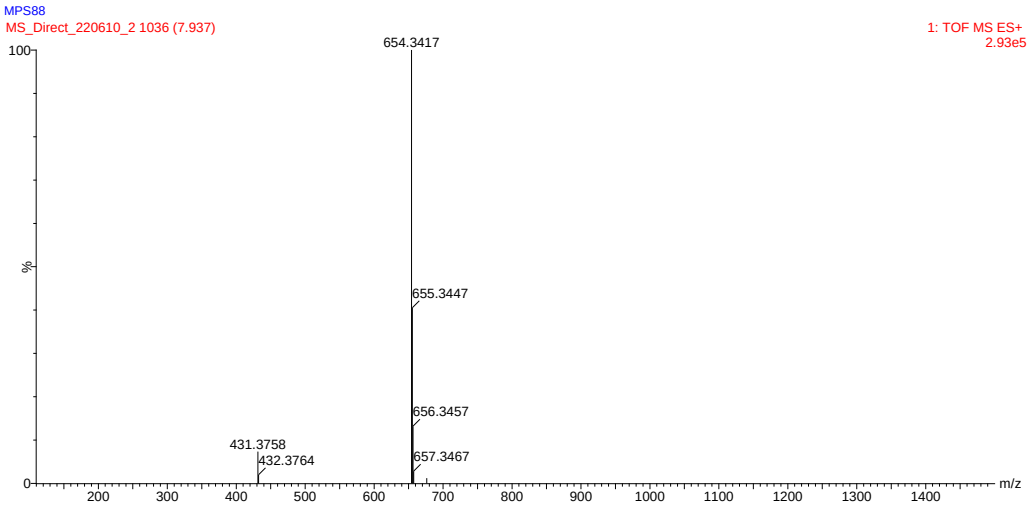

Figure 16-69: Mass spectrum of a mixture of Compound 22 and 26.

16.1.24Compound 22

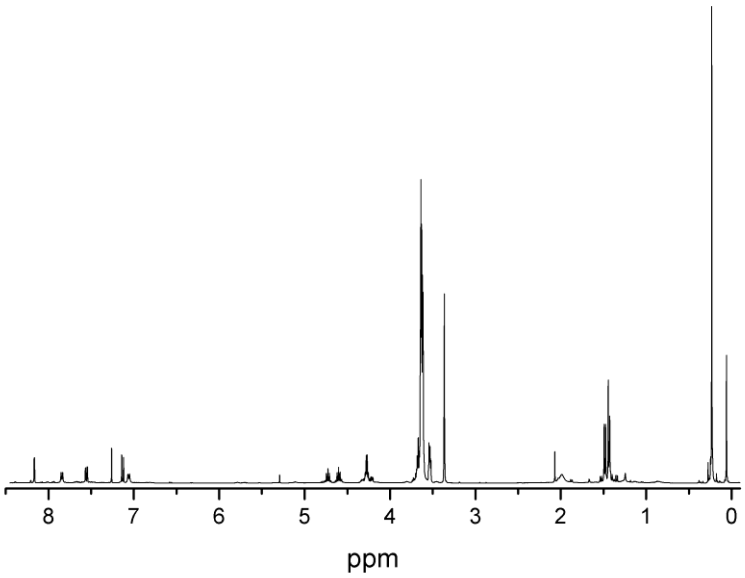

Figure 16-70: ^{1}H NMR of compound 22.

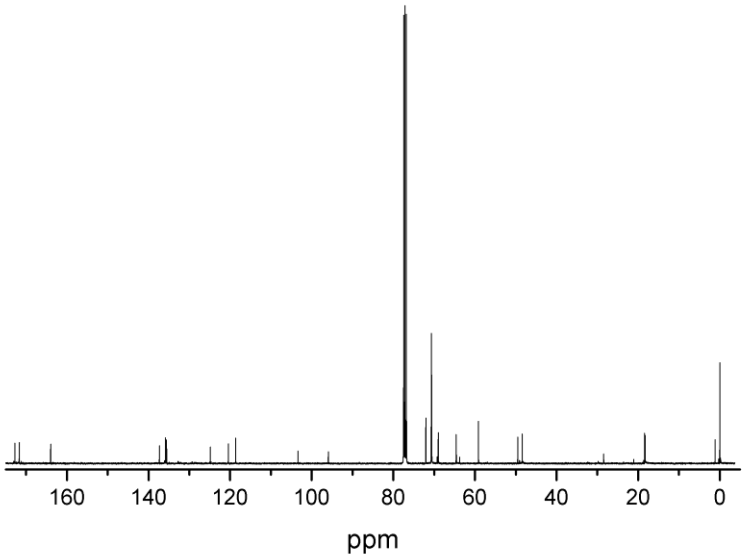

Figure 16-71: ^{13}C NMR of compound 22.

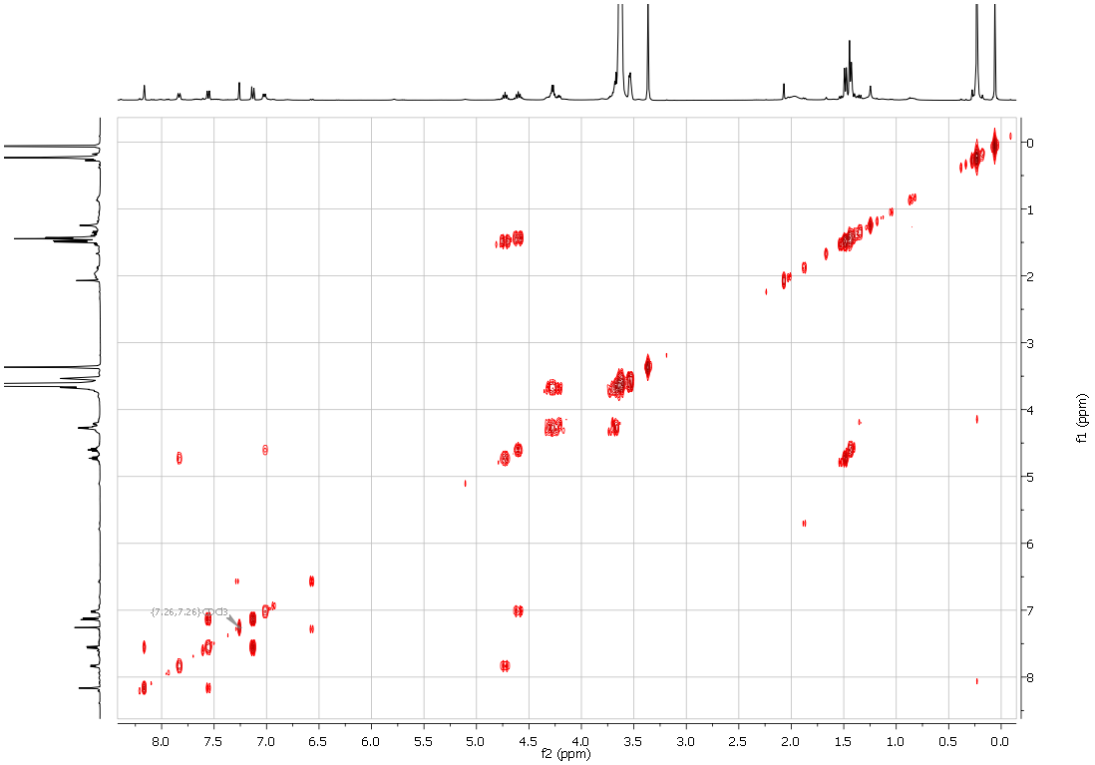

Figure 16-72: COSY of compound 22.

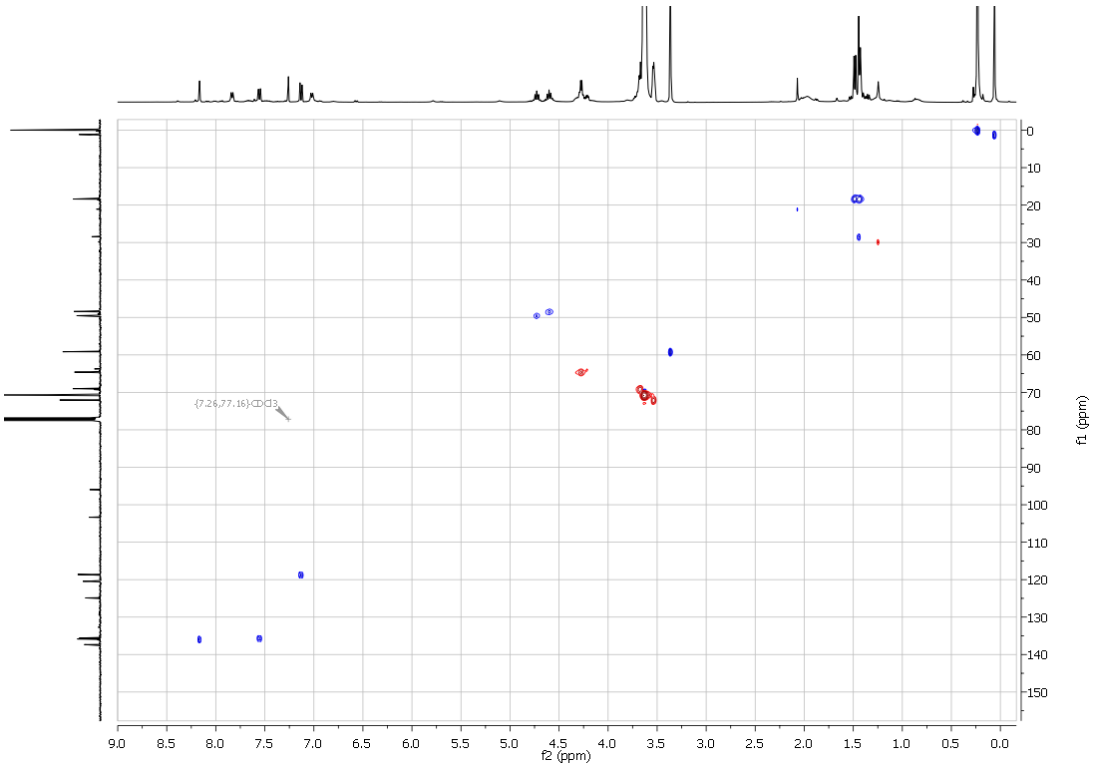

Figure 16-73: HSQC of compound 22.

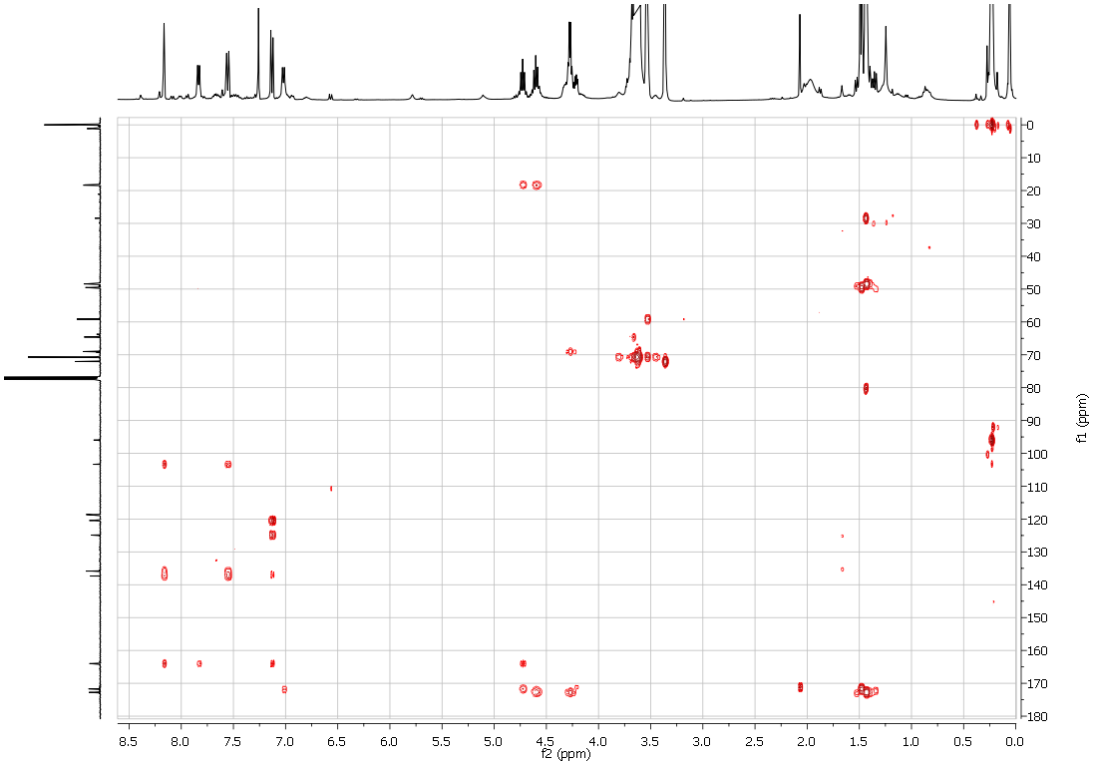

Figure 16-74: HMBC of compound 22.

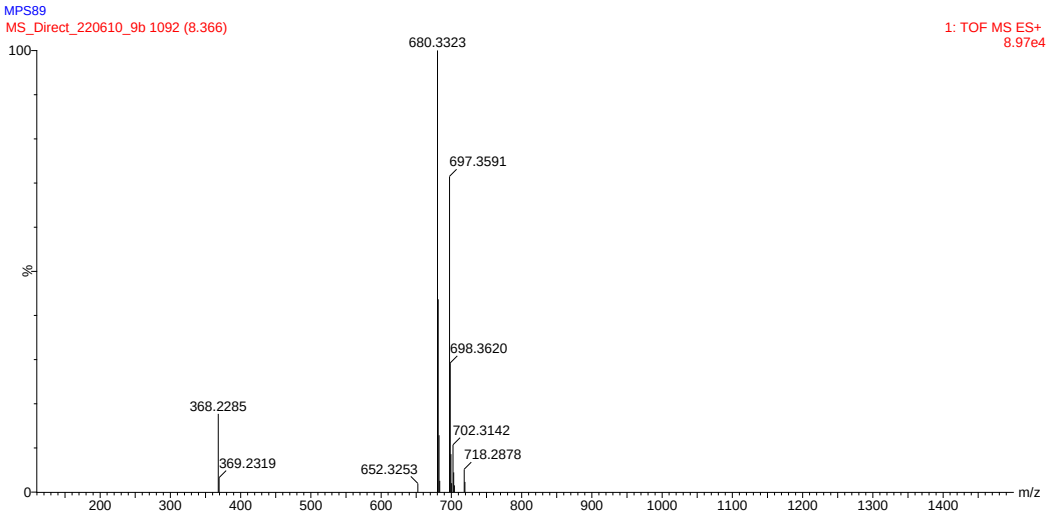

Figure 16-75: Mass spectrum of compound 22.

16.1.25Compound 27

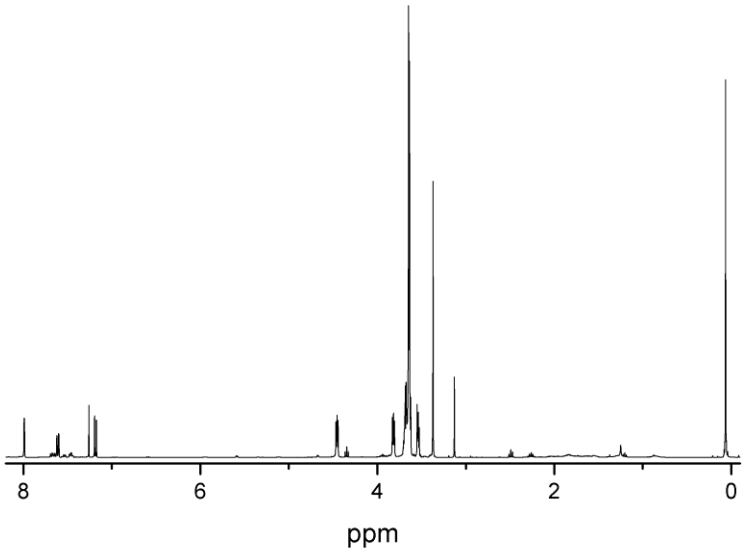

Figure 16-76: ^{1}H NMR of compound 27.

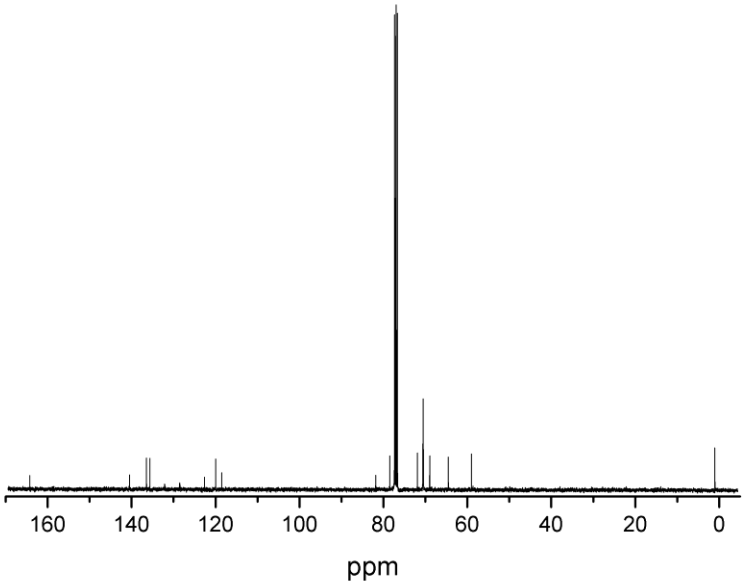

Figure 16-77: ^{13}C NMR of compound 27.

16.1.26Compound 28

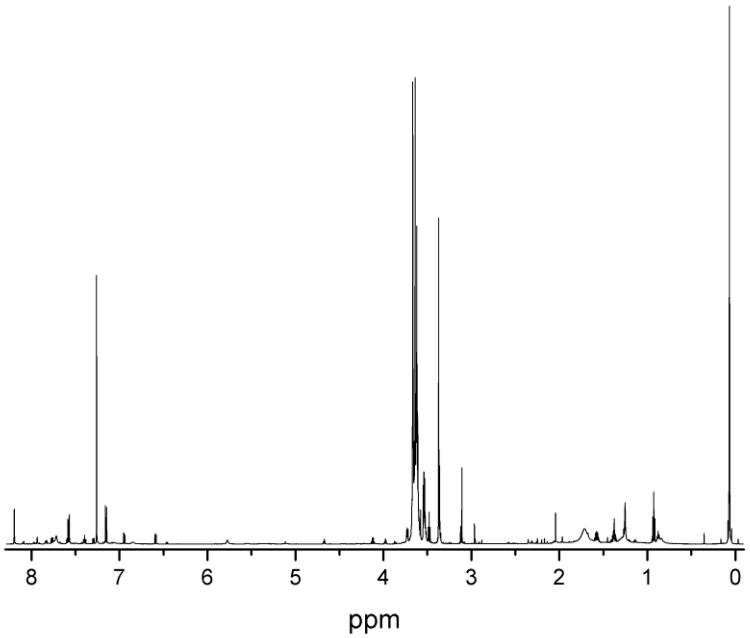

Figure 16-79: ^{1}H NMR of an impure compound 28.

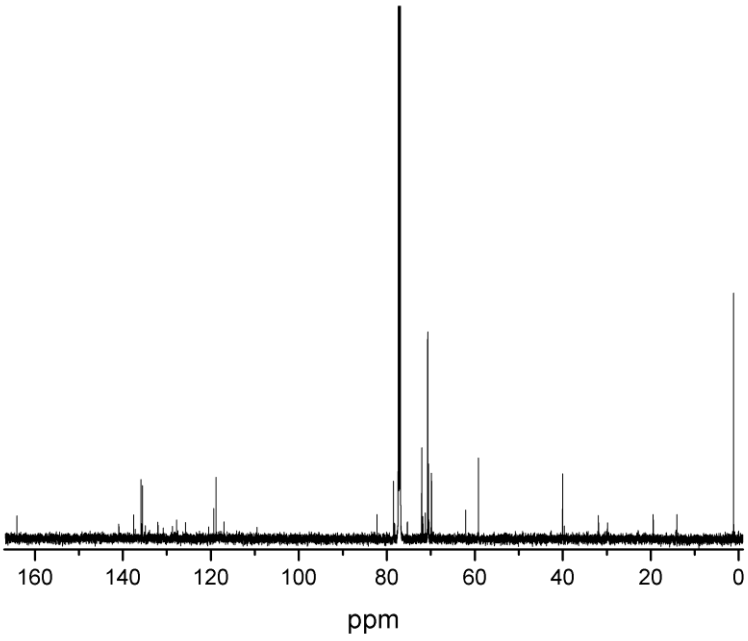

Figure 16-78: ^{13}C NMR of an impure compound 28.

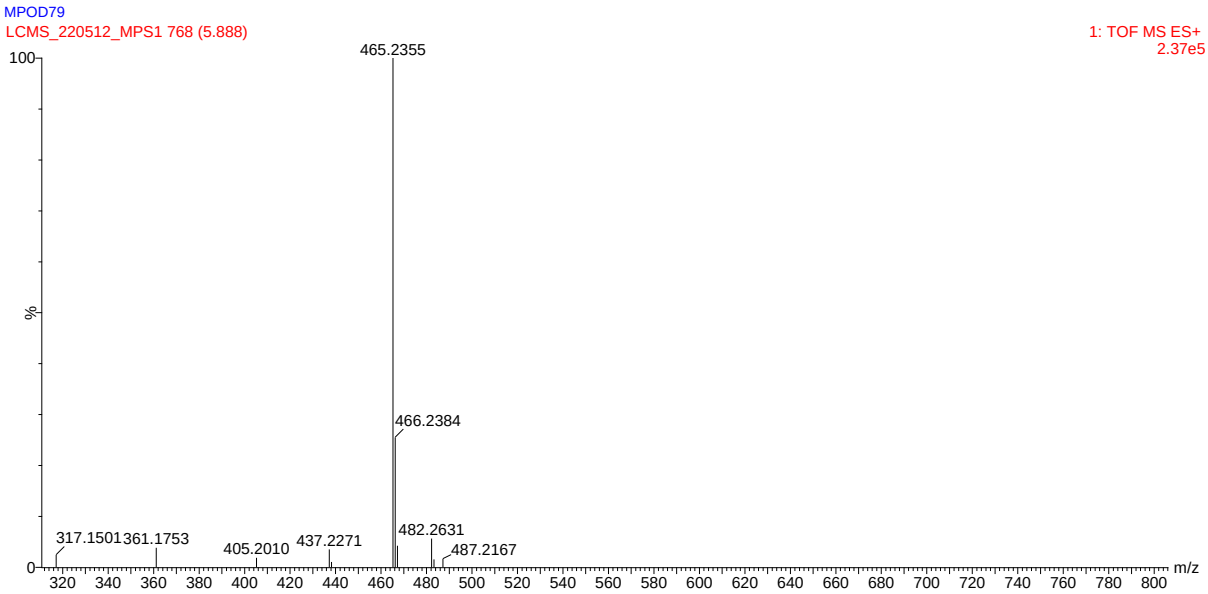

Figure 16-80: Mass spectrum of compound 28.

16.1.27Compound 29

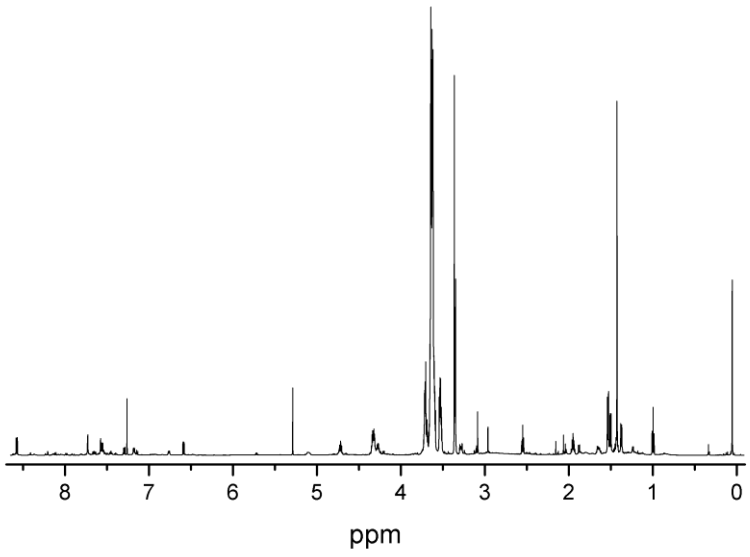

Figure 16-81: ^{1}H NMR of an impure compound 29.

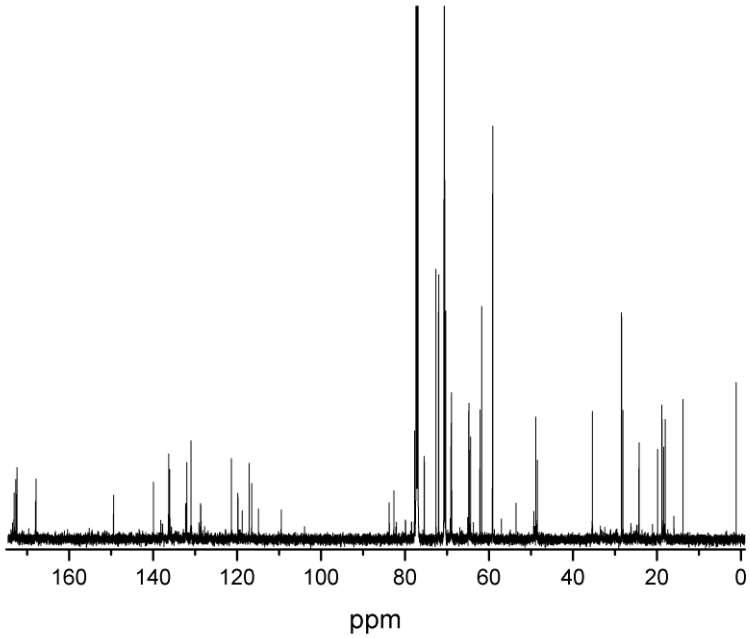

Figure 16-82: ^{13}C NMR of an impure compound 29.

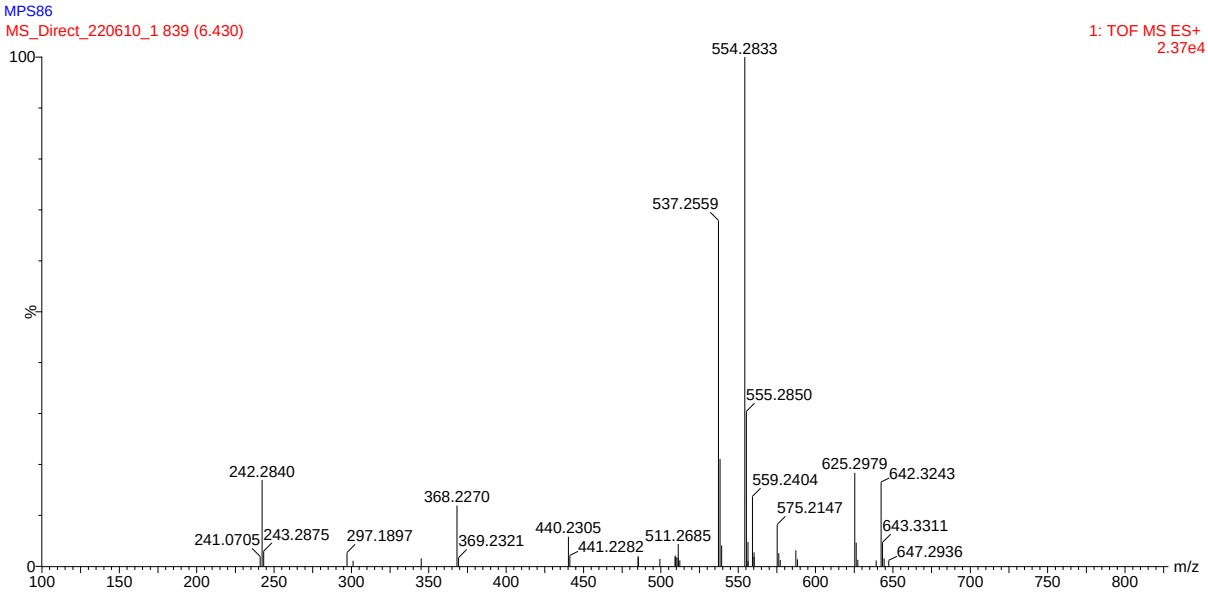

Figure 16-83: Mass spectrum of compound 29.

16.1.28Compound 30

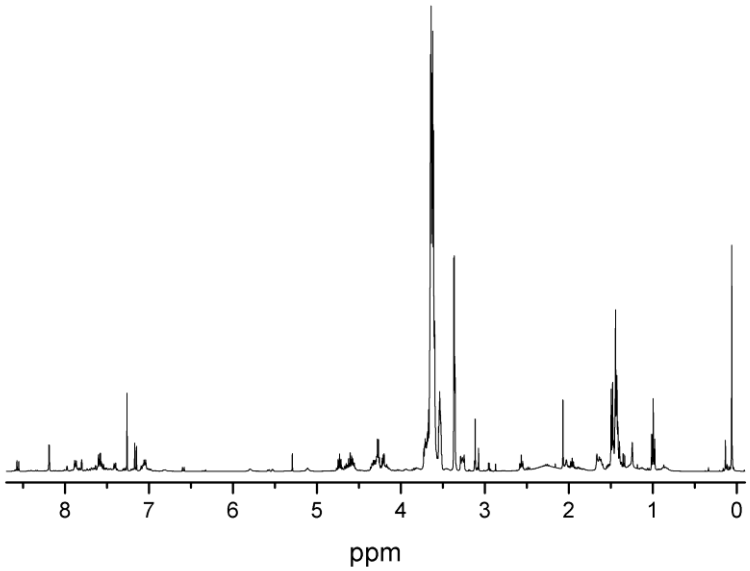

Figure 16-84: ^{1}H NMR of an impure compound 30.

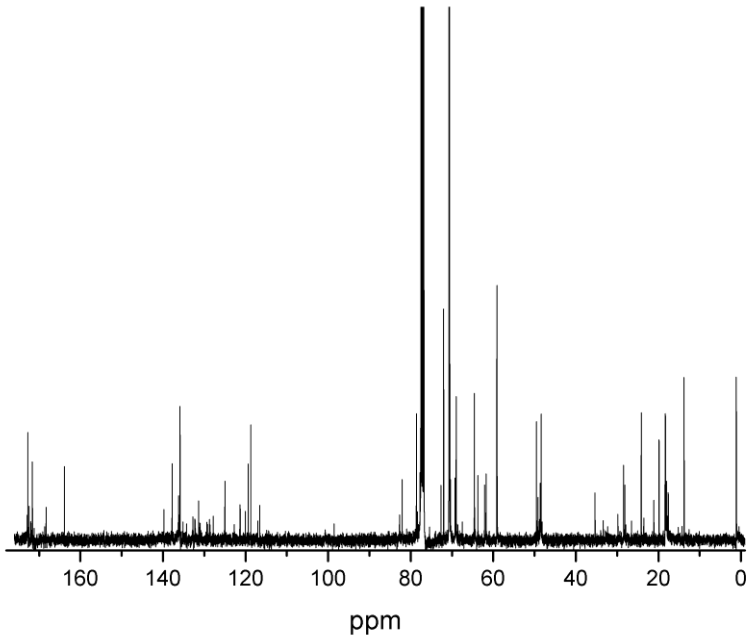

Figure 16-85:^{13}C NMR of an impure compound 30.

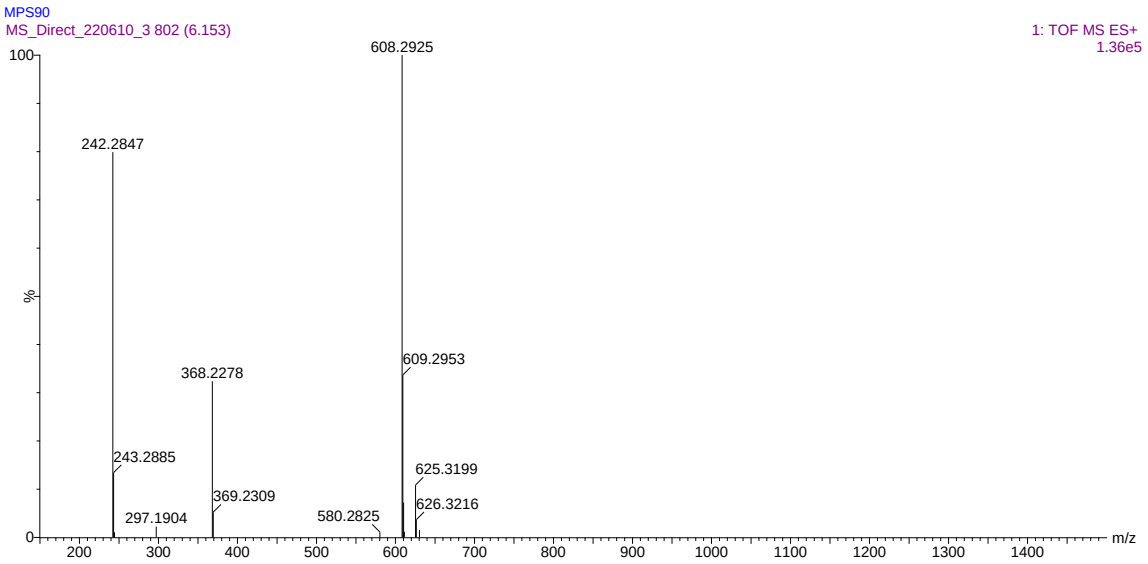

Figure 16-86: Mass spectrum of compound 30.

16.1.29Polymer 1

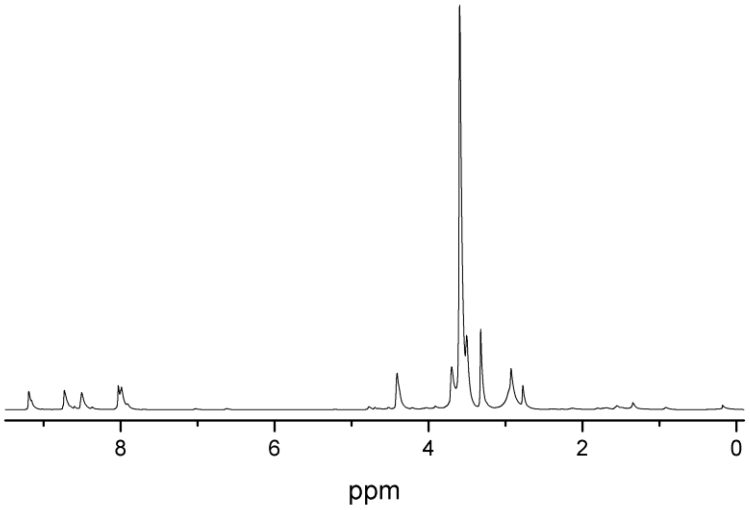

Figure 16-87: ^{1}H NMR of polymer 1 in DMF-d_7.

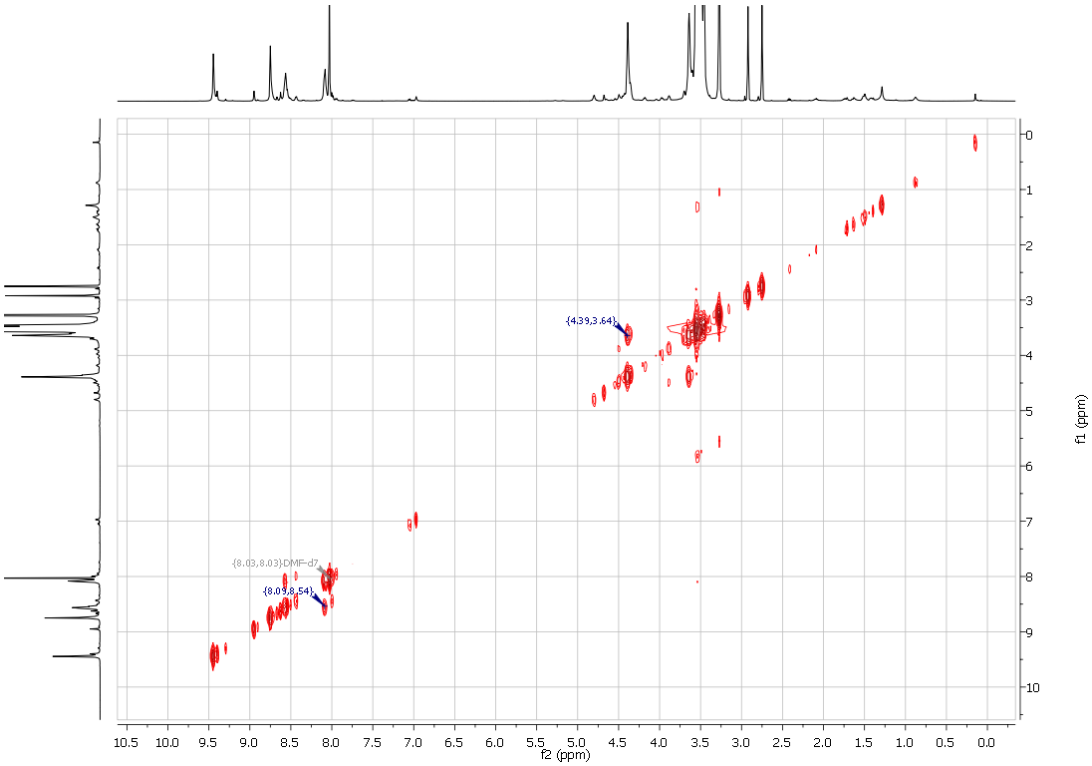

Figure 16-88: COSY NMR of polymer 1 in DMF-d_7.

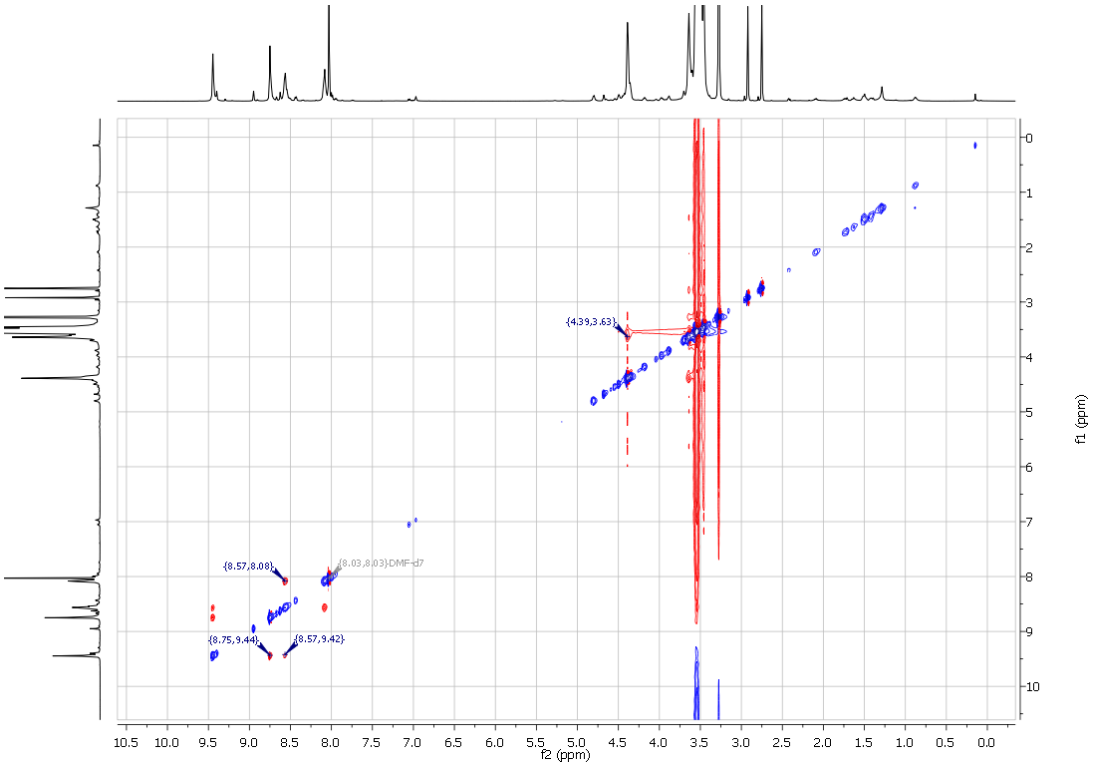

Figure 16-89: ROESY NMR of polymer 1 in DMF-d_7.

16.1.30Polymer 2

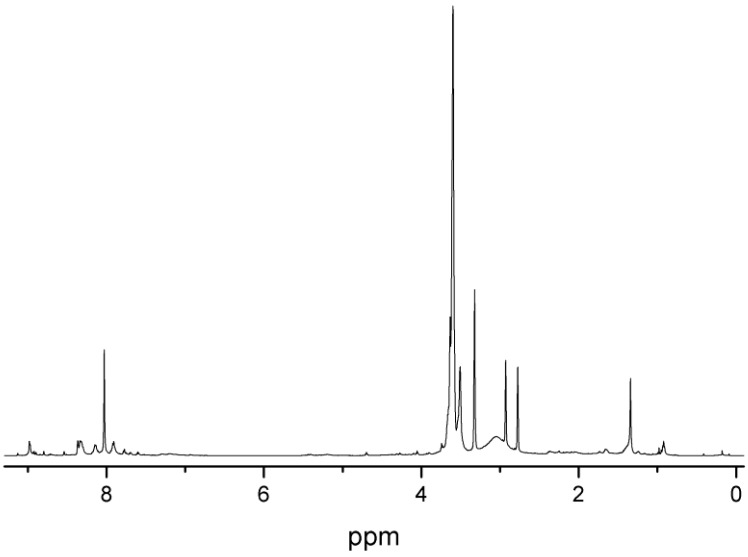

Figure 16-90: ^{1}H NMR of polymer 2 in DMF-d_7.

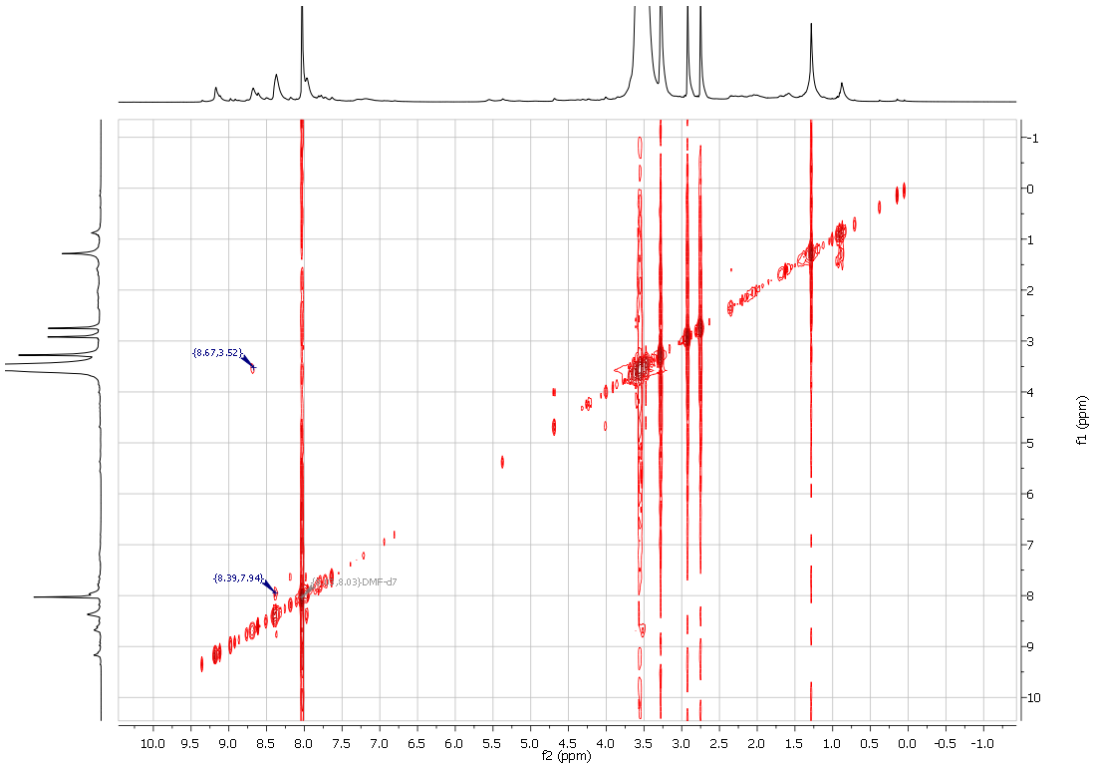

Figure 16-91: COSY NMR of polymer 2 in DMF-d_7.

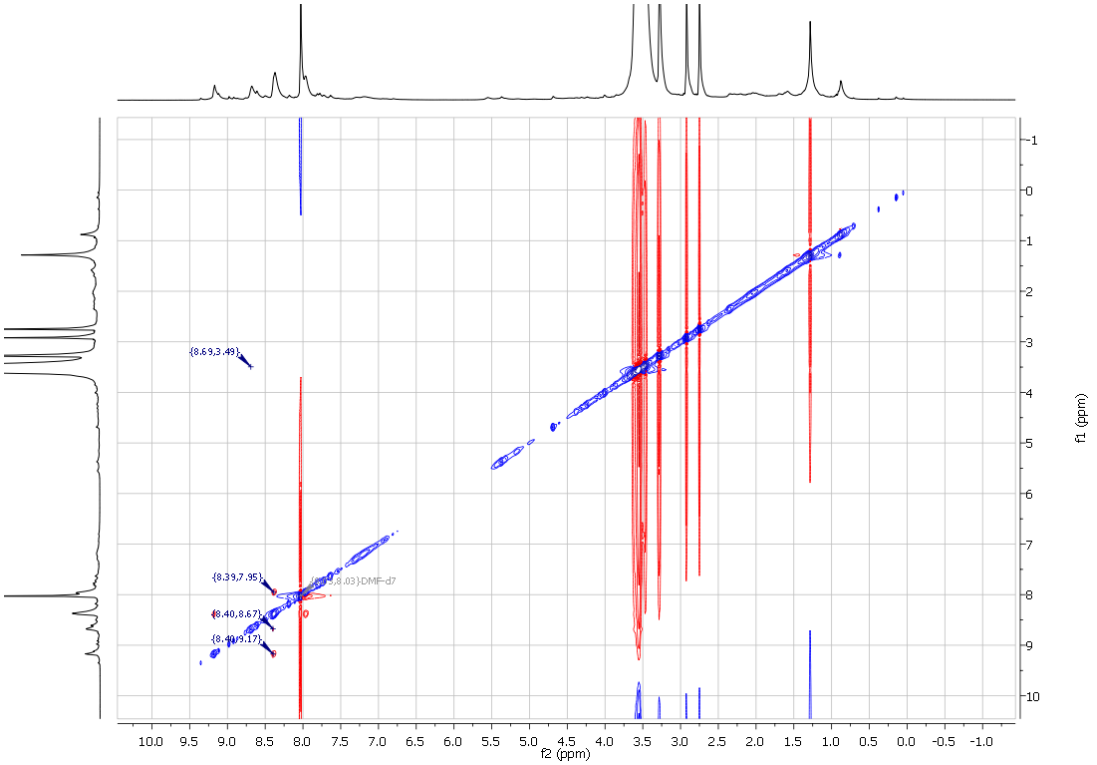

Figure 16-92: ROESY NMR of polymer 2 in DMF-d_7.

16.1.31Polymer 3

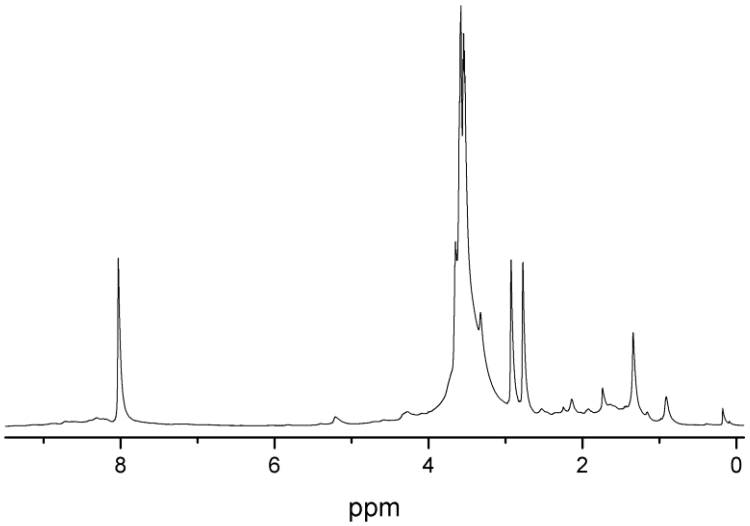

Figure 16-93: ^{1}H NMR of polymer 3 in DMF-d_7.

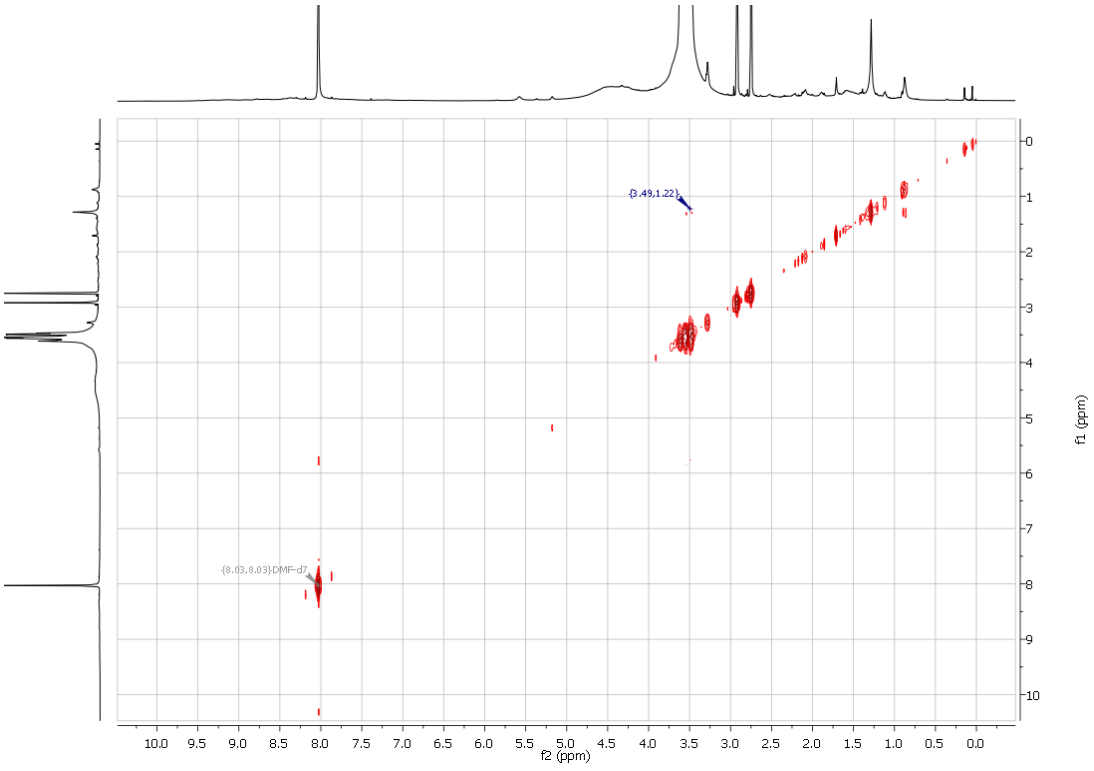

Figure 16-94: COSY NMR of polymer 3 in DMF-d_7.

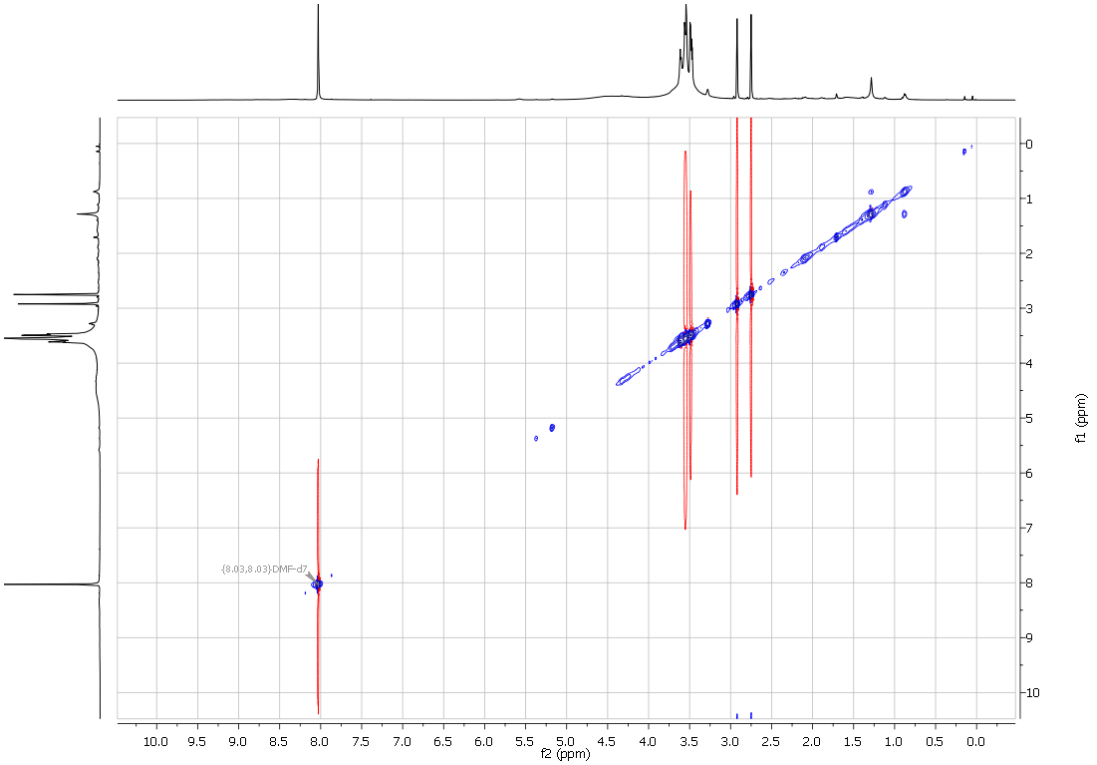

Figure 16-95: ROESY NMR of polymer 3 in DMF-d_7.

16.1.32Polymer 4

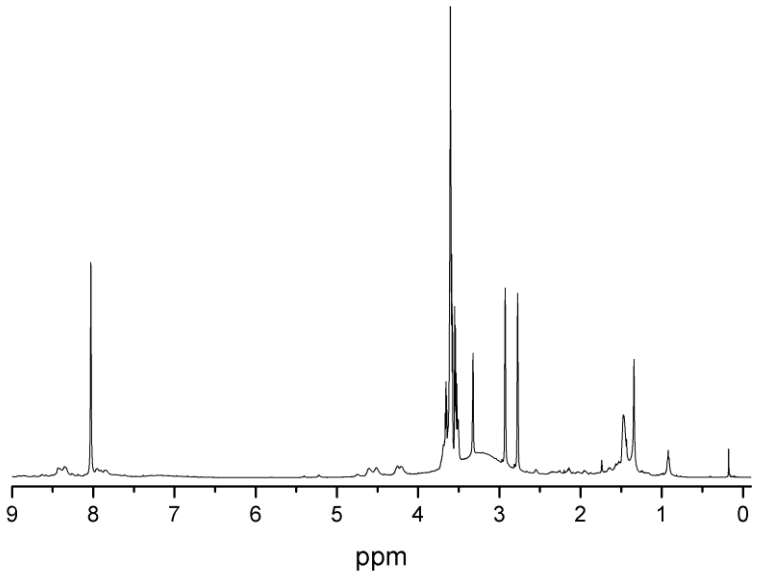

Figure 16-96: ^{1}H NMR of polymer 4 in DMF-d_7.

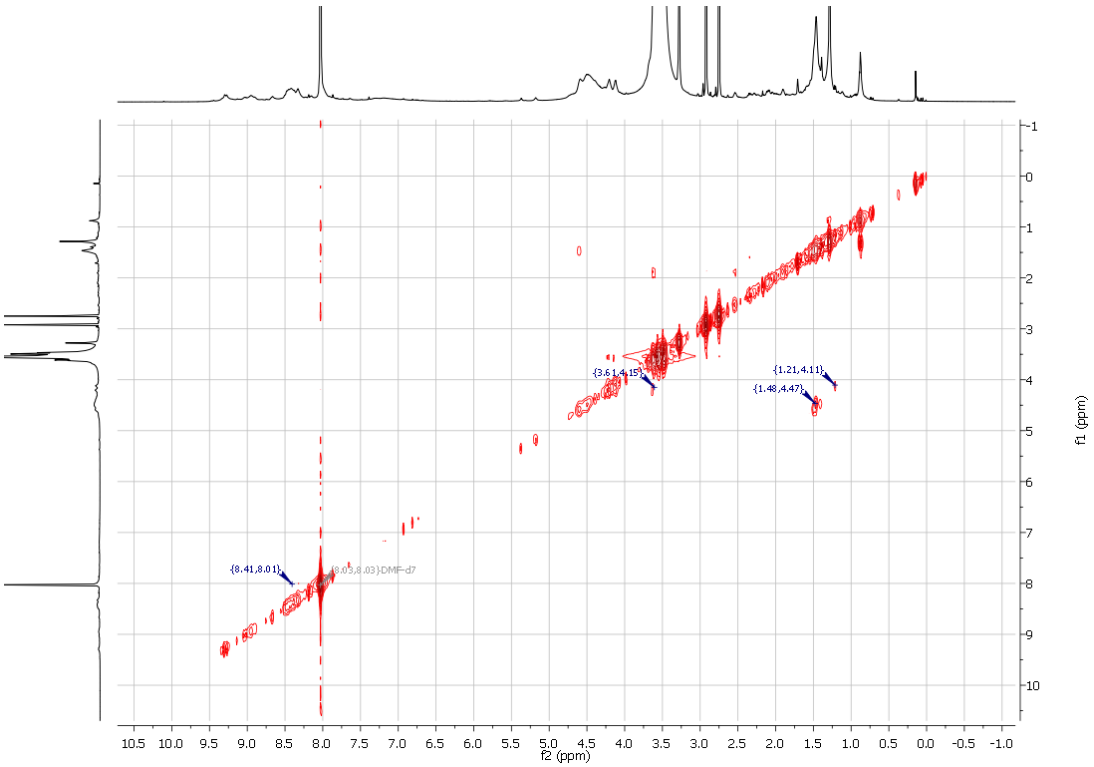

Figure 16-97: COSY NMR of polymer 4 in DMF-d_7.

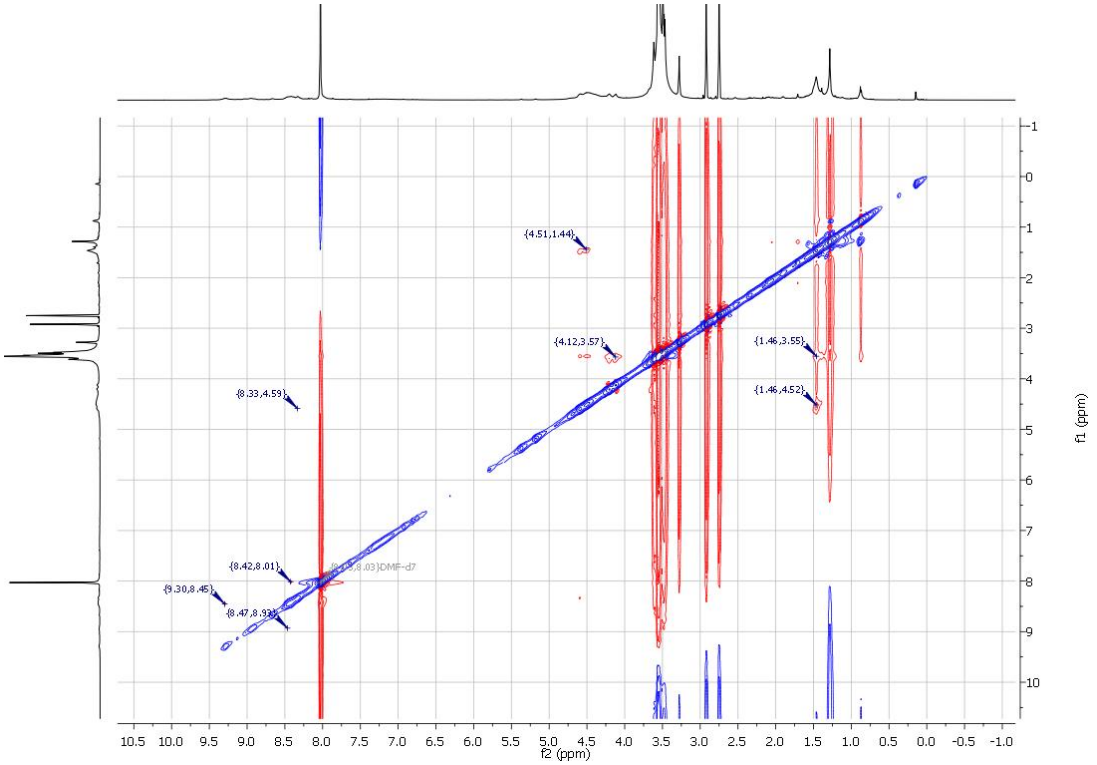

Figure 16-98: ROESY NMR of polymer 4 in DMF-d_7.